ANNUAL REPORT
"INVESTIGATION OF IN SITU PHYSICAL PROPERTIES OF SURFACE AND SUBSURFACE SITE MATERIALS BY ENGINEERING GEOPHYSICAL TECHNIQUES" Project

Joel S. Watkins, Editor and Project Chief

U. S. GEOLOGICAL SURVEY LIBRARY
MAY 9 1967
DENVER

67-272

This report is preliminary and has not been edited or reviewed for conformity with U. S. Geological Survey standards and nomenclature.

DEPARTMENT OF THE INTERIOR
UNITED STATES GEOLOGICAL SURVEY
OPEN FILE REPORT

MAY 1967

Work done on behalf of
National Aeronautics and Space Administration

CONTENTS

Contents--Continued

Contents--Continued

Contents--Continued

ILLUSTRATIONS

Illustrations--Continued

Illustrations--Continued

Illustrations--Continued

Illustrations--Continued

Illustrations--Continued

TABLES

SUMMARY AND HIGHLIGHTS

This report includes the first substantive body of in situ density, bearing strength, shear strength, and moisture content data measured by Project personnel. Emphasis in this fiscal year's measurements was on low-density materials since available data suggest that the upper meter or so of the lunar surface consists of low-density material. In situ densities ranged upward from 0.43 g per cc, and bearing strengths ranged from 3.4×10^4 to 4.6×10^7 dynes per cm^2 (0.5 to 607 psi).

Tabulation of compressional wave data indicates that for 90 percent of the data, ground particle velocities at 30 m from a 0.05 kg dynamite shot are between 0.23 and 16×10^{-3} cm per sec with a median value of 2.1×10^{-3}. Ranges of particle velocities at other distances have been tabulated and approximate empirical conversion coefficients for ratios of energy due to dynamite charges of various size, 45-kg weight drops, and blasting caps are presented.

Physical properties studies made in the laboratory on cores from six lunar analog sites show little correlation between seismic wave properties and densities or strengths. In situ measurements at 23 sites show that the density (ρ) and the compressional wave velocity (V_p) are related by the formula

$$\rho = 0.454 \ln V_p - 1.46.$$

The rms deviation of observed data from calculated values is 0.24 g per cc.

Geologic documentation of lunar analog sites has continued during the past fiscal year and reports covering geologic investigations of five lunar analog sites are presented in this report.

Petrographic examination of cores from the Sonora Pass granite indicates that the rock is homogeneous quartz monzonite. The dry bulk density averages 2.62 g per cc and the porosity averages 1.8 percent.

Examination of core and surface samples from the Mono Ash site show that the material at the surface consists of dry lapilli ash of Late Pleistocene-Recent age probably derived from the adjacent Mono Craters. A tuff (probably equivalent to the Bishop Tuff) occurs at and below 47 m in the core hole. Density of material above the tuff averages about 1.26 g per cc.

Geologic mapping of the Southern Coulee indicates that the coulee consists of three main parts: the dome, where the flow was vertical; the flow, where the flow was lateral; and the talus slope surrounding the flow. Three lithologic units were distinguished (mainly within the flow) on the basis of variations of density. Analyses of samples from different localities indicate that the flow is chemically homogeneous.

Examination of surface samples and cores from the Bishop Tuff site indicates that the rock at the site consists of 18.6 m of well-indurated pink rhyolitic tuff underlain by unconsolidated ash of similar composition.

Petrographic examination of core from a 107-m core hole on the south rim of Meteor Crater revealed a 10-m-thick debris zone at the top in which the stratigraphic sequence was inverted. The debris zone was underlain by a 10.1-m thickness of fine-grained calcareous sandstone of the Moenkopi Formation. The remaining 87 m consisted principally of sandy dolomite of the Kaibab Limestone.

Grain densities, bulk densities, porosities, compressional-wave velocities, shear-wave velocities, elastic moduli by static and pulse methods, compressive strength, tensile strength, and, in some cases, permeability measurements have been completed for cores from six analog test sites. These data are tabulated and presented in an appendix to this report.

Numerous other groups participating in the space program have requested data on the Southern Coulee to support various types of tests at this site. Plate 1 (in map pocket), a topographic map of the Southern Coulee

is being published with this report to aid other groups. Additional copies are available upon request.

Compressional wave data, including V_p, attenuation, and frequency measurements were completed essentially for all sites during the past fiscal year. These data are tabulated in an appendix to this report. Some problem areas may require reshooting after completion of further study of the data.

Drill logs for 2100 ft of diamond coring completed by Project personnel are tabulated along with hole locations in the appendix. In addition, the Project rig drilled over 9000 ft of shot holes.

Sixteen operational subroutines prepared by Project personnel are listed in the appendix, together with brief descriptions of the functions of the subroutines. Increasing amounts of data are being processed on digital computers and it is anticipated that most of the seismic data originally processed by hand will be reprocessed on digital computers during Fiscal Year 1967.

Shear-wave measurements have been completed at sites near Flagstaff, Arizona. It is anticipated that shear-wave measurements will be completed at the remainder of the sites during July 1966 and results summarized in the next Project report.

Status of seismic studies, geologic mapping, coring, petrography, laboratory physical properties measurements, and in situ physical properties measurements at all lunar analog sites is summarized in table 1.

Table 1.--Status of lunar analog site studies

[X--complete, /--partially complete, 0--not applicable, 1--shear wave data not complete, 2--relatively complete reports available from other sources, 3--no adequate means of coring exists. Petrology must be done from surface samples.]

Site	Seismic Data	Geologic Map	Cores	Petrography	Lab. Phys. Prop.	In Situ Phys. Prop.
Kana-a Flow	X	X	X	X	X	
Cinder Hills	X	0	3	3	/	/
S P Flow	X	X	3	X	X	/
Kaibab Limestone	X	0	X	0	X	0
Mono Ash	X1	0	X	X		/
Southern Coulee	X1	X	X	X	/	X
Bishop Tuff	X1	0	X	X	/	
Sonora Pass	X1	0	X	X	X	0
Amboy Flow	X1	X2	/	/2	X	
Pisgah Flow	X1	X2		/2		
Meteor Crater	X1	X2	X	X	X	/
Middle Mesa	X	/	X		/	/
Sierra Ancha	X	0				
Sacramento alluvium	X	0		0		
Lompoc	X	0	0	0		X
Inyokern	X	0	0	0	0	X
Olancha	X	0	0	0		X
White Sands	X	0	0	0	0	X

(page 7 follows)

IN SITU PHYSICAL PROPERTIES MEASUREMENTS

by Lawrence A. Walters

ABSTRACT.--In situ bulk density, moisture content, bearing capacity, shear strength, and compressional wave velocity were determined simultaneously on seven lunar analog sites. Bearing capacities ranged from 3.4×10^4 to 45.9×10^6 dynes per cm^2 (0.5-675 psi). Density ranged from 0.43 to 1.87 g per cc. A large range of properties for the same material was found for various physical states of the material.

Introduction

In situ bulk density, moisture content, bearing capacity, shear strength, and P-wave velocity were recorded simultaneously for the following lunar analog materials: S P blocky andesitic basalt, Meteor Crater rim material (previously shocked and fractured limestone and sandstone), Southern Coulee pumice, Olancha bentonite, Lompoc diatomite, Inyokern volcanic ash, and White Sands gypsum sand. Bearing capacities ranging from 3.4×10^4 to 45.9×10^6 dynes per cm^2 (0.5-675 psi), and bulk density ranging from 0.43 to 1.87 g per cc, were recorded for these diverse materials (table 2). A large range of properties for the same material was found for various physical states of the material, suggesting that lunar materials could have an equally large range of properties dependent upon their physical state.

This study is part of the continuing program of study of the interrelationships of various physical parameters of possible lunar analog materials whose tentative goal is to define the physical

Table 2.--In situ physical properties measurements on lunar analog sites

Material	Depth (meters)	Excavated (kilograms)	Volume (m^3)	Bulk Density (g/cc)	Moisture weight (percent)	P-Wave velocity (mps)	Dry bulk density calculated (g/cc)	Ultimate bearing capacity ($dynes/cm^2$)	Shear strength ($dynes/cm^2$)
S P FLOW									
Blocky andesitic basalt----	3	17,154.9	13.81	1.23	nil	450	----------	----------	----------
METEOR CRATER									
Loose sand and platy blocks of sandstone------	2	19,319.9	10.31	1.87	3	400	----------	----------	----------
SOUTHERN COULEE									
Pit No. 1									
Blocky pumice with intermixed ash----------	2	4,484.0	4.61	0.97	15	260	0.82	11.0×10^6 (15-cm dia. platen)	----------
Pit No. 2									
Loose black pumice blocks with minor ash----------	2	3,002.6	4.23	0.71	8	---	0.65	----------	----------
Pit No. 3									
1-m thick unit of ash with minor amounts of rhyolite rubble----------	1	1,540.4	1.15	1.34	20	140	1.14	9.3×10^6 (15-cm dia. platen)	----------
OLANCHA BENTONITE talus									
Loose bentonite talus------	---	------	---	0.50-1.0	3-13	120	----------	approx. $3.4\text{-}6.8 \times 10^4$	$6.8\text{-}13.6 \times 10^4$
Compacted bentonite talus at depth----------	---	------	---	0.90-1.0	15-18	260	----------	$3.7\text{-}4.4 \times 10^5$ (30-cm dia. platen)	$6.4\text{-}7.4 \times 10^5$
"IN PLACE" BENTONITE									
Compacted stratified bentonite with loose material on top----------	---	------	---	0.70-1.10	3-16	300	----------	$13.6\text{-}20.4 \times 10^6$ (15-cm dia. platen)	----------
LOMPOC DIATOMITE Talus									
Loose diatomite talus------	---	------	---	0.43- .54	14-16	120	----------	$6.8\text{-}13.6 \times 10^4$ (15-cm dia. platen)	----------
Compacted diatomite talus at depth----------	---	------	---	0.50- .70	25-35	200	----------	$3.4\text{-}4.7 \times 10^6$ (15-cm dia. platen)	6.3×10^5
"IN PLACE" DIATOMITE									
Stratified diatomite waste with interbedded clay----------	---	------	---	0.65- .72	16-40	195	----------	$40\text{-}45.9 \times 10^6$ (5.5-cm dia. platen)	----------
INYOKERN									
Upper 10 cm loose volcanic ash----------	---	------	---	0.80- .90	10-30	---	----------	approx. $6.8\text{-}13.6 \times 10^4$	----------
1-m compacted volcanic ash-	---	------	---	0.80-1.05	40-70	170	----------	$2\text{-}10 \times 10^5$ (30-cm dia. platen)	$4.7\text{-}17.0 \times 10^5$
WHITE SANDS									
Fine-grained gypsum sand on top of a 10 m high dune--	---	------	---	1.71	20	730	----------	----------	----------
Coarse-grained gypsum sand on lee side of a 5 m high dune----------	---	------	---	1.22	nil	410	----------	----------	----------

parameters of materials by geophysical techniques.

Techniques

In situ bulk density was measured by two techniques:

1. A _____ gamma ray backscatterer with a 4.5 millicurie source was used to determine the density of materials whose maximum block size did not exceed 12.5 cm. Pits were excavated to get subsurface density measurements because the maximum depth of penetration of the gamma ray backscatterer probably did not exceed 25 cm. A limiting diameter of 1 m at the base of these pits was necessary to prevent backscattering interference from the walls.
2. The bulk density of blocky materials whose largest dimension exceeded 12.5 cm was determined by excavating and weighing a large sample of material whose volume was known. The volume of the excavated pits was determined by lining the pits with plastic and filling them with water (Walters, 1966).

Bearing capacities were measured by forcing steel platens into surface materials with a hydraulic jack anchored to the frame of a one-ton truck. Ultimate bearing capacities were determined from load-settlement curves (fig. 1). Loading increments never exceeded 25 percent and seldom exceeded 10 percent of the failure load. Each load increment settled for 0.5-1.0 hrs. Most bearing capacities in this report are subject to rechecking with larger platens when suitable loading apparatus is acquired.

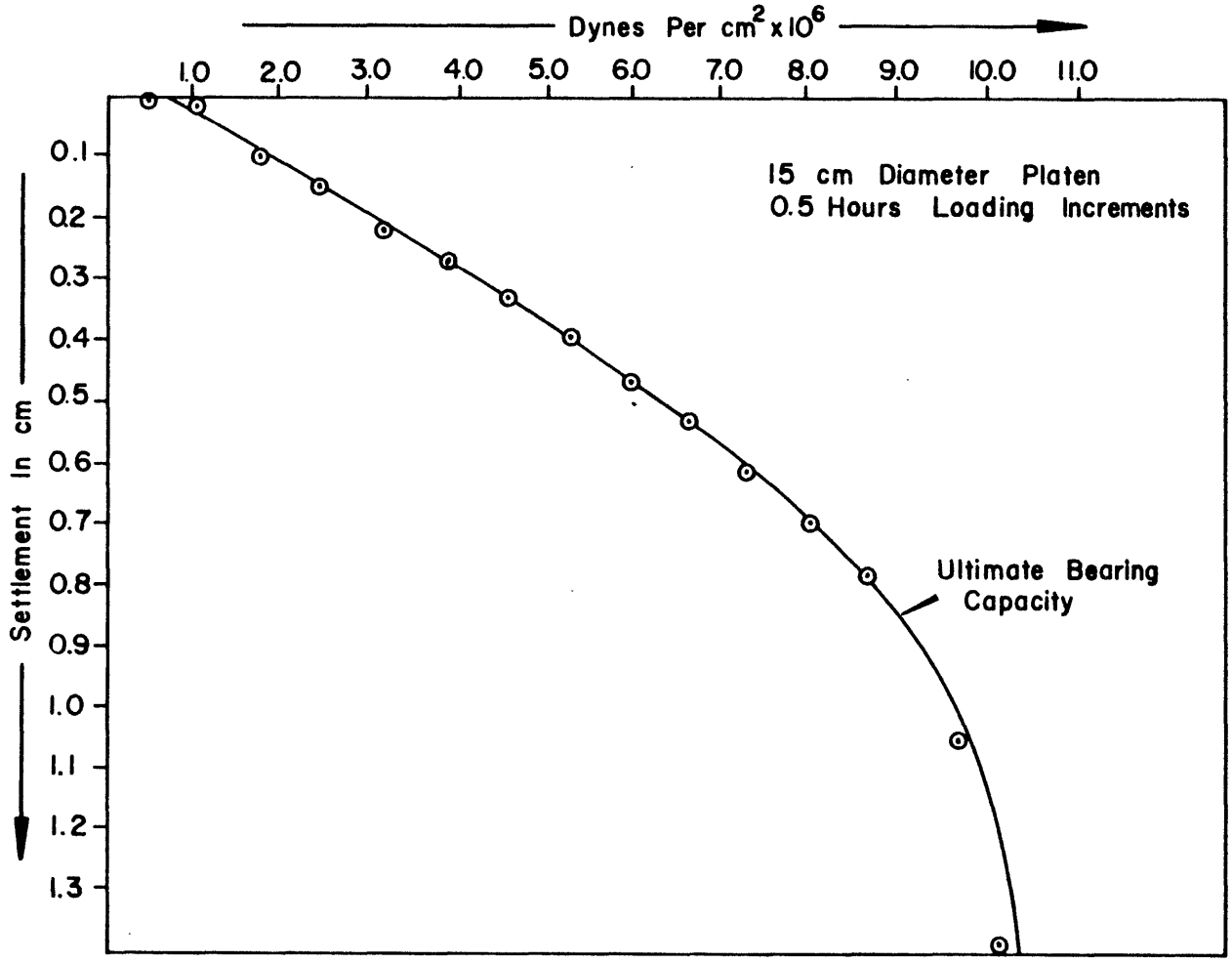

Figure 1.--Load-settlement curve for Southern Coulee Ash area near pit 3.

Moisture content was determined by wet and dry weights and by the neutron-moisture apparatus. The density apparatus is converted to a moisture content measurer by the addition of a chemical neutron source and by an appropriate voltage adjustment on the scaler.

Shear strength was determined at various depths with an Acker vane shear tester equipped with a precision torque head.

S P Flow

The S P Flow is a highly fractured, blocky andesitic basalt flow located in the northern part of the San Francisco volcanic field near Flagstaff, Arizona. The flow extends 7.2 km north from the base of S P Crater and reaches a maximum width of 3.0 km. The maximum thickness probably does not exceed 60 m.

The flow consists of loosely packed, angular polygonal blocks of vesicular lava ranging in size from less than 2.5 cm to greater than 1.5 m. Abundant fines consisting of ash and residual weathering products occur in voids between the blocks of lava.

A bulk density pit was dug 3 m deep on the thickest part of the flow. The bulk density was 1.23 g per cc (table 2).

Meteor Crater

A bulk density test pit was dug in the debris layer atop the overturned flap on the southern rim of Meteor Crater near Winslow, Arizona. Excavated material consisted of loose sand and platy blocks of sandstone whose maximum size was 40 cm x 40 cm x 90 cm. The pit was excavated to a depth of 2 m and the bulk density was 1.87 g per cc with a moisture content of 3 percent by weight (table 2).

Southern Coulee

Southern Coulee is the largest of four Recent, pumiceous, rhyolitic flows of the Mono Craters area in eastern California (Loney, this report). Three bulk density pits were dug on the coulee on seismic lines DEF (pit 1) and PQR (pit 3), and in an area southeast of line STU (pit 2). Locations are shown in figure 2. Compressional wave velocities, bearing capacities, and moisture content were determined at the same time density measurements were made (table 2).

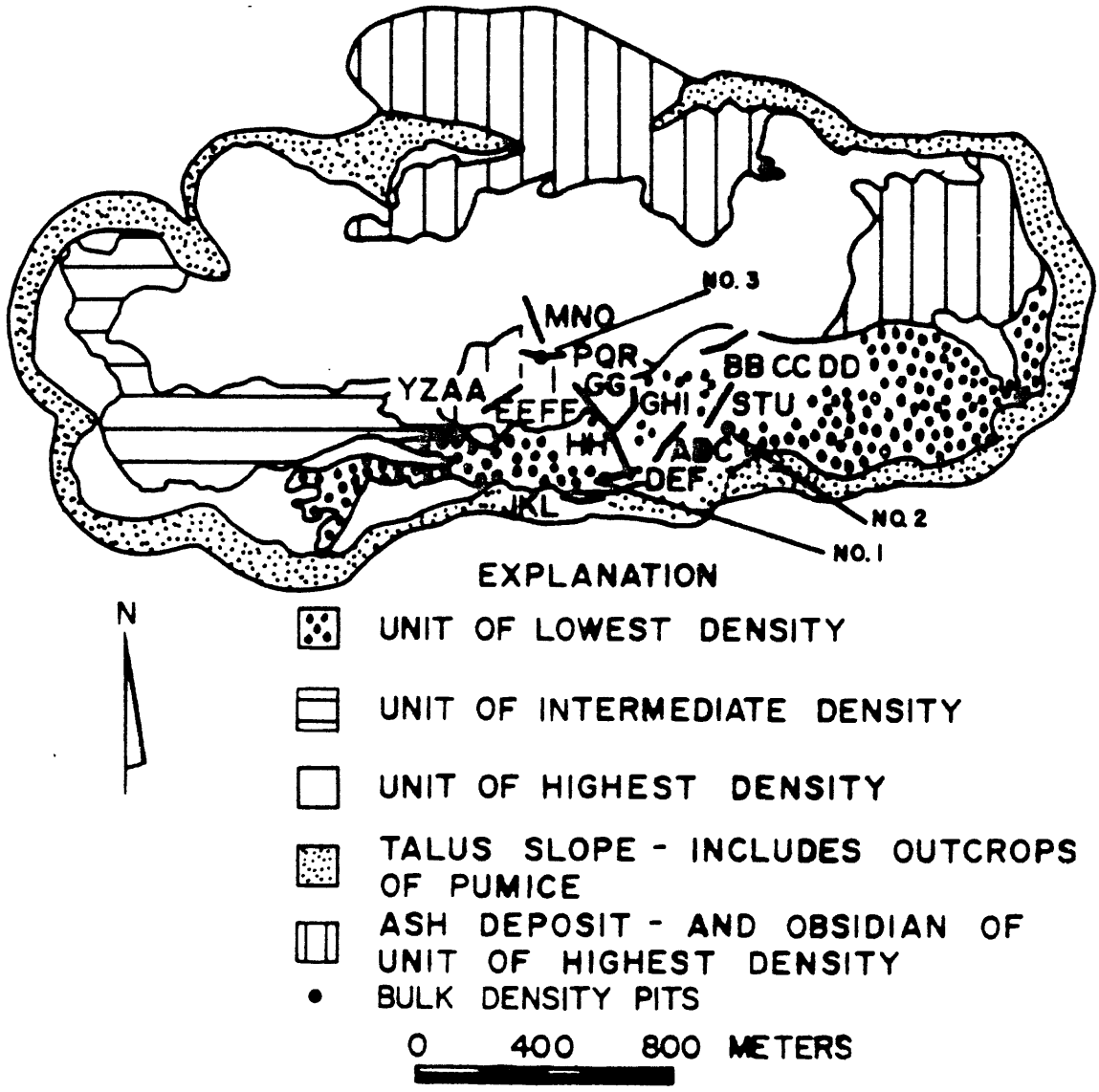

Figure 2.--Location of bulk density pits on Southern Coulee relative to refraction profiles and lithologic units (after Hassemer and others, 1965).

Olancha Bentonite

The Olancha bentonite site is located 16 km east of Olancha, California, at the southern end of Owens Valley. The material is a non-swelling montmorillonite clay that has been extensively mined for use as a filter aid and insecticide carrier.

The bentonite talus site consists of material mined from adit 29 and dumped on the slope in front of the mine adit (fig. 3). Minor amounts of an overlying dense volcanic rock are intermixed with the bentonite. The bentonite talus is underlain by talus composed of predominently dense volcanic rock (fig. 4). Talus fragments range in size from fine lumps to blocks 30 cm x 30 cm x 7.5 cm (fig. 5).

The "in place" site (fig. 6) is underlain by at least 3.5 m of compact bentonite which is in turn underlain by a clayey siltstone. Data are tabulated in table 2.

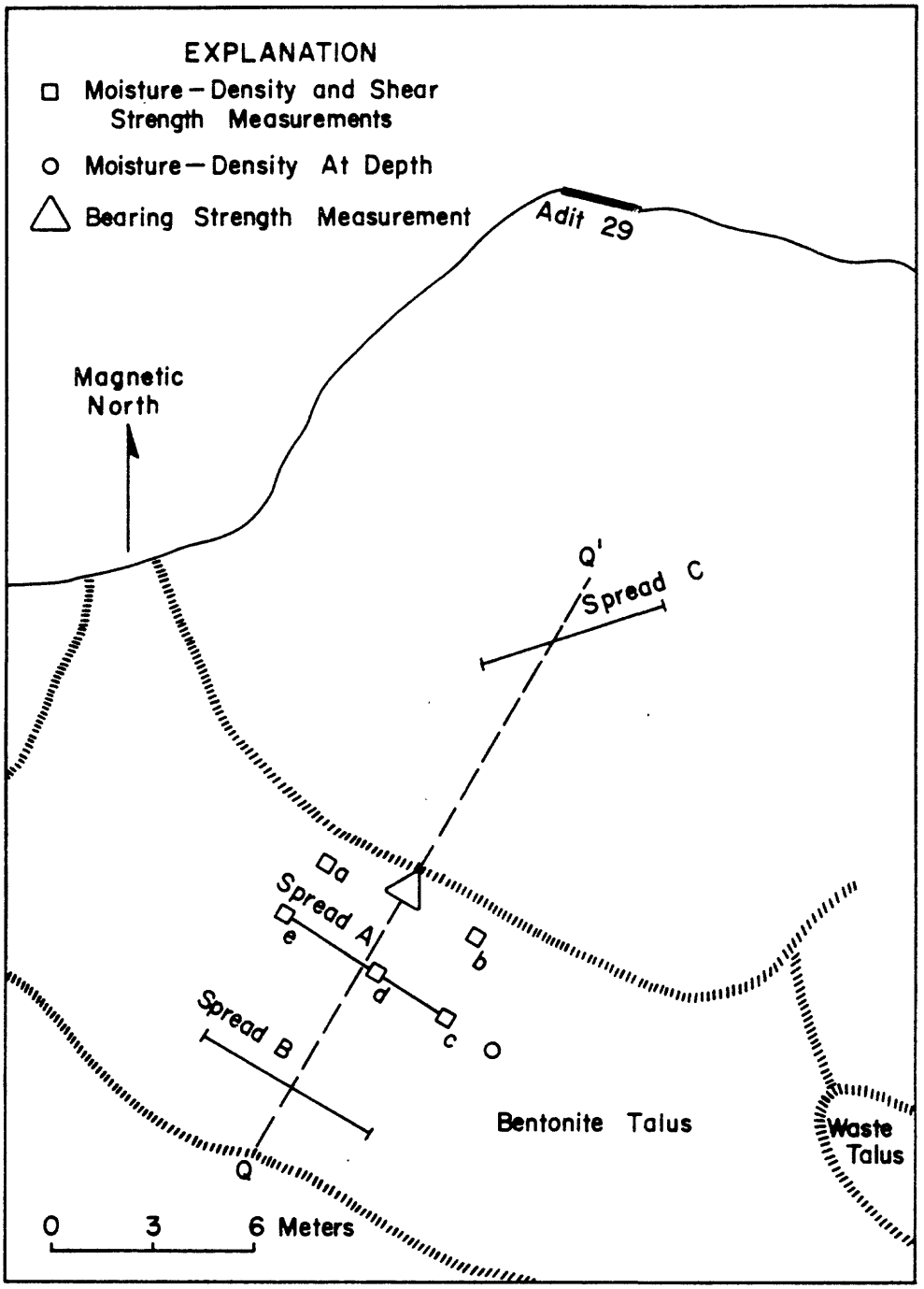

Figure 3.--Olancha, California, bentonite talus site. Cross section Q - Q' is shown in figure 4.

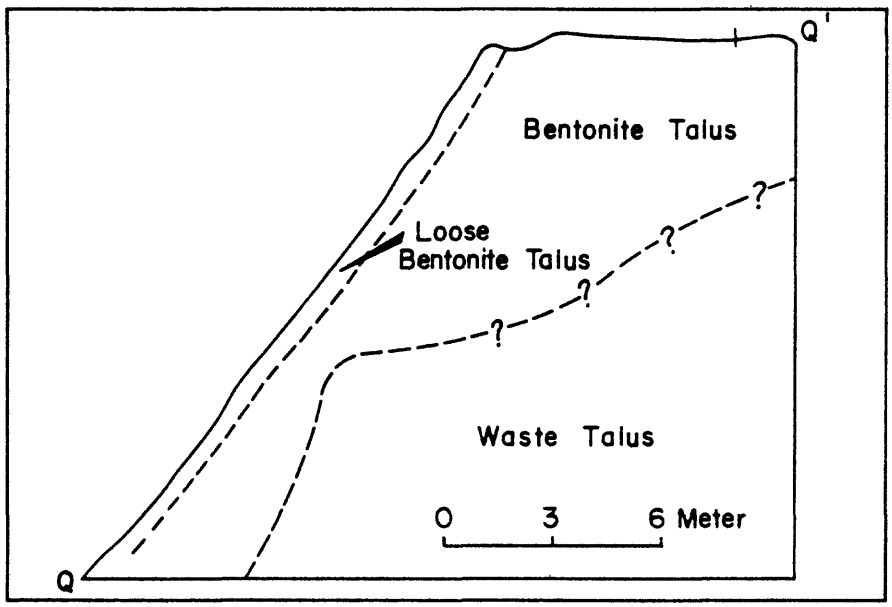

Figure 4.--Cross section of Olancha, California, bentonite talus site.

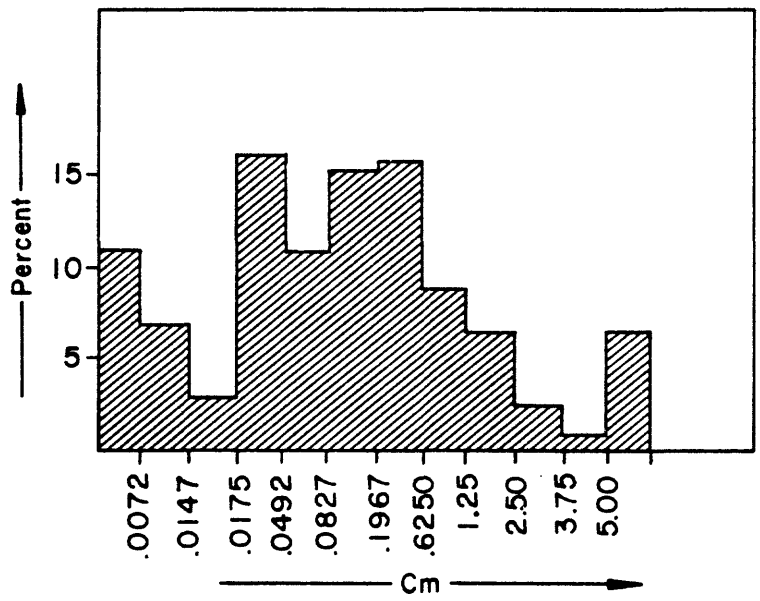

Figure 5.--Grain-size distribution of 10 kg of Olancha, California, bentonite talus sample.

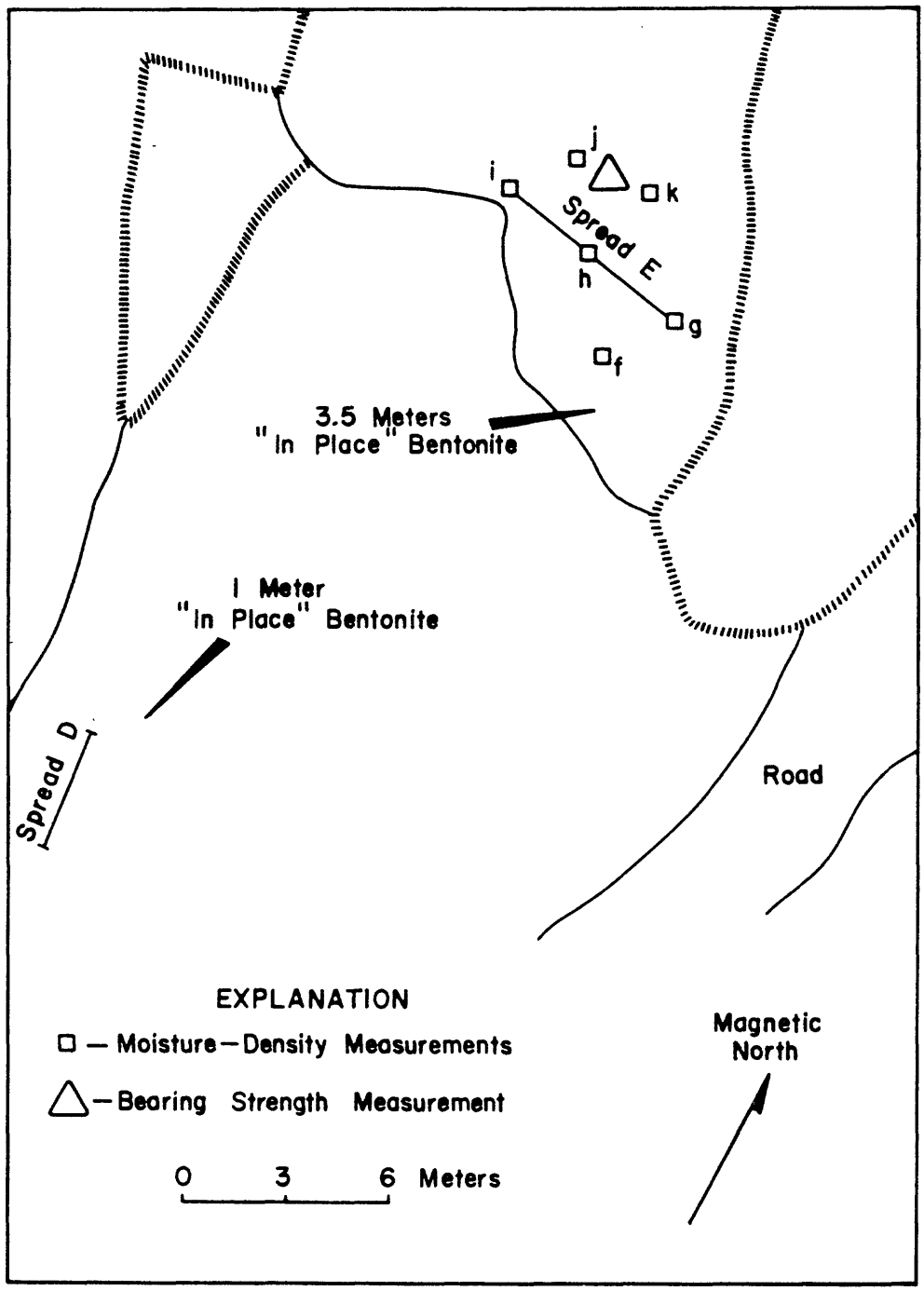

Figure 6.--Olancha, California, "in place" bentonite site.

Lompoc Diatomite

The Lompoc diatomite site is a few kilometers south of Lompoc, California, This diatomite occurs in the Miocene-Pliocene Sisquoc Formation.

The diatomite talus site is on a low-grade stockpile (no. 15) (fig. 7). The stockpile is about 3.2 m thick and is underlain by a more compacted diatomite stockpile and "in place" diatomite waste material. The diatomite talus material ranges in size from very fine aggregates to lumps of material 25 cm x 25 cm x 5 cm (fig. 8).

The "in place" site is on the crest of an anticlinal structure on hill 24 (fig. 9) and consists of at least 30 m of "waste diatomite". The "waste diatomite" is diatomite interbedded with clay and admixed clay.

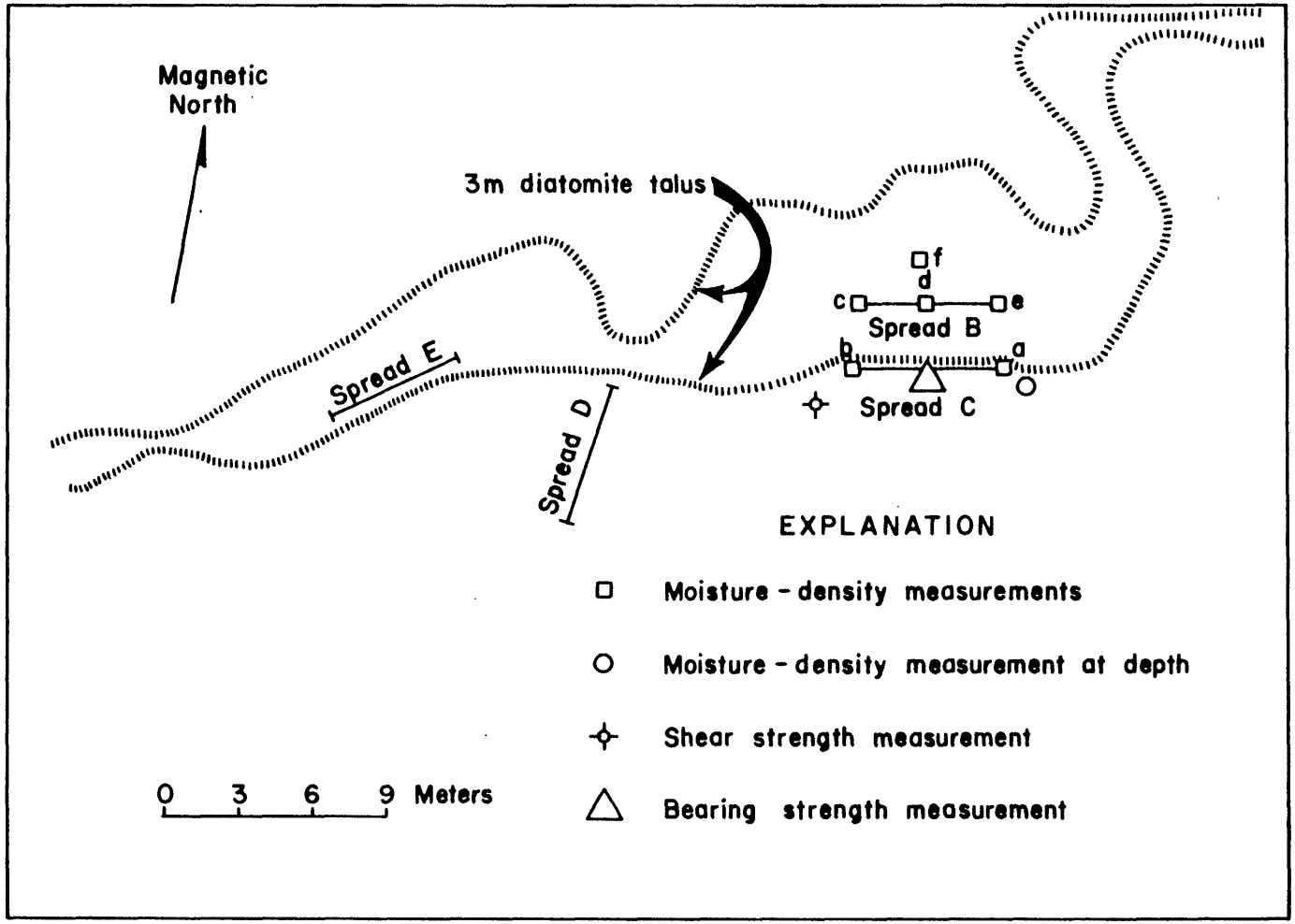

Figure 7.--Lompoc, California, diatomite talus site on low-grade stockpile number 15.

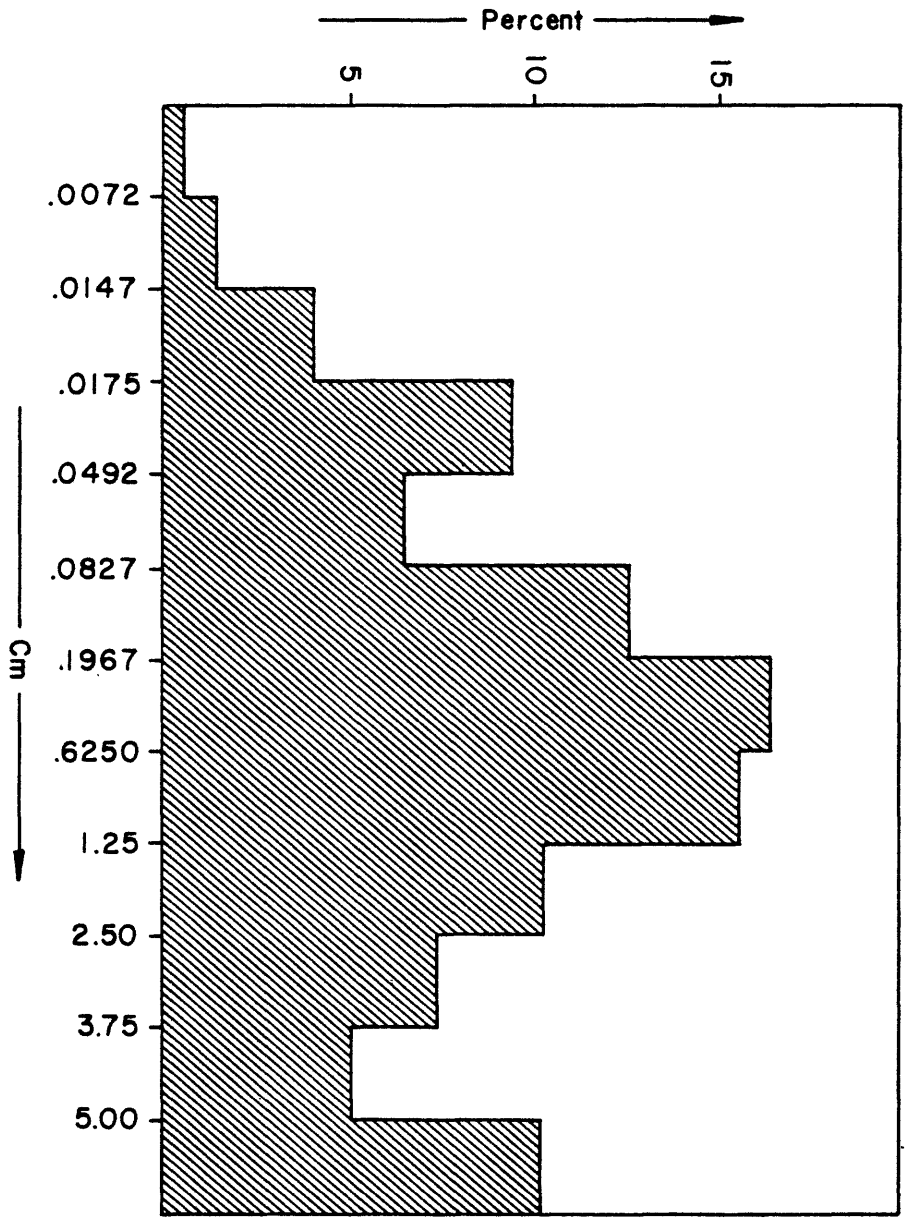

Figure 8.--Grain-size distribution of 10 kg of Lompoc, California, diatomite talus sample.

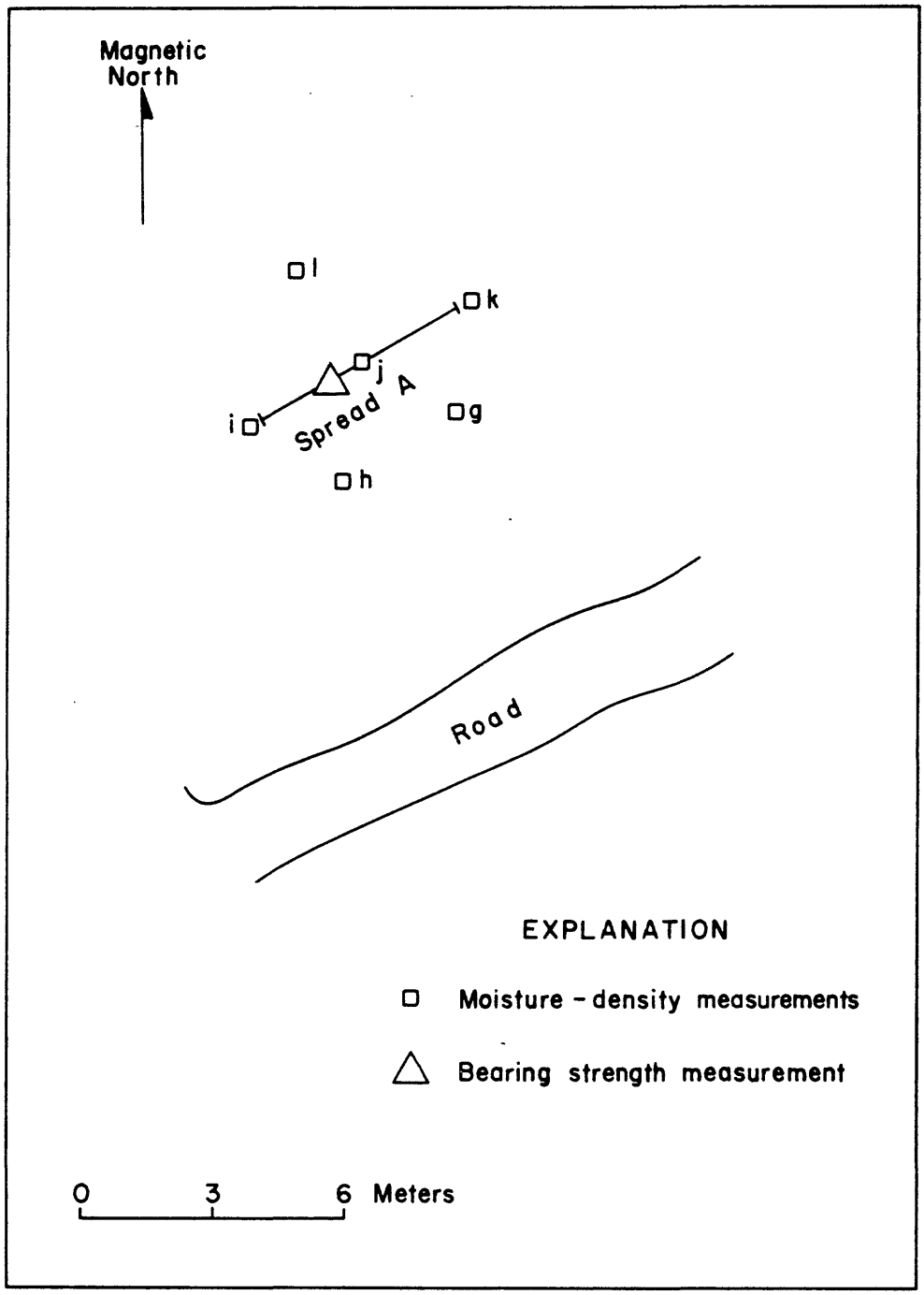

Figure 9.--Lompoc, California, "in place" diatomite waste site on hill 24.

Inyokern Volcanic Ash

The Inyokern volcanic ash site is located 23 km south of Inyokern, California, The material consists of volcanic ash with varying degrees of alteration (kaolinization?) (fig. 10).

The volcanic ash stockpile is approximately 3 m thick. It is stratified vertically into various density and moisture units (table 2).

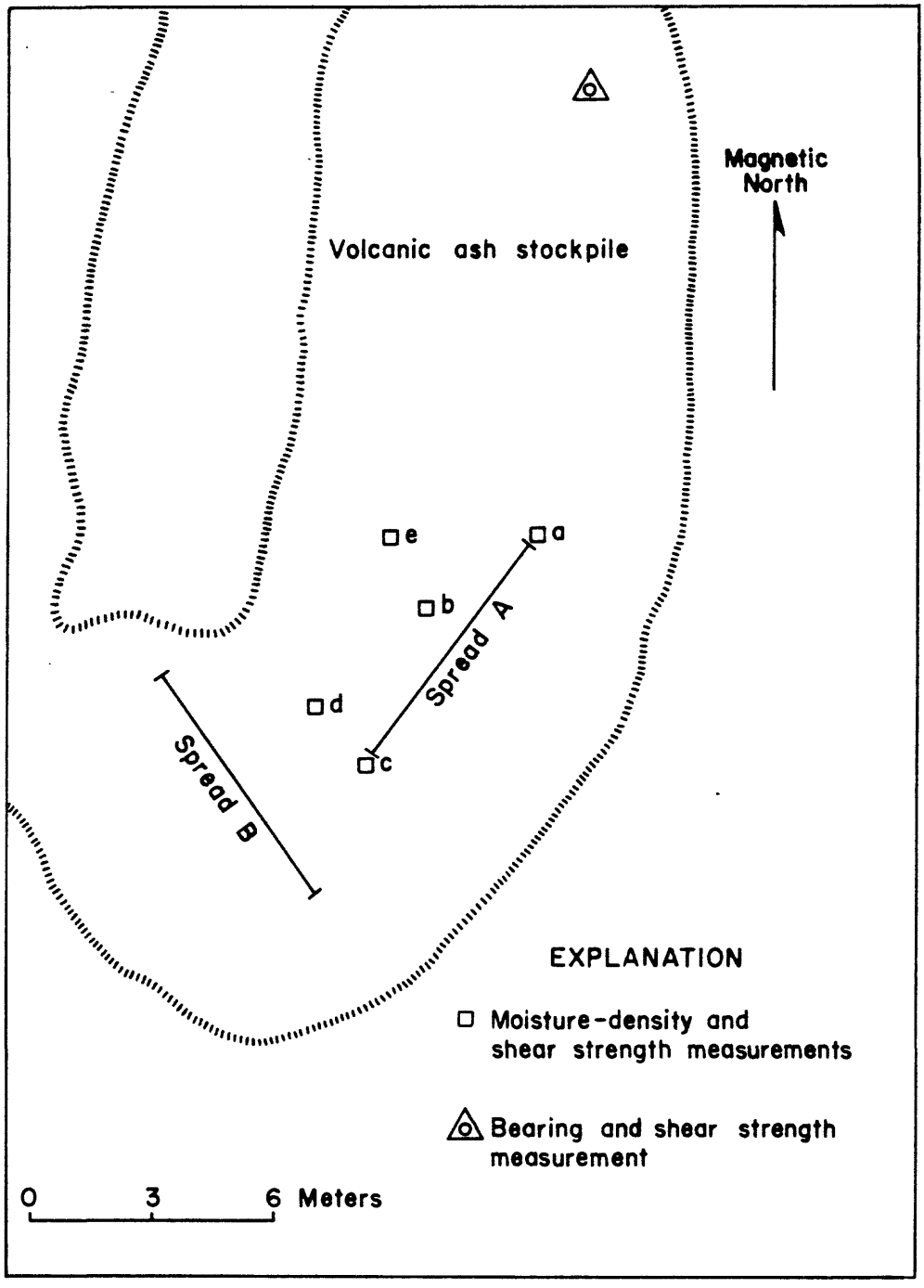

Figure 10.-- Inyokern, California, volcanic ash stockpile.

White Sands Gypsum

Bulk densities, moisture content, and P-wave velocities were measured for fine- and coarse-grained gypsum sand (table 2) at the White Sands National Monument, New Mexico.

References

Hassemer, Jerry H., 1965, Southern Coulee refraction studies, in In situ, Project quarterly rept., Oct. 1, 1965-Dec. 31, 1965: Flagstaff, Arizona, U.S. Geol. Survey, Br. of Astrogeology, p. 55-66.

Walters, L. A., 1965, In situ bulk density measurement at S P Flow, Arizona, in In situ Project quarterly rept., Oct. 1, 1965-Dec. 31, 1965: Flagstaff, Arizona, U.S. Geol. Survey, Br. of Astrogeology, p. 87-92.

CORRELATION OF PHYSICAL PROPERTIES--FROM LABORATORY MEASUREMENTS AND FROM IN SITU MEASUREMENTS

by Joel S. Watkins, Carl H. Roach, and Ralph P. Christian

ABSTRACT.--Physical properties data have been measured in the laboratory from cores taken from the more than 600 m of NX diameter core collected at 10 lunar analog sites during the past 18 months.

Core data from six sites have been examined in detail including preparation of 48 scatter diagrams in an attempt to find relationships between the measured physical properties. Correlations from the laboratory measurements have been poor at best and generally unrewarding.

Correlation of 23 in situ measurements of bulk density and P-wave velocities are encouraging.

During the last 18 months of the In Situ Physical Properties program, over 600 m of NX diameter core have been recovered from a variety of lunar analog sites. These cores have been sampled at intervals, and measurements of grain density, bulk density, porosity, P-wave velocity (V_p), S-wave velocity (V_s), elastic moduli, unconfined compressive strength, and in some cases, tensile strength and magnetic susceptibility have been made in Geological Survey laboratories. These measurements were made as part of a detailed documentation program of the lunar analog test sites, and also in hopes that some relationships might be observed between the various physical properties.

Briefly, the measurement techniques were as follows: (1) sonic properties were measured on one-inch diameter core specimens taken from the axial region of larger NX cores; (2) dry bulk density and

porosity measurements were made on the same core specimens; and (3) static properties were measured on segments of NX-core immediately adjacent to locations where the smaller one-inch diameter cores were taken.

Electrically-excited barium titanate transduced P-wave energy into rock cylinders and P-wave velocities (V_p) were measured directly. S-wave velocities (V_s) were obtained from two barium titanate transducers in combination with two AC cut quartz transducers that converted P-waves into S-waves and transmitted the S-waves longitudinally through core specimens. Elastic constants were calculated from values of V_p, V_s, and bulk density.

Bulk density and porosity measurement techniques for small core specimens were summarized by Roach and Johnson (1966). Some sonic measurements were made by the bar-resonance technique described by Birch (1937).

For compressive strength tests, rock core with length versus diameter of 2:1 and with ends plane parallel to within 0.001 inch were fitted with four SR-4 strain gauges on the outside surface of each along a plane perpendicular to the long axis and passing through the geometric center of the core. Pairs of gauges were diametrically opposed and oriented normal to each other. One pair averaged longitudinal deformation and the other averaged lateral deformation.

The core was placed in a static load press. Each core was cycled twice at approximately 50 psi per sec to a load of about 0.25 expected failure pressure. On the third cycle the load was applied until rock failure occurred.

Electrical energy supplied by the load cell and resistance changes in the strain gauges were recorded simultaneously by two X-Y recorders, one of which plotted Young's modulus and the other Poisson's ratio. A continuous plot was made until rock failure occurred, but moduli quoted in this report were derived from the early linear part of the first cycle of loading.

Physical properties data collected in the laboratory from cores from six sites were examined in detail, including preparation of 48 scatter diagrams in an attempt to find relationships between the physical properties measured.

Three of the six sites sampled were basaltic or andesitic basalt lava flows located near Sunset Crater, Arizona, (Kana-a basalt flow); Amboy, California, (Amboy pahoehoe basalt flow); and the S P Flow approximately 30 miles north of Flagstaff, Arizona, (andesitic basalt flow). Two of the sites consisted of late Paleozoic and Mesozoic sedimentary rocks. The Kaibab Limestone site consisted of interbedded arenaceous limestone and calcareous sandstone; the Meteor Crater site included fragments of the Coconino Sandstone, Kaibab Limestone, and Moenkopi Sandstone, which had been badly broken and brecciated during formation of Meteor Crater. The sixth site consisted of a massive granite cropping out near the Sonora Pass of the Sierra Nevada in eastern California. More detailed information can be obtained for most of these sites from previous project reports.

Scatter diagrams include plots of density (ρ) as a function of V_p, V_s, unconfined compressive strength (ucs), and Young's modulus (E); V_p as a function of ρ, porosity, ucs, and E; V_s as a function

of ρ, porosity, ucs, and E; porosity as a function V_p, V_s, and ucs; unconfined compressive strength as a function of ρ, V_p, V_s, porosity, E, and Poisson's ratio; Young's modulus as a function of ρ, V_p, V_s, and ucs; and Poisson's ratio as a function of ucs.

Correlation of the unrelated properties was poor and not significant. Those few instances where correlations can be inferred generally show scatter large enough to render the correlations virtually useless as a method of estimating one property from another. One of the best correlations, relationship of porosity and V_s obtained from cores taken at S P Flow, Arizona, is shown in figure 11. Insofar as grain densities of cores from S P Flow are relatively uniform, V_s also correlates reasonably well with bulk density (ρ), as does V_p.

Figure 12 shows the relationship of V_p and ρ for S P Flow, Kana-a Flow, and Amboy Flow samples. Figure 13 is a similar diagram showing the relationship of V_p and ρ for cores from sedimentary rocks at Meteor Crater and the Kaibab Limestone site in Arizona. Figure 14 shows the relationship between unconfined compressive strength and V_s; and between unconfined compressive strength and porosity of samples from S P Flow. It is difficult to detect any meaningful trend or correlation in any of these three figures.

Figures 15, 16, and 17 show relationships between parameters that are mathematical functions of one another. Figure 15 shows relationships between V_p and E for samples from the Kana-a Flow; figure 16 shows the relationship of ρ and E from cores from S P Flow; and

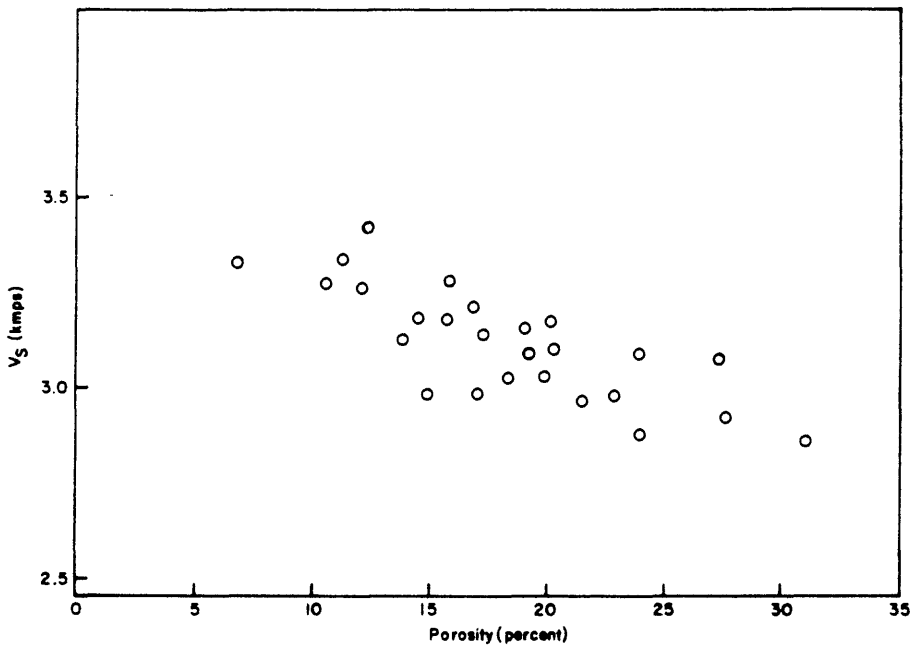

Figure 11.--Relationship of porosity and shear wave velocity (V_s) (bar resonance method), S P Flow, Arizona.

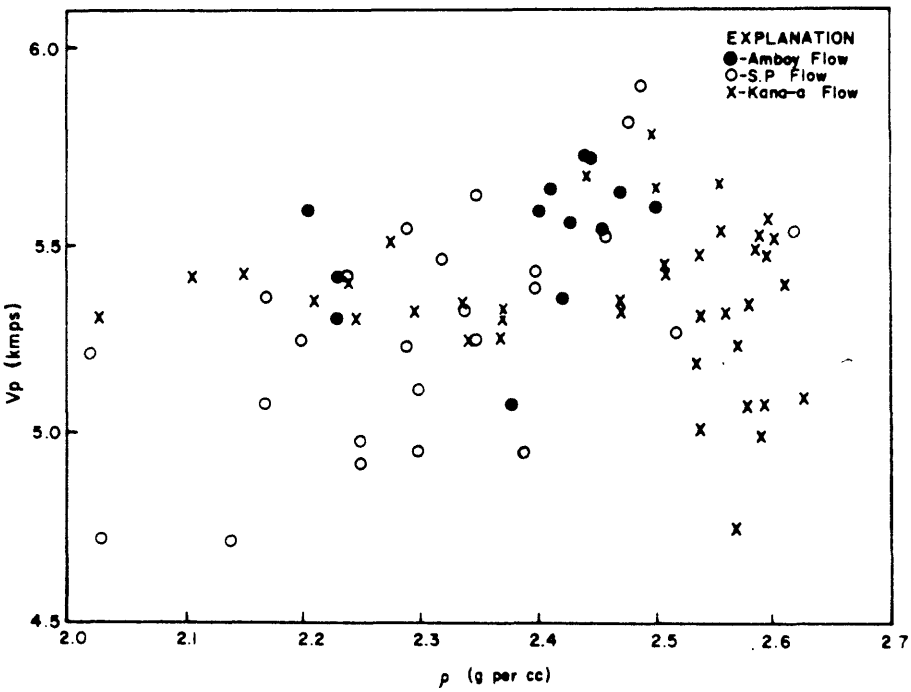

Figure 12.--Relationship of dry bulk density (ρ) and compressional wave velocity (V_P) (pulse method), S P Flow, Kana-a Flow, Arizona, and Amboy Flow, California.

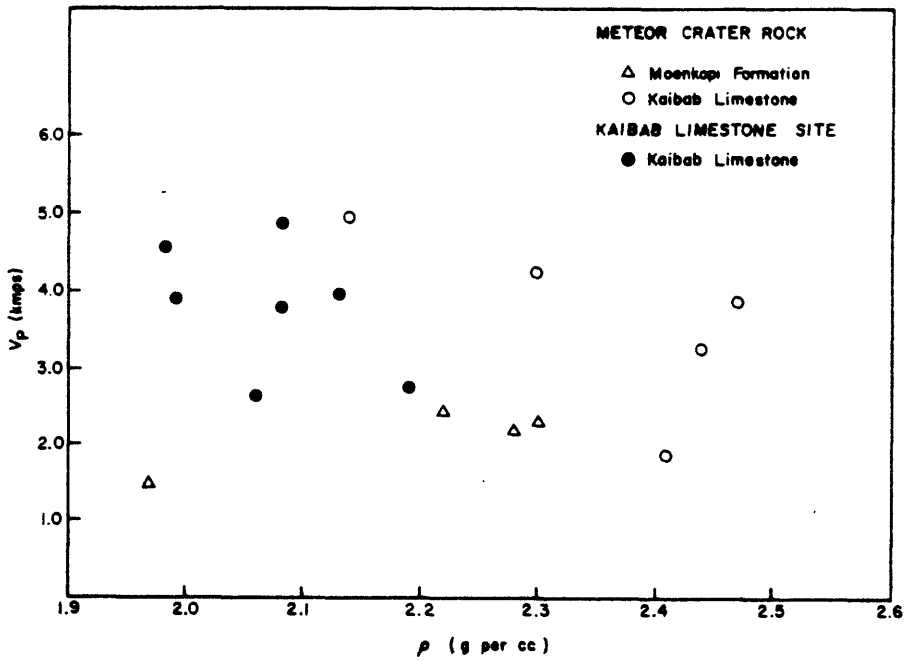

Figure 13.--Relation of dry bulk density (ρ) and compressional wave velocity (V_p) (pulse method). Meteor Crater and Kaibab Limestone sites, Arizona.

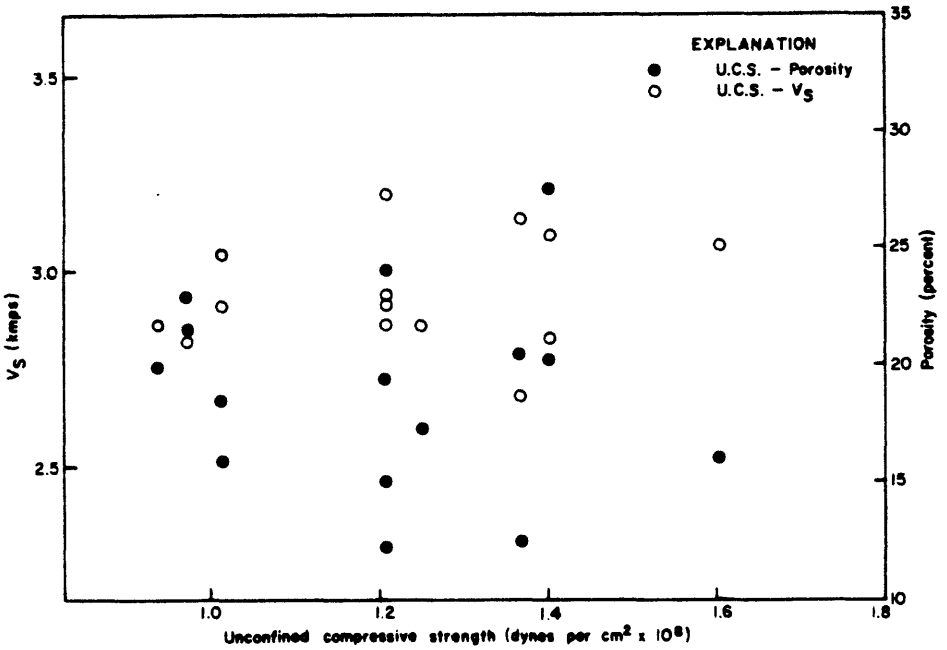

Figure 14.--Relations of unconfined compressive strength, shear-wave velocity (V_s) (pulse method), and porosity, S P Flow, Arizona

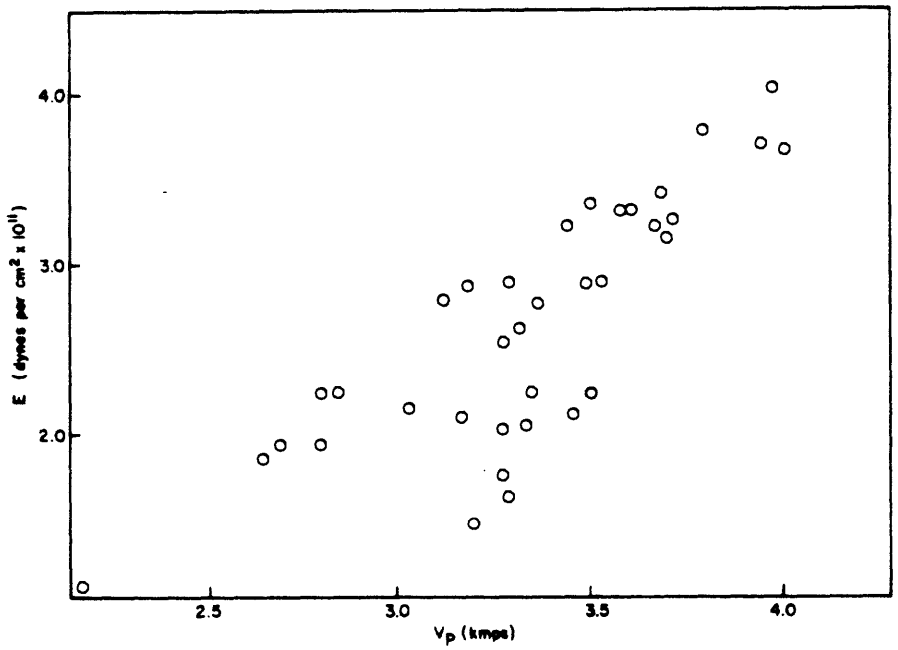

Figure 15.--Relation of compressional wave velocity (V_p) and Young's modulus (E) (pulse method), Kana-a Flow, Arizona.

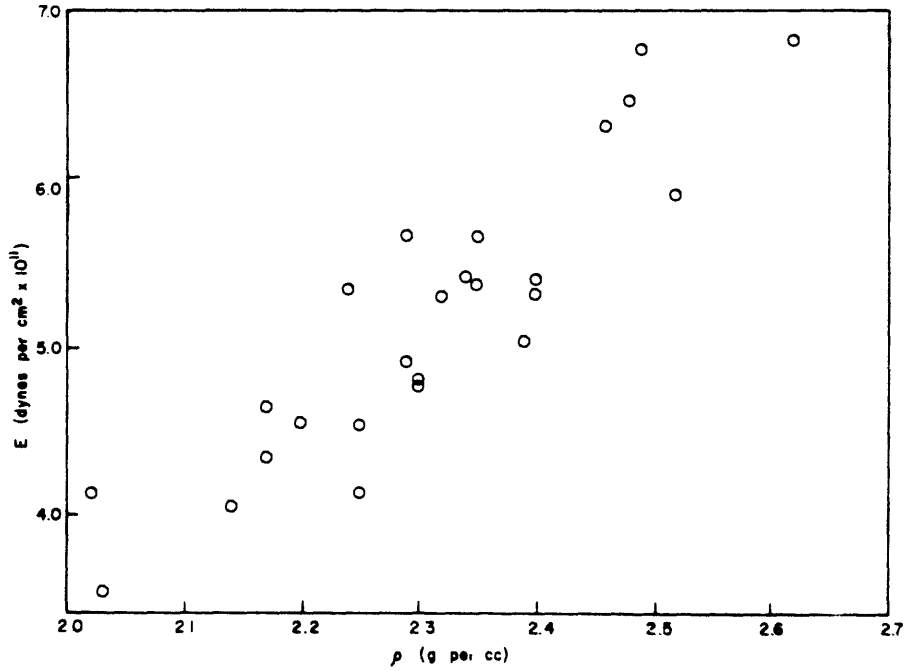

Figure 16.--Relation of dry bulk density (ρ) and Young's modulus (E) (pulse method), S P Flow, Arizona.

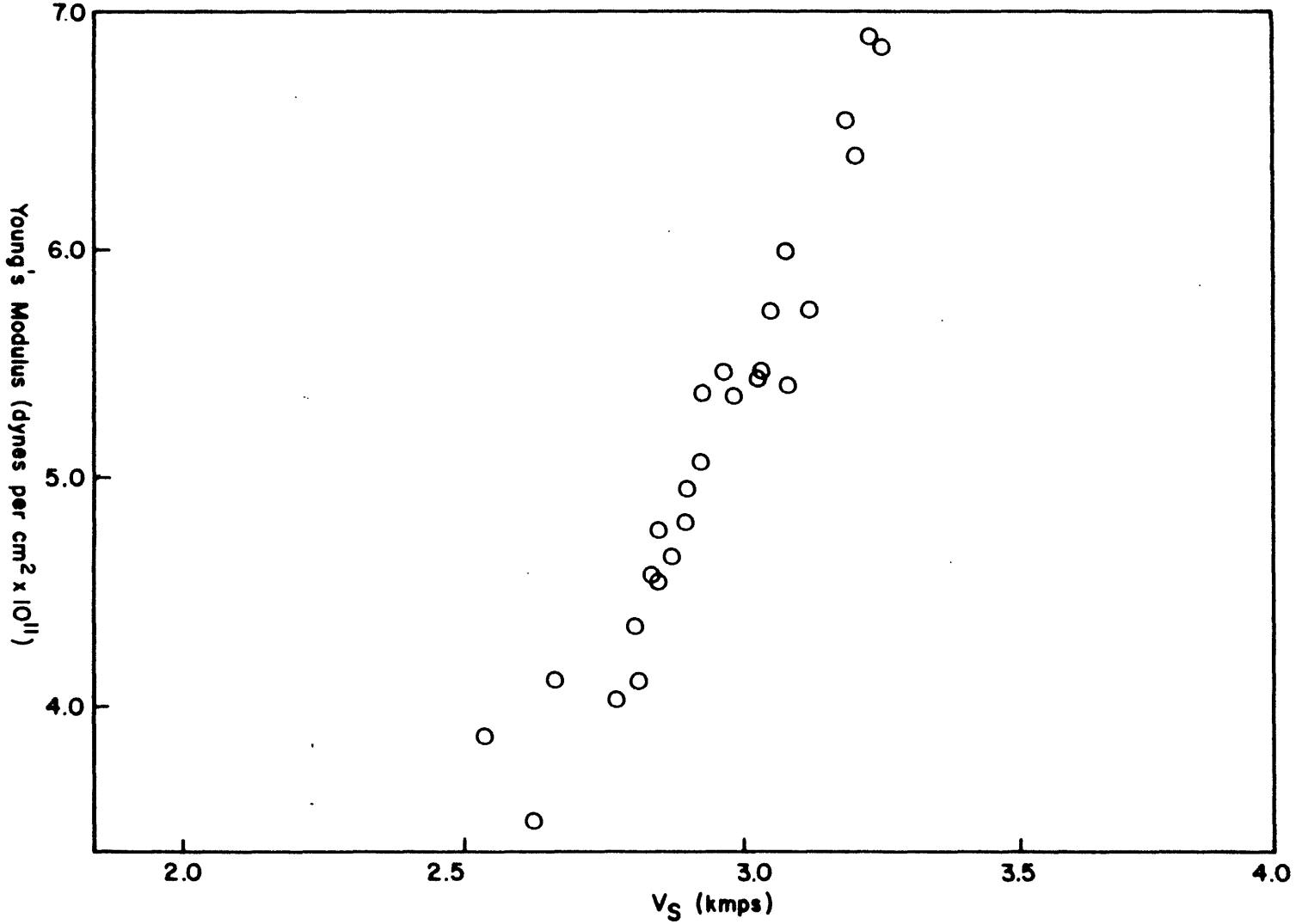

Figure 17.--Relation of shear wave velocity (V_s) and Young's modulus (E) (pulse method), S P Flow, Arizona.

figure 17 shows the relationship of V_s and E from cores from S P Flow, Arizona. The relatively good correlations between these functions result from the fact that E is a function of ρ, V_p, and V_s. In actual field data, the range in ρ is relatively small at a given site, and V_s is roughly proportional to V_p.

In situ physical property measurements, which are discussed in more detail elsewhere in this report, have been more difficult to obtain than the laboratory measurements, but 23 measurements show promise of significance. Figure 18 shows the relationship between V_p and in situ bulk density (ρ).

In figure 18, the least squares fit

$$\rho = 0.454 \ln V_p - 1.46$$

and has an rms error of .24 g per cc.

Better correlation of in situ data probably results from decreased effect of small cracks, pore orientation, and bedding. These factors tend to average in the in situ measurements but are dominant factors in measurements of very small core samples.

Correlations of laboratory measurements have been unrewarding and will be continued only to the extent that data will be computerized and least square fits will be computed with standard deviations.

Correlation of in situ measurements of bulk density (ρ) and V_p are encouraging. However, more and better data, especially with respect to the bulk density, are required.

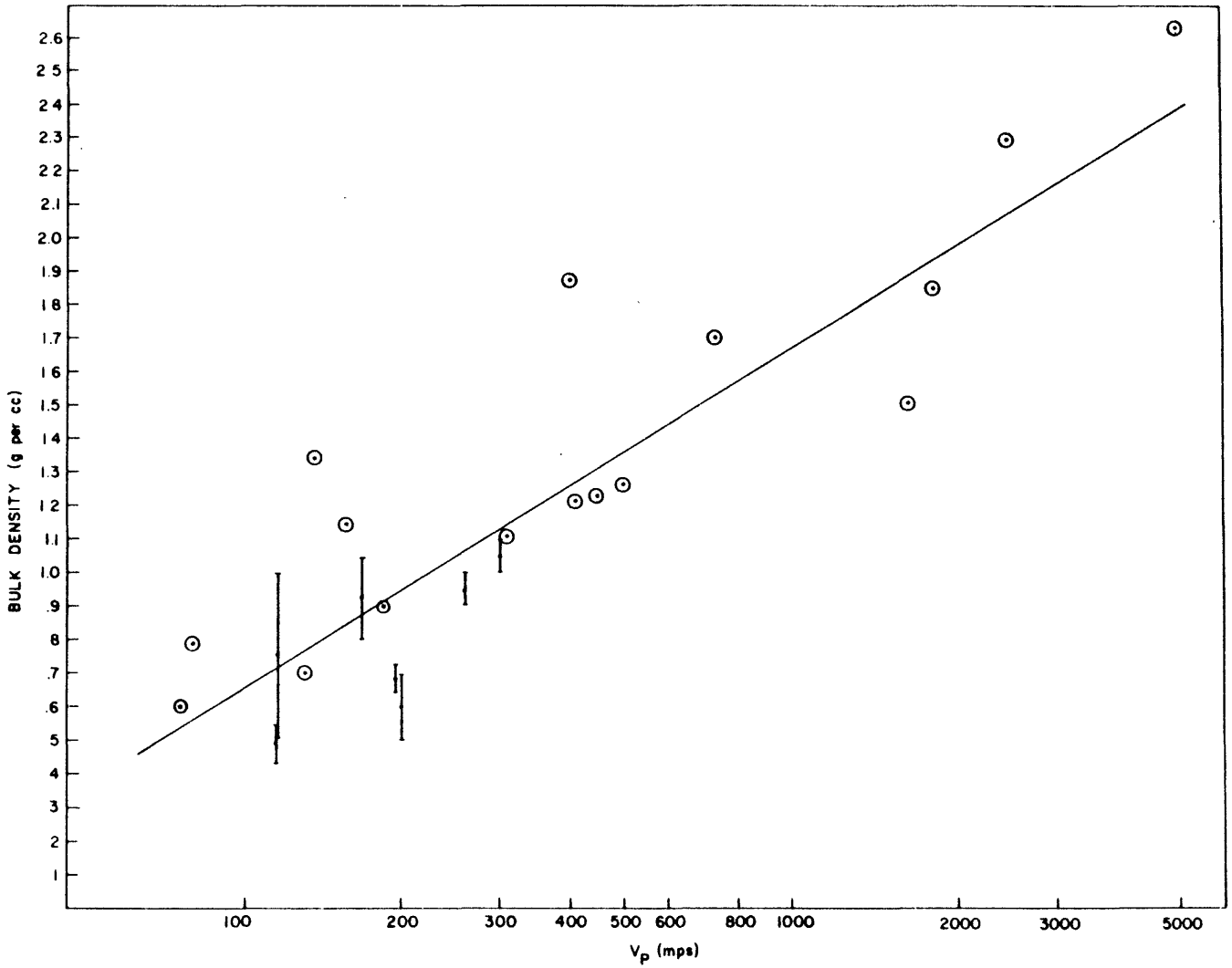

Figure 18.--In situ bulk densities (ρ) and P-wave velocities (V_ρ) for 23 lunar analog sites. Ranges of densities are shown where measured. Least square line for arithmatic mean of density data is $\rho = 0.454\ \ln V_\rho - 1.46$ in g per cc. The standard deviation is 0.24 g per cc.

References

Birch, Francis, 1937, The effect of pressure on the modulus of rigidity of several metals and glasses: Jour. Appl. Physics, v. 8, p. 129-133.

Roach, C. H., and Johnson, G. R., 1966, Field verification of in situ physical properties, in Investigation of in situ physical properties of surface and subsurface site materials by engineering geophysical techniques, Project quart. rept., Oct. 1, 1965-Dec. 31, 1965: Flagstaff, Arizona, U.S. Geol. Survey, Br. of Astrogeology, p. 9-46.

(page 37 follows)

IN SITU DRILLING PROGRAM

by Robert A. Elmer and Lawrence A. Walters

ABSTRACT.--In a 1.5 year period, the In Situ Project [redacted] drill rig has been used to drill 9,400 feet of shot holes and 2,100 feet of diamond core holes. This operation was achieved at a total operating cost of $51,740. It is estimated that this amount of work done on a contract basis would have cost $66,000 without yielding many of the intangible benefits derived from the project owned rig.

The In Situ Project has operated a drill rig on behalf of the National Aeronautics and Space Administration, Manned Spacecraft Center, Houston, Texas, since January 1965. This paper summarizes operating costs and work accomplishments for an 18-month period.

The drill rig is [redacted] mounted on a [redacted] truck with a gross carrying capacity of 15,000 lbs. It is equipped with a 31.5-ft hydraulically raised-and-lowered mast that can handle 20-ft lengths of drill rod. The rotary table has a 7.5 in opening. The power feed is capable of exerting 15,000 lbs on the drill string. The rig is capable of drilling holes from 4 in to 5.6 in diameters to depths of 1,000 ft using water. The rated capacity for the same size holes is 500 ft using air. A driller and a driller's helper are required to operate the rig and the supporting water truck.

Table 3 tabulates the capital investment for the drill rig and nonexpendible accessories. Capital investment will be depreciated on a straight-line basis over a 7-year period for calculation purposes.

Table 3.--Capital expenditures for in situ drilling program

[Straight-line depreciation at 14.28% per year over a 7-year period]

Drilling	
Cab and chassis	$ 6,500
Front wheel drive and 25-ton winch	3,000
combination rig	19,350
7.5-in opening rotary table	1,500
Drill Pipe	
Four 20-ft drill collars	1,250
Nine 20-ft flush joints	900
Four 20-ft external upsets	275
Core Barrels	
Four 3 1/2-in-outside diameter barrels	1,500
Three 5 3/4-in-outside diameter barrels	1,500
Accessories for above	500
Drilling Accessories	
Mud pan	200
Subs	300
Drive hammer	100
Reusable casing	1,500
Hand tools	1,250
TOTAL	$39,625

Table 4 tabulates the recurring expenditures for a 1.5-year period.

For the period January 1965-June 1966, $43,250 was spent for operating costs and expendible supplies. To this amount must be added 21.42 percent of the capital investment to get a total cost of $51,740 for the operating period.

During this 1.5-year period a total of 9,400 ft of shot holes and 2,100 ft of diamond coring was accomplished. Using average prices for drilling as $3 per ft for shot holes and $12.50 per ft of NX diamond cores, approximately $54,000 of work was realized. Footage costs take moving costs into account for inaccessible areas and overburden costs. Contracted work would have included a $12,000 salary of an experienced drilling supervisor. Hence, a comparable amount of work would have cost the In Situ Project $66,000.

Intangible benefits, such as availability of drilling equipment when it was needed, reliable personnel familiar with attempted problems and willingness to undertake problems that many experienced companies are reluctant to attempt, cannot be adequately evaluated in terms of dollars.

The greatest benefit derived from this program was excellent core recovery, a factor which cannot be achieved with a contract driller primarily interested in footage.

Appendix A shows locations and drill logs for the In Situ diamond drilling program. All of the Kana-a drilling was contracted and footage figures for these holes are not included in the cost operations calculations.

Table 4.--Recurring expenditures for in situ drilling program for the period January 1965-June 1966

Expendible equipment		
Diamond drill bits		$ 5,000
Rock bits		1,500
Supplies, mud, cement, core boxes, blocking, etc.		1,900
Maintenance costs		
Drill rig		1,350
Rock bits		250
Operating costs		
Drill rig		2,350
Water truck (surplus)		1,500
Pickup (rental)		3,500
Wages of driller and helper		
Wages		17,800
Overtime		5,500
Per diem		2,600
	SUB TOTAL	$43,250
Depreciation		8,490
	TOTAL	$51,740

LIMITS OF HEAD-WAVE AMPLITUDES FOR SHORT SPREADS FROM VARIOUS CHARGE SIZES, BLASTING CAPS, AND 45-KG WEIGHT DROP

by Hans D. Ackermann

ABSTRACT.--Measurements of head-wave amplitudes obtained with various charge sizes at 12 in situ test sites have been normalized to a standard distance (30 m) and charge size (.05 kg dynamite). The upper and lower bounds of head-wave amplitudes as a function of distance for the standard charge have been estimated and empirical relationships determined to predict such bounds when other charge sizes, blasting caps, or 45-kg weight drops are used as the energy source. Only distances less than 300 m are considered.

Introduction

This paper reviews the relationship between the velocity of ground-particle motion of initial head waves from various energy sources released near the ground surface at 12 in situ sites: Amboy Flow, Bishop Tuff, Cinder Hills, Kana-a Flow, Middle Mesa, Mono Ash, Pisgah Flow, Sacramento Valley, Sierra Ancha, Sonora Pass, Southern Coulee, and S P Flow.

The Bishop Tuff, Mono Ash, Sonora Pass, and Southern Coulee sites are described elsewhere in this report. Kana-a and S P flows have been described in previous project reports; other sites, except Sacramento Valley, a thick alluvium deposit, have been summarily described in the FY-66 Work Plan.

Energy Sources

Energy was released within 0.6 m of the ground surface and was initiated by either a charge of dynamite weighing between 0.03 and 4.5 kg (1/16 and 10 lbs), an electric blasting cap, or by a 45-kg (100 lbs) weight dropped from a height of 2.4 m. Charge size was selected so that the first half cycle of the head wave could be measured with sufficient accuracy and had an adequate signal-to-noise ratio, but also so that the overdriving of amplifiers, caused by higher amplitude later arrivals, was minimized. After recording, amplitudes were measured in equivalent volts input to the seismic amplifiers and converted to displacement velocity from velocity seismometer calibration curves.

Data Reduction

Comparison of signals generated by caps, weight drops, and dynamite necessitated normalization of amplitude data to a standard distance and charge size. A short distance (1-10 m) seemed preferable; but on many spreads the nearest seismometer to the shot point was 30 m from it which was too far for confident projection of signal attenuation data. Hence, 30 m and .05-kg dynamite, respectively, were chosen. The symbol $A_{d,E}$ will be used to denote signal or wave amplitude at distance, d, resulting from charge E. Thus, normalized amplitude is represented by $A_{30,0.05}$.

It was observed from sites where a range of charge sizes were used that a tenfold increase in charge roughly doubled signal amplitude. This is equivalent to the expression $A_{30,E} \sim E^{0.3}$ which is used

for normalization. The observed relationship seems consistent with expected energy loss in shallow holes. Observed data are badly scattered, and the general use of this relationship is by no means conclusive.

Values of signal amplitude recorded at 30 m from the shot were tabulated from attenuation plots and normalized graphically to $A_{30,0.05}$.

Amplitude-Distance Relationships

If $\underline{a}$ is defined as

$$\underline{a} = \frac{\pi \nu}{Q_\alpha \alpha}$$

where ν is the modal frequency of the head wave, Q_α is a constant, and α is the head wave velocity, then an expression for amplitude of the head wave (A) at some distance, d, is

$$A = Ke^{-\underline{a}d}$$

where K and $\underline{a}$ are constants (see Godson and others, 1965, p. F11). Thus, $\underline{a}$ is an attenuation coefficient. A log-normal graph of A as a function of d is a straight line with slope $-\underline{a}$, and each attenuation plot therefore results in a value for attenuation coefficient, $\underline{a}$, and normalized amplitude, $A_{30,0.05}$. For i (number of attenuation plots) the pairs ($A^i_{30,0.05}$, $\underline{a}^i$) then define a set of signal amplitude curves for 0.05 kg dynamite as a function of distance,

$$(A_{d,0.05} = A^i_{30,0.05}\ e^{-a^i(d-30)}).$$

The amplitude at 30 m is $A^i_{30,0.05}$ and the slope is $-\underline{a}^i$ (see fig. 19). Figure 20 shows the pairs $(A^i_{30,0.05}, \underline{a}^i)$ for 178 attenuation measurements from the sites previously mentioned with the attenuation coefficient as a function of amplitude. This is a convenient form of presentation for the following analysis.

In order to determine bounds on values of signal amplitude for 0.05 kg dynamite as a funtion of distance it is necessary to determine the upper and lower bounds for the set of 178 curves $A_{d,0.05} = A^i_{30,0.05} e^{-a^i(d-30)}$. The upper and lower values for bounds at d = 30 m are values of $A_{30,0.05}$, which will bound a desired percentage of the values $A^i_{30,0.05}$. To bound 90 percent of $A^i_{30,0.05}$, the upper bound, $A^U_{30,0.05}$ is 16×10^{-3} cm per sec and the lower, $A^L_{30,0.05}$ is $.23 \times 10^{-3}$ cm per sec. These are obtained directly from figure 20. (Five percent or 9 of the values of $A^i_{30,0.05}$ are to the left of $A_{30,0.05} = .23 \times 10^{-3}$ cm per sec and 5 percent to the right of $A_{30,0.05} = 16 \times 10^{-3}$ cm per sec.)

For a curve bounded at d = 30 m, the slope $\underline{a}^i$ may be such that it will leave the bounds at a larger distance (fig. 19). Similarly, a curve outside the bounds at d = 30 m later may become bounded. The total percentage bounded will be maintained approximately for all distances. This can be accomplished by choosing a value of $\underline{a}$ for the lower bound ($\underline{a}^L$) and one for the upper bound ($\underline{a}^U$) which will similarly bound the desired percentage of the values $\underline{a}^i$. These are also obtained from figure 20, and for 90 percent values, $\underline{a}^L = 0.155\ m^{-1}$ and $\underline{a}^U = 0.025\ m^{-1}$.

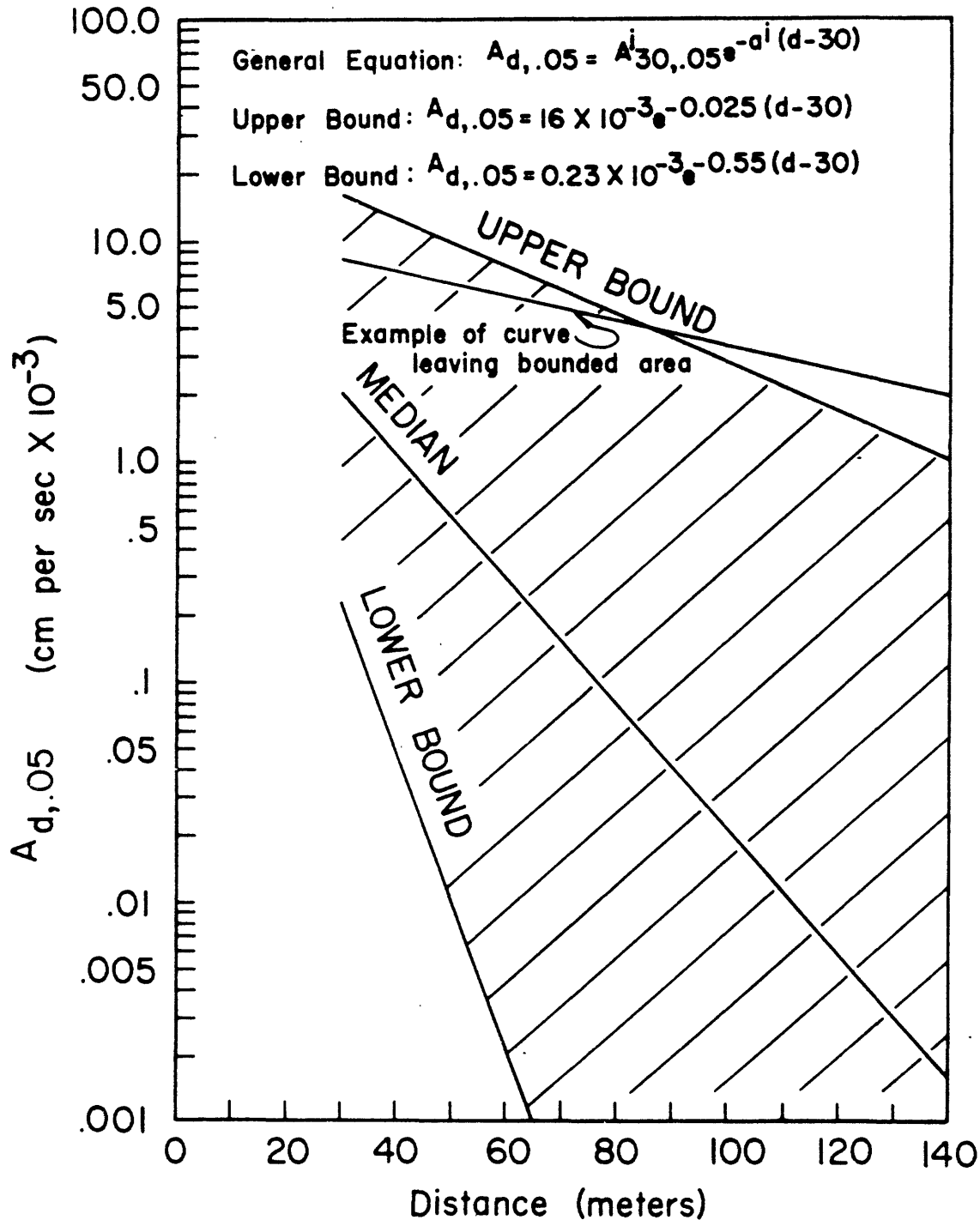

Figure 19.--Curves bounding approximately 90 percent of the values of $A_{d,0.05}$.

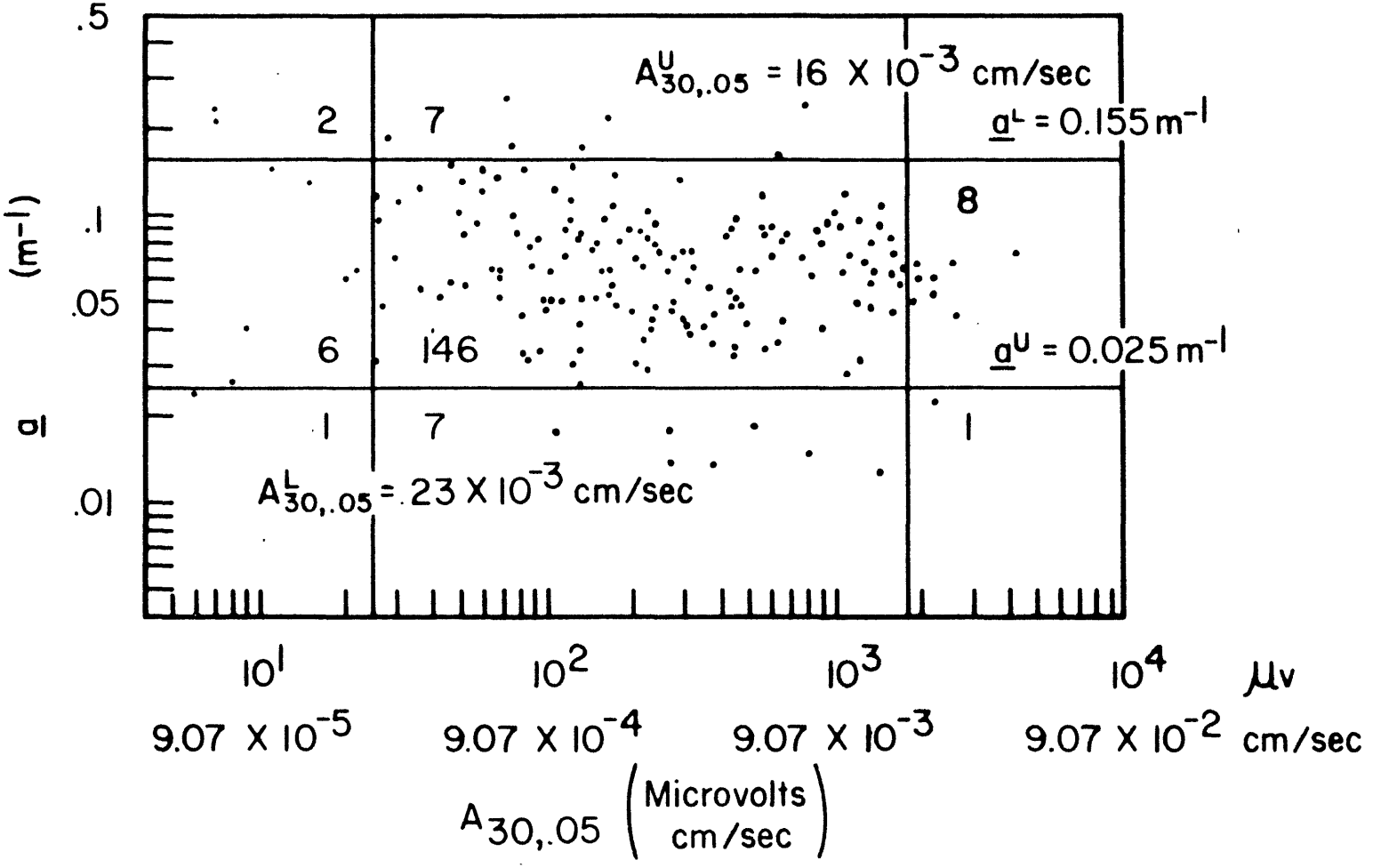

Figure 20.--Values of normalized amplitude and attenuation coefficient $(A^{i}_{30,0.05}, \underline{a}^{i})$ for attenuation measurements.

Curves bounding 90 percent of the values of $A_{d,0.05}$ are plotted in figure 19. A curve representing the median values of $(A^{i}_{30,0.05}, \underline{a}^{i})$ also is shown.

Comparison of Signal Amplitude

In addition to dynamite, blasting caps or weight drops were used as an energy source at nine sites. The weight drop consisted of a 45-kg lead weight dropped from a height of 2.4 meters. Signal amplitudes from the caps and weight drops at 30 m ($A_{30,cap}$ and $A_{30,wd}$) were read from the attenuation plots and tabulated. For each of the nine sites, the means ($\bar{A}$) and the medians (A^{*}) of $A_{30,0.05}$, $A_{30,wd}$ and $A_{30,cap}$ were determined and were denoted respectively as $\bar{A}_{30,0.05}$, $A^{*}_{30,0.05}$, $\bar{A}_{30,wd}$, $A^{*}_{30,wd}$, $\bar{A}_{30,cap}$, and $A^{*}_{30,cap}$.

Table 5 summarizes ratios of cap versus normalized dynamite amplitudes, weight drop versus normalized dynamite amplitudes, and weight drop versus cap amplitudes; and shows the number of measurements for each energy source. Data from table 5 suggest that signal amplitudes generated by the 45-kg weight drop were slightly greater than those generated by a cap. Signal amplitudes from both caps and weight drops generally are between one and ten percent of those generated from 0.05-kg dynamite.

Table 5.--Mean and median value ratios of $A_{30m,0.05}$, $A_{30,wd}$, and $A_{30,cap}$

Site	No. of Dyna. shots	No. of Cap shots	No. of weight drops	$\frac{\bar{A}_{30,cap}}{\bar{A}_{30,0.05}}$	$\frac{A^*_{30,cap}}{A^*_{30,0.05}}$	$\frac{\bar{A}_{30,wd}}{\bar{A}_{30,0.05}}$	$\frac{A^*_{30,wd}}{A^*_{30,0.05}}$	$\frac{\bar{A}_{30,wd}}{\bar{A}_{30,cap}}$	$\frac{A^*_{30,wd}}{A^*_{30,cap}}$
Bishop Tuff	15	8	0	0.013	0.011				
Cinder Hills		6	4					1.1	1.5
Middle Mesa	17		12			0.35	0.86		
Mono Ash	17	7		0.015	0.018				
Sacramento Valley	10		3			0.11	0.18		
Sierra Ancha	23		11			0.079	0.065		
S P Flow	5	5		0.0070	0.011				
Southern Coulee	21	8		0.065	0.030				
Sonora Pass	3	2		0.074					

Conclusions

Measurements of head-wave amplitudes for 178 attenuation measurements at 12 in situ test sites, obtained with various charge sizes, have been normalized to a standard distance (30 m) and a charge size (0.05 kg). Field measurements using different dynamite charges have given an approximate empirical relationship between amplitude and charge size, $A_{30,E} \sim E^{0.3}$, which is used to normalize data to the standard charge. The upper and lower bounds for signal amplitudes resulting from 0.05-kg dynamite as a function of distance have been determined (fig. 19) from these normalized amplitudes ($A^{i}_{30,0.05}$) and corresponding attenuation coefficients ($\underline{a}^{i}$). These bounds with the relation $A_{d,E} \sim D^{0.3}$ can be used to predict signal amplitudes for varying distance and charge size.

An empirical relationship between seismic energy released by a 0.05-kg dynamite charge, a cap, and weight drop has been established. This information combined with that in figure 19 can be used to estimate limits of head-wave amplitudes at sites where caps, weight drops, or similar energy sources are used.

References

Godson, R. H., Watkins, J. S., and Loney, R. A., 1965, Velocities and attenuation of head-wave amplitudes observed in lunar analog rocks, in Investigation of in situ physical properties of surface and subsurface site materials by engineering geophysical techniques--Project ann. rept., FY 1965: Flagstaff, Arizona, U.S. Geol. Survey, Br. of Astrogeology, p. F1-F25.

(page 51 follows)

STRUCTURE AND COMPOSITION OF THE SOUTHERN COULEE, MONO CRATERS, CALIFORNIA--A PUMICEOUS RHYOLITE FLOW

by Robert A. Loney

ABSTRACT.--The Southern Coulee is the southernmost and largest of the four Recent pumiceous rhyolite coulees, or stubby flows, of the Mono Craters, eastern California. It is one of the youngest volcanic deposits of the Mono Craters and is mostly bare and uneroded. The coulee is 3.6 km long and averages 1.2 km wide and has a minimum thickness of 150 m. It was protruded from a north-trending fissure, beneath and parallel to the crest of the Mono Craters ridge.

The coulee has three main parts: the dome, located over the orifice, where flow was about vertical; the flow, where movement was lateral; and the talus slope, which surrounds the coulee and which formed from the advancing steep flow front. Three small areas of air-fall, pumice ash occur on the coulee and seem to be remnants of an ash eruption that took place during an early phase of the coulee eruption.

Three distinct lithologic units based on rock density or degree of vesicularity have been mapped as follows: unit of lowest density ($\overline{\rho}$ = 0.65); unit of intermediate density ($\overline{\rho}$ = 1.20), and unit of highest density ($\overline{\rho}$ = 1.75). Contacts between units are abrupt in spite of the fact that core drilling has shown the coulee to be a jumbled mass of blocks down to at least a depth of 45 m. The two less dense units, which consist of highly inflated, thick-bedded pumice, form two connecting, boat-shaped outcrops along the entire south margin of the coulee. These units are probably not over 25 m thick and are underlain by the unit of highest density, which seem to form the rest of the coulee. The dense unit consists of thin- to medium-bedded, dense pumice and lesser amounts of obsidian.

Distribution of lithologic units was probably caused by the eruption of all the units from the southern part of the fissure, while only the unit of highest density erupted from the northern part. The lava protrusion involved several streams that had an anastomosing flow pattern. This complex flow modified the original spatial relations of lithologic units.

The petrographic and chemical data indicate a uniform composition for the lava that belies its heterogeneous aspect. The lava is composed almost entirely of clear glass (average n_D = 1.488 ± .001) and contains only trace amounts of microlites and cristobalite-sanidine spherulites. Eight chemical analyses show a silica range of from 74.7 to 76.2 percent and indicate a rhyolite of the sodi-potassic subrange. This composition is characteristic of glassy fluidal rhyolites.

Introduction

The Southern Coulee (Russell, 1889; Putnam, 1938) is the southernmost and largest of the Recent pumiceous rhyolite flows, or coulees, of Mono Craters, eastern California (fig. 21). The coulee extends east-west 3.6 km, roughly normal to the trend of the Mono Craters ridge with about two-thirds of the coulee lying west of the crest of the ridge. It averages about 1.2 km wide and has a minimum thickness of 150 m. The maximum altitude of the coulee is 2,717 m on the surface and the minimum altitude at the western toe is 2,250 m.

According to Kistler (in press), the northward arcuate trend of the Mono Craters is probably controlled by a major ring fault that bounds a circular area of subsidence, centered about 4 miles west of the craters (fig.21). A major fault zone beneath the southern end of the craters was revealed during the construction of the Mono Craters Tunnel (Gresswell, 1940, p. 202).

Southern Coulee is one of the youngest deposits of the Mono Craters. It overlaps rhyolitic domes and associated craters on both sides. The major part of its surface is free of the pumice ash deposits that blanket most of the Mono Craters and the surrounding country. Other coulees in the northern part of the craters are also young deposits, mostly free of ash.

Southern Coulee was selected for study by the In Situ project because it is an excellent example of a pumiceous,fluidal,silicic lava flow that is virtually untouched by erosion and alterations,

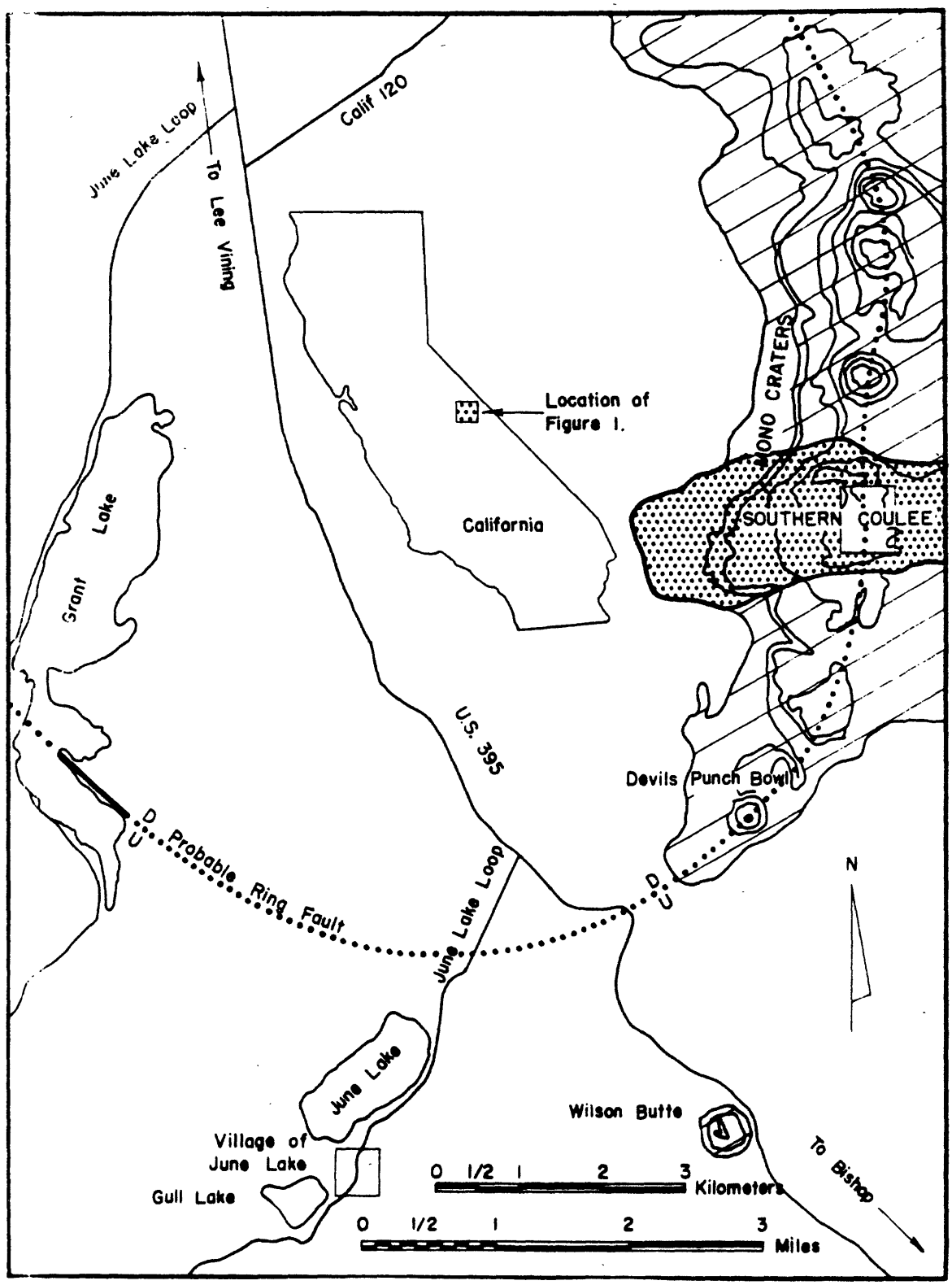

Figure 21.--Index map showing location of Southern Coulee.

and yet is accessible to heavy vehicles. The uneroded fresh condition of the coulee makes it analogous to lunar volcanic terranes. Access by vehicles to the surface of the coulee was limited to the southeastern part, where pumice blocks are being quarried.

The upper surface consists of extremely rugged hills and ridges of loose rubble as much as 25 m high. Spires of solid pumice project through the loose rubble (fig. 22). The terrain is extremely difficult to traverse. The coulee is surrounded by a steep talus slope that ranges from 60 to 90 m high. The rubble of the slope lies at the angle of repose or perhaps locally at greater angles where permanently frozen (fig. 23).

Morphology

Topographic features of the coulee are mostly constructional and related to the extrusion of the coulee. The Southern Coulee can be divided into four parts (fig. 24): (1) the dome, in which the movement of lava was mostly vertical; (2) the flow, in which the movement of lava was mostly lateral; (3) the ash deposit, which is air-fall, pumiceous ash and lapilli and (4) the marginal talus slope. The ash deposit is not directly related to the coulee and may be entirely foreign to it. The talus slope is a secondary feature formed during and after the advance of the steep-sided flow.

Dome.--The dome makes up most of the high part of the coulee and probably overlies the vent from which lava was protruded.

Figure 22.--Rugged topography in higher part of Southern Coulee, California (dome).

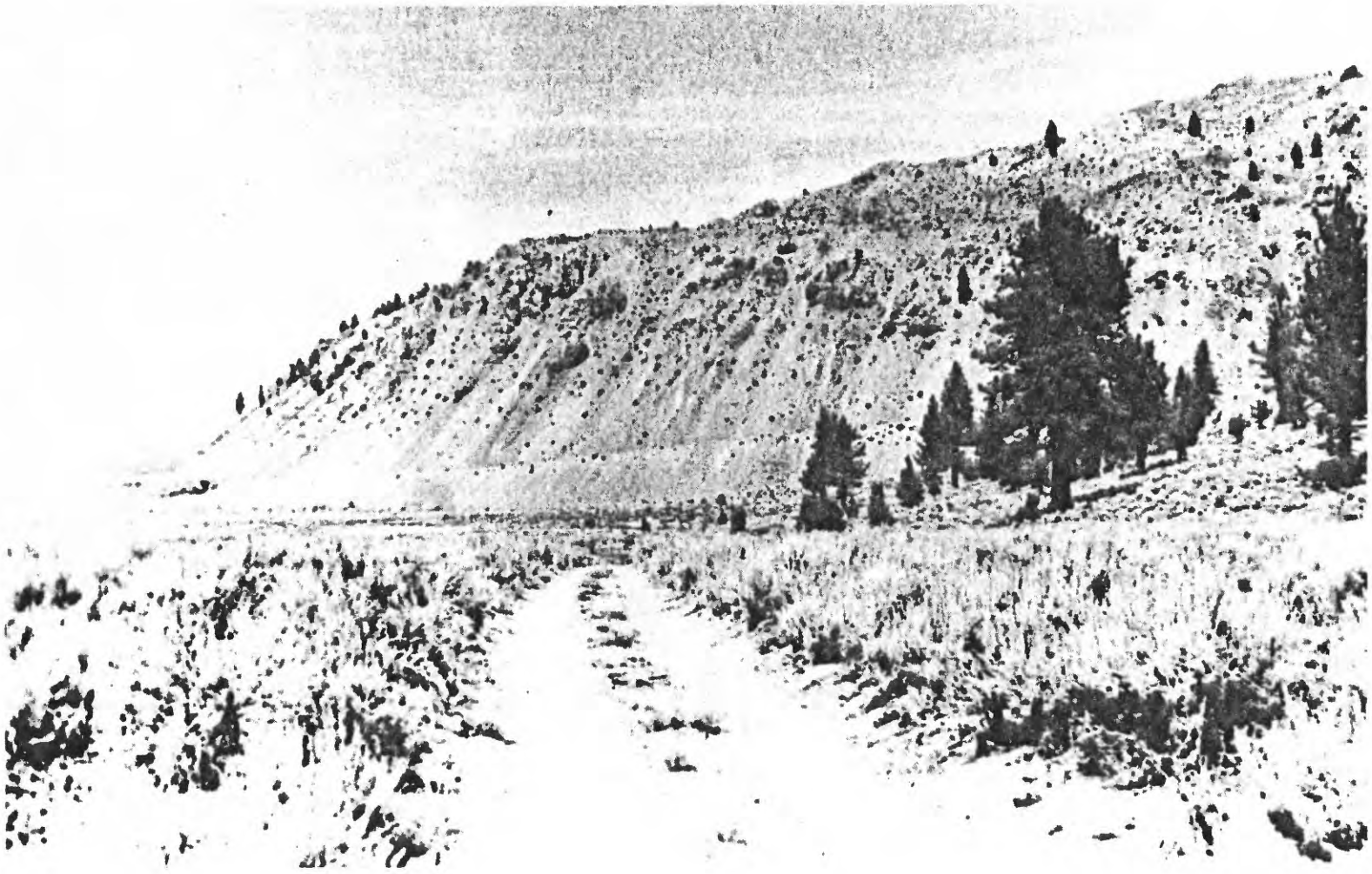

Figure 23.--Talus slope at toe of Southern Coulee.

67-272

EXPLANATION

- t — Talus deposits, at margin of Southern Coulee
- Older volcanic deposits, in section A-A' only
- Ash deposits - includes small outcrops of obsidian and dense pumice

FLOW UNITS

- Unit of lowest density (0.65g per cc avg.)
- Unit of intermediate density (1.20g per cc avg.)
- Unit of highest density (1.75g per cc avg.)
  (Hypothetical flow lines shown in section)
- Outer boundary of Southern Coulee
- Contact between lithologic units and outer border of Coulee
- Boundary of lava stream
- Approximate boundary of domal area
- 80 — Strike and dip of flow layering in spires
- Strike of vertical flow layering in spires
- Direction of flow
- 2 — Core hole and number, map
- 2 — Core hole and number, section

0 1/2 1 2 Kilometers

Contour Interval : 20 Feet

Figure 24.--Geologic map and cross-section of Southern Coulee, California.

no page 58

Borders of the dome are poorly defined, owing to the streams of lava that extend out from it and obscure its margins. The dome is characterized by numerous spires or pinnacles that project through the rubble. Most of the spires show prominent vertical striations and grooves, which indicate upward protrusion through orifices in already solidified lava (fig. 25). A few spires are composed of lightly cemented rubble (fig. 26) pushed up by still-liquid lava from below. Spires range from sharp to blunt. They show stages of their normal development, during which they protrude upward and eventually tend to fall over (Williams, 1932, p. 55-57). This process accounts for much of the surface rubble of the dome.

Flow.--The flow extends east-west from the dome. Movement of lava in the flow is distinctly lateral, and vertically grooved spires are absent. Ridges of rubble are commonly developed normal to the direction of flow and in places are convex downstream (fig. 24). Surface layers of the flow are composed of loose rubble comprised of angular blocks of pumice averaging 0.7 m across. The rubble was produced mostly from the breaking up of the thick, highly fractured crust during movement of the underlying still-fluid lava. Locally, larger slablike masses are tilted at various angles. Slabs in the ridges tend to strike parallel to the ridges and dip off on either flank. Arrows in figure 24 show direction of flow inferred from large-scale streaks of prominent rock types (such as black obsidian) which contrast markedly with the dominant gray pumice.

The flow can be divided into individual streams of lava that have complex flow patterns. These streams seem to have moved at

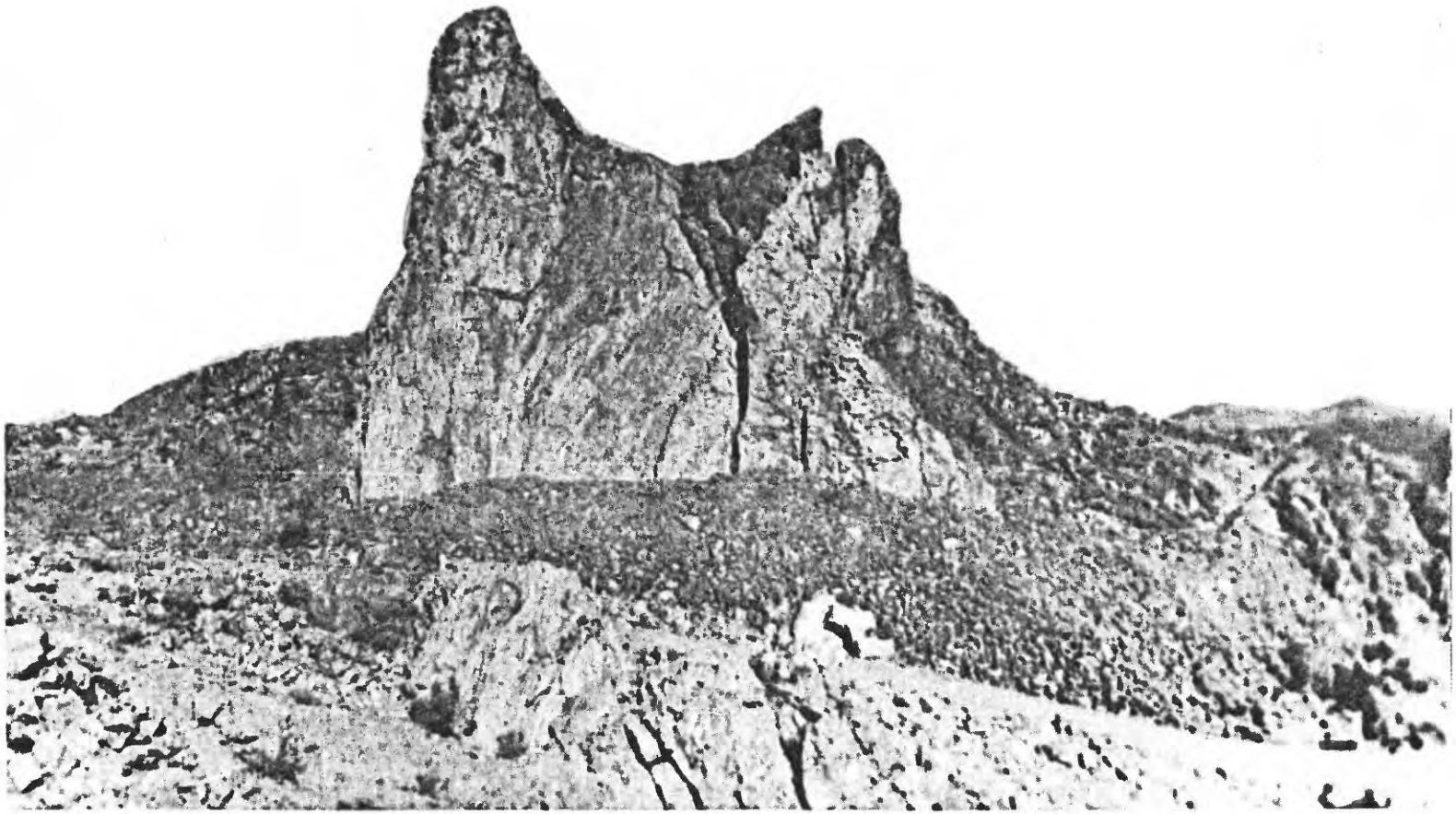

Figure 25.--Well-preserved spire on dome, Southern Coulee, California. Vertical streaks are grooves and the patches of dark rock on the right side and top are masses of rubble carried up by the protrusion of the spire.

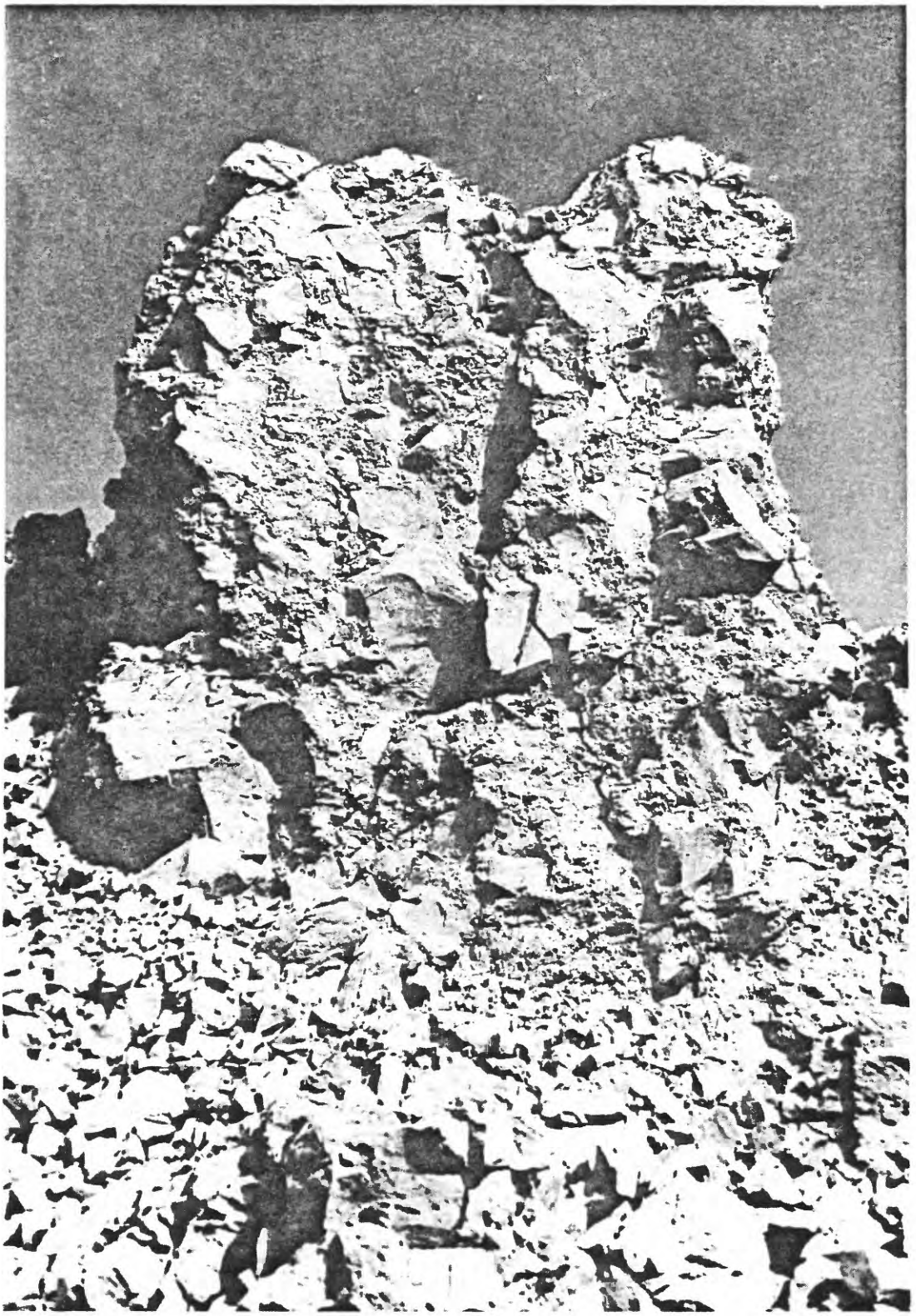

Figure 26.--Spire of lightly cemented rubble, dome of the Southern Coulee.

different times, or at least different rates, originating at different parts of the orifice. The most perfectly defined stream extends westward from the northern part of the dome and forms most of the northern half of the flow west of the dome. The crescentic ridges in this stream are well developed and help define the sides of the stream that seem to be bounded by shear zones. This stream seems to be a late feature that cuts across, and, in places, disturbs earlier streams. This cross-cutting relation is supported by its generally higher altitude relative to adjacent streams and suggests that it flowed out over parts of the adjacent streams.

Streams in the flow to the east of the dome are much shorter and less well defined than those to the west. A large area of ash obscures the northeastern part of the eastern area, and quarry operations have obscured an equally large area in the southern part. The most distinct ridges are in the central part immediately east of the dome where a small stream, with distinct ridges, has flowed east. Farther east, near the border of the large ash area, the direction of the ridges is confused.

Ash deposits.--Ash deposits comprise three areas of air-fall, pumiceous ash and lapilli. Scattered masses of blocky pumice and obsidian project up through the ash from the flow below. The largest area of ash lies in the northeastern part of the coulee, and supports a substantial growth of pine trees. A smaller area of ash is in the south central part of the flow, west of the dome, and is covered with pines. The third area of ash lies along the north-central margin of the coulee and forms high dunelike hills, mostly bare of vegetation.

It is thought that the ash and lapilli deposits were originally part of an extensive blanket erupted early and were subsequently disturbed by later eruptions of lava. The deposits seem to rest on pumice of the highest density lithologic unit, part of which must represent a pre-ash flow. Large parts of the densest unit, together with the least dense and intermediate units, are virtually ash-free and are later than the ash fall. It seems improbable, in view of the generally widespread distribution of ash from known eruptions (Powers and Wilcox, 1964), that late ash deposits would be restricted to small patches now present on the coulee.

The ash and lapilli deposits show a much higher degree of crystallinity than do the flow rocks of the Southern Coulee. Quartz, plagioclase, biotite, and possible potassium feldspar have been identified by x-ray diffraction. This higher degree of crystallinity suggests a source for the ash other than the coulee.

Talus slope.--The talus slope is composed of debris from the steep edges of the coulee (fig. 23), and mostly consists of blocks of pumice similar to those found on the surface; but also includes finer pumice and obsidian fragments, and ash and lapilli in places. The talus slope encircles the coulee except where covered by the deep ash deposits on the north margin. Its location can be distinguished easily in figure 24 by the regular close-spaced contours. Outcrops of pumice and obsidian of the flow project through the talus slope about three-quarters the distance from the bottom and form a nearly continuous belt around the coulee (fig. 27).

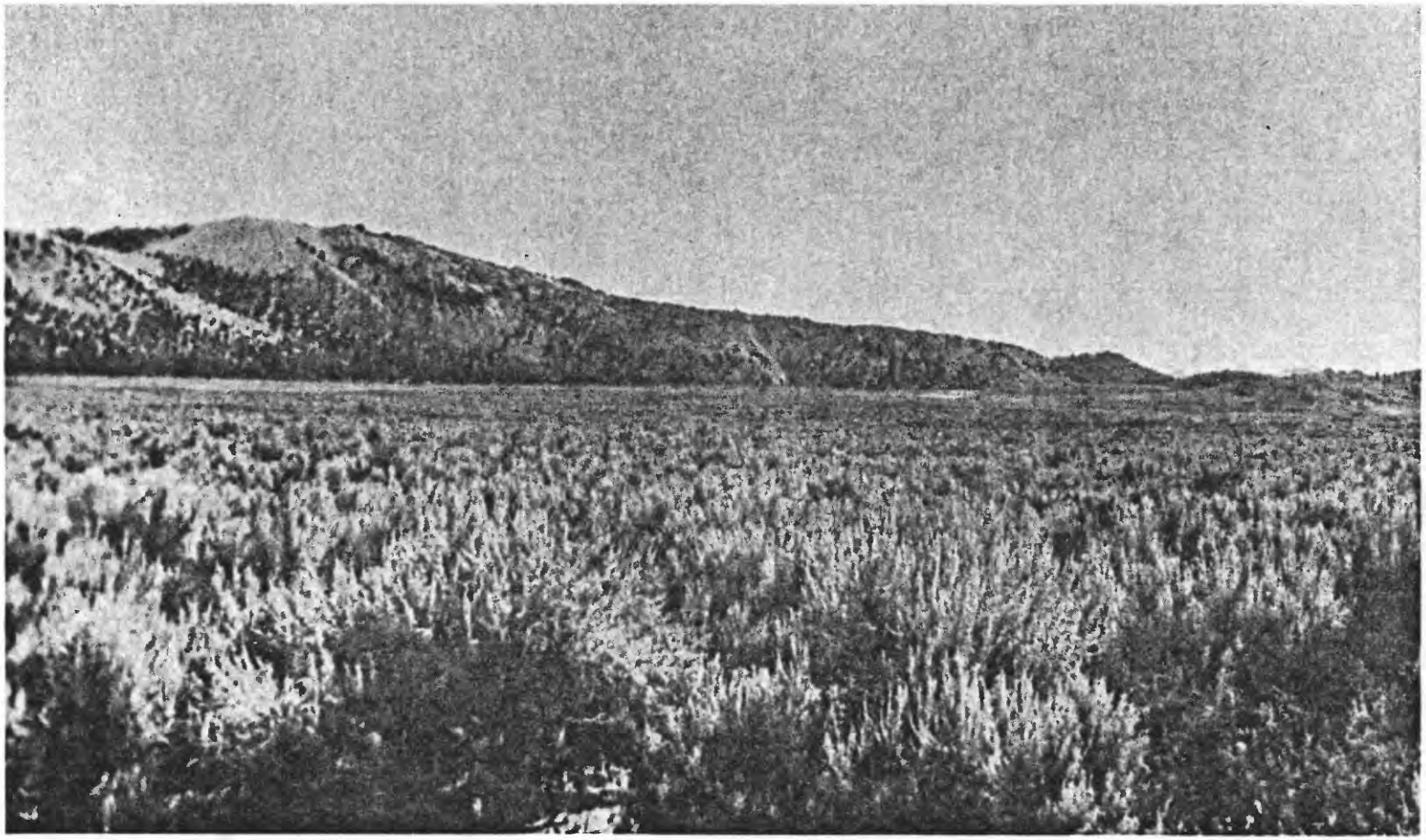

Figure 27.--View of the Southern Coulee from the north, showing a belt of outcrops below top of talus slope; talus slope and outcrops on left near top of coulee are buried by light gray dune of ash.

Lithology

Three lithologic units have been mapped in the lava of the Southern Coulee (fig. 24). Each unit has a characteristic range in density and distinctive physical characteristics related mainly to the degree and nature of vesicularity. No significant compositional differences between the units have been recognized (table 6). Quarry operations are confined to the least dense of the lithologic units.

An individual lithologic unit is not homogeneous and contains subordinate layers and laminae of rock types that also occur in the other units. The general discussion of lithologic features that follows holds for all units. Contacts were based generally on abrupt changes in the character of the rock types in the rubble because the surface of the coulee is mostly rubble. No gradational contacts between units were seen. Little mixing of rock types occurs along these contacts, and every indication is that the rubble has been moved but slightly by erosional processes and closely reflects the underlying rock. In most instances, the rubble seems to have either broken up in place or merely rolled down a nearby slope.

Major lithologic units extend east-west parallel to the direction of flow. Units seem analogous to different streams of ice in a large valley or piedmont glacier that result from coalescence of smaller tributary valley glaciers. The areal distribution of these units suggests that they came from different parts of an orifice that was elongate in a northerly direction, parallel to the trend of the Mono Craters. Lava flowed east and west from the orifice below the dome, but the majority of it flowed west, probably because of lower altitude and fewer obstacles.

Table 6.--Chemical analyses and petrographic data, Southern Coulee

[Southern Coulee major oxides by rapid rock analysis, by Paul Elmore, Sam Botts, and Lowell Artis, U.S. Geological Survey. Minor elements by quantitative spectrographic analysis, by J. D. Fletcher, U.S. Geological Survey]

Lithologic Unit	Lowest Density		Intermediate Density			Highest Density			Glass Mtn. Calif.	West Yellowstone, Mont.
	1	2	3	4	5	6	7	8	9	10
	Major oxides, in weight percent									
SiO_2	75.4	75.7	75.5	75.3	75.3	74.7	75.5	76.2	73.00	75.8
Al_2O_3	13.5	13.1	12.6	12.5	12.6	12.5	12.8	12.6	13.87	12.0
Fe_2O_3	.42	.62	.37	.23	.31	.61	.34	.34	.58	.8
FeO	.50	.44	.66	.72	.58	.54	.60	.33	2.21	1.2
MgO	.10	.05	.05	.05	.41	.10	.05	.05	.16	.18
CaO	.42	.64	.62	.62	.52	.52	.62	.51	1.80	.57
Na_2O	3.8	4.0	4.0	4.0	3.9	3.8	3.7	4.1	3.95	3.4
K_2O	4.8	4.5	5.1	5.1	4.9	5.0	5.1	5.1	3.85	4.9
H_2O^-	.17	.09	.16	.16	.19	.21	.15	.08	nil	--- .32
H_2O^+	.71	.71	.71	1.0	1.0	1.5	.70	.33	.10	---
TiO_2	.04	.05	.04	.04	.03	.04	.05	.03	.25	.20
P_2O_3	.00	.05	.10	.07	.10	.12	.07	.05	tr	.02
MnO	.05	.06	.06	.05	.11	.06	.05	.06	nil	.06
CO_2	.08	< .05	.06	.07	.09	.07	.07	.06	nil	---
Sum	100	100	100	100	100	100	100	100	99.77	99.1

n_D	1.489	1.487	1.488	1.495	1.489	1.495	1.489	1.483
± .001	---	---	1.485	1.485	---	1.488	---	---
						1.486		
Density								
Glass(gm/cc)	---	---	---	---	---	---	---	2.33
Rock	.60	.78	1.22	1.24	1.59	1.87	1.92	2.33

C.I.P.W. Norms

q	33.8	33.9	31.5	31.2	32.2	32.5	33.1	32.0
c	1.5	.6	---	---	.4	.3	.4	---
or	28.4	26.6	30.1	30.1	28.9	29.5	30.1	30.1
ab	32.1	33.8	33.8	33.8	33.0	32.1	31.3	34.7
an	1.6	2.5	1.4	1.1	1.4	1.4	2.2	.9
wo	---	---	.3	.4	---	---	---	.4
en	.2	.1	.1	.1	1.0	.3	.1	.1
fs	.6	.3	.9	1.2	1.0	.5	.8	.4
mt	.6	.9	.5	.3	.4	.8	.5	.5
il	.1	.1	.1	.1	.1	.1	.1	.1
ap	---	.1	.2	.2	.2	.3	.2	.1
cc	.2	.1	.1	.2	.2	.2	.2	.1
salic	97.4	97.5	96.8	96.3	95.9	95.9	97.1	97.7
femic	1.7	1.7	2.3	2.5	2.9	2.2	1.9	1.7

Table 6.--Chemical analyses and petrographic data, Southern Coulee--continued

Minor Elements

Lithologic Unit	Lowest Density		Intermediate Density			Highest Density			Glass Mtn. Calif.	West Yellowstone, Mont.
	1 (PPM)	2 (PPM)	3 (PPM)	4 (PPM)	5 (PPM)	6 (PPM)	7 (PPM)	8 (PPM)		
Pb	40	30	30	30	40	40	30	40		
Ag	< 1	< 1	< 1	< 1	2	2	< 1	< 1		
Cu	2	3	2	1	2	2	1	2		
Ga	17	16	17	15	16	17	18	16		
Mn	300	270	280	285	275	285	280	295		
Cr	2	< 1	2	2	2	2	2	2		
B	30	40	40	40	40	40	40	40		
Co	< 2	< 2	< 2	< 2	< 2	< 2	< 2	< 2		
Ni	1	< 1	2	2	1	2	1	1		
Ba	33	39	36	38	36	28	34	30		
Sr	12	22	12	12	12	11	11	10		
V	< 5	< 5	< 5	< 5	< 5	< 5	< 5	< 5		
Be	3	4	3	3	3	4	4	4		
Nb	10	20	10	10	10	10	10	10		
Sc	3	4	3	3	3	3	3	3		
La	< 50	< 50	< 50	< 50	< 50	< 50	< 50	< 50		
Mo	3	< 2	3	3	3	3	3	3		
Y	20	27	21	20	20	21	21	20		

Zr	110	88	115	140	110	110	125	115
Li	55	27	58	47	55	55	57	57
Cs	6	4	5	5	5	5	5	5
Rb	195	235	175	155	175	160	180	185

Elements looked for but not found: Au, Hg, Ir, Pt, W, Ge, As, Sb, Sn, Bi, Zn, Cd, Ti, Th, Ta, U, and P.

Southern Coulee, California (1-8)

1. Medium greenish gray pumice, sparsely streaked with faint, darker gray, more dense pumice laminae (avg. .4-mm thick); vesicles are tubular and range in width from .03 mm to 1 mm. Microlites generally sparse; average .01 mm long.
2. Light-gray pumice and very sparse, faint, denser laminae; rock similar to 1; vesicles very elongate tubes that average .5 mm in width; microlites extremely sparse and average .7 mm long.
3. Medium dark-gray pumice having crenulated layers and lenses of markedly different vesicle size that range from 1 mm to 5 mm in thickness; vesicles are tubular and range from .1 to 5 mm in width. Microlites very sparse; average .015 mm in length.
4. Medium-gray pumice having darker gray denser pumice lenses (less than 1 mm thick); vesicles tubular, average .3 mm wide and 1 mm long; microlites very sparse, average .008 mm in length.
5. Light-medium-gray, homogeneous pumice; vesicles elongate tubes that range from .002 mm to 1 mm in width; microlites very sparse, average .015 mm in length.
6. Light-gray, homogeneous pumice; vesicles generally less than .008 mm wide, very elongate tubes; microlites very sparse, ranging from .08 mm to .1 mm in length.
7. Dark-gray, distinctly layered pumice; layering due to alternation of thin (average 1 mm) dense laminae and lenses 3 to 10 mm thick of highly inflated pumice with vesicles as much as 10 mm wide. Microlites more abundant than most, but probably less than 1 percent, concentrated into very thin layers .2 to .3 mm thick; microlites average about .008 mm in length.
8. Black, homogeneous, nonvesicular obsidian with faint streaks of dark gray; microlites sparse, range in length from .004 to .1 mm.

Glass Mountain area, California

9. Rhyolite obsidian (Anderson, 1933, table 1, no. 7; analysis by Frank Herdsman).

West Yellowstone area, Montana

10. Rhyolite obsidian (Hamilton, 1963, p. C80, specimen 9; analysis by Paul Elmore, I. Barlow, S. Botts, and G. Chloe, U.S. Geological Survey).

Southern Coulee consists of predominantly layered pumice (density 0.53-2.01 g per cc; see table 6) that lacks megascopically visible crystals. Densities of pumice were determined by weighing cylindrical cores of known volume. Obsidian (density 2.33 g per cc), a minor but ubiquitous constituent of all units, occurs as lenses and laminae in the pumice (fig. 28). The obsidian also lacks megascopically visible crystals, but contains sparse spherulites that range in diameter from less than 1 mm to more than 40 mm and average about 2 mm. The spherulites can be locally abundant. They are partially leached out near former fumaroles, a condition that gives the obsidian in such localities a false appearance of coarse vesicularity, which it generally lacks. X-ray diffraction indicates that the spherulites are composed of sanidine and well-ordered cristobalite.

Permanent clear ice occurs in fractures and open pores in the rocks of the coulee from a few feet below the surface down to an unknown depth. Its presence often delays quarrying operations. Core drilling shows it to be abundant down to about 23 m and in trace amounts down to at least 45 m. This decrease in the abundance of ice below about 23 m coincides with an abrupt decrease in porosity of the pumice below that depth. The ice is probably frozen ground water that has become permafrost (chemical analyses show that the water is relatively pure) owing to a combination of low mean annual temperatures and the low heat-conductive properties of the pumice.

Although flow layering is nearly present everywhere, it varies

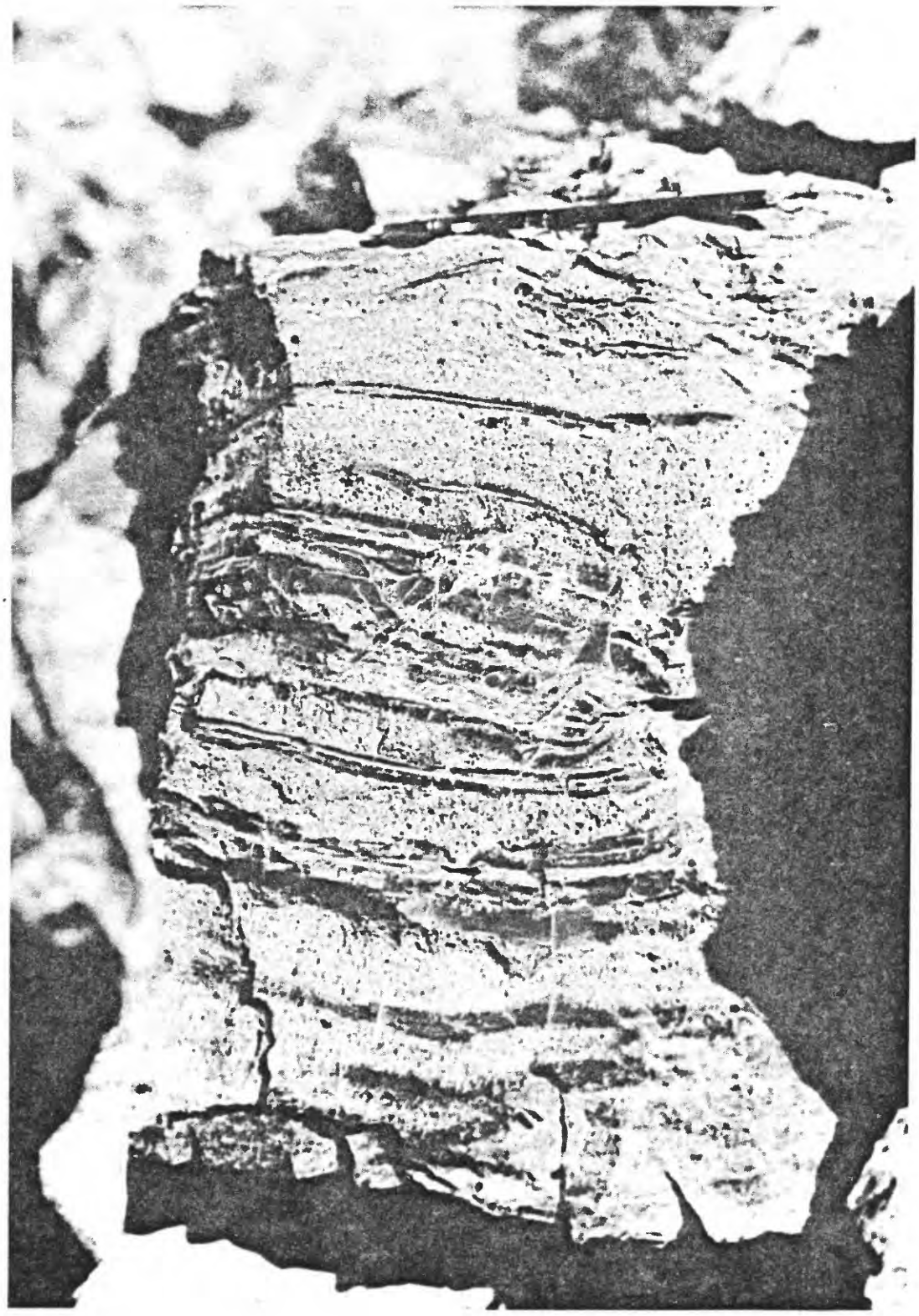

Figure 28.--Thin layers of black obsidian in light gray, highly inflated pumice, intermediate-density unit, Southern Coulee.

considerably in aspect. The pumice appears massive in places, but generally close inspection shows that this appearance is due either to medium-to-thick beds of homogeneous rock separated by thin inconspicuous laminae or to a very thin, subtle layering. Generally the layering is represented by differences in the degree and form of vesicularity. In a few places, surfaces of flow layers are coated by pale pink very fine-grained material, which has been shown by x-ray diffraction to be a mixture of sanidine and well-ordered cristobalite similar in composition to the spherulites in the obsidian. The pink coatings and pumice layers are broken in places, apparently due to more plastic behavior of adjacent layers, and the fragments scattered along the flow layers.

The pink sanidine-cristobalite material commonly fills fractures and coats the surfaces of the pumice blocks. The skins formed by coatings on the pumice blocks are cut by numerous fractures (fig. 29). The common sigmoidal form of the fractures indicates contemporaneous fracturing and differential plastic flow of the skins. The material in the interior of the blocks has been squeezed into the fractures which indicate that interiors of the blocks were still plastic after the fractures were formed. Skins occurring on several surfaces of blocks suggest that blocks formed while the lava was still hot.

The color of the rocks of the units ranges from black (in obsidian) to light gray (in pumice); pumice shows all gradations from light-to-dark gray. The thicker the walls of the glass framework of the pumice, the darker is the color. However, the darker gray rocks are not necessarily the densest because the presence

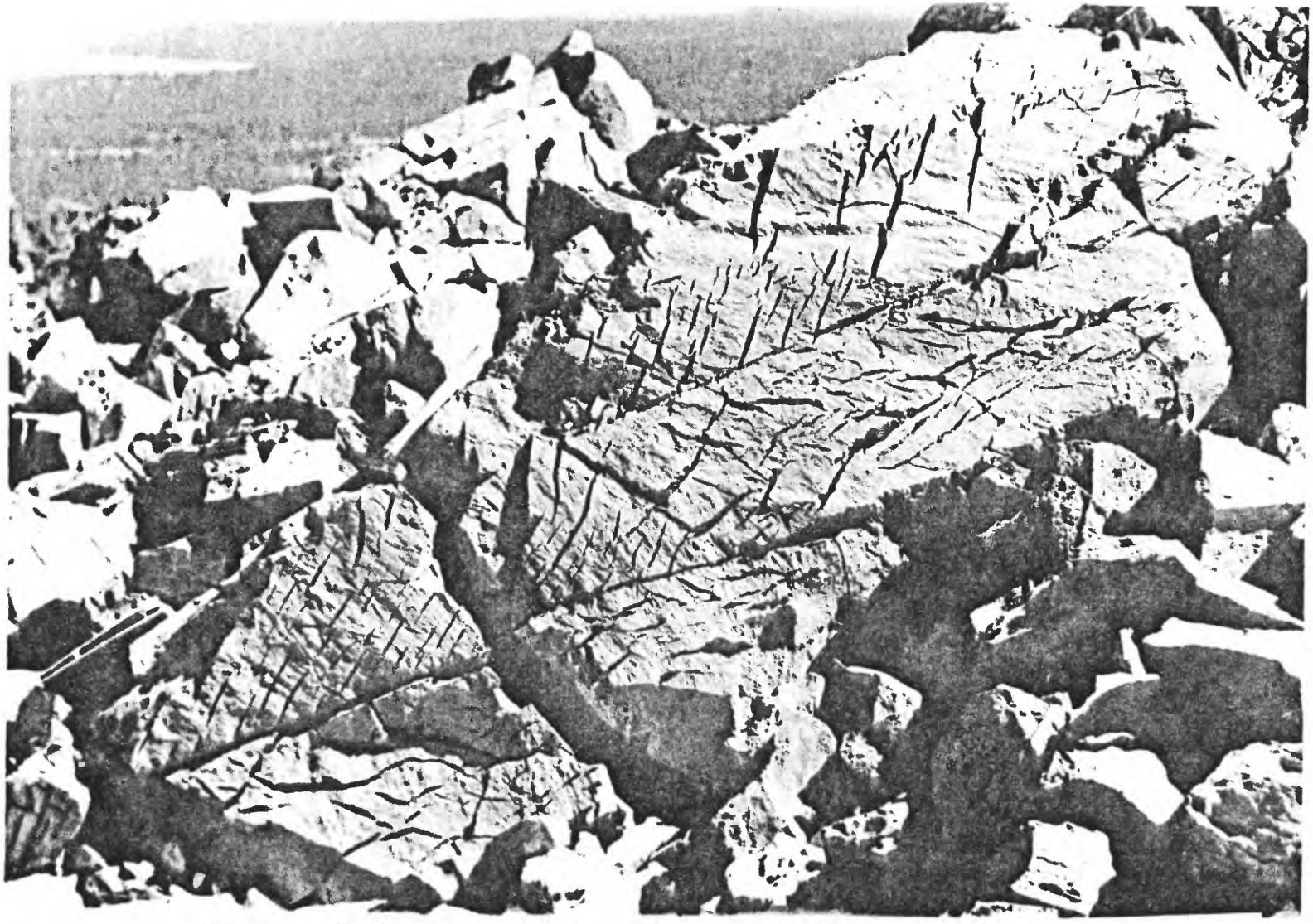

Figure 29.--Fractures in siliceous skin on pumice blocks, intermediate-density unit, Southern Coulee.

of large vesicles may more than compensate for the thick walls.

Vesicles are most commonly flattened tubes that tend to be elongated parallel to the direction flow. Intersection of the elongate vesicles and flow surfaces produces many of the widespread fine striations. Lenses of coarse vesicularity occur in finely vesicular pumice or in nonvesicular obsidian in places. These coarse vesicles are seldom flattened or much elongated and seem to represent pockets between layers of flowing lava where pressure was released normal to the layering. In other places, vesicles in large masses of pumice are elongated at a high angle to the flow layering, which is expressed by thin layers of lower vesicularity that show marked elongation parallel to the layering. This phenomenon is particularly widespread in the rather coarsely vesicular, dark-gray phase of the lowest density unit. The above observations suggest that, for a given viscosity, the form and orientation of vesicles seem to be mostly a result of three conflicting stress fields: (1) gravity, which results in an upward release of pressure; (2) plastic flow, which results in a release of pressure parallel to the direction of flow; and (3) shear, which results in a more complex force distribution. Stress due to plastic flow dominates.

Lowest density unit.--The lowest density unit is characterized by pumice that has a density range from 0.51 to 0.78 g per cc. Minor amounts of denser pumice (1.00 to 1.75 g per cc) and obsidian are interlayered with the less dense rocks. The unit narrows to the west and pinches out in a series of complicated fingers (fig. 24). The northernmost of the fingers is in contact with the narrow upper

east end of the intermediate-density unit, but the relations between the two units are not clear. The intermediate unit may be closely related to the lowest density unit, but the rubble contact is abrupt and no indications of gradation or intertonguing between the two units are found.

The pumice of the unit is generally homogeneous and layering is inconspicuous. This is partly because flow layering is represented by very small subtle variations in size and shape of the vesicles, and partly because of the presence of thick (1 to 2 m) homogeneous beds separated by thin (2 to 10 mm) layers of only slightly different texture. Its homogeneous character and low density make the pumice of the unit a valuable commodity.

Generally, the pumice color in the low-density unit grades from light gray along the south margin to dark gray along the north margin. Different hues of pumice form east-west bands roughly parallel to the direction of flow. In detail the bands are irregular and some are discontinuous. The pumice of all hues is light brown to yellowish brown in an extremely thin surface layer, which may be due to weathering or alteration while the lava was still hot.

The lighter hued pumice is finely vesicular with average vesicle diameter in the medium-gray of about 0.6 mm, in light-gray less than 0.1 mm, and in the dark-gray as much as 3 mm.

Intermediate-density unit.--The intermediate-density unit (average density is about 1.20 g per cc) is confined to the western part of the flow and may be part of the same flow unit as the low-density unit. Dominant rocks are of relatively low-density pumice

types that resemble those in the lowest density unit, but the rock is much more heterogeneous. Laminae and thin beds of denser pumice and obsidian are more abundant (fig. 28). Fractured surface skins of siliceous material and glass are widespread (fig. 29) in contrast to the low-density unit where they are scarce. The dominant, less dense pumice commonly shows the same light-brown to yellowish-brown surface that is generally in the lowest density unit.

The northern contact of the unit seems to grade into the highest density unit and trends diagonally across a conspicuous, younger lava stream composed of pumice of the two units. The contact seems to be laterally displaced to the right at the south margin of the stream, but field relations are not clear. This displacement would be expected if, as suggested by morphologic evidence, the conspicuous stream with the crescentic ridges is younger, or contemporaneous and more rapidly flowing, than adjacent streams.

Highest density unit.--The highest density unit is characterized by a dominance of pumice whose density ranges from 1.37 to 2.07 g per cc. Smaller amounts of less dense pumice and obsidian are interbedded with denser pumice throughout the unit. Obsidian is much more abundant in this unit than in the others. Pumice and obsidian are medium-to-thin bedded giving the unit a characteristic well-bedded aspect (fig. 30). Various layers of different hues of gray and of different densities are typical. The rock breaks along surfaces of flow layering, producing abundant slablike fragments in contrast to the more equant fragments of the less dense units.

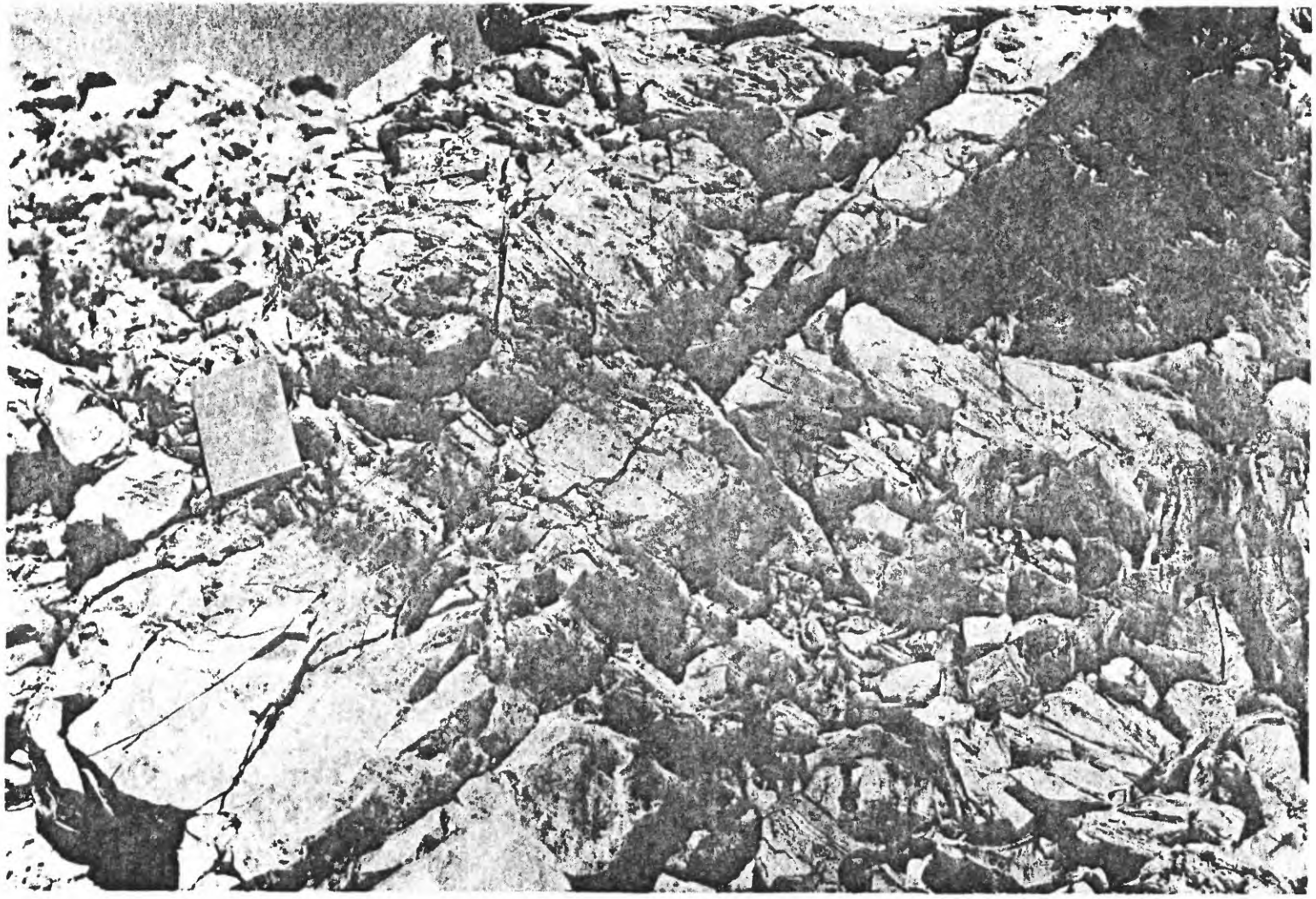

Figure 30.--Interbedded light-gray dense pumice and black obsidian, highest density unit, Southern Coulee

The layering surfaces have a distinctive sheen due to coatings of glass or siliceous material. The color of the denser pumice is hues of gray and the pumice lacks the brown surface color of other units.

Rocks included in this unit are possibly some of the youngest and oldest, or at least lowest exposed rocks, of the coulee (see section on structure). They form part of the previously mentioned younger stream, and are the only rocks to be seen projecting through the talus slope at the sides of the coulee (fig. 27) where they are especially rich in obsidian. Rocks of the densest unit also are the only ones that project upward through ash deposits. The last occurrence strongly suggests that parts of the densest unit are pre-ash eruption in age.

Vesicles of the densest pumice are smaller (commonly of microscopic dimensions) and less abundant than those of the other units. Fresh surfaces of this pumice have a pearly luster that results from the network of fine filaments of glass that compose the framework of the rock surrounding the vesicles. Perlitic fractures are lacking.

Structure

Because of the jumbled, fragmental character of the lava, no attempt has been made here to study the structure of the coulee by means of the geometrical analysis of flow layering and linear structures. These structures are described on the next few pages; but the discussion of the overall structure of the coulee is based on the consideration of gross features.

Surface structures.--The previously described flow layering is the dominant and most pervasive structural feature of the coulee. Almost as widespread are lineations, chiefly streaks, striations, and grooves that lie in the plane of the flow layering and are parallel to the direction of flow. Streaks and some striations represent the intersections of the flow surfaces and elongate bodies, including walls of vesicles that were extended plastically parallel to the direction of flow. Grooves and other striations were caused by the movement of flow layers over one another.

Fold and related crenulations tend to be normal to the direction of flow and are less common linear structures. Folds range from open warps to isoclinal folds. Open folds tend to have the characteristic form of flexural slip or parallel folds in which folded layers maintain their thickness throughout the fold (Wynne-Edwards, 1963). In such folds, layers are competent and folding is accomplished by flexure and slip between layers. The isoclinal folds (fig. 31) show the thick hinges and thin limbs of flow or similar folds, in which layers behave passively and folding results from non-uniform lamina-flow along invisible planes parallel to the axial plane of the fold (Wynne-Edwards, 1963). The open, parallel folds form in surface layers of obsidian where, because of cooling, viscosity, and competence of layers may be relatively high. On the other hand, isoclinal folds appear most often in the interior parts of thick pumice and obsidian masses where the temperature was probably relatively high and viscosity low.

Pressure ridges seem to be large-scale open folds that correspond

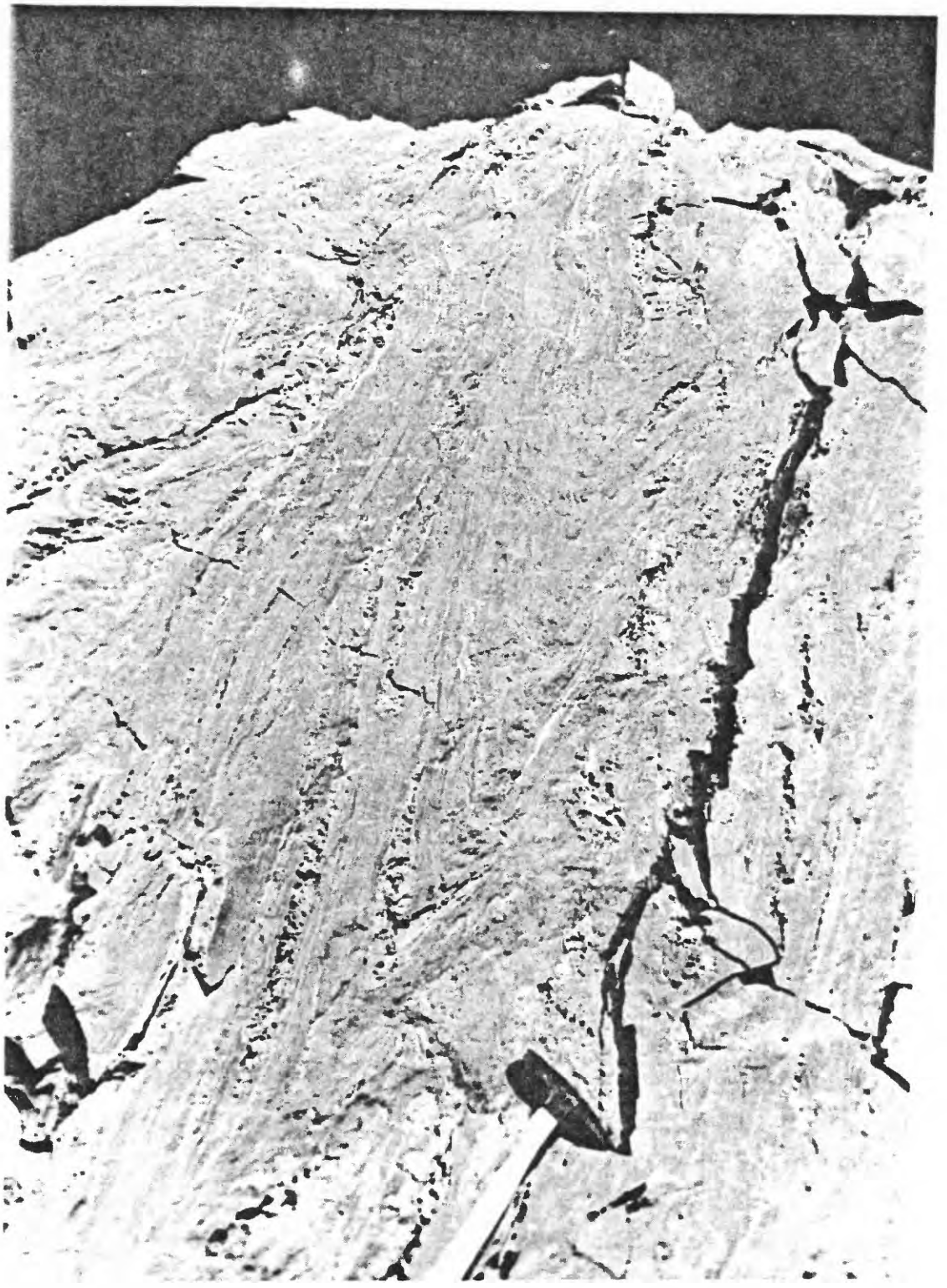

Figure 31.--Isoclinal folds in pumice, highest density unit, Southern Coulee.

to the smaller scale flexural slip folds above. Large slabs on flanks of ridges dip away from the crest in a manner that suggests the ridges represent large-scale wrinkles or flexures in the crust of the flow. Such wrinkles appear to be analogous to the thin, wrinkled crust of highly fluid pahoehoe basalt flows (see Parker, 1963, p. 11-12). The crust of a highly viscous flow of the Southern Coulee type would be much thicker and the wrinkles produced in it of much larger scale (deSitter, 1956, p. 189-190).

Locally, strain-slip or fracture cleavage occurs and contains numerous paper-thin glassy or siliceous laminae whose physical properties contrast sharply with those of the pumice. The cleavage is identical to that found in metamorphic rocks (see Turner and Weiss 1963, p. 98) and consists of parallel planes intersecting and layering at high angles (fig. 32). The strain-slip cleavage in metamorphic rocks is a late feature developed in already foliated rocks, and it probably developed in solidified, layered lava as the result of stresses created by nearby movement of still fluid lava.

Subsurface structure.--Interpretation of the internal structure of Southern Coulee is based mostly on the cores obtained during the present work and their correlation with the surface features. Unfortunately, the base of the coulee was not reached due to the difficulties in drilling the highly porous, fragmental lava. Four core holes were drilled, all located in the lowest density unit and in the flow part of the coulee (fig. 24). Of these, only core holes 2 and 4 drilled through this unit into the highest density unit. The contact between the two units seems to be abrupt, much

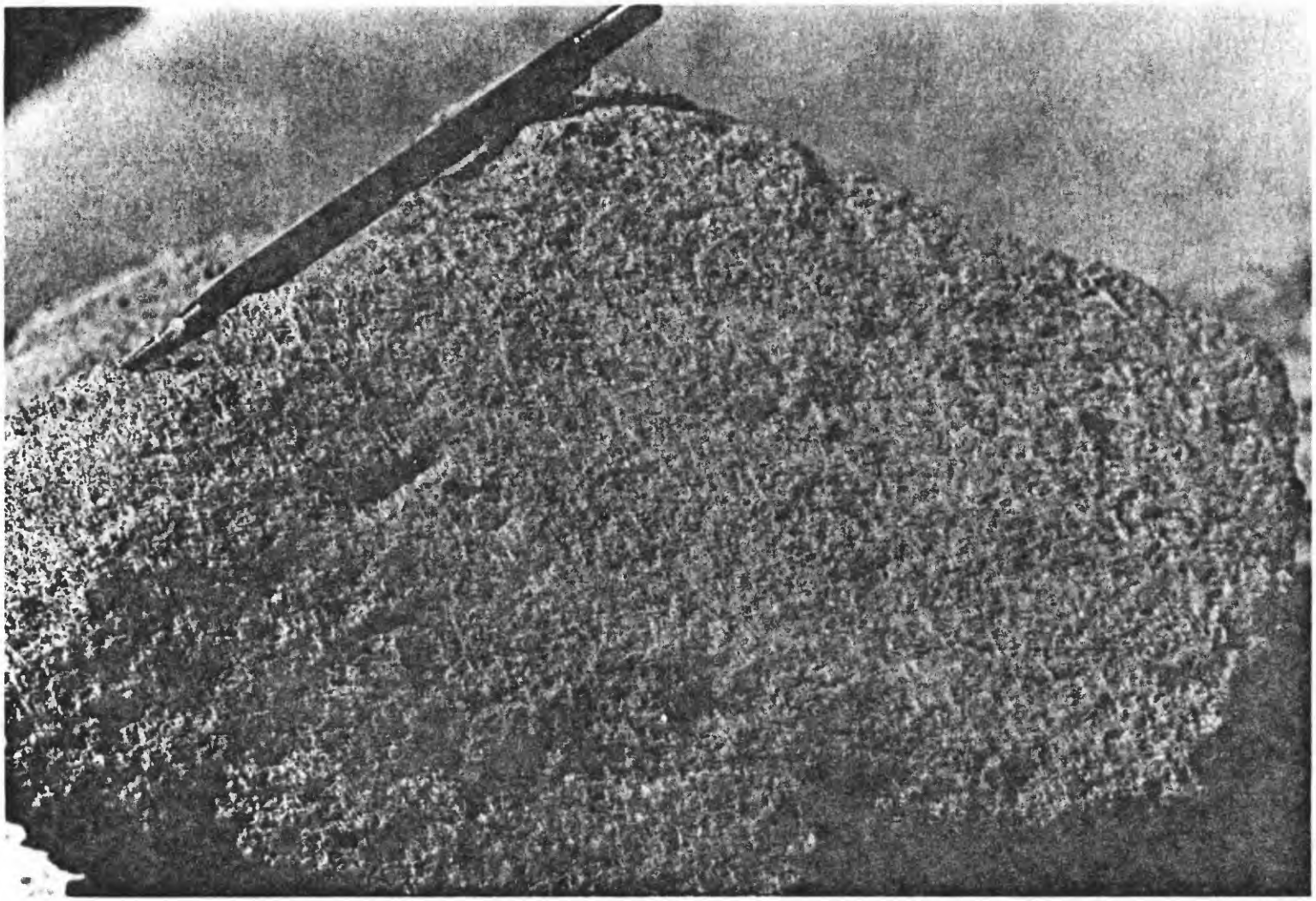

Figure 32.--Strain-slip cleavage in pumice, lowest density unit; flow layering dips gently to right and is cut by cleavage that dips steeply to right.

like surface contacts between the units. The lower 20 or 30 feet of the least dense unit may contain more layers of denser pumice than is usual, but this is a common occurrence near the contacts at the surface. The lower 10 feet of core hole 4 (fig. 33) is especially rich in obsidian that contains abundant spherulites. Similar thick obsidian layers are exposed at the surface, but spherulites are generally sparse or lacking. The spherulitic obsidian layer may represent the top of a very dense, spherulitic unit similar to that seen in the small, partly disrupted rhyolitic flow, about 1 mile south of the southern margin of the coulee.

All core holes penetrated broken jumbled rock their entire depth. Hence, flow-layering attitudes in cores are highly variable and probably reflect attitudes of single blocks rather than that of the original flow of lava. Ice in highly variable amounts was encountered down to the deepest level, but is more abundant near the surface.

According to the core evidence, the least density unit is an elongate, boat-shaped layer, having a thickness of at least 25 m. It lies on a substratum composed of the densest unit, which may pass downward into a still denser spherulitic unit. The form of the intermediate-density unit seems similar to that of the least dense unit.

The above evidence suggests that lower density units represent frothy top layers floating on a generally more dense lava. This frothing apparently occurred at the southern end of the fissure-like orifice, thus the low-density units are confined to the

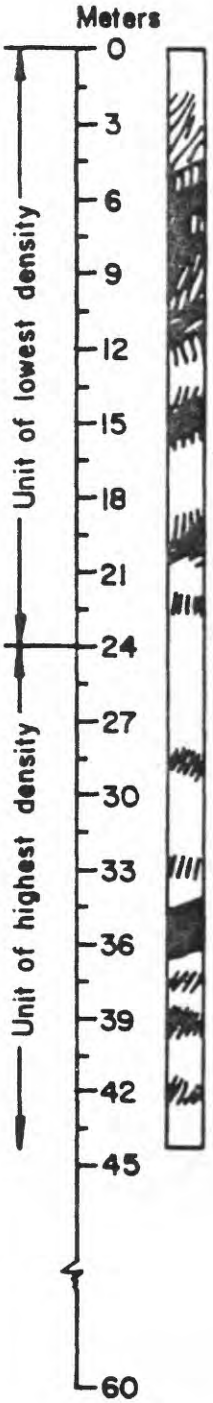

2,654 m Top of coulee. Light gray, massive pumice of low density

Pumice, light gray, low density, broken-ice in cavities @ 4.5 m.

Pumice, light gray to light brown, low to medium density; broken; ice in cavities.

Pumice, light gray to light brown, low to medium density, broken, ice in cavities.

Pumice and thin streak of black obsidian; pumice, medium density, medium gray; ice in cavities; broken.

Pumice, light brownish gray, low density with sparse laminae of black obsidian; broken; ice in cavities.

Pumice, light gray, dense; scattered black obsidian layers, broken; trace of ice in cavities.

Pumice, light gray, dense and scattered black obsidian layers. Broken; ice in cavities.

Pumice, light gray and abundant spherulitic black obsidian in irregular streaks veins; broken; scattered ice in cavities.

Same as above.

Same as above.

Black spherulitic obsidian and light gray, dense pumice irregularly interlayered; broken; scatterd ice in cavities.

Total Depth. 44.8 m.

Estimated base of coulee.

Figure 33.--Log of Southern Coulee core (SCC) 4; lines in column show orientation of flow layering; location of lines show interval of core recovered.

southern part of the coulee. Lack of strict correlation between the mapped density units and the lava streams, probably resulted from the complex, anastomosing pattern of within the flow part of the coulee. Individual streams of lava flowed at different rates, at different times, and took different courses. This process may have disrupted original spatial relations of density units at the orifice.

Petrography

Both pumice and obsidian of the Southern Coulee consist predominantly of clear, colorless, undevitrified glass, which lack phenocrysts. Other constituents, microlites, spherulites, and xenocrysts constitute only a small fraction of 1 percent of the total rock, although locally, microlites and spherulites may approach 1 percent. Xenocrysts are rare; the few that were seen are plagioclase grains 1-2 mm long.

Elongate microlites and vesicles show a preferred orientation parallel to the flow direction when seen is thin section. Although generally the orientation in a single section is fairly uniform, in some, trains of microlites are contorted into whirls. In others the preferred orientation of microlites is weak and flow direction obscure.

Refractive index of the glass ranges from 1.483 to 1.495 (table 6) with 1.488 (± .001) being the most commonly obtained value. Variations are not gradational and represent the indices of discrete masses of glass whose shape and extent are difficult to determine. A particular range of indices and hence of composition could not be

identified with a particular rock type of lithologic unit; variations within a single specimen (4 and 6, table 6) nearly span the total index range.

Regular polarizing microscope and phase-contrast microscope observations showed that vesicles are commonly surrounded by rims of higher index. For example, in specimen 6 (table 6), rims have an index of 1.495, whereas glass between rims has an index ranging from 1.486 to 1.488. Rims range in width from less than 5 microns to as much as 20 microns. Thin zones (less than 10 microns) of probable higher index occur along a generally polygonal pattern of fractures. Both vesicle rims and fracture zones show faint birefringence. For this reason, together with higher index and occurrence at places of water accessibility, it is suggested that they represent zones of hydration (Ross and Smith, 1955; Friedman and Smith, 1960). Hydration could have occurred either at the time of eruption or later when the coulee was penetrated by groundwater.

Other types of index distribution were not observed. Hydration zones vary markedly in abundance from specimen to specimen, and are obviously related to the degree of vesicularity and fracturing. This relation of index and vesicles probably accounts for the fact that only one index was encountered in the nonvesicular obsidian (col. 8, table 6), and 2 or 3 indices in some of the highly vesicular pumices.

Chemical composition

Eight chemical analyses (table 6) of the Southern Coulee represent not only a wide range of physical rock types but also a

wide range of localities on the coulee. The analyses are remarkably similar and indicate a nearly uniform composition for the coulee as a whole. Similar uniformity of composition for similar glassy rhyolitic flows and domes have been noted by Anderson (1933) at Glass Mountain, northern California, and by Hamilton (1963) near West Yellowstone, Montana. Composition of rhyolites of these two areas (table 6, nos. 9 and 10) are similar to composition of Southern Coulee rhyolite.

The uniform composition is reflected in the narrow range of refractive indices. The average silica percentage is 75.4 percent and the most common index is 1.488. These data, when plotted on the silica refractive index diagram of George (1924, fig. 3), define a point very close to his curve for natural glasses.

Chemical composition of the rocks of the Southern Coulee indicates a rhyolite of the sodipotassic subrange of the C.I.P.W. classification, as does the analyses from Glass Mountain and West Yellowstone. Bowen (1928, p. 129) noted that, of the 44 rhyolite obsidian analyses at his disposal, 31 were of the sodipotassic subrange and 13 were dosodic; none were extreme potassic or sodic types. Glassy rhyolitic rocks seem, therefore, to have a much more restricted compositional range than do the crystalline silicic rocks.

Bowen (1928, p. 125-132) considered glassy rocks to be the only igneous rocks whose composition undoubtedly corresponded to a liquid (allowing for possible loss of volatiles on cooling). He took their restriction in composition, as compared to their crystalline counterparts, to be caused by the more restricted compositional

course of the changing liquid during a crystallization sequence as compared to the wide range of possible compositions of the crystalline products of the magma.

The projection of the composition of the rhyolite of the Southern Coulee (salic constituents less anorthite as per Bowen, 1937, p. 16-17) on the equilibrium diagram of the system $NaAlSiO_4$-$KAlSiO_4$-SiO_2, falls in the salicic end of the low-temperature trough (fig. 34). Bowen (1937; also see Benson, 1941) found that compositions of a large number of igneous rocks rich in alkali-alumina silicates (phonolites, trachytes, syenites, granites, rhyolites, etc.) plotted in the low-temperature trough. From this he concluded that these rocks were the products of fractional crystallization of a differentiated magma in which crystal-liquid equilibrium was the principal control. Had they been products of another process, their compositions would scatter out of the low-temperature trough. Laws of crystal-liquid equilibrium may also govern the process of partial melting (Barth, 1962, p. 124), and the rocks whose compositions fall in the low-temperature trough in figure 34 may represent the early melting fraction instead of the "residue" of a differentiated magma. Holmes (1932, p. 545-546) and Waters (1955, p. 712-715) have emphasized the potential of partial melting and assimilation of crustal rocks in the production of different magma types.

Which processes led to production of the Mono Craters cannot be decided with certainty from the present data but differentiation from a basalt magma seems unlikely in view of the relatively small

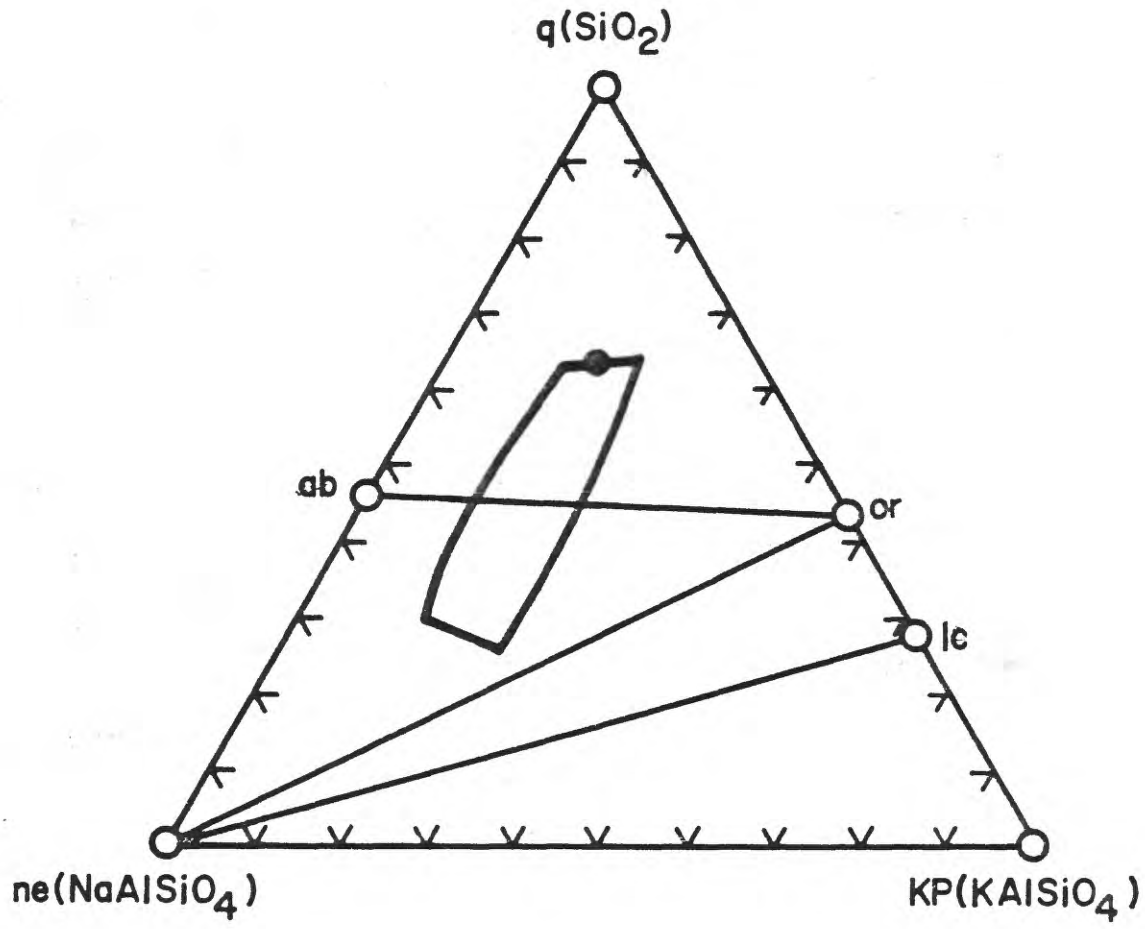

Figure 34.--Normative nephaline (ne), quartz (q), and Kaliophilite (Kp) diagram after Bowen (1937) showing average composition of Southern Coulee rhyolite (dot) in low temperature trough (heavy lines); ab = albite, or = orthoclase, lc = leucite.

volume of basalt of appropriate age in the Mono Craters area (Kistler, 1966). Granitic residuum of such a magma would be less than a tenth of the original magma volume (Barth, 1962, p. 122). Therefore, it seems more probable that the Mono Craters came from a granitic magma derived from crustal rocks by partial melting. This magma may have come to the surface along the arcuate fracture zone beneath the craters, which is the eastern arc of a large-scale ring structure whose center lies about 4 miles to the west (Kistler, in press).

References

Anderson, C. A., 1933, Volcanic history of Glass Mountain, northern California: Am. Jour. Sci., 5th ser., v. 26, no. 155, p. 484-506.

Barth, T. F. W., 1962, Theoretical petrology, 2d ed.: New York, John Wiley and Sons, Inc., 416 p.

Benson, W. N., 1941, Cenozoic petrographic provinces in New Zealand and their residual magmas: Am. Jour. Sci., v. 239, no. 8, p. 537-552.

Bowen, N. L., 1928, The evolution of the igneous rocks: Princeton, N. J., Princeton Univ. Press, 332 p.

_____1937, Recent high-temperature research on silicates and its significance in igneous geology: Am. Jour. Sci., 5th ser., v. 33, no. 193, p. 1-21.

de Sitter, L. U., 1956, Structural geology: New York, McGraw-Hill Book Co., 552 p.

Donath, F. A., and Parker, R. B., 1964, Folds and folding: Geol. Soc. America Bull., v. 75, no. 1, p. 45-62.

Friedman, I., and Smith, R. L., 1960, A new dating method using obsidian--Pt. 1, The development of the method: Am. Antiquity, v. 25, no. 4, p. 476-522.

George, W. O., 1924, The relation of the physical properties of natural glasses to their chemical composition: Jour. Geology, v. 32, no. 5, p. 353-372.

Gresswell, W. K., 1940, Short report on the geological formations encountered in driving the Mono Craters Tunnel: Calif. Jour. Mines Geol., v. 36, p. 199-204.

Hamilton, W. B., 1963, Petrology of rhyolite and basalt, northwestern Yellowstone Plateau: U.S. Geol. Survey Prof. Paper 475-C, p. C78-C81.

Hatch, F. H., Wells, A. K., and Wells, M. K., 1961, Petrology of the igneous rocks, 12th ed.: London, Thomas Murby Co., 516 p.

Holmes, Arthur, 1932, The origin of igneous rocks: Geol. Mag. [Great Britain], v. 69, p. 543-558.

Kistler, R. W., 1966, Geologic map of the Mono Craters quadrangle, Mono and Tuolumne Counties, California: U.S. Geol. Survey Geol. Map GQ-462.

_____196 , Structure and metamorphism in the Mono Craters quadrangle, Sierra Nevada, California: U.S. Geol. Survey Bull. 1221-E (in press).

Parker, R. B., 1963, Recent volcanism at Amboy Crater, San Bernardino County, California: California Div. Mines and Geology, Spec. Rept. 76, 21p.

Powers, H. A., and Wilcox, R. E., 1964, Volcanic ash from Mount Mazama (Crater Lake) and from Glacier Peak: Science, v. 144, no. 3624, p. 1334-1336.

Putnam, W. C., 1938, The Mono Craters, California: Geog. Rev., v. 28, no. 1, p. 68-82.

Ross, C. R., and Smith, R. L., 1955, Water and other volatiles in volcanic glasses: Am. Mineralogist, v. 40, nos. 11-12, p. 1071-1089.

Russell, I. C., 1889, Quaternary history of Mono Valley, California: U.S. Geol. Survey, v. 8, pt. 1, p. 261-394.

Turner, F. J., and Weiss, L. E., 1963, Structural analysis of metamorphic tectonites: New York, McGraw-Hill Book Co., 545 p.

Waters, A. C., 1955, Volcanic rocks and the tectonic cycle, in Poldervaart, Arie, ed., Crust of the earth--a symposium: Geol. Soc. America Spec. Paper 62, p. 703-722.

Williams, Howel, 1932, The history and character of volcanic domes: Calif. Univ. Dept. Geol. Sci. Bull., v. 21, no. 5, p. 51-146.

Wynne-Edwards, H. R., 1963, Flow folding: Am. Jour. Sci., v. 261, no. 9, p. 793-814.

GEOLOGY AND PETROGRAPHY OF THE SONORA PASS SITE MONO COUNTY, CALIFORNIA

by David V. Haines

ABSTRACT.--The Sonora Pass site is located in the Sierra Nevada on a quartz monzonite pluton. Outcrops consist of relatively unweathered, jointed, sheeted, and exfoliated rock. Rock surfaces are generally smooth with rounded edges. Slopes are usually less than 15 degrees. Irregularities in the terrain are due to erosion along joints by running water. Petrographic examination of drill core to a depth of 12.2 meters indicates the rock is a homogenous, medium-grained porphyritic quartz monzonite consisting of pink microcline, zoned plagioclase, quartz, biotite, and minor accessory minerals.

Introduction

The Sierra Nevada consists of pre-Cretaceous metamorphic and metasedimentary rocks and Mesozoic plutonic rocks, chiefly granite, granodiorite, and quartz monzonite. Plutons range from a fraction of a mile to 20 miles across, with sharp crosscutting relationships indicating multiple injection (Ross, 1958; Bateman and others, 1963). Tertiary rocks include early Cenozoic auriferous gravels, Miocene rhyolite ignimbrite, and Pliocene andesite mudflows. Subsequent erosion carved deep narrow canyons through the volcanic rocks into the crystalline basement. These canyons have been modified by Pleistocene glaciation, which locally mantled the surface with moraine. A region 55 km wide along the crest of the range was intensely glaciated. Fault movements along the eastern escarpment have continued into Recent time.

Geology

The test site consists of a relatively unweathered plutonic bedrock outcrop. Topography and rock type may be analogous to conditions in the lunar highland regions. The test site is located on the eastern slope of the Sierra Nevada approximately 4.5 air km southeast of Sonora Pass (fig.35). The test site is accessible via paved highway (California Highway 108). The nearest sizeable community is Bridgeport, California, about 32 air km east southeast of the test site. Elevations at the test site range from approximately 2,550 m to 2,600 m MSL (mean sea level).

The major part of the test site consists of outcrops of medium-grained quartz monzonite, which are part of a large pluton (fig. 36). Rock surfaces show a variety of slope directions and angles ranging from vertical to horizontal, and are generally smooth and rounded on the edges but not polished. Minor irregularities in the rock surfaces are due to exfoliation and differential weathering (fig. 37). On a larger scale, more prominent irregularities in the terrain are due to weathering and erosion along joints and to rock sheeting probably caused by the exfoliation process or by unloading.

Water

Surface water consists of small rivulets that carry meltwater across the test site in the spring. These small streams probably dry up in the summer months. During the spring, meltwater forms pools on the more level rock surfaces; these pools are often discolored by algae.

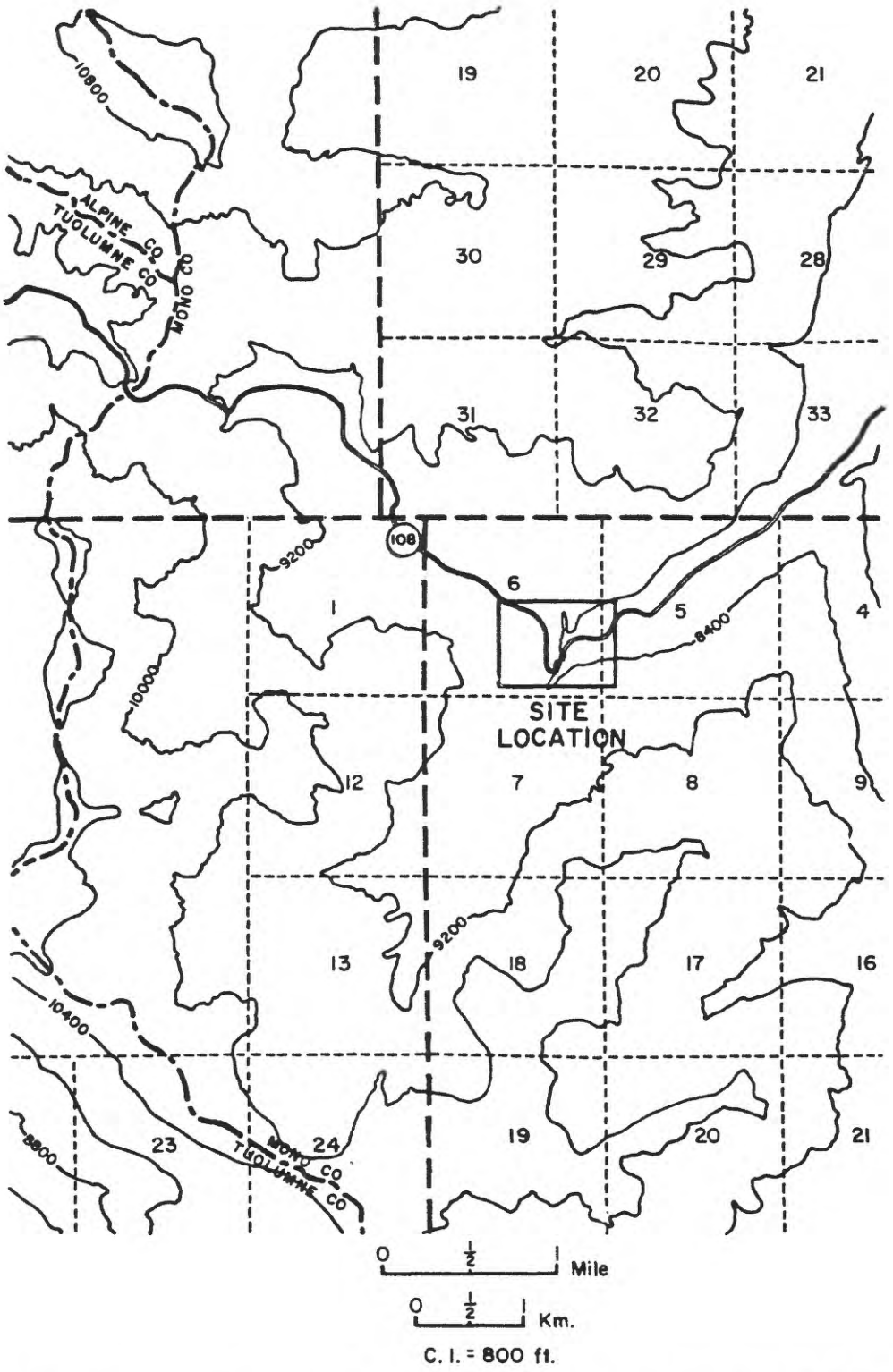

Figure 35.--Topographic map, Sonora Pass site, Mono County, California.

Figure 36.--Aerial photograph shows seismic-spread layout, drill-hole location, and quartz monzonite outcrops, Sonora Pass site, California.

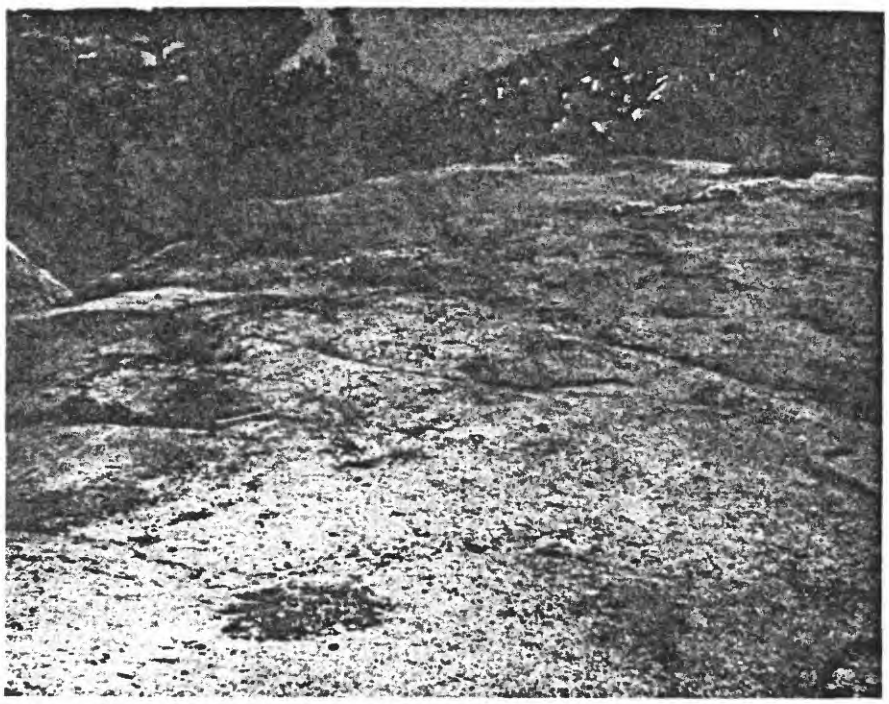

Figure 37.--Exfoliation on rock surface sloping southwest. Boulders are transported quartz monzonite, similar to underlying rock, Sonora Pass site, Mono County, California.

Subsurface meteoric water occurs in the joints of the rock and probably contributes small amounts of effluent water to Leavitt Creek during the summer. A spring on the test site issues from the quartz monzonite and has formed a small terrace consisting of brown tufa. The channel taken by the spring is coated reddish brown on bottom and sides with limonitic sludge, and the banks for several feet on either side contain white efflorescences of salts.

Rock structure

The quartz monzonite is medium-grained, massive, hard, well-indurated, and solid in most of the exposures. The rock is cut by steeply dipping joints trending in different directions. The most prominent set of joints trends approximately east-west. The joints are spaced, on the average, about 1 meter apart and the majority are tight with little surface expression. Sheeting is expressed as a more or less horizontal to low-dipping joint set.

The quartz monzonite is intruded by dikes of white aplite 15 cm or less thick, and by pegmatitic dikes containing pinkish feldspar and quartz, which are up to 67 cm thick.

Weathering and Erosion

The smooth rock surfaces and the irregularities observed in the ground surface are the result of four processes: exfoliation,

frost heaving, erosion by running water, and glaciation. Exfoliation tends to produce the rounded edges and smooth rock surfaces shown in figure 37. Frost heaving tends to widen the joints in the rock and probably assists in stripping the rock surface of exfoliation plates. The relatively large grain size of the rock also permits frost to wedge out mineral grains to form grus (fig.38). Grus may also form by shattering of the rock caused by expansion of the lattices of biotite and plagioclase, as a result of weathering (Wahrhaftig, 1965). Erosion by running water also assists in widening and deepening joints so that narrow defiles are sometimes produced. Grus tends to be washed into joints or deposited in swales in the rock surface.

The quartz monzonite is superficially weathered to a maximum depth of about 15 cm. Large, broken fragments of the rock, which are strewn along the shoulder of the highway, show the depth of weathering by an abrupt change in color. The weathered rock in most places is almost as firm and hard as the fresh rock. Locally, outcrops of especially coarse-grained weathered rock have a rougher surface texture than usual, and are slightly friable. Some mineral fragments can be scratched off the surface with a hammer, but the friability is very superficial. Large phenocrysts of microcline are most resistant to weathering and tend to project outward on the rock surfaces. Relatively thin aplite dikes, which cut the quartz monzonite, are also resistant to weathering and tend to stand out an inch or two above the surface of the quartz monzonite. The weathering colors are yellowish and brownish hues but are

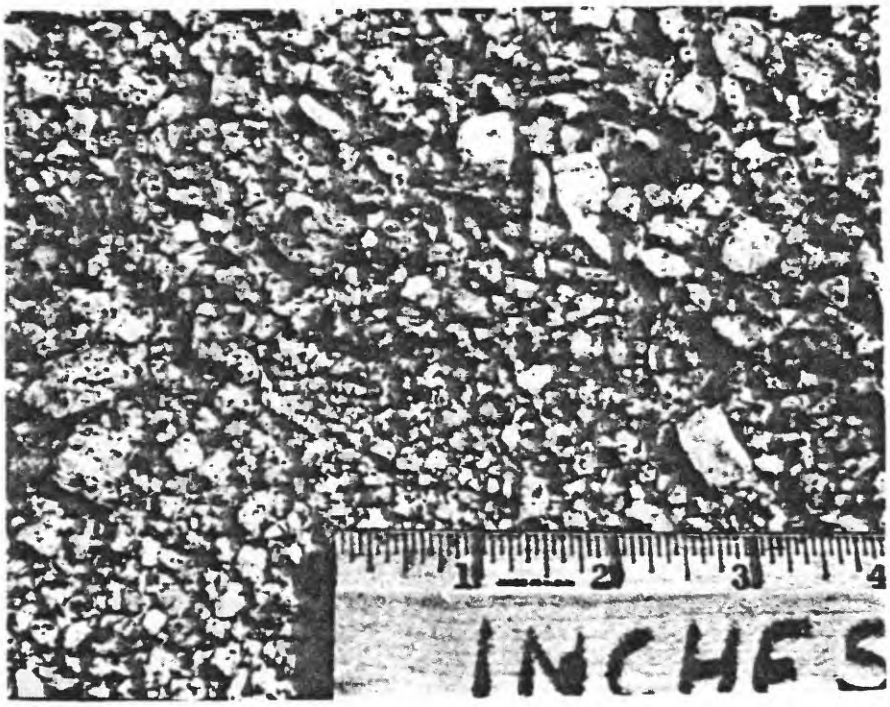

Figure 38.--Close-up view of grus derived from weathering of quartz monzonite; grus accumulates in joint cracks and swales in rock surface, Sonora Pass site, Mono County, California.

only locally present in the quartz monzonite.

Drill Hole Sonora Pass 1

Drill hole Sonora Pass 1 is located in the SE 1/4, sec 6, T.5N., R.22E., Mt. Diablo Base Line and Meridian (see fig. 36). Drilling was begun on August 6, 1965, and completed on August 13, 1965, at a depth of 12.2 m. Elevation at the collar of the hole is approximately 2,585 m above mean sea level. Average rate of NX diameter core drilling was 33.6 cm per hour and core recovery was 98 percent. Ground water entered the hole through joints in the rock between 1.8 and 2.7 m.

Petrography

General description

Large phenocrysts of pink microcline set in a medium-grained groundmass are megascopically visible. Biotite, plagioclase, quartz, and sphene can also be recognized. The rock has a holocrystalline, granular texture of interlocking grains typical of plutonic rock. The color is somewhat mottled due to the large pink phenocrysts and to black biotite grains, but is predominantly white in slightly weathered rock and faint bluish gray in fresh rock. Microscopically, the texture is hypidiomorphic-granular. Plagioclase is locally marked by myrmekitic texture, and microcline sometimes shows perthitic texture. Grain size averages 3 mm. Modal analyses and texture indicate the rock is a porphyritic quartz monzonite.

Microcline

Megascopically, microcline occurs as large phenocrysts of grayish pink color which are anhedral and rectangular in shape with a maximum size of about 10 cm in length by 5 cm in width (see fig.39). Phenocrysts contain inclusions of plagioclase, biotite, magnetite, and sphene. Microscopically, a grid-twinning is characteristic but is not always present and two good cleavages almost at right angles can be observed in some crystals. The mineral surface in plane light, shows clots of dust-like sericite particles particles that are elongated along one of the cleavage directions (fig. 40). Perthitic texture is formed in some crystals by lenticular wormy inclusions of sodic plagioclase; perthitic structure in other thin sections consists of oriented rounded blebs of plagioclase (fig. 41). Plagioclase is the most abundant inclusion found in the microcline phenocrysts. Average grain size of the microcline is about 5 mm.

Quartz

Megascopically, quartz occurs as colorless, transparent to light gray crystals with anhedral crystal development and equant to elongated shapes. Crystals reach a maximum size of about 15 mm. Microscopically, the quartz crystals are usually equant and anhedral. The grains contain irregular fractures and frequently show undulose extinction. Average grain size is 3 mm. The irregular fractures are commonly filled by sericite or fine-grained biotite. Veinlets of sericite may cut across and through several quartz

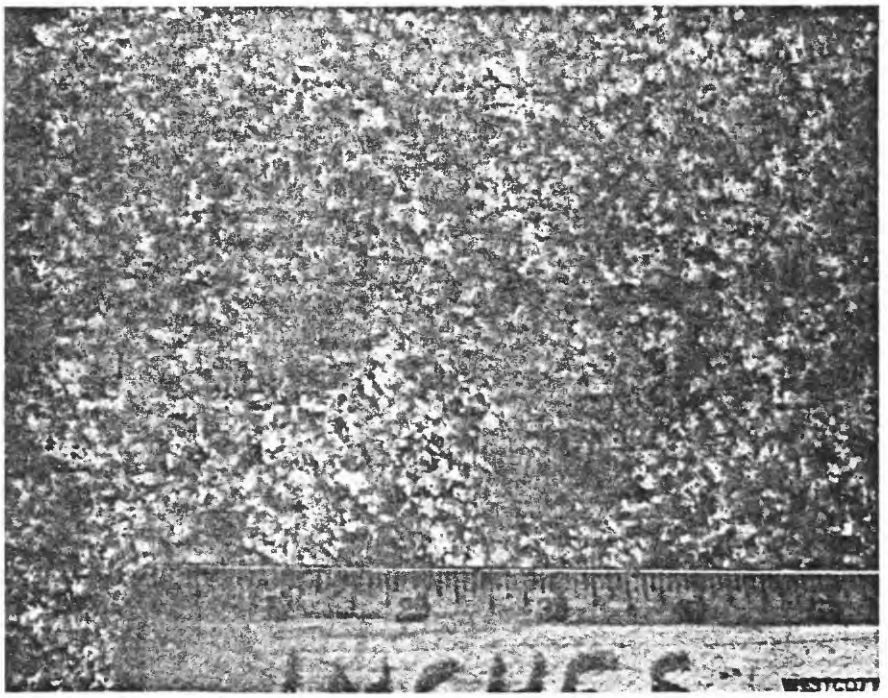

Figure 39.--Close-up view of weathered quartz monzonite surface. Note microcline phenocryst at upper left. Sonora Pass site, Mono County, California.

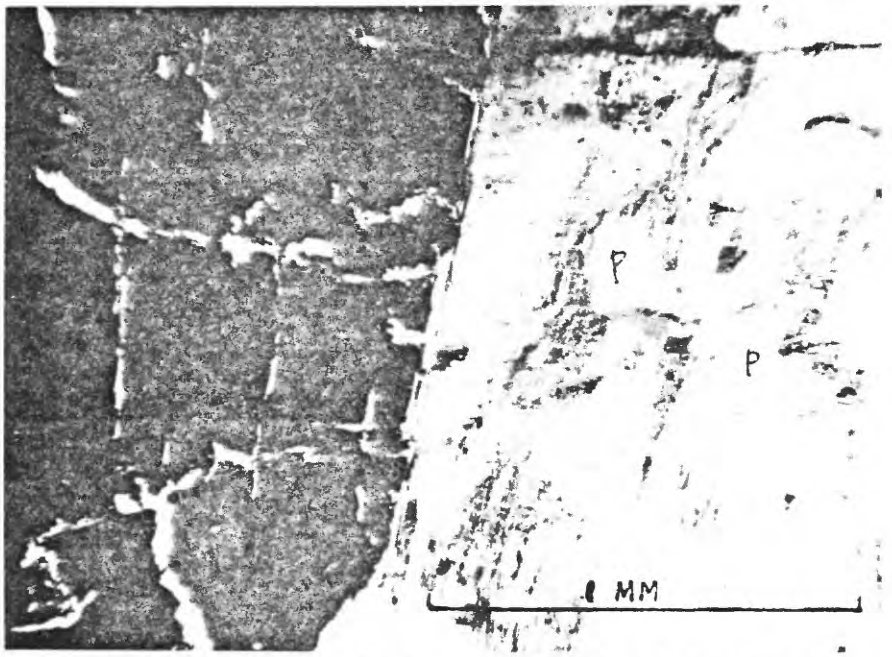

Figure 40.--Photomicrograph shows microcline (right) and quartz (left). Irregular fractures in quartz are filled with sericite: dark streaks in microcline are sericite; inclusions of plagioclase (p) in microcline. Crossed nicols. Sonora Pass 1.

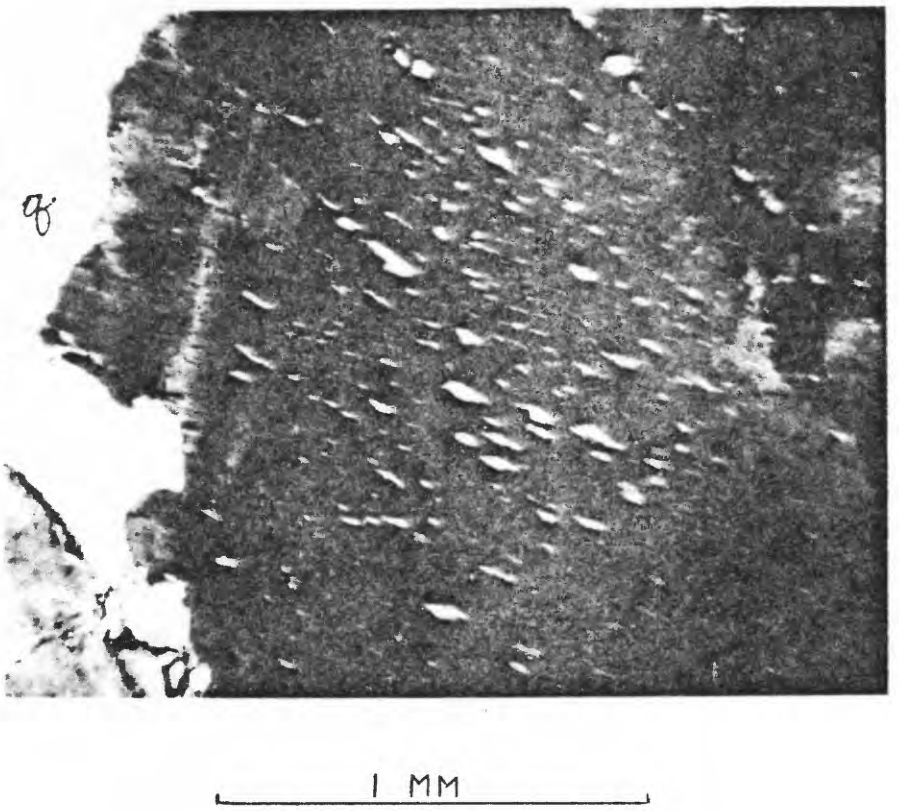

Figure 41.--Photomicrograph shows perthitic texture in microcline. Crossed nicols. Sonora Pass 1.

crystals and appear to be stopped at the contact with microcline (fig. 42). Myrmekite texture occurs locally where plagioclase contacts microcline and consists of vermicules of quartz.

Two generations of quartz seem to exist in the rock. Younger quartz can be observed to cross-cut older quartz (fig. 42).

Plagioclase

Megascopically, plagioclase occurs as white, euhedral to subhedral, translucent, elongated, striated crystals averaging about 3 mm in length. Microscopically, albite twinning and carlsbad twinning are characteristic of the mineral. The crystals usually show strong zoning and undulatory extinction. Stringer-like veinlets of sericite or fine-grained biotite are generally oriented parallel to each other and cut across the albite twinning. Cores of some crystals are sericitized (fig. 43). Plagioclase contains inclusions of optically dissimilar equant plagioclase, prismatic amphibole, sphene, and quartz. Plagioclase crystals usually show myrmekitic structure where grains are in contact with microcline (fig. 44). Minor amounts of plagioclase occur as zoned inclusions in microcline averaging 0.5 to 1.0 mm. Extinction angles measured on combined albite-carlsbad twins cut normal to (010) indicate that the composition of the zoned plagioclase ranges from cores of An_{30} to rims of An_{22}.

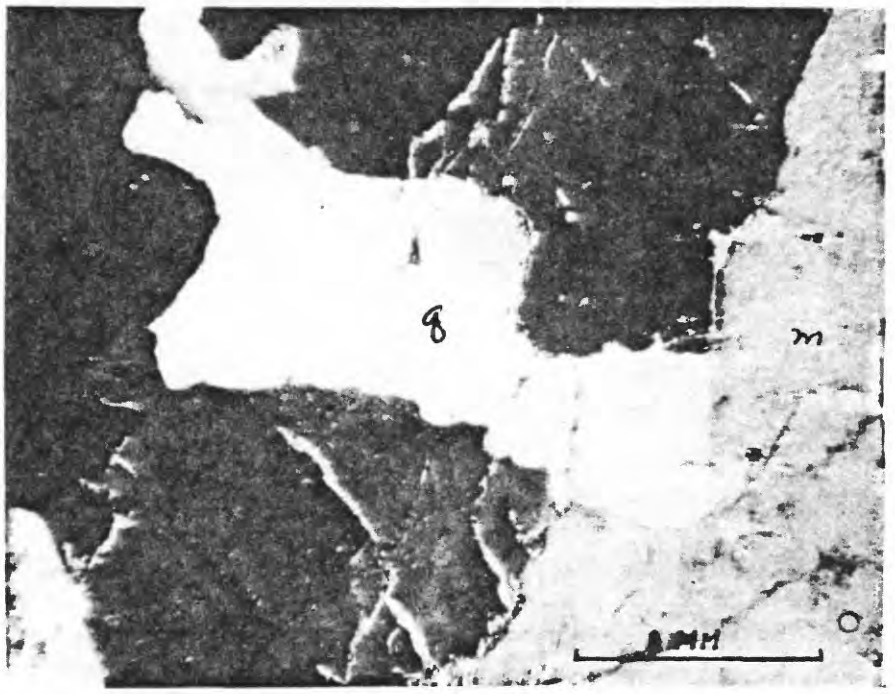

Figure 42.--Photomicrograph shows quartz (q) intruding earlier quartz and microcline (m). Sericite veinlets cut early quartz as well as late quartz. Crossed nicols. Sonora Pass 1.

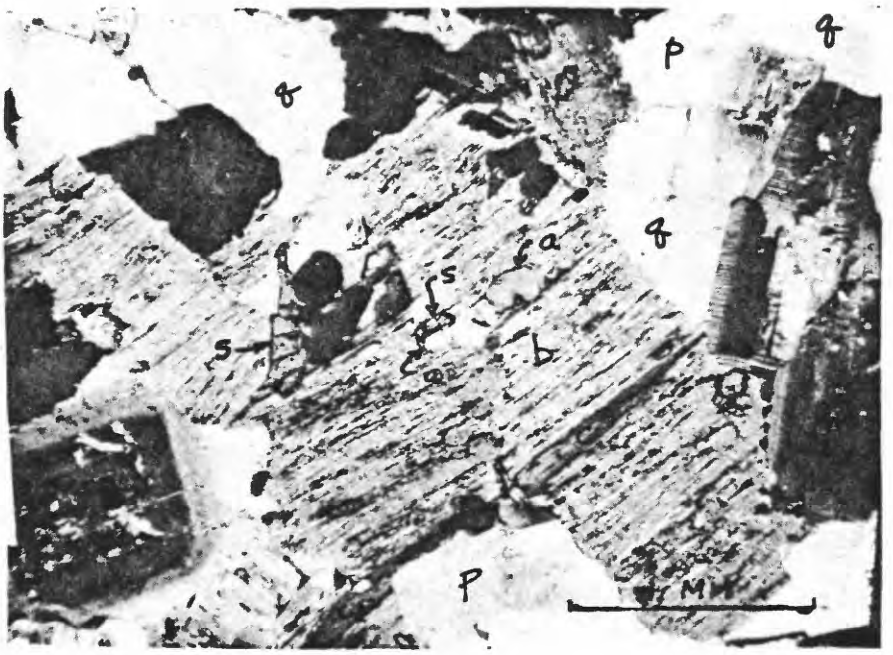

Figure 43.--Cluster of biotite (b), chlorite (c), sphene (s), magnetite (opaque), plagioclase (p) and apatite (a). Note zoning in plagioclase crystals. Partially crossed nicols. Sonora Pass 1

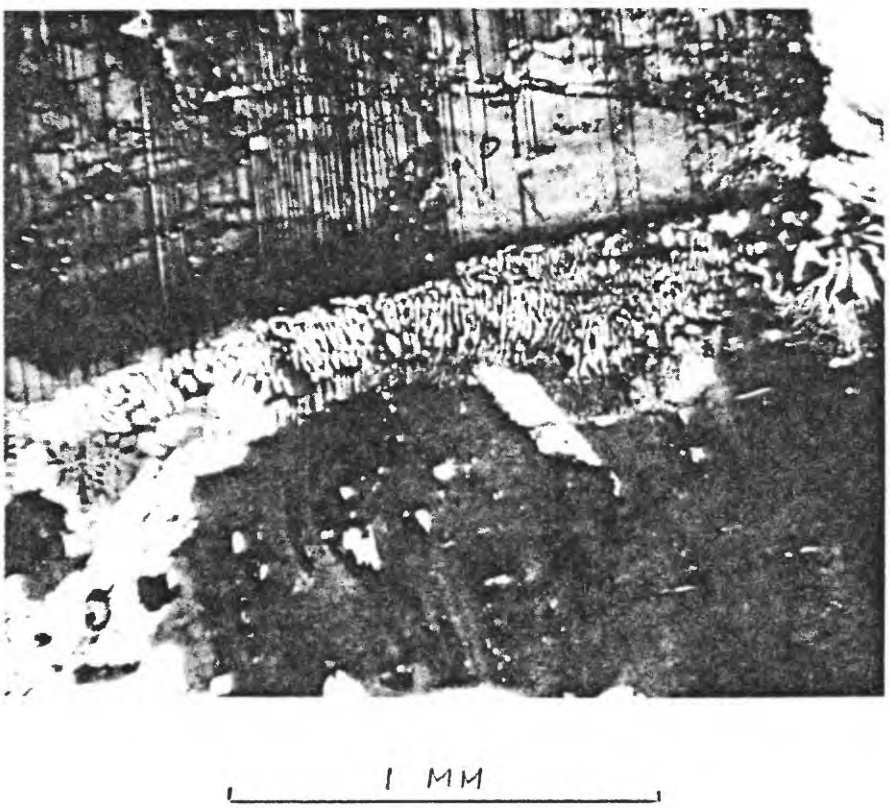

Figure 44.--Photomicrograph shows myrmekite texture in plagioclase (p) at contact with microcline (m). Crossed nocols. Sonora Pass 1.

Biotite

Megascopically, biotite occurs disseminated throughout the rock as irregular-shaped knots or lenses and smaller books. Knots average 5 mm in diameter; individual books average about 1 mm. The biotite sometimes shows euhedral hexagonal outlines. The color is greenish black to black. The mineral also occurs in minor quantity as inclusions in quartz and microcline. Alteration to chlorite has taken place along some foliation planes of the biotite. Microscopically, biotite usually occurs as anhedral, elongated flakes with irregular angular outlines. Alteration to chlorite is visible along some cleavage planes. Inclusions of sphene, apatite, and magnetite are fairly common. Fine-grained biotite or sericite fills some of the minute fractures in quartz, plagioclase, and other minerals. In one instance, the fractures seem to emanate from a flake of biotite.

Sphene

Megascopically, sphene occurs as dark yellowish orange, subhedral to euhedral, transparent crystals. The crystals average 0.5 mm,and reach a maximum size of about 2 mm. Sphene is usually closely associated with biotite,but occurs as individual inclusions in quartz and microcline. Microscopically, sphene usually occurs in clusters with magnetite and biotite. Crystals are mostly euhedral and lozenge-shaped, but a few crystals are prismatic. Sphene occurs as inclusions in biotite, plagioclase, quartz, and microcline.

Magnetite

Megascopically, magnetite is difficult to identify because of the small grain size. Microscopically, the mineral occurs in equant, anhedral to subhedral grains averaging 0.2 mm in diameter. It usually occurs in clusters of several grains (fig. 43), closely associated with sphene and biotite. Magnetite also occurs as inclusions in sphene and is sometimes found as discontinuous lenses along the foliation planes in biotite and chlorite, where it is probably the result of a deuteric chemical reaction.

Apatite

Apatite is difficult to recognize megascopically because of the small grain size. Microscopically, it occurs sparsely as euhedral hexagonal crystals or in prisms ranging from 0.1 to 0.3 mm in size. The inconspicuous crystals are closely associated with clusters of magnetite, sphene, and biotite (fig. 43).

Amphibole

Amphibole is not readily identifiable megascopically due to scarcity of the mineral and the small grain size. Microscopically, amphibole is closely associated with chlorite, biotite, sphene, and magnetite. It occurs in colorless prismatic forms or anhedral elongated masses from 0.1 to 1 mm in length. It forms cores of some plagioclase crystals, or occurs in plagioclase and microcline as inclusions.

Chlorite

Megascopically, chlorite is visible as a greenish alteration product that occurs along the cleavage planes in biotite. Microscopically, the chlorite laminae have sharp contacts with the biotite, but tend to wedge out in short distances (fig. 43). Chlorite comprises approximately 5 percent of the biotite.

Mode and classification

Modal analyses were made by averaging 3 vertical and 3 horizontal traverses across each thin section with a mechanical stage. The results are presented in table 7 . Mineral composition of the rock indicates a classification of quartz monzonite, while the phenocrysts of microcline indicate a porphyritic texture.

Physical Properties

The average of the physical properties measurements of the quartz monzonite from the test site are as follows (Roach and Johnson, 1966):

Dry Bulk Density (g per cc)	2.62
Saturated Bulk Density (g per cc)	2.64
Grain Density (g per cc)	2.67
Total Porosity, percent	1.8

The rock is uniform in physical properties but is jointed and affected by exfoliation and unloading. The petrography and geologic occurrence of the rock indicate a uniform composition

Table 7.--Petrographic modal analyses, Sonora Pass drill hole 1, Mono County, California.

[Qtz = quartz, Micro = microcline, Plag = plagioclase, Biot = biotite, Sph = sphene, Mag = magnetite, and Amph = amphibole (Percent by volume)]

Depth (meters)	Qtz	Micro	Plag	Biot	Sph	Mag	Amph
1.6	27.2	38.6	31.2	2.0	0.5	0.1	0.4
3.0	20.9	27.0	48.9	2.7	0.3	0.2	---
4.6	42.55	27.6	27.0	2.8	---	0.05	---
7.6	41.3	21.8	33.5	2.0	0.6	0.8	---
10.8	18.7	57.6	20.2	2.6	0.8	0.1	---
12.0	24.55	33.9	38.2	3.1	0.05	0.2	---
Average	29.2	34.4	33.2	2.5	0.4	0.2	0.1

and texture typical of a batholitic rock. Some variation in rock properties may occur near margins of the pluton.

Seismic Properties

The seismic velocity in the quartz monzonite is a uniform 5,000 meters per second. This velocity is the highest encountered at any of the test sites (Godson, Watkins, and Loney, 1965) and is typical of unweathered granitic rock.

References

Bateman, P. C., Clark, L. D., Huber, N. K., Moore, J. G., and Rinehart, C. D., 1963, The Sierra Nevada batholith--A synthesis of recent work across the central part: U. S. Geol. Survey Prof. Paper 414-D, 46 p.

Godson, R. H., Watkins, J. S., and Loney, R. A., 1965, Velocities and attenuation of head wave amplitudes observed in lunar analog rocks, in Investigation of in situ physical properties of surface and subsurface site materials by engineering geophysical techniques--Project ann. rept., FY 1965: Flagstaff Arizona, U.S. Geo. Survey, Br. of Astrogeology, p. F1-F25.

Roach, C. H., and Johnson, G. R., 1966, Field verification of in situ physical properties; in Investigation of in situ physical properties of surface and subsurface site materials by engineering geophysical techniques--Project quart. rept., October 1, 1965-December 31, 1965: Flagstaff, Arizona, U.S. Geol. Survey, Br. of Astrogeology, p. 9-46.

Ross, Donald C., 1958, Igneous and metamorphic rocks of parts of Sequoia and Kings Canyon National Parks, California: California Dept. Nat. Resources Div. Mines, Special Report 53, 24 p.

Wahrhaftig, Clyde, 1965, Stepped topography of the southern Sierra Nevada, California: Geol. Soc. America Bull., v. 76, p. 1165-1190.

(page 115 follows)

PETROGRAPHY AND GEOLOGY OF BISHOP TUFF AND MONO ASH SITES, CALIFORNIA

by David V. Haines

ABSTRACT.--Two test sites, selected on the basis of geologic lunar analogies, indicate petrographic and physical characteristics pertinent to lunar exploration and interpretation of lunar terrains.

The Bishop Tuff site is located on a gently sloping, predominantly flat tableland broken by northerly-trending faults and underlain by Pleistocene Bishop Tuff in a youthful stage of erosion. A thin regolith overlies the tuff. Steep fault scarps, angular breccia on the ground surface, and wind-deposited sand impede foot or vehicle movement. Drilling indicates the presence of well-indurated tuff to 18.6 m, underlain by unconsolidated ash.

The Mono Ash site is located on a gently sloping, predominantly flat surface underlain by pyroclastic debris derived from the adjacent Mono Craters. The surface soil is loose, dry lapilli ash of Late Pleistocene to Recent age, and is underlain by similar moist soil. The lapilli ash consists chiefly of pumice fragments and has an approximate dry density of 1.26 g per cc and a void ratio of 0.85. Cone penetrometer tests indicate that the relative density is fairly uniform except on two embankments that cross the test site and on small pumice sand dunes at the margins of the site.

Excavation of the lapilli ash is easy but large blocks of pumice may be found scattered through the deposit. Drill core shows the surface soil to be underlain by ash and consolidated pumice to a depth of 47 m. Occasional beds of clastic sand, up to 3.7 m thick, are interbedded with the pumice and ash and represent deposits formed in pluvial Lake Russell. Tuff (probably equivalent to the previously mentioned Bishop Tuff) occurs below a depth of 47 m. Strongly eutaxitic texture, spherulitic structure developed in pumice inclusions, and flattened lenses containing obsidian indicate higher temperature and pressure conditions during deposition than occurred at the Bishop Tuff site. Petrographic features can be correlated with higher bulk density and lower porosity of the tuff at the Mono Ash site.

Introduction

This report describes the (1) petrographic characteristics of the Bishop Tuff and other pyroclastic rocks as observed in rock thin sections prepared from drill core obtained at two widely

separated sites, (2) results of field measurements of cone penetration resistance, moisture content, and density of the surface soil, and (3) geology.

The sites are located near Bishop, California, (Bishop Tuff site) and in the Mono Basin area, California, (Mono Ash site) and were selected because of possible analogies to parts of the lunar surface. The Bishop Tuff site is an example of a surface covered by pyroclastic tuff and may be analogous to proposed lunar vacuum welding. The Mono Ash site is an example of a surface covered by low-density lapilli ash. Surfaces at both sites are relatively unweathered and uneroded.

Core was obtained from one NX-diameter drill hole at each site. Core logs are given by Elmer and Walters, Appendix A, in this report. Seismic surveys were carried out in the summer and fall of 1964. Brief geologic examinations and physical measurements at the sites were made in April 1966.

The test site is located a few miles north of Bishop, California, on a volcanic plateau underlain by the Bishop Tuff Formation. The southern edge of this plateau or tableland is marked by a steep escarpment about 61 m high (fig. 45). Elevation ranges from 1,260 m above mean sea level (MSL) at Bishop to 1,362 m above MSL at the test site, which is approximately 1.6 km north of the escarpment, in sections 13 and 14, T. 6 S., R. 32 E., Mt. Diablo BL & M. Much of the surface of the tableland is comparatively flat and gently sloping toward the east and southeast. The tableland has an east-west width of about 24 km and extends in a north-south direction

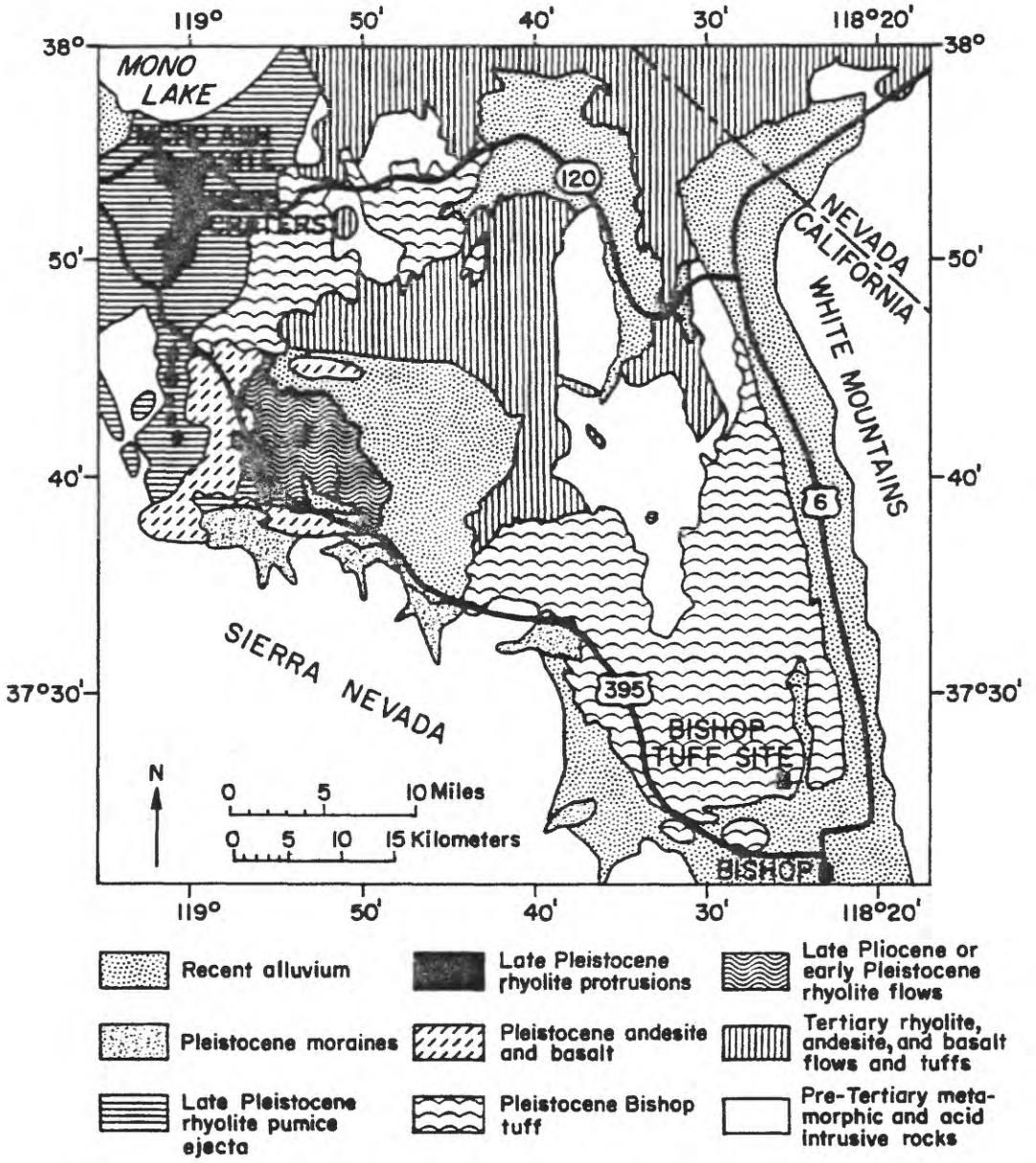

Figure 45.--Generalized geologic map, vicinity of Bishop Tuff site and Mono Ash site (after Gilbert, 1938).

for about 29 km. The Pleistocene Bishop Tuff occurs elsewhere outside of the tableland shown in figure 45 chiefly in similar tablelands west of Adobe Valley and southeast of Mono Lake. The total area covered by the Bishop Tuff amounts to about 1,040 sq km. The formation is believed to have originated as a highly mobile nuée ardente which had a source possibly in Long Valley (Gilbert, 1938). The tuff averages between 122 and 152 m thick having a total volume of about 143 cu km. Fault trends observed at the Bishop Tuff site parallel those of the nearby Sierra Nevada and White Mountains and are believed to be controlled by faults in the older rocks underlying the tuff (Gilbert, 1938).

The Bishop Tuff is a massive rock, more or less uniform in appearance. Bedding is generally absent or poorly developed. Where obscure and gradational bedding has been noted (Gilbert, 1938) the time interval between deposition was probably short. Potassium-argon dating indicates an age of 700,000 years for Bishop Tuff (Dalrymple, Cox, and Doell, 1965).

The upper surface of the tuff is characteristically flat, and columnar jointing is commonly present. Margins of the formation are often marked by steep, abrupt escarpments.

Geology

The test site is generally flat with a gentle slope toward the southeast. Minor undulations of sharp declivities in the slope are caused by relatively short northerly-trending faults which are probably normal and steeply dipping. Weathering prevents identification

of fault features indicative of movement, but height of rock faces along faults suggests that maximum vertical movement may exceed 10 m. The fault pattern resembles horst-and-graben structure.

Figure 46 is an aerial photograph of the test site and adjoining areas; figure 47 is a surface photograph of the site. Eight faults in the test site area are indicated (A through H) and are shown in figure 46 which also includes locations of seismic lines.

Water.--Surface water was not observed on the test site nor was subsurface water encountered in Bishop drill hole 1 which terminated at a depth of 58.5 m. Pore properties of the tuff tend to make it a poor aquifer.

Rock and soil conditions.--The surface of the ground at the seismic survey site is covered by numerous subrounded to angular fragments of well indurated, pitted tuff up to 1.2 m in length, but averaging 12.5 cm (fig. 48). Fragments are usually equant but a minor amount of platy fragments occur. The interstitial space between the boulder- and gravel-size fragments is filled by micaceous sand, silty sand, and sandy silt. The upper 2-5 cm of the ground surface seems to be wind-winnowed of the finer particles, so that the interstitial soil is predominantly sand. A few centimeters below the ground surface, however, the proportion of silt increases and the soil is essentially an undisturbed sandy silt. The overlying sand seems to be chiefly a wind-winnowed semiresidual soil. Accumulations of wind-deposited sand occur along the base of the fault scarps, and cover a large area west of fault A. Examination of a sample of sand trapped in joints along fault G shows that it

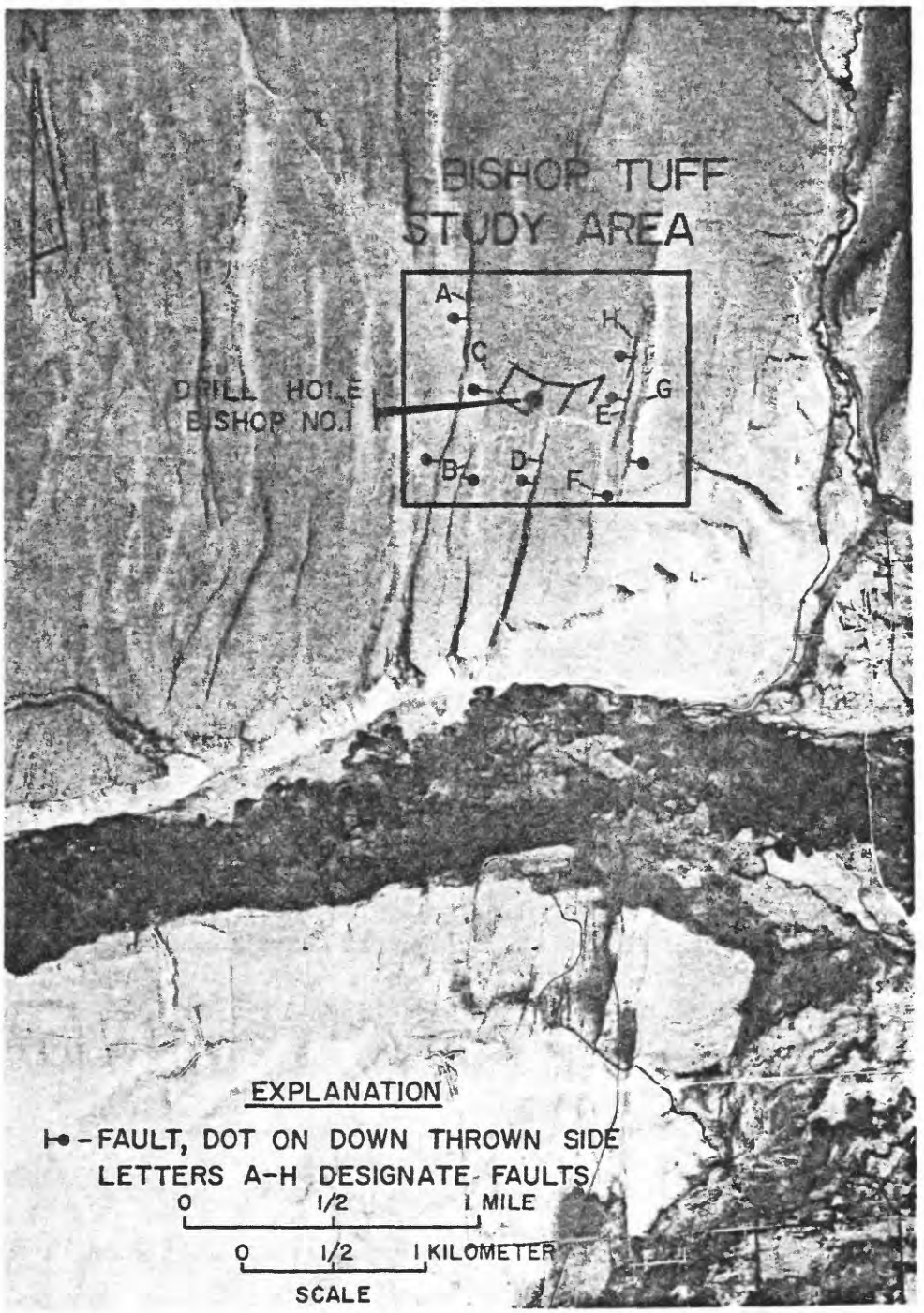

Figure 46.--Aerial photograph showing faults, drill-hole location, and seismic spread layout, Bishop Tuff site, California.

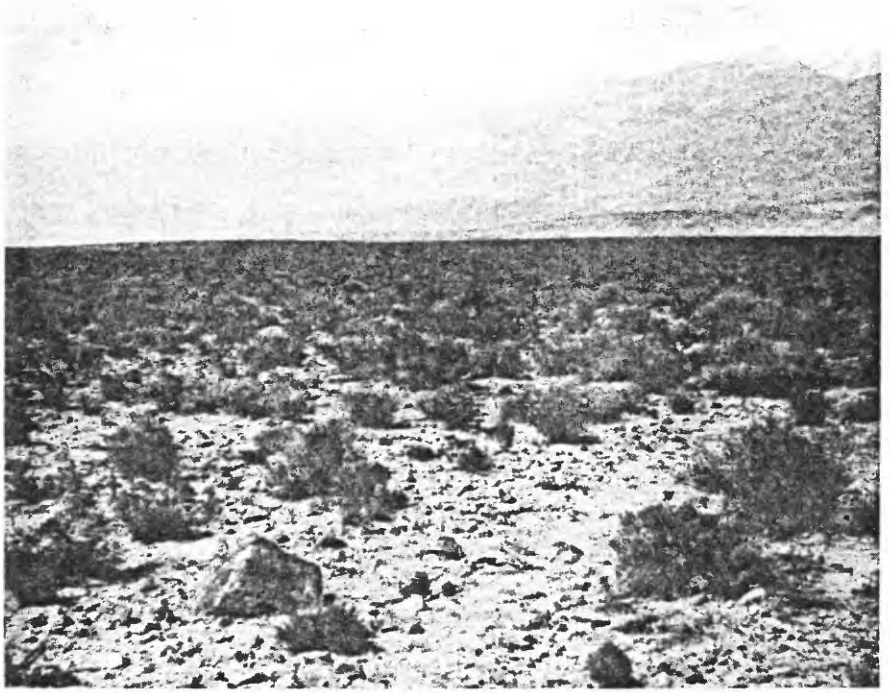

Figure 47.--View looks north across area of seismic survey toward the White Mountains, Bishop Tuff site, California.

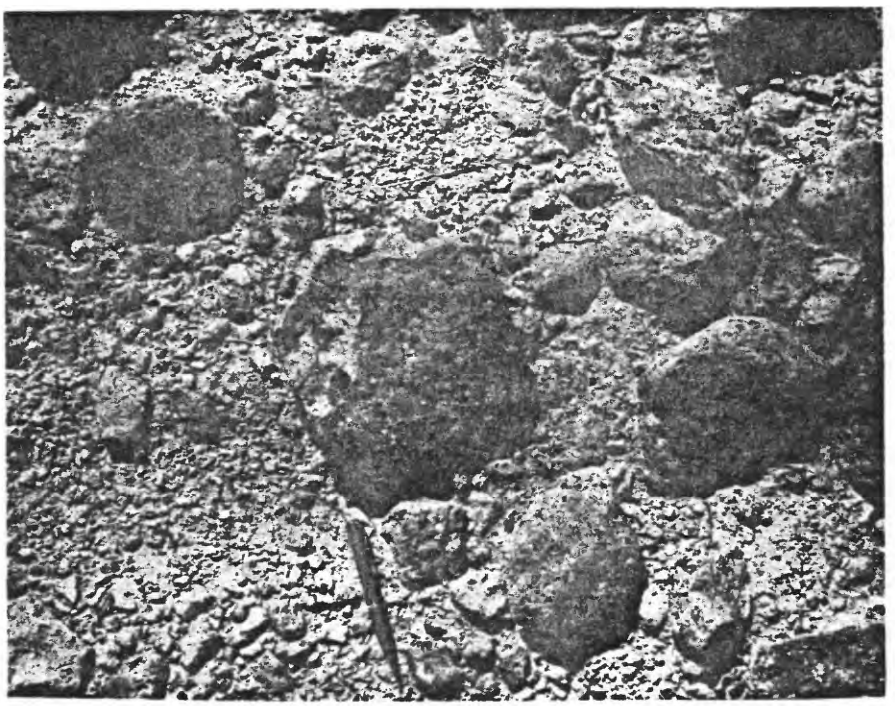

Figure 48.--Vertical view of ground surface at seismic survey site showing fragments of Bishop Tuff. Pencil is 10 cm long.

consists of medium sand made up of 75 percent quartz and sanidine; 20 percent pumice and tuff; 3 percent magnetite; and a small amount of biotite, ferromagnesian minerals, obsidian, and olivine. The composition of the sand indicates that it is derived from the Bishop Tuff.

The regolith at the test site averages about 20 cm deep and lies on the flat upper surface of relatively undisturbed Bishop Tuff. Joints are filled with regolith that probably extend down several feet.

A bulldozed area on the test site exposed tuff coated with clay, and these exposures also are locally coated or encrusted with caliche. A test pit dug on the site showed that gravel and larger-sizes (over 7.5 cm) make up about 50 percent of the regolith and sandy fines make up the remaining 50 percent. Moisture was encountered 15 cm below the ground surface. A large boulder or bedrock surface was found at a depth of 20 cm on one side of the pit and another rock surface at a depth of 48 cm on the other side of the pit. A weathered clayey silt zone having discontinuous lenses and stringers of caliche was found at depths ranging from 40 to 50 cm.

Weathering.--Pits up to 2.5 cm long (fig. 49) usually occur in fragments in the tuff of the regolith and exposures of tuff along the fault scarps. These pits are due to weathering out of certain constituents of the tuff, chiefly pumice inclusions. Such pits occur in drill core to depths of about 7.7 m, but may have been accentuated by drilling vibrations. Pits are not found in fresh rock.

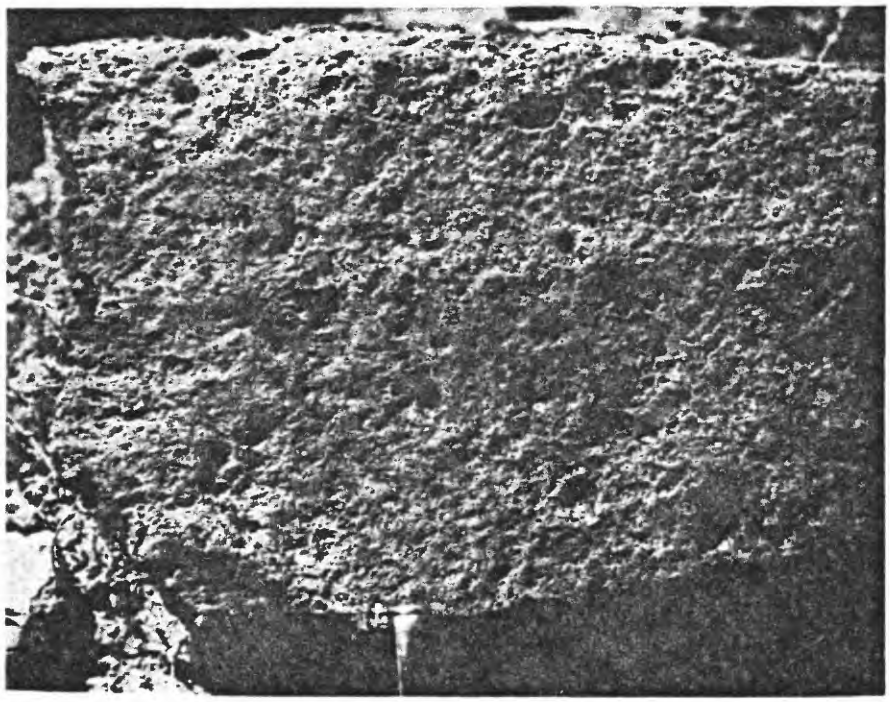

Figure 49.--Close-up view of weathered pits in Bishop Tuff specimen.

Lack of significant chemical weathering in the sand grains examined from fault scarp G suggests that the exposed tuff breaks down chiefly by mechanical means but chemical weathering is evidenced by clay coatings on tuff in the bulldozed area and clayey silt found near the bottom of the test pit.

Tuff exposed along faults consists generally of large rounded boulders which show marked exfoliation and effects of wind erosion. Rock surfaces are frequently covered by desert varnish. Severe weathering has affected the rock to a depth of 1-2 cm, but depth of weathering can be greater in outcrops where exfoliation is well developed. Curvilinear and spheroidal fractures cutting entirely through some large boulders may be related to exfoliation. Exfoliation plates are usually 2.5 cm thick, can be pried loose from the rock in many places, and locally pave the regolith.

Tuff a few meters below the surface is massive and relatively unjointed in a small quarry near the test site.

Cone penetrometer tests.--Cone penetrometer tests were not possible in the rocky soil at the site of the seismic survey.

Bishop Drill Hole 1

Bishop drill hole 1 is located in the NE 1/4, sec 14, T6 S, R32 E, Mt. Diablo BL & M, Inyo County, California (fig.46). The vertical hole was spudded in on September 9, 1965, and completed on September 17, 1965, at a depth oi 58.6 m. Drilling was begun by reaming through 0.3 m of rocky soil and 1.5 m of tuff in order to accommodate the 1.5 m long coring barrel. Coring was attempted

from 1.8 to 3.5 m deep using air circulation and a carbide bit, but the core was ground up. The cuttings consisted of tuff. The carbide bit at 3.5 m was removed and replaced by a 3 3/4-inch outside diameter, 2 1/8-inch inside diameter NX diamond core bit. Core recovery to a depth of 18.9 m ranged from 90 to 100 percent with this bit. Unconsolidated ash was encountered and core recovery fell to zero. Drilling mud was then placed in the hole and core recovery ranged from zero to 100 percent, averaging 52 percent, to the bottom of the hole. The core log is shown in Appendix A (Elmer and Walters).

Tuff from the Bishop Tuff Site

The rock is moderately well indurated in the upper 18.3 m. An aphanitic matrix with minor amounts of crystals and inclusions is the most prominent feature of the rock. The rock is unconsolidated ash below 18.9 m, and extends to the bottom of the hole at 58.6 m.

Induration.--The rock can easily be scratched by a knife blade and, below 9.0 m, the rock leaves a powdery or dusty coating on the hand when handled. Core emits a dull thud rather than a ringing sound when struck by a hammer. The rock became dented under the hammer, but usually did not fracture (Gilbert, 1938, p. 1835). These properties are probably due to the very fine grained particles of the matrix, to the relatively loose packing structure of the particles, and to weak cementation of the upper few feet of the tuff.

Texture.--The texture of the matrix is microfelsitic and the luster is dull. Under 15 X or more magnification, texture is felted, particulate, and consists largely of randomly oriented minute rod-shaped or plate-like glassy fragments. Disseminated throughout the matrix are relatively large and abundant crystals of sanidine up to 2.5 mm in diameter and inclusions of pumice up to 20 mm in diameter (figs. 50, and 51). Pumice fragments are elongated and oriented in subhorizontal layers. The structure is slightly eutaxitic. Cavities are present, mostly in the upper 6 m, and make up about 12 percent of the rock at a depth of 3.5 m. The cavities are partly filled by fragments of pumice. The groundmass contains sparsely disseminated flakes and small books of biotite averaging about 1 mm long. Occasional rock fragments also can be observed in the matrix. A small amount of quartz, plagioclase, obsidian, and pyroxene occur in the matrix as relatively large grains, averaging about 0.5 mm in diameter. Very minute grains of magnetite and limonite are present throughout the matrix in small amounts.

Mode

Megascopic observations indicate a modal mineral composition as follows:

Groundmass, probably vitric	75 - 90 percent
Sanidine	5 - 10
Pumice fragments	5 - 15
Biotite, quartz	Less than 1

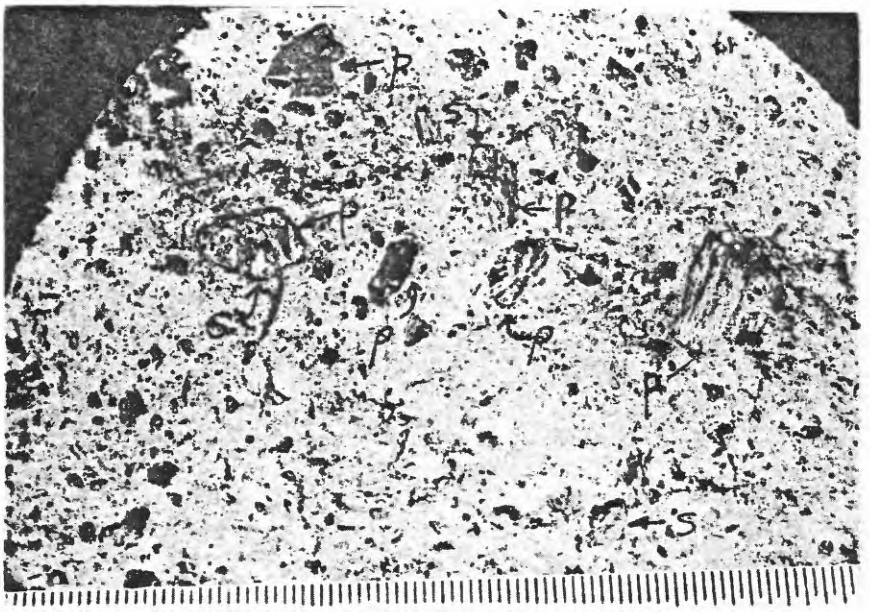

Figure 50.--Tuff from Bishop drill hole 1 shows horizontal fracture plane. Larger fragments are pumice enclosed in fine-grain glassy matrix containing sanidine crystals, quartz, and minor constituents. Scale is graduated in 0.5-mm divisions. 3.5 m deep.

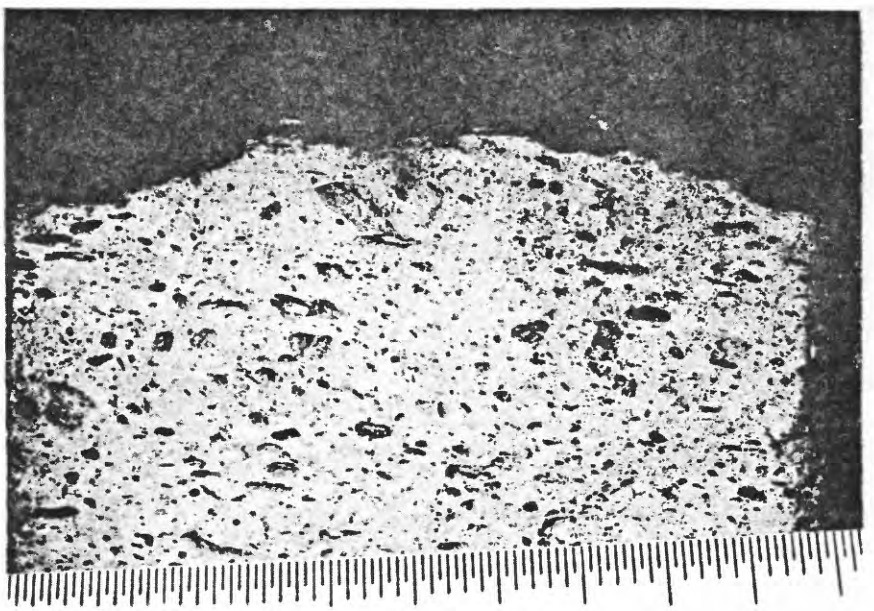

Figure 51.--Vertical section of tuff from Bishop drill hole 1. Sub-horizontal lenses of pumice set in fine-grain groundmass. Scale is divided into 0.5-mm divisions. 3.5 m deep.

Mineral Descriptions

Sanidine

Sanidine occurs in very clear, transparent, colorless crystals with a vitreous luster. Crystals are generally anhedral with uneven to conchoidal fracture surfaces. Subhedral crystals are fairly common and a few euhedral crystals were observed. Crystals range in size from 0.5 to 3 mm and are usually equant in shape. Cleavages intersecting at right angles can be observed in some crystals. Sparse white opaque spherulites can be seen as inclusions in a few crystals. Sanidine occurs either as discrete individual crystals set in the matrix of the rock in random locations, or as inclusions within pumice fragments that are randomly distributed throughout the matrix (figs. 52 and 53). Sanidine crystals may be as small as 0.1 mm, but average 0.5 mm in thin section. Clear glass occurs as rounded globules included within sanidine or as fillings of cracks in sanidine (fig. 54) and in some embayments. Similar occurrences of clear glass were also observed in quartz. Disorganized and broken carlsbad twins occur in some sanidine crystals and wavy extinction is common. Under crossed nicols, the crystal surfaces sometimes show a mosaic pattern of dark and light surfaces which is probably due to fracturing. Some sanidine crystals show rims or partial rims that extinguish at a slightly different angle from the main part of the crystal that indicates a slightly different composition in the rim material. Inclusions of biotite and plagioclase occur in some sanidine crystals.

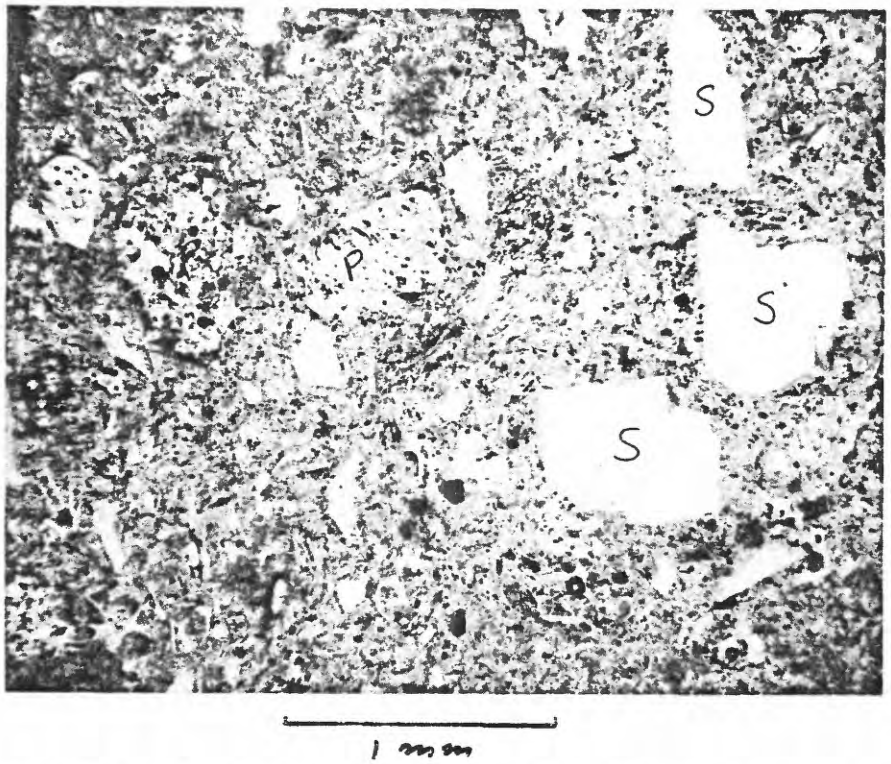

Figure 52.--Photomicrograph of Bishop(?) Tuff. Sanidine crystals (s) and pumice fragments (p) embedded in groundmass of glass shards. Plane light. 18.6 m deep.

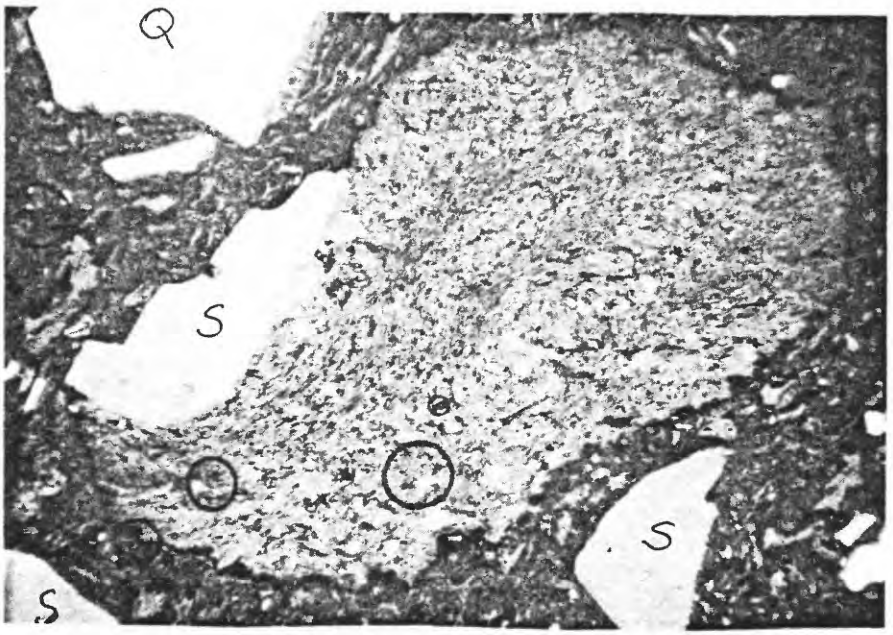

Figure 53.--Photomicrograph of Bishop(?) Tuff. Inclusion of sanidine (s) in pumice fragment. Quartz (q) at upper right is partially rimmed by clear glass. Partially crossed nicols. 9.1 m deep.

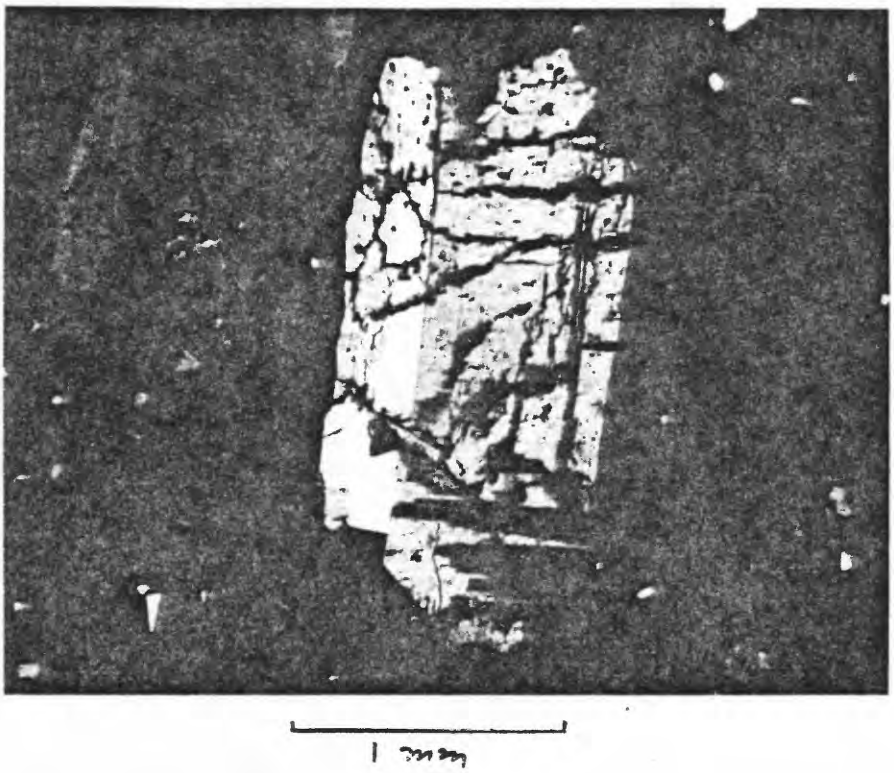

Figure 54.--Photomicrograph of Bishop(?) Tuff. Carlsbad twin of sanidine, fractured and filled with clear glass. Crossed nicols. 16.8 m deep.

Groundmass

The groundmass consists of colorless glass shards embedded in a moderate brown (5YR4/4) glassy matrix. Shards generally show curved and branching forms and the texture is vitroclastic, although a few fragments of vesicular glass with unbroken bubbles are present (fig. 55). Shards average about 0.1 mm in length, but may be as long as 1.1 mm. Elongated shards show a preferred horizontal orientation and are moderately aligned around pumice inclusions and crystals. At less than 7.5 m deep, larger shards and pumice fragments contain rims of low birefringent cryptocrystalline material representing devitrification products (fig. 56). With increasing depth, the thickness of the devitrified rims gradually decreases until, at a depth of about 7.5 m, the rims are no longer present. Rims may consist of elongated fibrous crystals oriented at right angles to the shard outline or pumice fragment boundary, or may consist of equant grains forming a mosaic or granular texture. Groundmass becomes lighter in color between 16.5 and 18.9 m, with slight devitrification in this interval as well as a decrease in the induration of the rock.

Pumice

Pumice fragments are distributed throughout the tuff and range up to 20 mm in length, but average about 1 mm. The pumice fragments in the horizontal plane present a variety of shapes (fig. 50), but many fragments in the vertical plane show lens-shaped cross sections

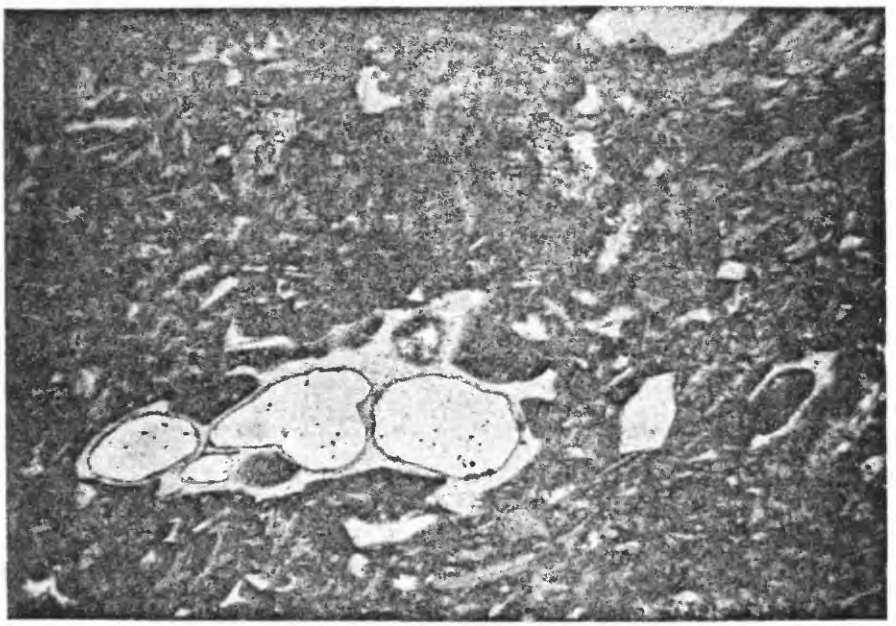

Figure 55.--Photomicrograph of Bishop(?) Tuff. Fragment of cellular pumice with large unbroken bubbles included in groundmass. Lath of biotite is at upper right. Plane light.

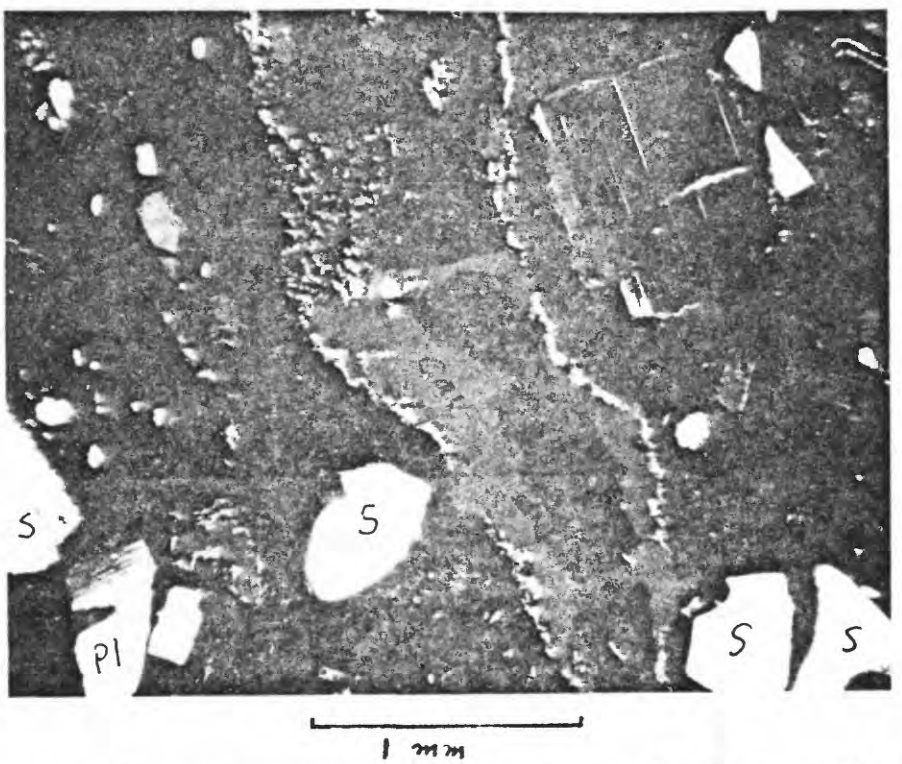

Figure 56.--Photomicrograph of Bishop Tuff. Fibrous pumice fragment outlined by devitrification products; note cavity (cav). Plagioclase crystal (Pl) to right of pumice is zoned. Partially crossed nicols. 3.5 m deep.

(fig. 51). Pumice fragments that are not flattened in the horizontal plane are fairly abundant. Pumice fragments above 6 m in depth, seem to be enclosed in vugs where much space partially surrounds each fragment (fig. 56). Pumice fragments below 6 m in depth, are tightly included in the matrix and lack the surrounding space found at shallower depths. Fragments consist of aggregates of parallel, closely-packed, slender fibers or tubes, or cellular masses containing vesicles and hollow bubbles of ovoid to rounded shape. Fibrous pumice in thin section, contains relatively little pore space compared to the cellular pumice (fig. 57).

Quartz

Quartz occurs as disseminated crystals throughout the matrix and as inclusions within pumice fragments (fig. 58). Crystals range in shape from irregular to euhedral, and are characterized by numerous curving fractures. Some crystals in thin section show an unusual mosaic-like texture of dark and light angular surfaces similar to that observed in some sanidine crystals, an effect believed caused by intersecting fractures. Quartz tends to show rounded outlines, and embayments and inclusions of glass are more common than in sanidine. Fractures in broken crystals are often filled with clear colorless glass (fig. 58). Quartz usually shows sharp extinction. Larger quartz crystals show partial rims of clear glass which, in some instances, have pumiceous texture (fig. 53).

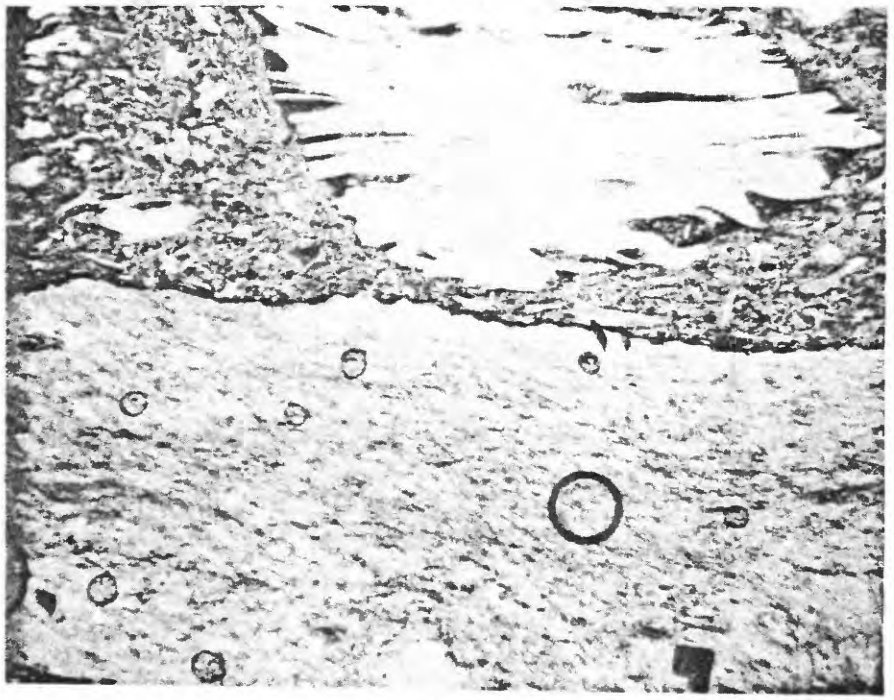

Figure 57.--Photomicrograph of Bishop Tuff. Fibrous pumice is below; cellular pumice is above. Plane light. 9.1 m deep.

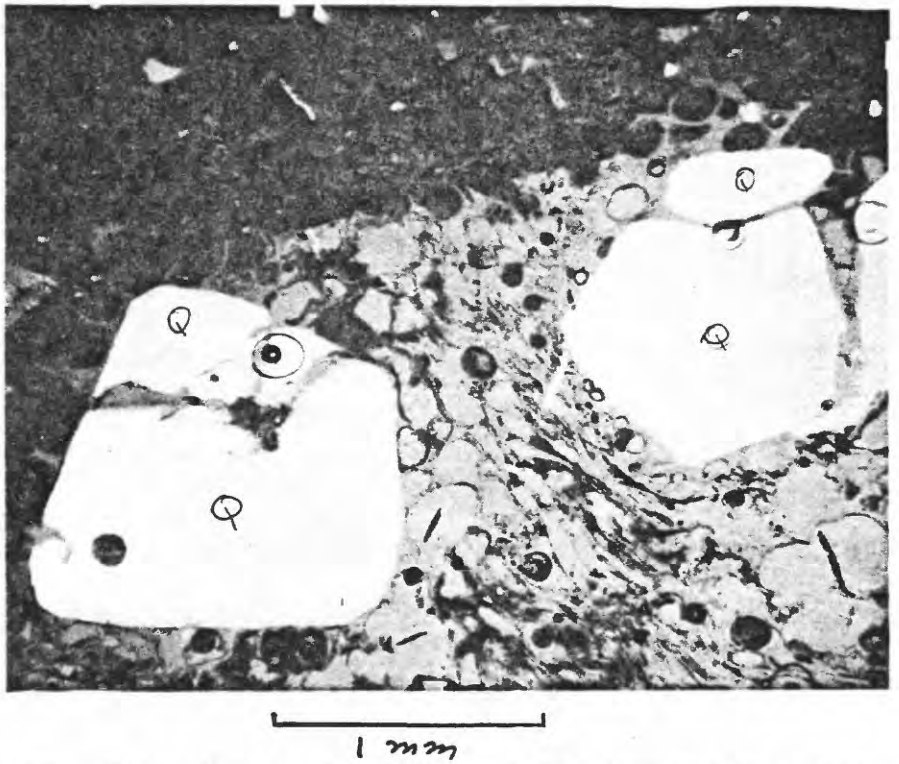

Figure 58.--Photomicrograph of Bishop Tuff showing two quartz crystals (q) included in cellular pumice fragments. Quartz crystals are broken and filled with clear glass. Partially crossed nicols. 15.2 m deep.

Plagioclase

Irregular to euhedral plagioclase crystals are disseminated in the matrix or associated with pumice fragments in a manner similar to that of sanidine and quartz. They occur as tabular shaped crystals which show combined carlsbad and albite twinning, or albite twinning only and wavy extinction is common. Plagioclase has been identified as oligoclase by Gilbert (1938). A few crystals are zoned, some are broken and filled by clear glass, and a few contain inclusions of biotite. Crystals are occasionally observed as inclusions in sanidine.

Biotite

Biotite occurs in minor amounts as small brown laths and plates averaging 0.2 mm in diameter scattered through the matrix, or it occurs as inclusions in pumice, plagioclase, and sanidine. Some laths are bent at one end and cleavage traces are wavy. Slight reaction rims, probably iron oxide, are present around the biotite fragments.

Pyroxene

Pyroxene occurs in minor amounts as black, anhedral to euhedral grains, disseminated through the matrix and as inclusions in pumice.

Obsidian

Obsidian in thin section is colorless, lacks vesicles, and occurs as individual grains in the matrix (fig. 59). It is often ~~irregularly fractured and shows no devitrification exeept for~~

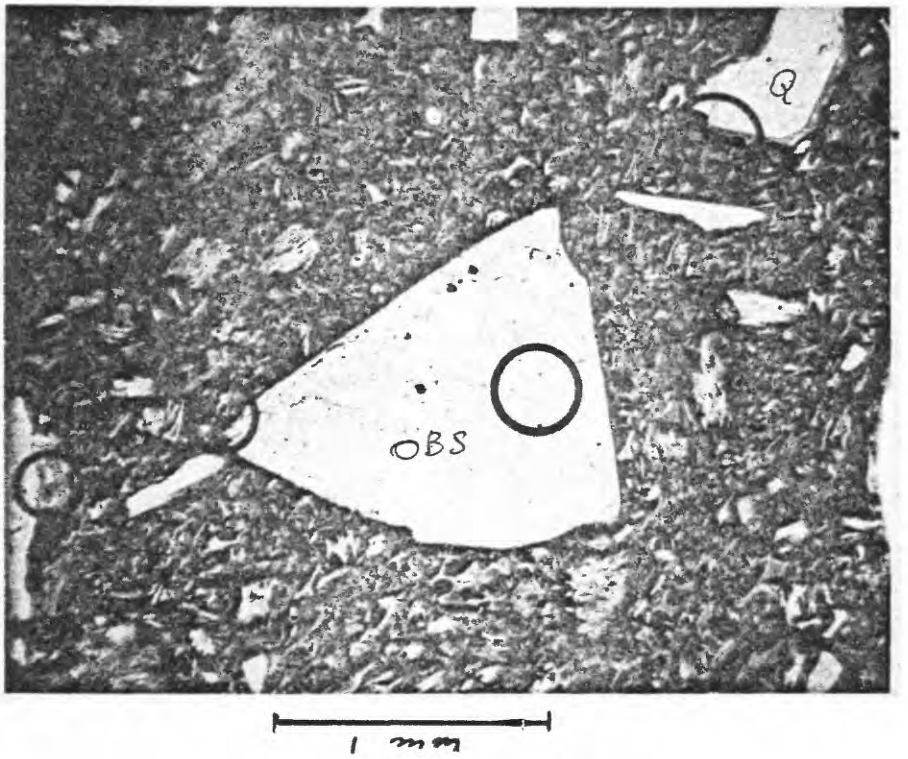

Figure 59.--Photomicrograph of Bishop Tuff shows angular-shaped grain of obsidian (obs) embedded in groundmass of glass shards. Note partial rim of glass around crystal of quartz (q). Plane light. 10.7 m deep.

incipient crystallites. Particle size ranges up to 2 mm.

Modal Composition

Modal analyses were calculated for each thin section by making vertical and horizontal traverses across each slide with a mechanical stage. Six traverses were made in each slide and results were averaged to obtain the mineral composition for that slide. All thin sections were oriented vertically. Results for each slide are tabulated in table 8. Average composition of the tuff indicates glassy groundmass, pumice fragments, and obsidian account for 89 percent of of the volume of the tuff, and crystals and cavities occupy 11 percent. The tuff can therefore be classified as a vitric tuff. Since crystalline minerals are mainly sanidine, quartz, and sodic plagioclase, the term rhyolitic has also been applied to the tuff. Devitrification products may account for up to 1 percent by volume of the rock at a depth of 3.5 m.

Table 8.--Summary of petrographic modal analyses from Bishop drill hole 1, California.

[Gm = groundmass, Pum = pumice, San = sanidine, Plag = plagioclase, Bio = biotite, Qtz = quartz, Pyro = pyroxene, Rock = rock, Obs = obsidian, and Cav = cavities (Percent by volume)]

Sample Depth (meters)	Gm	Pum	San	Plag	Bio	Qtz	Pyro	Rock	Obs	Cav
3.5	76.5	2.2	6.1	1.5	0.1	1.1	---	---	---	12.5
4.9	81.4	4.4	5.0	0.9	0.1	0.7	---	---	---	7.5
6.3	84.0	5.4	5.0	0.2	0.2	0.8	0.1	0.3	---	4.0
7.8	81.3	9.2	5.4	1.0	0.2	1.6	---	---	---	1.3
9.1	82.9	8.7	4.7	1.3	0.2	1.9	0.1	0.2	---	---
10.7	78.0	9.7	6.3	0.9	0.3	1.6	---	0.9	2.3	---
12.4	74.2	19.3	3.1	0.1	0.2	2.3	---	---	0.8	---
13.7	78.1	11.5	6.0	0.2	0.3	2.3	---	1.0	0.6	---
15.2	68.7	21.4	2.4	0.1	0.1	4.6	---	2.0	0.7	---
16.8	74.8	16.6	3.5	0.5	---	2.8	0.2	0.1	0.6	0.9
18.6	74.5	15.5	2.5	0.3	0.2	1.8	0.4	0.2	2.0	2.6
Average	77.7	11.3	4.5	0.6	0.2	2.0	0.1	0.4	0.6	2.6

Mono Ash site, California

The Mono Ash site is located in eastern California about one km south of Mono Lake (fig. 60) on a broad plain formerly covered by the waters of ancestral Lake Russell.

Volcanic activity during late Pleistocene time formed the Mono Craters, a series of rhyolitic obsidian domes and flows that extend 30 km south from Mono Lake in a nearly continuous chain. The domes are nearly circular with steep sides that are covered with talus. Explosive volcanic activity associated with the rise of the domes deposited pyroclastic debris as far east as 48 km (Putnam, 1949).

Geology

The test site is located near the south end of Mono Lake and east of the Mono Craters, in sections 27 and 34, T.1 N., R.27 E., Mt. Diablo Base Line and Meridian. Part of the test site lies between Northwest Coulee and Northern Coulee. State Highway 120 crosses the test area at a point 10.5 km from its junction with U.S. Highway 395 (fig. 60). Much of this area is underlain by tuff (probably Bishop Tuff of Pleistocene age).

The test site lacks appreciable vegetation and is flat to gently undulating with a gentle slope toward the north and northeast (fig. 61). Windblown sand dunes consisting of fine-grained pumice and obsidian fragments occur at the northeastern end of the test site, and reach a maximum height of about 2 m. Two embankments cross the test site trending approximately east-west. The southernmost embankment is the more prominent and averages about 2.5 m high (fig.62); the northern averages about 0.6 m high.

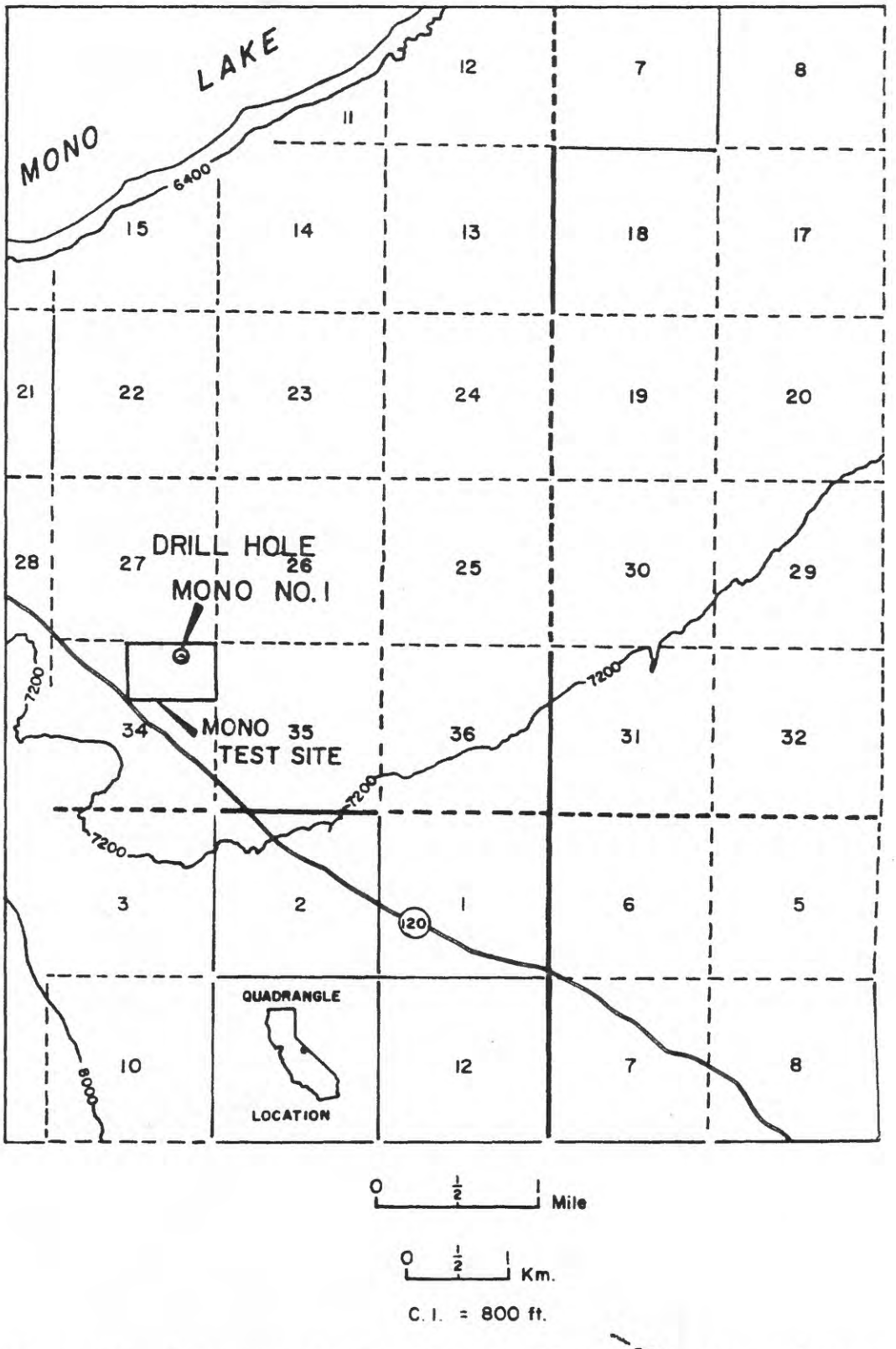

Figure 60.--Index map showing location of Mono Ash site and Mono drill hole 1, California.

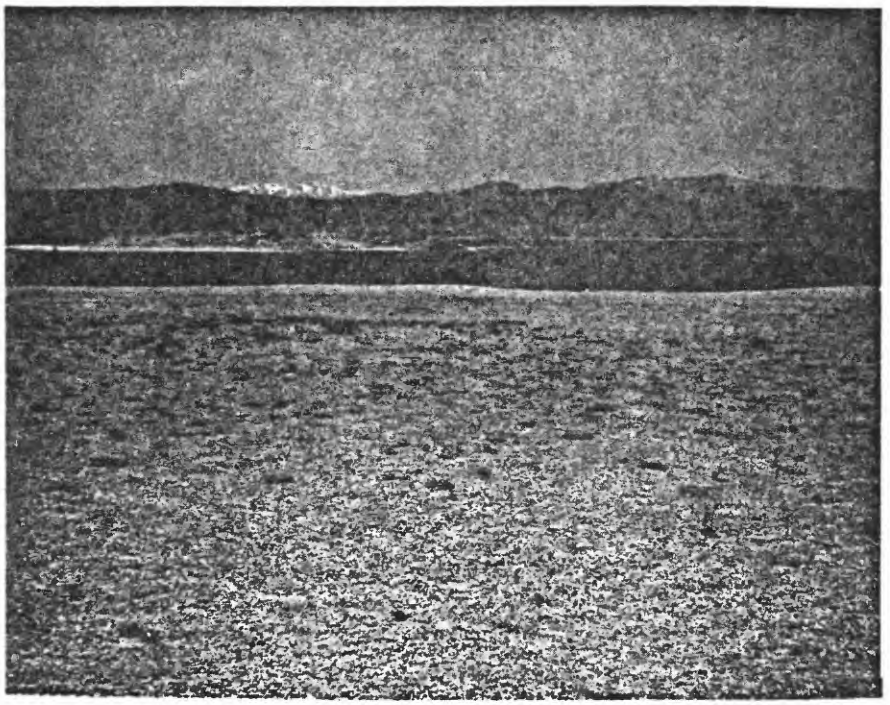

Figure 61.--Mono Ash site, California, looking northwest across area of seismic survey; Mono Lake and Paoha Island in background.

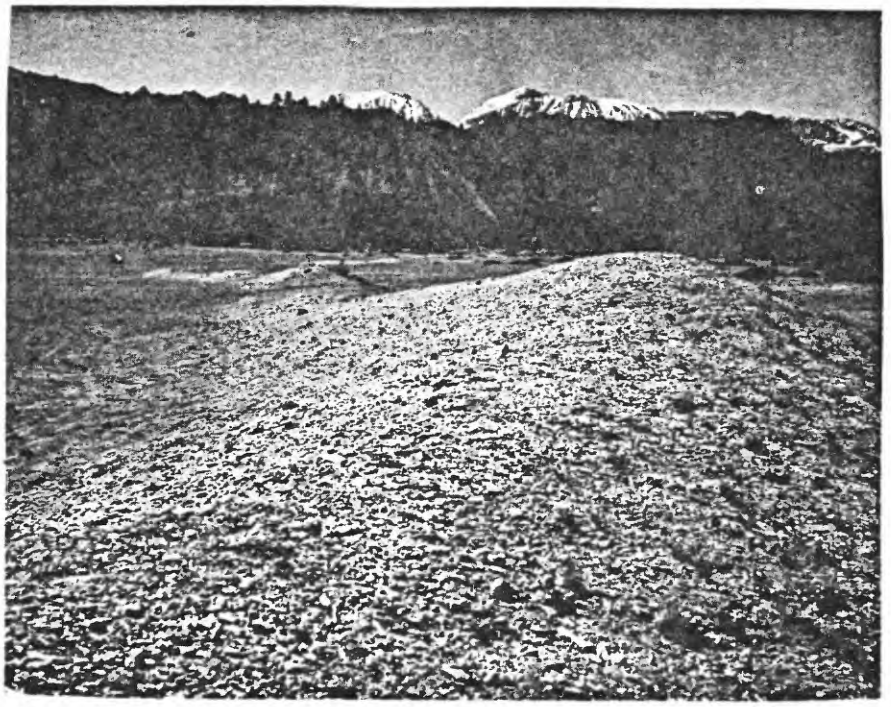

Figure 62.--Mono Ash site looking west along top of southernmost embankment.

Water

Moisture is present a few inches below the surface, but no ground water was encountered in Mono 1 (52.5 m total depth).

Soil Conditions

The surface of the test site is covered with 3-5 cm of loose, dry lapilli ash generally consisting of angular to subrounded equant fragments of pumice (90 percent) and obsidian (10 percent) (fig. 63). Maximum particle size is about 19 mm and averages about 3 mm. Minor amounts of platy and elongated fragments occur. Surface soil is probably wind-winnowed of the finer sizes. Mechanical analyses of six samples of the soil from various locations on the test site were made. The two most widely different samples are plotted in the form of gradation curves in figure 64. In the Unified Soil Classification, the soil is classified as sandy gravel (GW) and gravelly sand (SP). Fifteen samples of underlying moist soil from various locations on the test site, from depths ranging from 5 to 15 cm, were sieved and the three most different gradations are plotted in figure 65. The soils are classified as gravelly sand (SW), silty sand (SP-SM), and silty sand (SM), and are lithologically similar to the loose, dry surface soil.

Patches of larger pumice fragments occur locally at the test site and one large block of pumice (2.4 m in length) was found embedded in the lapilli ash.

Figure 63.--Vertical view of ground surface near southwest end of seismic line DEF shows typical particle size. Light-colored fragments are pumice; dark fragment in upper middle left is obsidian.

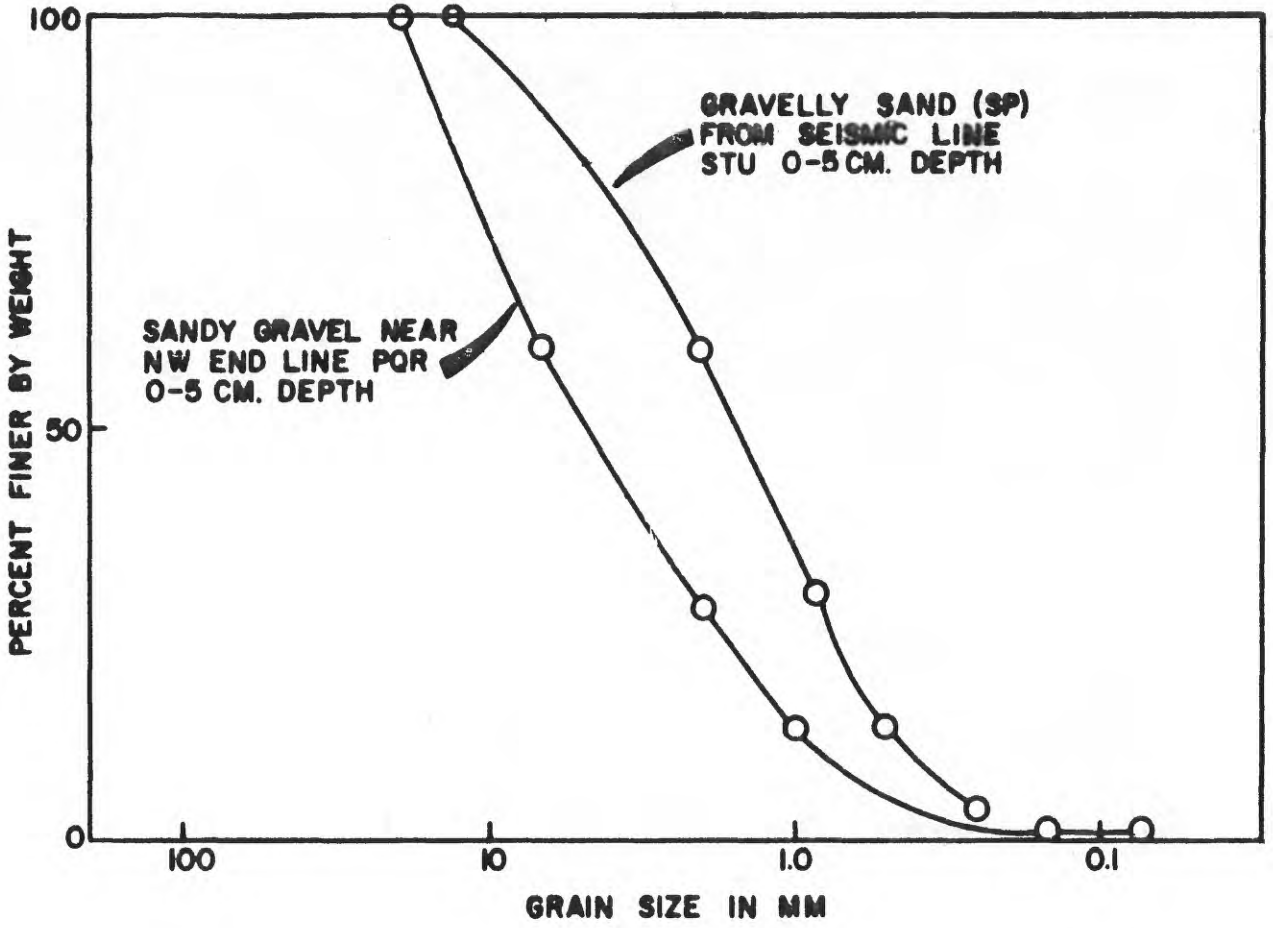

Figure 64.--Mono Ash site. Gradation curves, 0-5 cm depth.

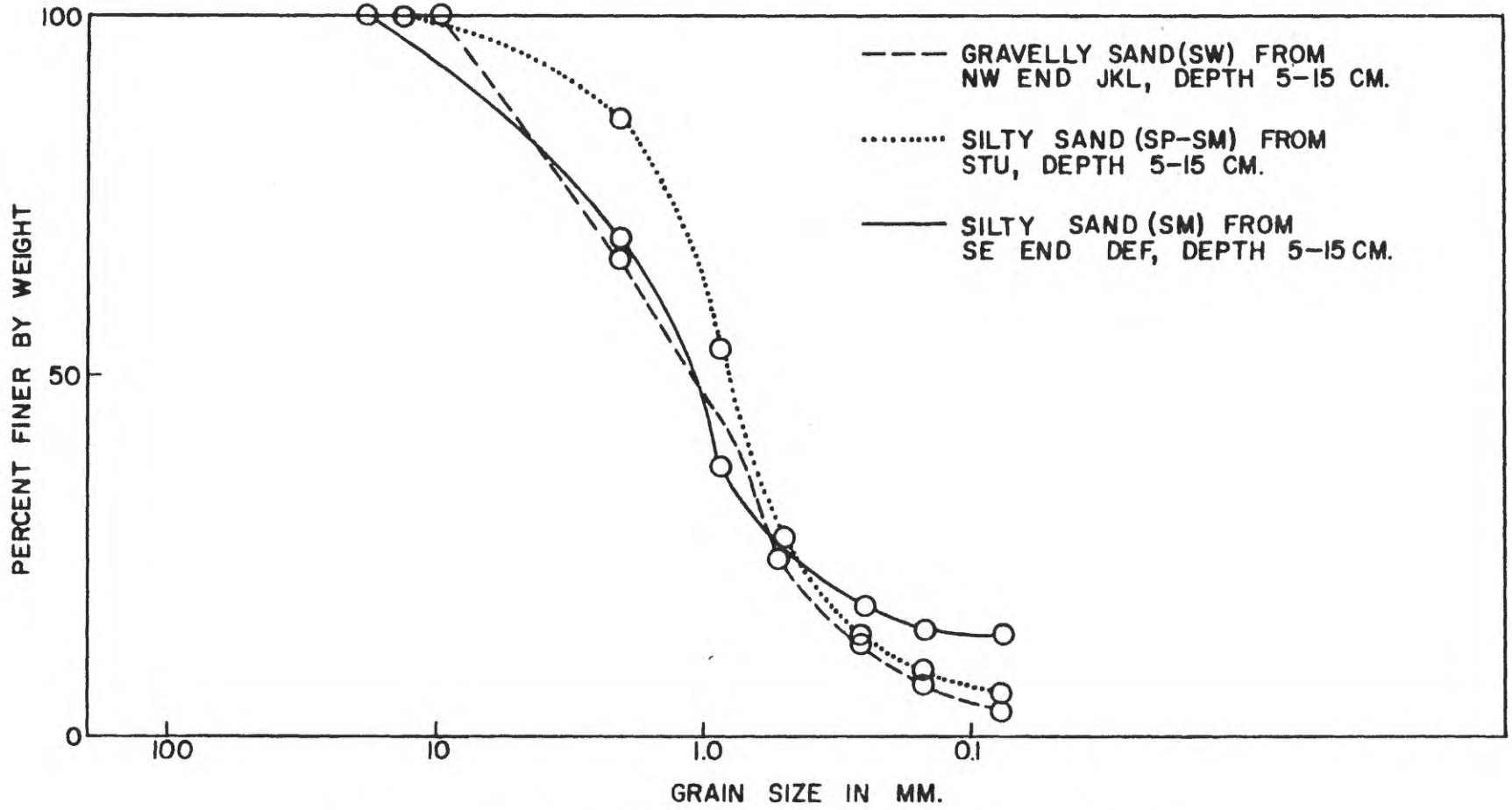

Figure 65.--Mono Ash site. Gradation curves, 5-15 cm depth.

Cone penetrometer tests

Cone penetrometer tests were made at 60-m intervals along each of the seismic lines (fig. 66). Refusal was usually encountered at depths 10-18 cm below surface soil. The embankment soil is much looser than the soil elsewhere on the ash flat, and in some tests refusal was not encountered the full depth of the penetration rod (90 cm) or the penetration rod with added extension rod (140 cm).

Moisture-density measurements

Density and moisture content were determined for samples taken from ends of each seismic line. Loose, dry lapilli ash was sampled separately from the underlying moist lapilli ash. In sampling the loose, dry soil a metal cylinder open at both ends was hand pressed vertically into the soil and the loose dry soil was scopped out from the inside of the cylinder to the top of the underlying moist layer. Excavated soil was then measured in a graduated cylinder to obtain the volume.

In sampling the underlying moist soil, the open-ended cylinder was replaced by a closed-end cylinder pushed into the ground. Volume was determined by the amount of soil recovered in the cylinder.

The average depth of sampled soil varied from 4.5 to 15 cm. Samples were placed in plastic bags and sealed air-tight for laboratory weight and moisture measurements. Subsequently, dried samples were sieved, weighed, and classified, and representative

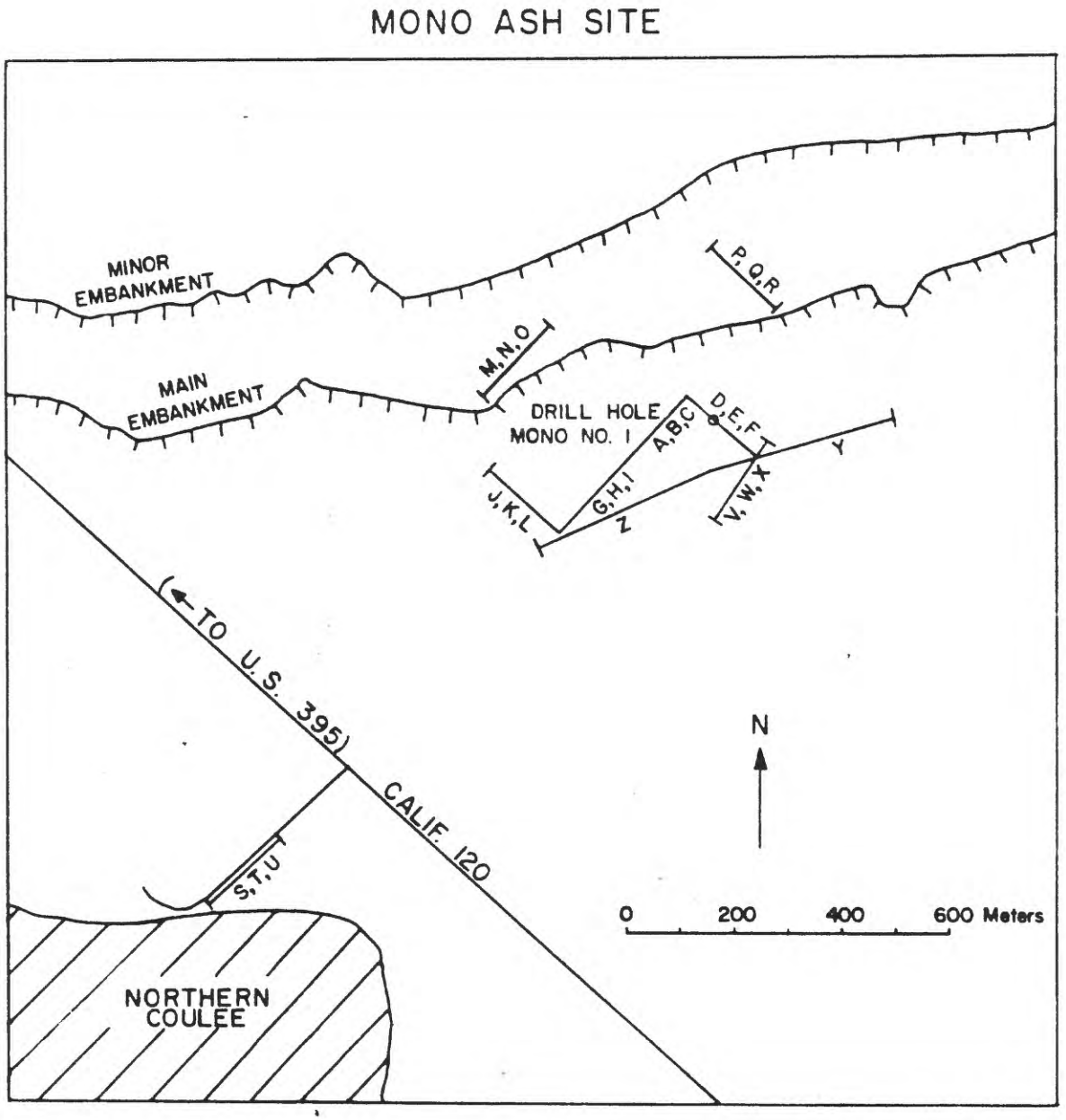

Figure 66.--Mono Ash site. Seismic spread layout.

gradation curves were prepared (see figs. 64 and 65). Results indicate that loose, dry surface soil (average depth of 4.5 cm) has an average dry density of 1.26 g per cc and a negligible water content. Underlying soil from an average depth of 4.5-15 cm has an average dry density of 1.26 g per cc and a negligible water content. Underlying soil from an average depth of 4.5-15 cm has an average dry density of 1.22 g per cc and a water content of 9.5 percent.

Assuming a value of 1.26 for the specific gravity of the soil and a value of 2.33 for the specific gravity of the solids (rhyolite glass), the volume of the solids is 0.540 liter. Pore volume, which includes the space between the pumice particles as well as space inside the particles, is 0.460 liter; void ratio (e) is 0.85.

Mono Drill Hole 1

Mono drill hole 1 is located in the NE 1/4, sec 34, T.1 N., R.27 E., Mt Diablo Base Line and Meridian, Mono County, California (fig. 60).

The vertical hole was spudded in on August 14, 1965 and completed on August 25, 1965. The total depth was 52.5 m. An initial attempt was made to core with air as the circulating agent, but no core was recovered to a depth of about 1 m. Cuttings indicated ash to this depth. Drilling mud was then used as the circulating medium. Because of the unconsolidated nature of the deposit, recovery of undisturbed material was not possible. A five-foot or ten-foot core barrel with NX-size diamond core bit was used throughout the drilling. Core recovery averaged 22 percent from 1 m to 34 m.

Best core recovery was obtained where layers of relatively well-indurated pumice occurred in the section. Caving of the hole and plugging of the bit caused minor delays. Core recovery improved to an average of 96 percent from 34 m to 47 m. The improved recovery was due to lower bit pressure and slower rotary speed. Bishop Tuff was encountered at 47 m, the bit pressure and rotary speed were increased and the recovery averaged 97 percent. The petrographic features of the core below 47 m are described in the following paragraphs.

Tuff from the Mono Ash site

Induration.--The rock is well-indurated and fractures under the hammer into discrete fragments having rough, uneven fracture surfaces.

Texture.--The rock is coarse-grained with average particle sizes of about 2 mm exclusive of the finer grained groundmass. The rock seems much coarser than rock from the Bishop Tuff site (compare figs. 51 and 67). The groundmass is less obvious in the Mono Ash drill core than it is at the Bishop Tuff site, although the matrix still makes up over half the volume of the rock. The pinkish matrix is generally aphanitic and massive-appearing with only faint granularity or microcrystallinity. Glass shards cannot be recognized megascopically in the matrix. The matrix seems to be little more than a cement.

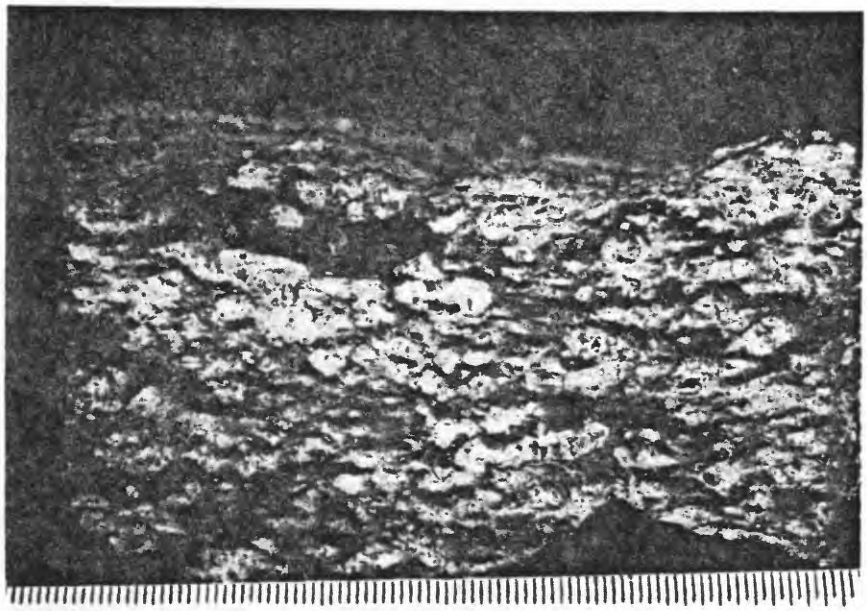

Figure 67.--Vertically sawed section showing lenses of devitrified pumice (gray); large lens of obsidian (black) in upper left. Light colored areas are matrix of microscopic glass shards. Scale marked in 0.5 mm divisions. 48 m deep. Mono drill hole 1.

Disseminated throughout the matrix are numerous crystals of sanidine, quartz, and minor constituents as well as prominent grayish and black lenses of devitrified pumice and obsidian. Lenses average only a few millimeters thick and usually 2.5 cm or less in length or breadth. They are slightly bent and give an impression, when viewed in the vertical plane, of discontinuous low-amplitude waves (fig. 67) or eutaxitic structure. This structure is best visible in the core near the top of the tuff formation because of greater contrast in colors.

The grayish and black lenses are inclusions of xenolithic pumice rock fragments subsequently altered by welding. Lenses are characterized by black obsidian, gray spherulites, and abundant sanidine. Spherulites are best observed in the horizontal plane on fresh fracture surfaces. The lenses consist almost entirely of obsidian, spherulites, and sanidine, and are very distinct in composition and texture from the surrounding matrix (figs. 68 and 69). Although the proportions of these three materials seem to vary slightly from one lens to another, sanidine usually predominates forming 40-50 percent of the volume of a typical lens; obsidian and spherulites occur in approximately equal amounts. Contact of the lenses with the matrix is sharp or fairly sharp.

Locally, the tuff is slightly iron stained. The source of the brown stains is not apparent, but they are probably the result of the breakdown of biotite and/or magnetite.

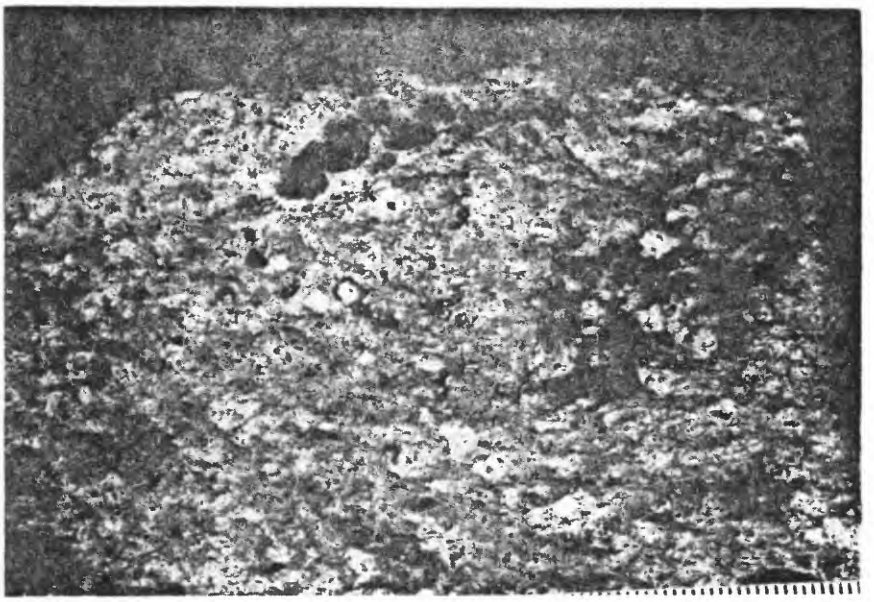

Figure 68.--Vertical surface showing dark-colored lens of obsidian, gray spherulites, and sanidine. Scale is marked in 0.5 mm divisions. 52 m deep. Mono drill hole 1.

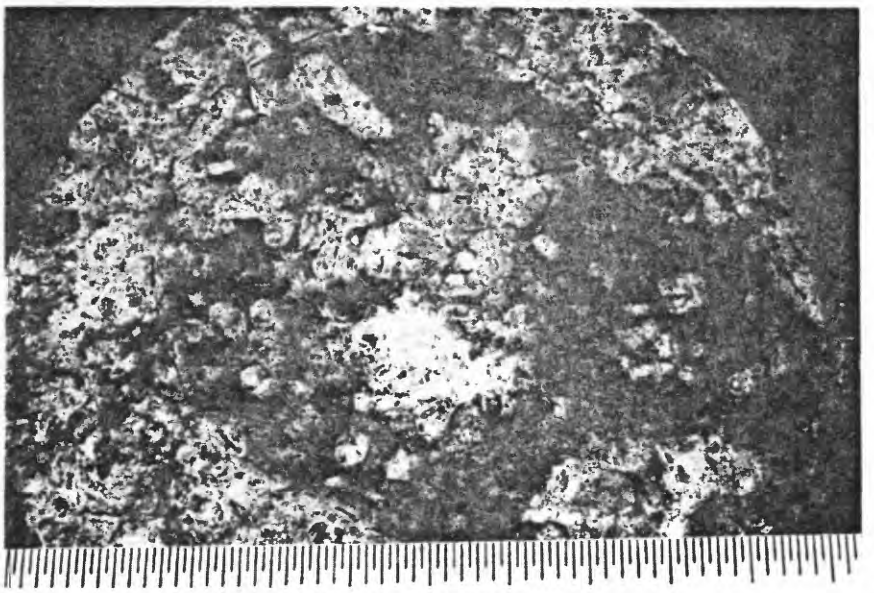

Figure 69.--Horizontal fracture surface showing a lens consisting of gray spherulites, obsidian and sanidine (area outlined by dashed line). Matrix consisting chiefly of glass shards is outside dashed line.

Mineral Descriptions

Sanidine

Sanidine crystals are similar in size, shape, and mode characteristics to those that occur at the Bishop Tuff site. The crystals are found scattered through the matrix either as individuals or in lenses with grayish devitrified pumice spherulites and obsidian.

Groundmass

Groundmass consists of glass shards set in a glassy featureless matrix. Typical shard structures are not well developed and appear fuzzy and blend indistinctly with the matrix on their outer margins. Shards are moderately devitrified and shard surfaces seem to be broken by many fine fractures. Shards are usually straight to gently curving in shape with an average length of 0.1 mm.

Devitrified Pumice

Lenses, representing highly compressed devitrified pumice fragments, commonly contain homogeneous material of uniform, medium-gray color. Larger lenses contain obsidian and sanidine. The lenses show on broken horizontal surfaces, that they are made up partly of spherulites. Spherulites are usually medium gray and are found together in botryoidal clusters up to 10 mm long, but also occur as individuals 1-2 mm in diameter (fig. 70). Some contain cores of sanidine. Other spherulites show concentric color bands as well as radial fibrous structure. The spherulites seem to have grown in the empty spaces in the vugs.

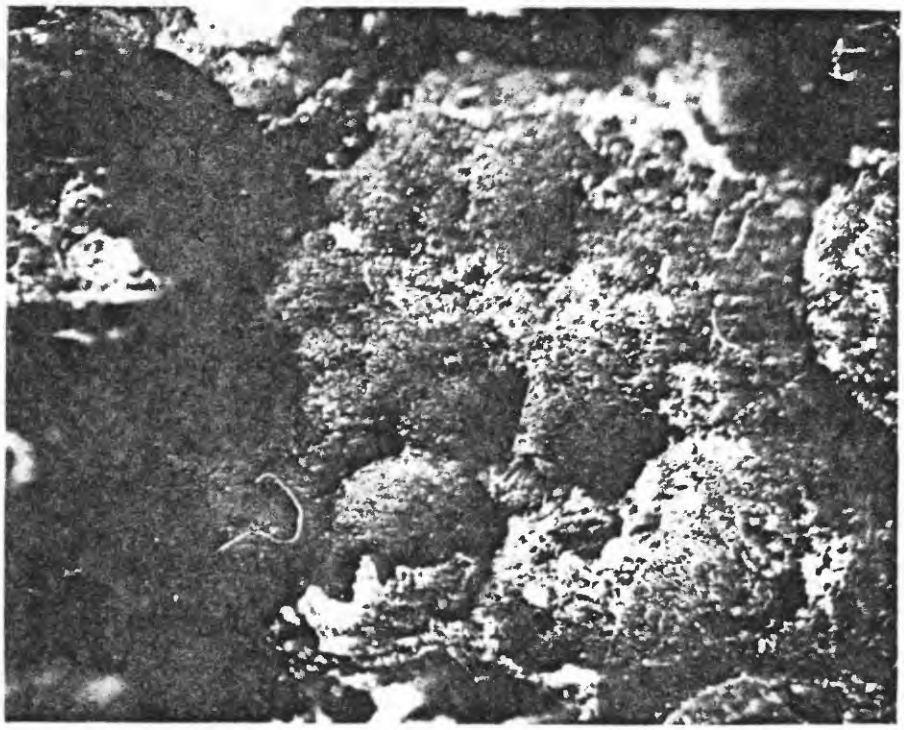

Figure 70.--Photomicrograph of tuff (10X) showing botryoidal mass of gray spherulites in horizontal plane. Reflected light. 47 m deep.

Devitrification is well advanced in lenses because over half the volume of a typical pumice fragment consists of devitrification products. The pumiceous texture in thin section is still visible in in most of the pumice fragments, although it is highly compressed. pression of parallel, closely-packed, slender fibers or tubes and welding have formed horizontally elongated lenses with flow-like textures. Subsequent devitrification superimposed a spherulitic structure over the flow-like texture (fig.71). Compression also has resulted in the bending and moulding of the lenses around crystals and inclusions. Devitrification apparently resulted in the production of two devitrification textures, spherulitic or fibrous form and mosaic or granular appearance, both of which may occur in the same fragment (fig. 72). Possibly the granular type of devitrification observed in the pumice fragments are actually fiber bundles cut perpendicular to their length and viewed end-on. Fibrous crystals making up the devitrification products are up to 0.4 mm long and are usually spherulitic. Fibrous crystals are arranged less frequently in subparallel rows at approximate right angles to the sides of a pumice fragment. The rows of subparallel fibers are similar in texture to those found in welded tuffs at other localities, where pectinate and axiolitic have been used to describe these textures. Both spherulitic and axiolitic fibrous structures cut across the compressed flow-like tubes of the pumice fragments. Spherulites were not observed outside of the devitrified pumice lenses. Devitrification in the groundmass is in the granular form and is finer grained than the devitrification products in the pumice lenses.

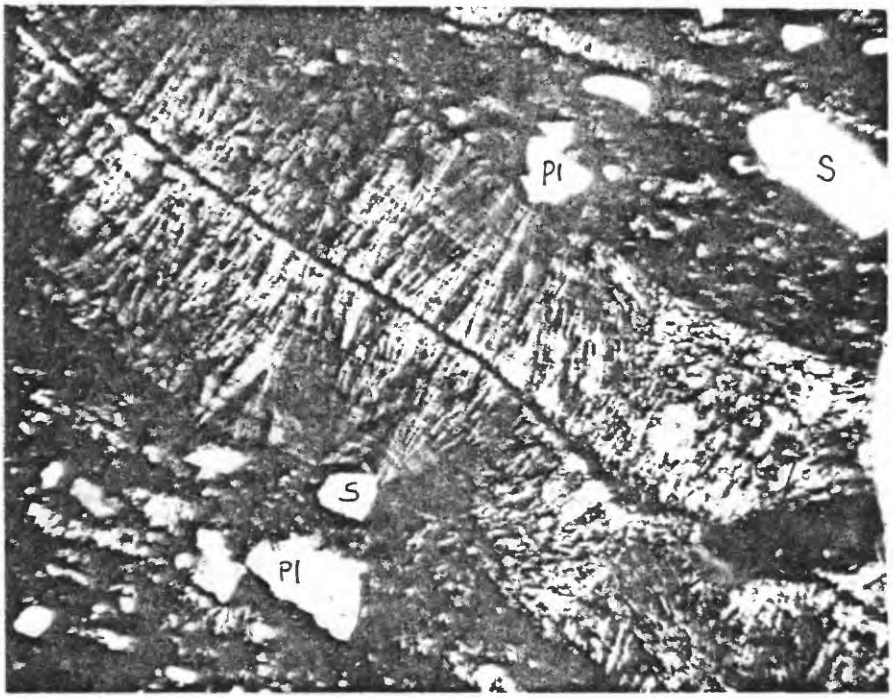

1 mm

Figure 71.--Photomicrograph of tuff showing spherulitic structure developed along margins of compressed fibrous pumice fragment. Spherulitic structure cuts across relict fibrous structure. Sanidine crystal at left (s) replaced by large amounts of clear glass (g). Crossed nicols. 47 m deep.

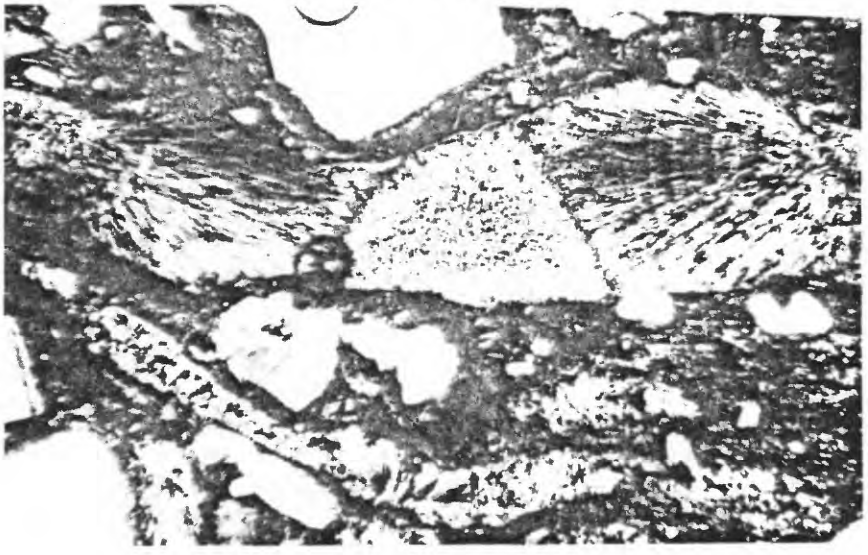

Figure 72.--Photomicrograph of devitrified pumice lens showing occurrence of spherulitic devitrification at ends of pumice fragment with mosaic type devitrification in center. The narrower pumice fragment at bottom of photomicrograph shows a reversed relationship. Crossed nicols. 52 m deep.

Obsidian

Obsidian is closely associated with spherulites in the larger pumice lenses. It occurs as rounded to subrounded equant to inequant polyhedral grains with vitreous luster and conchoidal fracture. Obsidian is usually black, but grayish-black, gray, and brown colors have been observed. Grains are 1-2 mm in diameter and sometimes occur as strings or beads of circular outline enclosing cores of sanidine. Some lighter colored glass has a sintered appearance. Obsidian fragments in thin section contain scattered unoriented globulites and irregular fractures. Obsidian-spherulite contacts are sharp. Some obsidian seems to have been lost in grinding the thin sections and the contact relations are seldom seen. The obsidian shows no devitrification.

Obsidian occurs in the groundmass outside of the pumice fragments at the Bishop Tuff site, and probably is xenolithic (fig. 59). Obsidian is abundant at the Mono Ash site. Its markedly different mode of occurrence reflect conditions of higher temperature and pressure and a process in which the obsidian was formed in situ.

Biotite

Laths and plates of black biotite are sparsely scattered through the matrix. The biotite locally shows a bronze reflection from cleavage surfaces.

Cavities

On the average, cavities occupy a larger volume of the tuff from the Mono Ash area than the tuff from the Bishop Tuff site. Although cavities at the Bishop Tuff site are of doubtful origin and may be due either to weathering or to factors involved in drilling the rock or making the thin sections, the cavities at the Mono Ash site seem to be natural vugs in the rock.

Modal Composition of the Tuff

Average modal analyses, calculated for each thin section by the same method as that previously described for the Bishop Tuff site (table 9), indicate that the glassy groundmass and undevitrified pumice inclusions comprise 65 percent of the rock. Devitrification products make up over half of the volume of the pumice inclusions and are present in the groundmass. They are not listed separately because of the difficulty of accurately measuring their extent in thin section. It is estimated that the average total volume of devitrification products is approximately 8 percent of the rock.

Glass and mineral composition of the tuff at the Mono Ash site indicate that the rock is a rhyolitic vitric tuff.

Petrography of Ash-Pumice Deposits

The upper part of Mono drill hole 1 consists chiefly of volcanic ash and silicic pumice. The coring of this friable and unconsolidated material was difficult and the recovered material was broken and mixed to some extent down to 6.4 m.

Table 9.--Summary of petrographic modal analyses of tuff, Mono drill hole 1.

[Gm = Groundmass, Dvp = devitrified pumice, San = Sanidine, Plag = plagioclase, Bio = biotite, Qtz = quartz, Pyro = pyroxene, Rock = rock, Obs = obsidian, Cav = cavities (47-52 m, percent by volume)].

Sample Depth (meters)	Gm	Dvp	San	Plag	Bio	Qtz	Pyro	Rock	Obs	Cav
47.0	61.1	14.5	12.3	2.5	0.5	3.5	0.1	0	0	5.5
48.0	59.1	15.0	11.1	0.7	0.5	2.8	0	0	1.8	9.0
50.0	57.1	12.5	11.6	1.2	0	10.2	0	0	1.5	5.9
52.0	55.0	14.1	14.2	1.5	0.4	2.6	0.2	1.7	1.8	8.5
Average	58.1	14.0	12.3	1.5	0.3	4.8	0.1	0.4	1.3	7.2

Material consisted of ash having angular fragments of pumice, tuff, and obsidian ranging up to 5 cm, and averaging 1.2 cm was found between 0 and 6.4 m. The ash contained colorless crystals of sanidine and quartz, as well as small fragments of fibrous pumice averaging 1 mm long. A few pumice fragments having flow banding also were observed. Larger angular fragments recovered with the ash may represent distinct layers or lenses of pumice and obsidian.

The fibrous pumice is white to medium-light-gray and small vugs, 1-2 mm in diameter, are present. The obsidian is black to medium-dark-gray and is homogeneous or finely laminated. Thin sections of selected fragments of pumice showed markedly wavy to crenulated flow lines (fig. 73) in some fragments. Devitrification of the pumice is well-advanced, as nearly all fibers show weak birefringence under crossed nicols. Under the microscope, laminated obsidian is made up of dark, finely fibrous laminae which alternate with white, homogeneous laminae (fig. 74). Devitrification is well advanced in the dark laminae and much less so in the white laminae.

Core consisted of alternating layers of lesser amounts of tuff, quartz sand, and greater amounts of silicic pumice was found between 6.4 m to 28 m. (See Elmer and Walters, this report.) Sand layers 1.5 m and 5.2 m thick may represent lake deposits when the test area was covered by pluvial Lake Russell of Wisconsin age. Steeply dipping pumice flow banding is locally present although pumice is generally homogeneous. Pumice varies from well-indurated to friable and contains inclusions of sanidine and quartz. Tuff is moderate

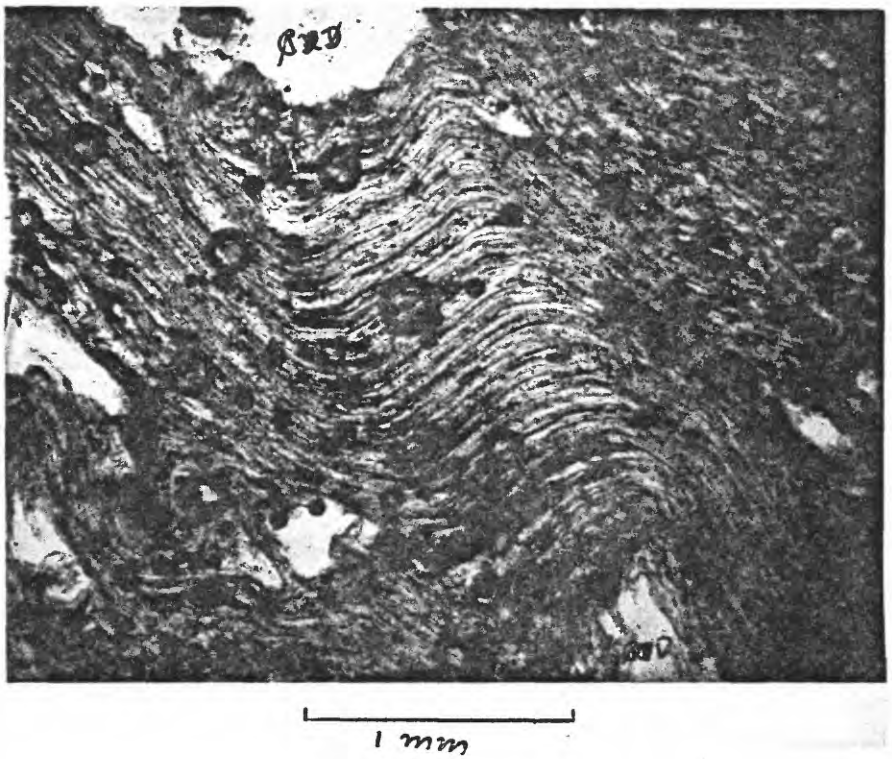

Figure 73.--Photomicrograph of ash-pumice deposit showing orenulated fibrous pumice molded around cavities (CAV). Plane light. 0.9-14 m deep.

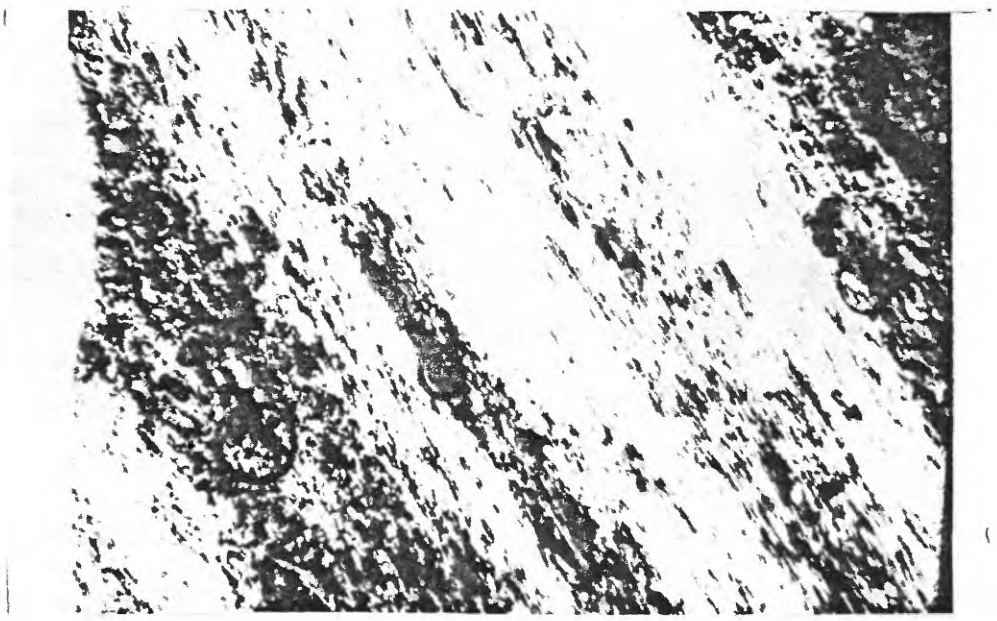

Figure 74.--Photomicrograph of ash-pumice deposit showing structure of laminated obsidian having very fine, fibrous, dark laminae and homogeneous light-colored laminae. Plane light. 4.3-6.4 m deep.

to poorly consolidated with fragments of pumice and obsidian, and crystals of sanidine and quartz.

The core consisted of gray ash from 28 m to 47 m.

Petrographic descriptions of the pumice at various depths are as follows:

6.4-7.9 m. Ten percent of the white cellular to very fine fibrous pumice has inclusions of sanidine, quartz, and plagioclase. Pumice fibers are moderately molded around inclusions. Sanidine is subhedral to anhedral in crystal form, inequant in shape, ranges from 0.5 to 1.5 mm in length, and makes up about 5 percent of the rock. Quartz is anhedral and equant, contains irregular fractures, is usually corroded or replaced by glass, ranges from 0.5 to 1.0 mm in diameter, and makes up about 4 percent of the rock. Corroded and fractured crystals are optically continuous (fig. 75). Plagioclase is subhedral, shows albite twinning, ranges from 0.5 to 1.0 mm in size, and makes up about 1 percent of the rock.

9.6 m. Ten percent of the fibrous pumice is composed of sanidine, quartz, and plagioclase crystals. Size ranges, crystal development, and shape of included crystals are similar to those described in the 6.4-7.9-m interval (above). Quartz makes up about 5 percent, sanidine 4 percent, and plagioclase 1 percent of the rock. Pumice fibers are moderately molded around inclusions. Inclusions are associated with tails of glass and areas of cellular pumice, as shown in figure 75. The

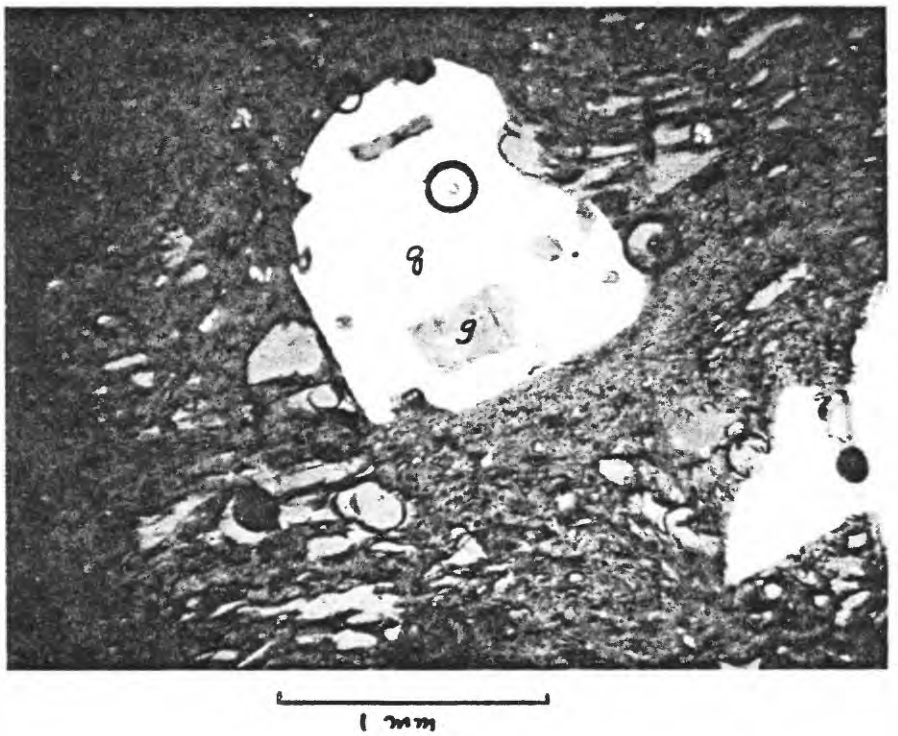

Figure 75.--Photomicrograph of ash-pumice deposit showing quartz crystal inclusion in pumice. Note replacement by glass (g) and proximity of cellular texture. Partially crossed nicols. 6.4-7.9 m deep.

groundmass contains numerous longulites of low birefringence that are thought to be incipient phenocrysts rather than devitrification products. Devitrification is slight.

12.2 m. White cellular pumice has round to oval vesicles up to 1 mm in diameter. Inclusions of quartz, sanidine, plagioclase, and biotite make up about 10 percent of the rock. Groundmass is molded around inclusions and is considerably devitrified.

Petrographic Analysis

Petrogenesis of the Mono ash-pumice deposits

Volcanic material consisting mostly of ash, overlies the tuff at 47 m in drill hole Mono 1. Pumice, obsidian, and tuff also occur from 0 to 28 m. In this interval, relatively dense thick-bedded pumice is locally a prominent constituent of the core over distances up to 2 m. Thick-bedded pumice contains flow banding at steep angles to the vertical axis of the drill core. Thickness and flow banding suggest that the pumice occurs as one or more flows associated with obsidian. Thick-bedded pumice, obsidian, and tuff appear to be bedded in situ, but also might be in the form of large breccia blocks in a flow. Interbedded pumice and obsidian of similar lithology occur at nearby Southern Coulee.

Ash deposits, most prominent from 28 to 47 m, suggest explosive eruption of a gas-charged magma of rhyolitic composition. The source was probably in the Mono Craters because the lithologies of the Mono Craters deposits and the Mono ash-pumice deposits are similar.

Petrogenesis of the Bishop Tuff

Lenticular elements, such as alignment and molding of glass shards around inclusions, vitroclastic texture, resorption of inclusions, and the development of eutaxitic, axiolitic, and spherulitic structures indicate that the Bishop Tuff is a welded ash flow. Tuff at the Bishop Tuff site is more porous and less dense than that at the Mono Ash site. Petrographic differences between the tuffs at the two test sites are summarized in the following paragraphs.

Mono Ash site tuff is much more highly devitrified than that at the Bishop Tuff site, probably because of the retention of a higher percentage of volatile gases in the tuff at the Mono Ash site, which lowers viscosity and promotes crystallization. Evidence for such gaseous retention is shown by vuggy lenses and spherulites within these lenses. Absence of significant devitrification at the Bishop site probably indicates more rapid cooling of the tuff.

Obsidian associated with the spherulites in vuggy lenses at the Mono Ash site seems to indicate a welding process that resulted in fusion and the production in situ of lenses of glass analogous to fiamme, black glassy tongue-like inclusions in welded tuff. The intrusion of the rhyolitic magma of the Mono Craters may have provided heat and locally accentuated some welding features. The fiammelike horizontal lenses of obsidian are typical of the lower part of the Bishop Tuff and are probably a syngenetic feature of the tuff. As these obsidian lenses are not present in the tuff at the Bishop Tuff site, it would indicate a higher temperature of deposition at the Mono Ash site and a lower temperature of deposition at

the Bishop Tuff site. Obsidian at the Bishop Tuff site occurs as discrete grains scattered through the matrix and seems to be xenolithic.

Shards in the matrix at the Mono Ash site are more nearly horizontal and more molded around larger inclusions than shards at the Bishop Tuff site suggesting a higher pressure at the Mono Ash site probably due to deeper burial within the ash flow. Gilbert (1938, p. 1835) noted that the amount of welding increased with depth and with thickness of the tuff.

The above differences in the tuff at the two sites can be explained by one or more of the following hypotheses:

1. Tuff deposited at the Mono Ash site was closer to the eruptive vent or fissure which was the source of the ash flow. Tuff at the Bishop site was more distant and cooler at the time of deposition.
2. Tuff at the Mono Ash site represents the uneroded remainder of a much thicker deposit where pressures and temperatures were much greater than at the Bishop site. The tuff at the Bishop Tuff site was deposited not only at the terminus of the ash flow, but in the upper part where pressure and temperatures were comparatively low.

Similarities in structure and miner mineralogy strongly suggest that the tuffs at Bishop Tuff and Mono Ash sites are stratigraphically equivalent. Outcrops can be physically traced throughout much of the area between the sites; hence, the two units are thought to be the same unit.

Physical Properties

The physical properties available for analysis are the dry bulk density, saturated bulk density, grain density, total porosity, effective porosity, and nitrogen permeability of the Bishop Tuff (Roach and Johnson, 1966). Generalizations concerning these properties are stated in the following paragraphs.

Bishop Tuff test site

Data show a decrease in the dry bulk density, saturated bulk density, and grain density from the top of the drill core to the bottom, and an increase in the total porosity from top to bottom (Roach and Johnson, 1966). Petrographic modal analyses shown in table 9 indicate that these changes in physical properties can be related to an increase in the proportion of pumice fragments and to decreasing induration, which are in turn related to the transition from well-indurated tuff to unconsolidated ash. This change is reflected in the increase in nitrogen permeability in samples from the lower 3 m of core.

Mono Ash test site

Physical tests (Roach and Johnson, 1966, written commun.) on cores of Bishop Tuff from the lower part of Mono drill hole 1 yielded the following mean results:

Total porosity, percent	11.6
Effective porosity, percent	10.2
Dry bulk density (g per cc)	2.24

Saturated bulk density (g per cc)	2.35
Grain density (g per cc)	2.49
Nitrogen permeability (Millidarcies, parallel to core axis)	1.67
Nitrogen permeability (millidarcies, normal to core axis)	2.92

The data show a significant difference in nitrogen permeability between core specimens oriented parallel to the core axis and those oriented normal to the core axis. This is probably related to the eutaxitic structure of the tuff, the more pronounced flattening and devitrification of horizontal lenses of pumice, and the presence of horizontally oriented cavities at the Mono Ash site.

The tuff at the Mono Ash site is less porous, less permeable, and denser when compared to the tuff at Bishop (Roach and Johnson, 1966). The difference may be related to the original depth of burial of the tuff at Mono Ash site and the thickness of the original tuff deposit. Petrographic characteristics of the Mono Ash tuff are typical of those found in the lower part of the Bishop Tuff at other localities; consequently, a relatively great thickness of overlying tuff may have been present at an earlier time and subsequently may have been eroded away. Weight of this tuff may have resulted in a denser compaction of the tuff near the base of the formation.

Seismic Properties

Velocity and attenuation of seismic waves are functions of the density, elastic, and inelastic properties of rock. The eutaxitic structure of the Bishop Tuff should result in some directional difference in elastic properties and consequently in

seismic wave velocities and attenuation. The columnar structure of the tuff should have a similar effect as well as other types of fractures and joints.

Bishop Tuff site

The variations in seismic velocity are relatively small and probably are caused by minor differences in composition, water content, and density of the tuff and by the number of fractures locally present. The average velocity of the Bishop Tuff is 1,690 meters per second from 26 seismic lines.

Mono Ash site

The average velocity of the Bishop Tuff is 1,940 meters per second from 10 seismic lines. The higher velocity at the Mono Ash site compared to the Bishop Tuff site probably is due to the greater induration and higher density of the tuff at the Mono Ash site. The average velocity of the ash-pumice deposit overlying the Bishop Tuff is 500 meters per second. The markedly lower velocity compared to the Bishop Tuff probably is due to the low density and lack of cementation.

References

Dalrymple, G. B., Cox, Allan, and Doell, R. R., 1965, Potassium-argon age and paleomagnetism of the Bishop Tuff, California: Geol. Soc. America Bull., v. 76, p. 665-674.

Gilbert, C. M., 1938, Welded tuff in eastern California: Geol. Soc. America Bull., v. 49, p. 1829-1862.

Putnam, W. C., 1949, Quaternary geology of the June Lake district, California: Geol. Soc. America Bull., v. 60, p. 1281-1302.

Roach, C. H., and Johnson, G. R., 1966, Field verification of in situ physical properties, in Investigation of in situ physical properties of surface and subsurface site materials by engineering geophysical techniques--Project quart. rept., Oct 1, 1965-Dec. 31, 1965: Flagstaff, Arizona, U.S. Geol. Survey, Br. of Astrogeology, p. 9-46.

PETROGRAPHY OF METEOR CRATER CORE 4, METEOR CRATER, ARIZONA

by David V. Haines

ABSTRACT.--A 107-m diamond drill core hole on the south rim of Meteor Crater recovered core from the debris zone, Moenkopi Formation, and Kaibab Limestone. The drill core and petrographic examination of thin sections indicate an inverted stratigraphic sequence in the debris zone, which is 10.0 m thick. The Moenkopi Formation beneath the debris zone is a very fine-grained calcareous sandstone 10.1 m thick, with shaly intervals comprising about 15 percent of the formation. The Kaibab Limestone, of which 87.3 m were cored, consists of sandy dolomite in the upper 25 percent of the section, very fine-grained sandy dolomite interbedded with dolomitic sandstone in the middle 60 percent of the section, and very fine grained calc-dolomitic sandstone in the lower 15 percent. Dolomite is relatively coarse-grained above 24.8 m and microcrystalline granular below 24.8 m.

Introduction

This report describes the petrography of drill core obtained from a diamond-bit, NX-size vertical hole MCC 4 drilled to a depth of 107.4 m on the south rim of Meteor Crater, March 1966. It is located in the NE1/4, sec 24, T.19N, R.12 1/2 E, Gila and Salt River Base Line and Meridian, Coconino County, Arizona. The location of the hole and the driller's log is shown by Walters and Elmer (Appendix A, this report). The elevation at the collar of the hole is about 1,740 m above mean sea level. The drill site is located on debris consisting of sand and fragments of the Coconino Sandstone. Outcrops on the crater slope and an artificial cut in the rim debris near the drill hole indicate the debris overlies tilted Moenkopi

Formation. The Moenkopi Formation was encountered in the drill hole between 10.0 and 20.1 m deep. Underlying the Moenkopi Formation from 20.1 m to 107.4 m deep is the Kaibab Limestone consisting mostly of very fine grained sandy dolomite and dolomitic sandstone. The geology of the crater and the stratigraphic relationships are discussed by Shoemaker (1963).

A total of 27 thin sections were examined including 2 from the debris zone, 4 from the Moenkopi Formation, and 21 from the Kaibab Limestone.

Petrography of the Kaibab Limestone

Half of each thin section was stained with a solution which colors calcite but not dolomite.

The Kaibab Limestone is generally a well-indurated, porous, very fine grained, white to pale yellowish orange, horizontally bedded sedimentary rock. The formation consists of varying amounts of dolomite, quartz sand, and minor calcite. Opaque substance, chalcedony(?), plagioclase, and microcline are present in small amounts. Cavities are present locally in the rock where fossil shell material has been dissolved. Rock strata consist of sandy dolomite, dolomitic sandstone, and sandy calc-dolomite. Most of the dolomite contains appreciable amounts of clastic quartz sand. Contacts between strata are gradational and the amount of quartz is not readily determinable by megascopic inspection. Thin sections

containing less than 50 percent quartz were classified as dolomite; those with more than 50 percent quartz as sandstone.

Dolomite

Carbonate is classified in this report as either dolomite or calcite on the basis of the staining effect. In most thin sections examined, the staining solution had little or no effect on the carbonate, and it is therefore considered to be dolomite.

Dolomite occurs as the following: (1) as a cement between grains of quartz or as a matrix containing quartz, (2) as clots up to 7 mm long comprised of minute, granular grains, (3) as anastomosing threadlike stringers, and (4) as relatively coarse grains up to 4 mm in diameter.. Dolomite is not evenly distributed in most thin sections.

Clots consist of aggregates of individual dolomite grains averaging about 0.01 mm in diameter. Grains are uniformly sized and approximately equant. They appear subrounded in some thin sections and rhomb-shaped in others. Clots are irregular in shape, generally free of quartz grains, and occur chiefly below a depth of 24.8 m. Margins of the clots usually show apophyses of dolomite extending outward between surrounding quartz grains. Clots range in size from 0.5 mm to 7 mm long, averaging about 2.5 mm, and are equant, ovoid, or elongated in shape. Most clots contain dolomite which is optically continuous. Some clots, however, are made up of two or more separate aggregates of particles which extinguish at different points under crossed nicols. Dolomite

also occurs in round to oval clots which have smooth, even contacts with the matrix and which may differ in origin from clots which have irregular margins and apophyses (fig. 76). The clots are sometimes megascopically visible in the rock where they are lighter colored than the matrix and produce a faint mottled texture.

Threadlike stringers of dolomite consist of similar very fine grained particles of dolomite. Stringers are also megascopically visible in the rock.

Dolomite also occurs as relatively coarse, anhedral, equant grains from 0.5 mm up to 4 mm in diameter, averaging 2.5 mm (fig. 77). This type of dolomite is most abundant from 20.2 to 21.0 and from 21.6 to 21.8 m, where the grains are interlocked (fig. 78). Relatively coarse grains are also present from 22.2 to 24.8 m but average 0.2 mm in diameter, and are less abundant (figs. 79 and 80).

Below a depth of 24.8 m, dolomite occurs in the microcrystalline granular form (fig. 81).

Calcite

Calcite occurs sparingly between 21.0 and 21.6 m where it occurs as scattered coarse colorless crystals averaging 3 mm in diameter embedded in dolomite (fig. 82). In thin section, calcite grains are anhedral with irregular interlocking contacts with the dolomite. Calcite fills occasional fossil casts, or possibly is primary shell material. Twinning is present. Calcite occurs as relatively coarse grains and as cement from 101 to 106 m. The

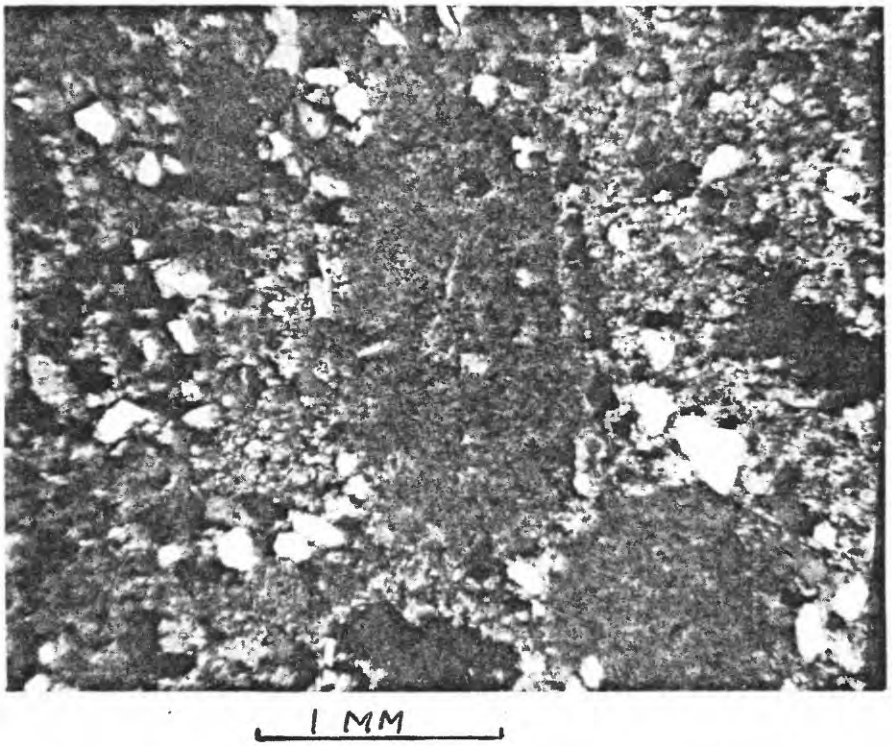

Figure 76.--Photomicrograph of Kaibab Limestone showing round to oval clots of microcrystalline dolomite set in a groundmass of clastic quartz and dolomite from Meteor Crater core 4. Crossed nicols. 67.5 m deep.

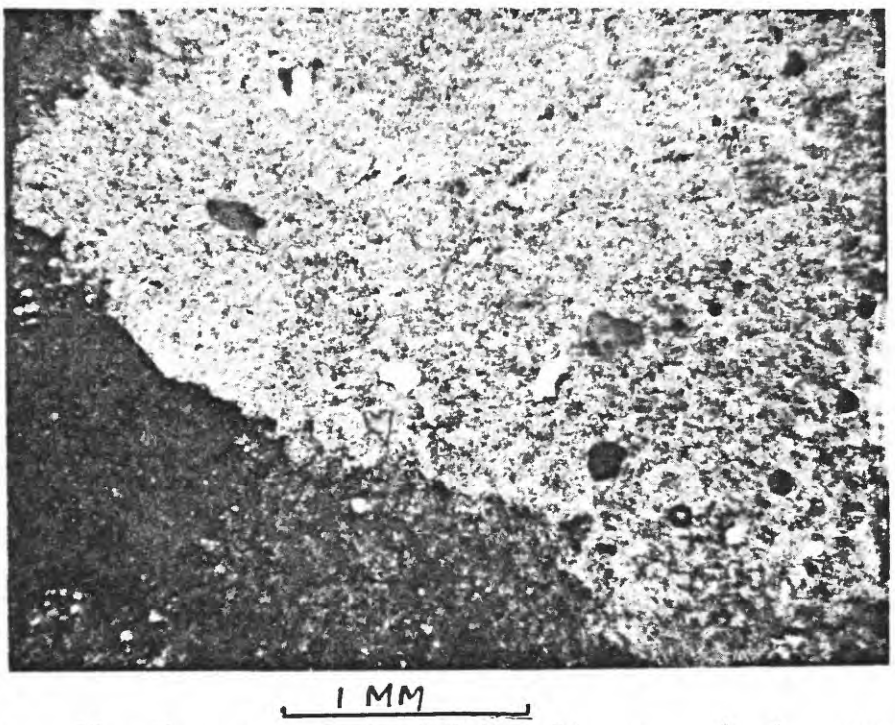

Figure 77.--Photomicrograph of Kaibab Limestone showing coarse-grain dolomite with clastic quartz grains from Meteor Crater core 4. 21.0 m deep.

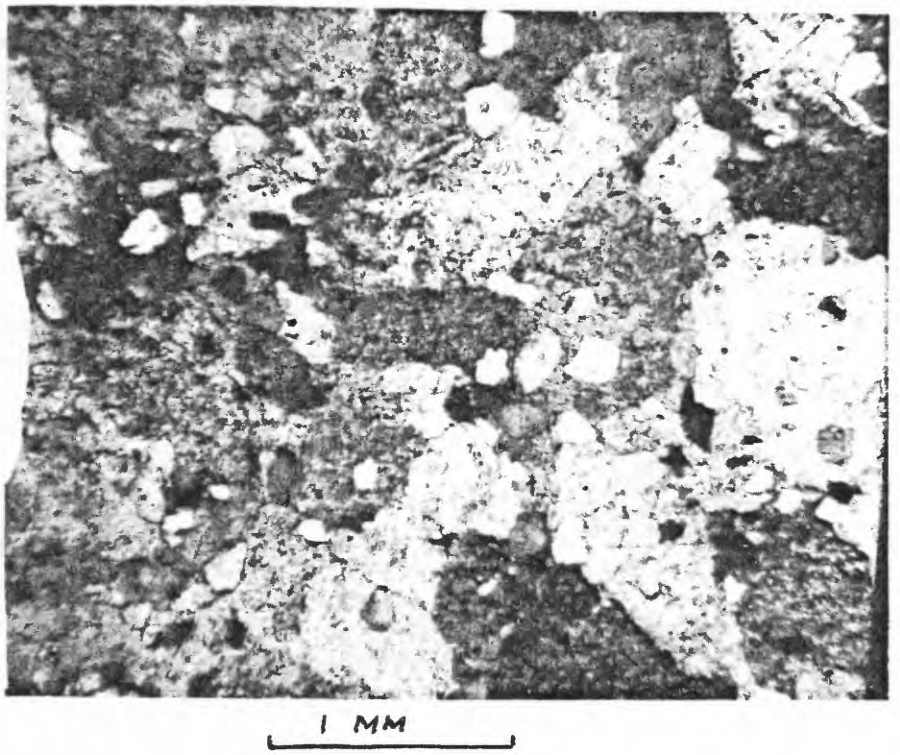

Figure 78.--Photomicrograph of Kaibab Limestone showing coarse-grain dolomite with clastic quartz grains from Meteor Crater core 4. Crossed nicols. 21.8 m deep.

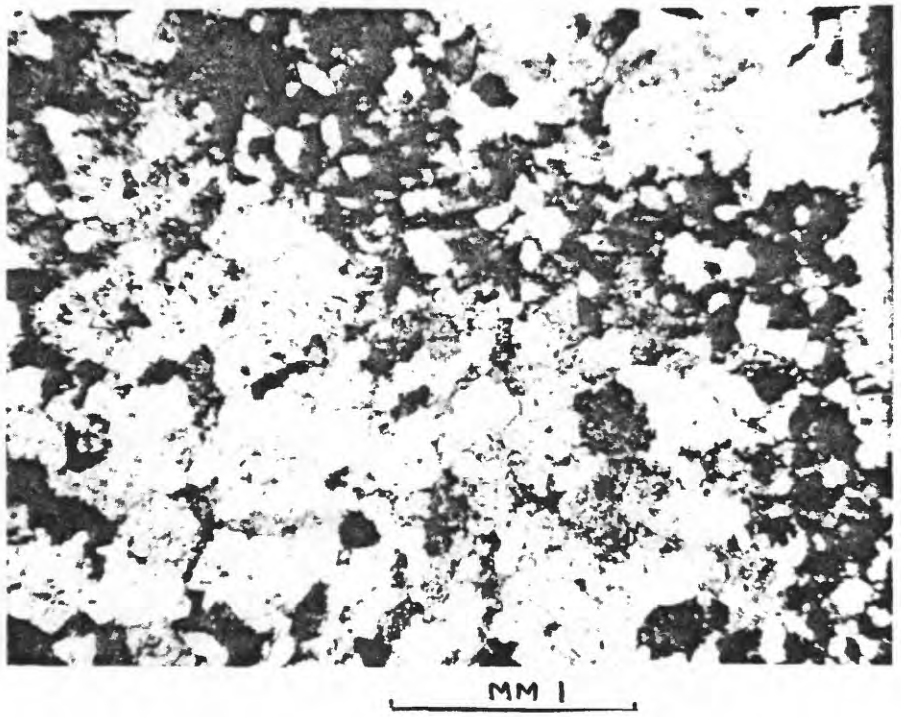

Figure 79.--Photomicrograph of Kaibab Limestone showing relatively coarse-grain dolomite with ribbon of clastic quartz grains from Meteor Crater core 4. Crossed nicols. 22.7 m deep

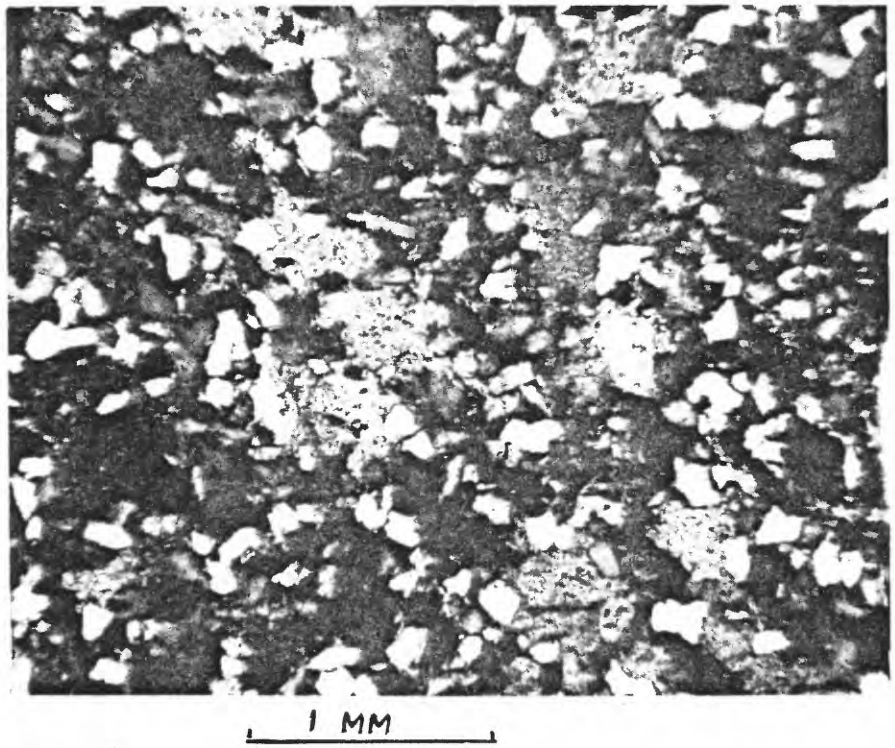

Figure 80.--Photomicrograph of Kaibab Limestone showing clastic quartz grains containing relatively coarse grains of dolomite from Meteor Crater core 4. Crossed nicols. 23.3 m deep.

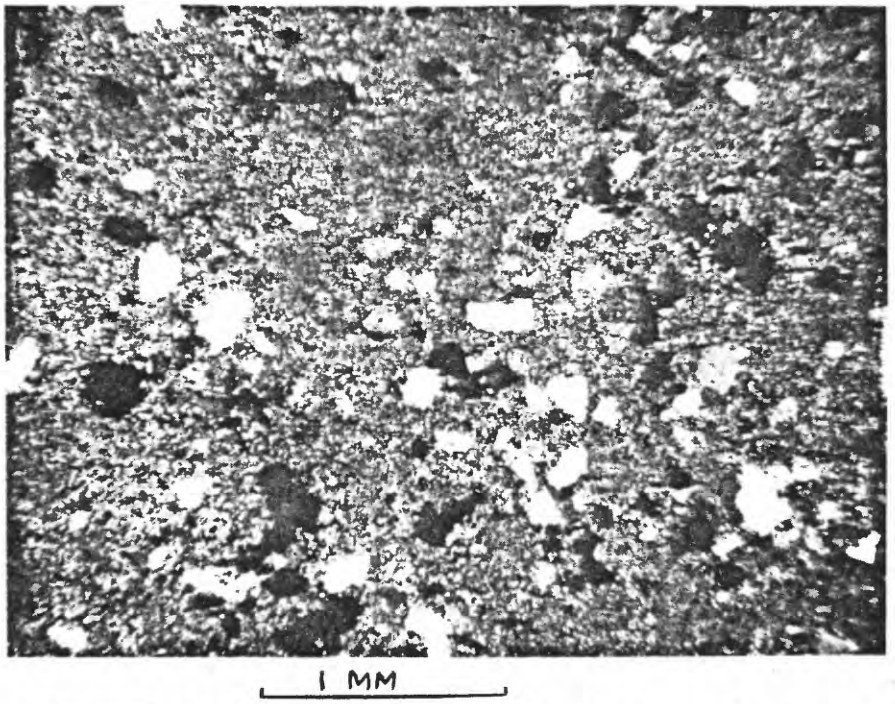

Figure 81.--Photomicrograph of Kaibab Limestone showing microcrystalline dolomite with grains of clastic quartz. Dark areas are mostly fossil shell solution cavities. Crossed nicols. 29.9 m deep.

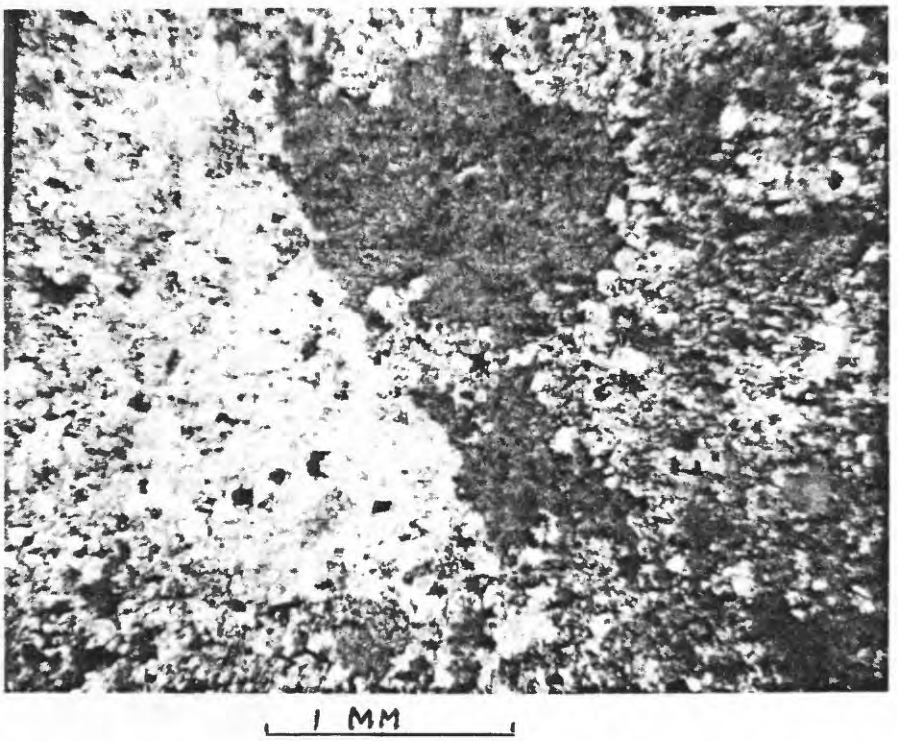

Figure 82.--Photomicrograph of Kaibab Limestone. Coarse calcite grain showing twinning embedded in dolomite. Crossed nicols. 21.4 m deep.

coarse grains, averaging 0.3 mm, are anhedral with irregular interlocking contacts with the quartz grains of the matrix. Grains are irregularly stained and it appears that approximately half of each grain consists of dolomite.

Quartz

The quartz is subangular to subrounded, equant to slightly elongated grains ranging in size from 0.01 to 0.6 mm and averaging 0.1 mm. The grains are well sorted. Grains larger than the average size are uncommon and tend to be rounded. Minute inclusions usually are present in the quartz grains. A few percent of the quartz grains show wavy extinction. Occasional, uncommon grains show fractures.

Feldspar

Anhedral grains of equant feldspar averaging 0.1 mm in diameter are present but occur in very minor amounts. Albite twinning, present in some grains, indicates the feldspar is plagioclase. Gridiron twinning, present in other grains, indicates microclines.

Chalcedony(?)

Scarce, irregular particles of fibrous material averaging 0.1 mm in diameter occur in the rock. The fibers form sheaflike aggregates of low birefringence and the particles are comprised

of many such sheaflike masses, each of which is randomly oriented. Optical properties and texture of the material are similar to chalcedony.

Opaque material

Opaque material consists of rounded to subangular, equant to elongated grains averaging 0.05 mm long. The grains are ubiquitous but occur in very small amounts. A brown stain is associated with a minor number of the grains but it is not prominent. In oblique reflected light the substance is pale-brown in color with a non-metallic luster. These properties are similar to those of limonite.

Cavities

Cavities, probably caused by solution of fossil material, are prominent locally in the drill core at various depths. The cavities usually occur as narrow, elongated lenses which are often curved (fig. 83). The cavities reach a maximum length of about 1.5 cm and locally make up as much as 20 percent of the rock by volume.

Sericite

A small amount of sericite occurs between quartz grains at a depth of 23.3 m, but was not noted elsewhere in the formation.

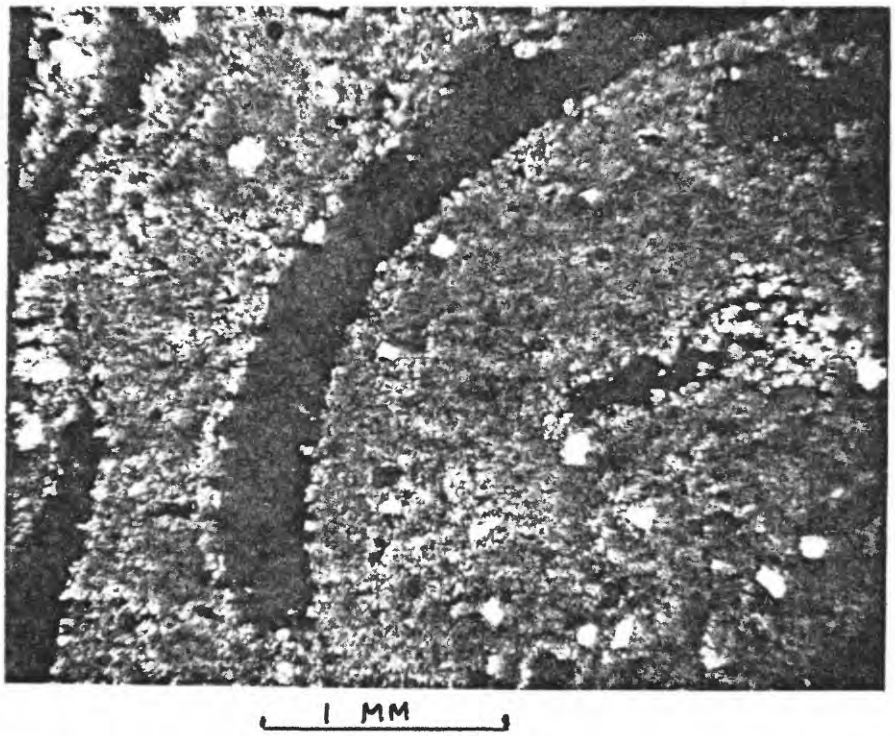

Figure 83.--Photomicrograph of Kaibab Limestone showing fossil shell solution cavities in microcrystalline granular dolomite. Crossed nicols. 32.6 m deep.

Petrography of the Moenkopi Formation

The Moenkopi Formation is pale reddish brown to grayish red in color and consists of quartz with minor calcite. Thin section examination indicates that the rock is a calcareous very fine grained quartz sandstone.

Quartz occurs as subrounded, equant, well-sorted grains averaging 0.1 mm in diameter. Occasional grains show wavy extinction. Quartz ranges from 50 to 7 percent of the rock by visual estimate in thin sections.

Calcite occurs as relatively coarse grains averaging 0.2 mm in diameter. Grains are anhedral with irregular margins that partially or wholly envelop quartz grains at the contact (fig. 84). At 20.1 m, calcite grains occur concentrated in relatively large aggregates of irregular shape, with smaller amounts of calcite irregularly distributed through the matrix as a cement (fig. 85). Patches reach a maximum length of 6 mm and show twinning. Quartz particles are abundantly included within the patches.

Very fine grained sericite(?) occurs in irregular, iron-stained, threadlike, anastomosing veinlets that traverse the rock in various directions. The matrix is stained a brownish color, possibly by iron oxide, which coats the quartz grains.

Feldspar, chalcedony(?), and opaque material occur in small amounts and total less than 1 percent of the rock by volume. The minerals are similar to those described from the Kaibab Limestone.

Examination of the drill core indicates that shaly intervals

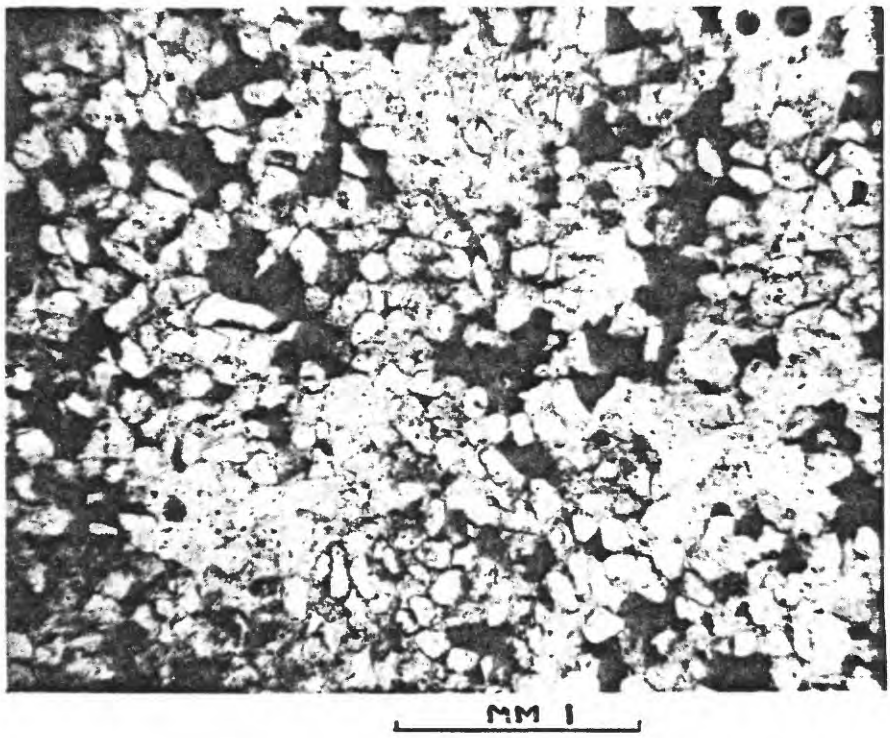

Figure 84.--Photomicrograph of Moenkopi Formation showing anhedral grains of calcite (dark) in clastic quartz from Meteor Crater core 4. Plane light. 11.4 m deep.

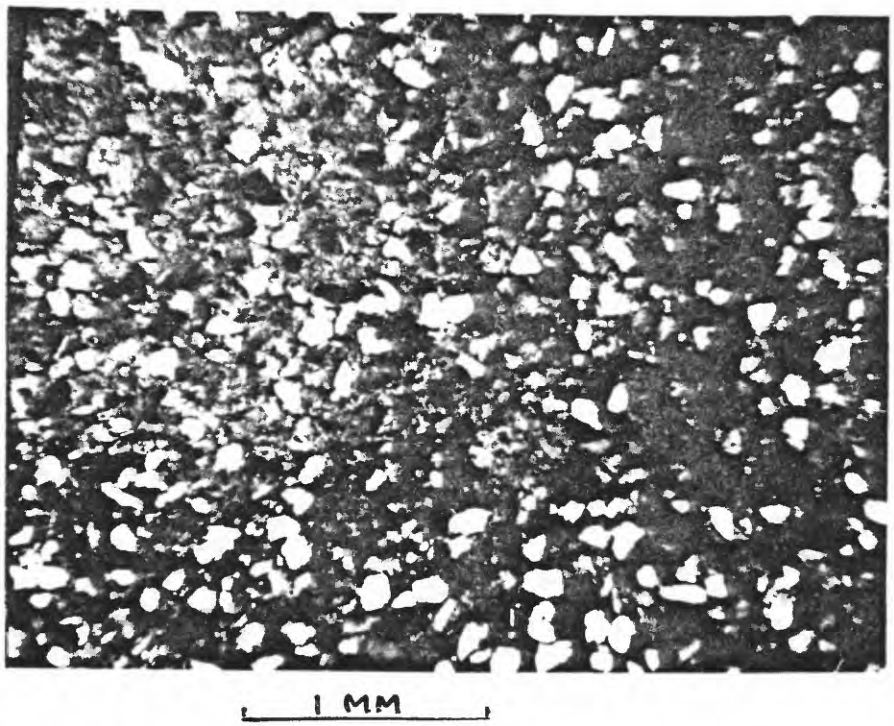

Figure 85.--Photomicrograph of Moenkopi Formation showing large calcite grain (upper left) in clastic quartz from Metero Crater core 4. Crossed nicols. 20.1 m deep.

occur in the Moenkopi Formation from 11.6 to 12.8 m, 14.8 to 14.9 m, and 19.8 to 20.0 m. The shaly rock intervals tend to split easily in a horizontal direction, are moderately well indurated, and can be easily scratched with steel in a manner similar to mudstone. Sericite and fine grained muscovite are particularly evident in the shaly rock intervals.

Debris zone

The debris zone overlies the Moenkopi Formation and is 10.0 m thick in MCC 4. The core to a depth of 4.9 m consists of sand and broken fragments of fine grained sandstone similar to the Coconino Sandstone. The recovered material from 4.9 m to 7.6 m consisted of unconsolidated sand, silty sand, and sandy silt containing rock fragments of calcareous sandstone and sandy dolomite up to 40 mm maximum length. The remainder of the core to 10.0 m consists of well-indurated sandy dolomite and dolomitic sandstone.

Petrographic examination of a thin section of dolomitic sandstone at 8.9 m, indicated gross textural and mineralogical similarities of the rock to strata in the Kaibab Limestone. The dolomite is the finely granular type that occurs in clots and as a cement and that is typical of the Kaibab Limestone below 24.8 m. The rock at 8.9 m contained notable amounts of sericite in threadlike veinlets and disseminated between quartz grains (fig. 86). A thin section of similar rock at 9.5 m contained sericite, but in lesser amounts.

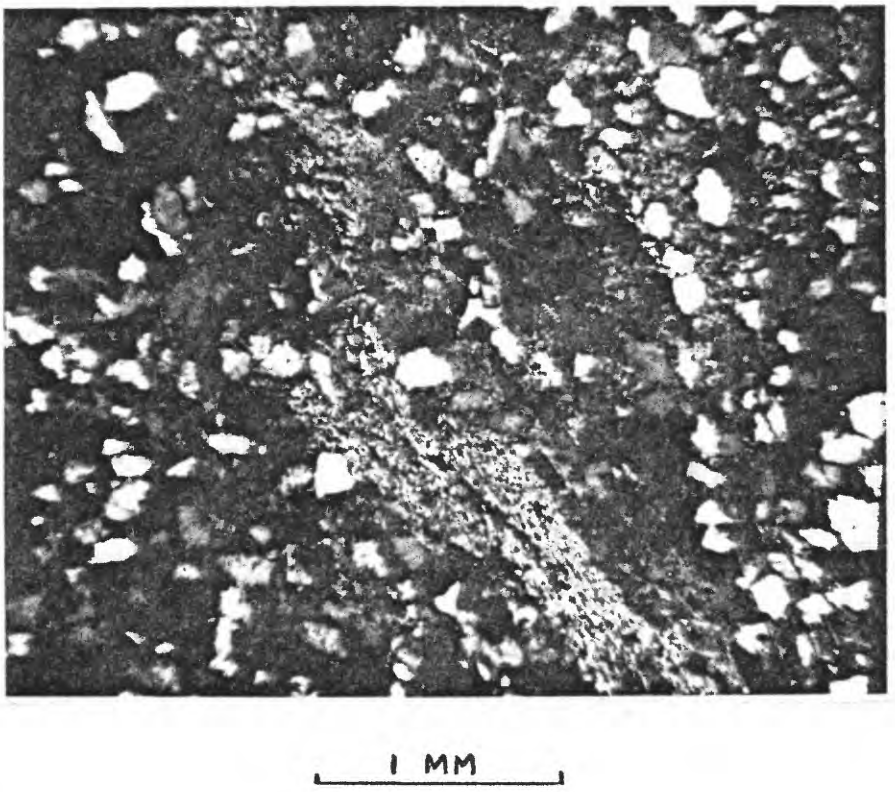

Figure 86.--Photomicrograph of debris zone. Threadlike veinlet of sericite in clastic quartz, fragment of Kaibab Limestone. Crossed nicols. 8.9 m deep.

Drill log

A summary of the drill core is shown in the drill log, table 10. Rock colors have been described according to the Munsell system, using the rock color chart published by the Geological Society of America. The drill core contains horizontal fractures averaging 2-3 inches apart. In 107.4 m of core, 1,059 fractures were counted.

Determinations of the sand content of the core were made at several depths by dissolving the carbonate portion of the rock in acid and then weighing the dried insoluble residue which consists almost entirely of very fine quartz sand. Results are summarized in table 11 and are shown in the drill log.

Visual estimates of the mode in each thin section examined are given in table 12.

Conclusions

An inverted stratigraphic relationship can be detected in the debris zone consisting of Coconino Sandstone near the surface and Kaibab Limestone at the base. Sericite in the Kaibab Limestone debris may be a shock-metamorphic mineral.

The Moenkopi Formation is essentially a calcareous very fine grained sandstone, although shaly rock intervals are present and comprise about 15 percent of the formation.

Table 10.--Meteor Crater drill hole 4 core log

Depth (m)	Thickness (m)	Description
0.0-1.2	1.2	Sandstone, yellowish-gray, fine-grained; grains rounded, average 0.25 mm in diameter; broken core.
1.2-4.9	3.7	Sand, yellowish-gray, fine; rounded grains average 0.25 mm in diameter.
4.9-6.1	1.2	Sand, silty, varicolored grayish-yellow and moderate reddish-orange; contains rock fragments up to 1.2 cm.
6.1-6.9	0.8	Silt, sandy, grayish-yellow; plastic; calcareous; contains rock fragments up to 1.2 cm.
6.9-7.6	0.7	Silt, sandy, moderate reddish-orange; contains broken rock fragments up to 40 mm in length; fragments are calcareous sandstone and sandy dolomite.
7.6-8.1	0.5	Dolomite, very pale orange, fine-grained; contains small lens-shaped cavities; broken core.
8.1-9.3	1.2	Sandstone, white, fine-grained; irregular pale yellowish-orange threadlike streaks; sand content at 8.8 m is 74 percent.
9.3-10.0	0.7	Sandstone, pale yellowish-orange, fine-grained; numerous pockets averaging 5 mm in diameter of white fine-grained, friable granular carbonate. Sand content at 9.5 m is 59 percent.
10.0-20.1	10.1	Sandstone, calcareous, pale reddish-brown to grayish-red, very fine-grained; scattered pockets of sericite and fine-grained muscovite; locally shaly from 11.6-12.8 m, 14.8-14.9 m, 19.8-20.0 m. Sand content at 11.4 m is 72 percent.

Table 10.--continued

Depth (m)	Thickness (m)	Description
20.1-20.2	0.1	Dolomite, grayish-orange, fine-grained.
20.2-21.0	0.8	Dolomite, light brown, coarse-grained aggregate; averages 2.5 mm in diameter with occasional lenses of colorless carbonate.
21.0-21.6	0.6	Calc-dolomite, pale yellowish-orange, fine-grained; 10 percent scattered coarse colorless calcite crystals averaging 3 mm; occasional vugs averaging 2 mm in diameter contains rhombs of dark yellowish-orange carbonate.
21.6-21.8	0.2	Dolomite, mottled moderate orange pink to pale greenish-yellow, coarse-grained; carbonate grains 1-3 mm in diameter; some pockets of fine-grained calcareous sandstone; rock is very well indurated.
21.8-22.2	0.4	Dolomite, pale yellowish-orange, fine-grained.
22.2-24.8	2.6	Dolomite, mottled moderate orange pink to pale greenish-yellow, fine-grained; average dolomite grain size is 0.2 mm; some pockets of fine-grained dolomitic sandstone. Sand content at 22.6 m is 25 percent.
24.8-39.6	14.8	Dolomite, very pale orange to white, fine-grained; fossil shell-solution cavities between 29.5 and 34.2 m. Sand content at 30.2 is 5 percent.
39.6-41.5	1.9	Dolomite, pale yellowish-orange to grayish-yellow, fine grained.
41.5-92.4	50.9	Sandstone and dolomite, white to yellowish-gray, fine-grained; gradational contacts. Sand content as follows: 45.5 m = 41 percent 61.0 m = 74 percent 75.6 m = 70 percent 91.5 m = 49 percent

Table 10.--continued

Depth (m)	Thickness (m)	Description
92.4-93.0	0.6	Dolomite, very pale orange, fine-grained.
93.0-95.5	2.5	Sandstone, white to yellowish-gray, fine-grained; sand content at 95.0 m is 76 percent.
95.5-107.3	39.6	Sandstone, pale yellowish-orange to grayish-yellow, fine-grained; fossil solution cavities at intervals from 96 m to 106 m; calcite with dolomite from 102 to 106 m; scattered round to oval pockets up to 10 mm in length of friable, very fine-grained white carbonate from 105 to 107 m. Sand content as follows: 98.5 m = 66 percent 101.5 m = 72 percent 106.0 m = 57 percent
107.3-107.4	0.1	Sandstone, white, fine-grained; consists of well sorted colorless quartz grains averaging 0.25 mm in diameter; disseminated minute black (opaque) grains 0.05 mm in diameter surrounded by rusty halos.

Table 11. Relative abundance of clastic quartz (insoluble residue) [percent by weight]

Depth (m)	Quartz (percent)	Formation
8.8	74.1	Debris zone (Kaibab Limestone)
9.5	58.8	" " " "
11.4	71.7	Moenkopi Formation
22.6	24.6	Kaibab Limestone
30.2	5.1	" "
45.5	41.4	" "
61.0	73.7	" "
75.6	69.6	" "
91.5	48.5	" "
95.0	76.4	" "
98.5	66.0	" "
101.5	71.5	" "
106.0	56.5	" "

Table 12. Visual estimate of modal composition from thin sections [percent by volume].

Depth (m)	Carbonate (percent)	Quartz (percent)	Cavities (percent)	Formation
8.9	15	85	--	Debris zone
9.5	40	60	--	" "
11.4	25	75	--	Moenkopi Formation
16.1	45	55	--	" "
18.3	20	80	--	" "
20.1	40	60	--	" "
21.0	97	3	Trace	Kaibab Limestone
21.4	95	2	3	" "
22.0	95	5	--	" "
22.7	65	35	--	" "
23.3	40	60	--	" "
29.9	75	10	15	" "
32.6	70	10	20	" "
37.5	75	25	--	" "
45.5	75	20	5	" "
53.4	75	10	15	" "
61.0	35	65	--	" "
67.5	75	10	15	" "
69.8	55	45	--	" "
75.7	44	55	1	" "
81.8	55	43	2	" "
87.4	60	40	--	" "

Table 12. Visual estimate of modal composition from thin sections--continued, [percent by volume].

Depth (m)	Carbonate (percent)	Quartz (percent)	Cavities (percent)	Formation
91.6	60	35	5	Kaibab Limestone
95.0	25	75	--	" "
98.5	40	60	--	" "
103.0	20	75	5	" "
106.0	40	60	--	" "

The Kaibab Limestone consists of sandy dolomite in the upper 25 percent of the formation, sandy dolomite interbedded with dolomitic sandstone in the central 60 percent of the stratigraphic section, and calc-dolomitic sandstone in the lower 15 percent of the cored section. The clastic quartz content is almost invariably high in the dolomite layers. Dolomite is relatively coarse-grained above 24.8 m, and microcrystalline granular below 24.8. The lithology suggests near-shore chemical precipitation.

Reference

Shoemaker, E. M., 1963, Impact mechanics at Meteor Crater, Arizona in The Moon, meteorites, and comets--The solar system, vol. IV: Chicago, Univ. Chicago Press, p. 301-336.

(page 195 follows)

"INVESTIGATION OF IN SITU PHYSICAL PROPERTIES OF SURFACE AND SUBSURFACE SITE MATERIALS BY ENGINEERING GEOPHYSICAL TECHNIQUES" PROJECT

FY 1967 WORK PLAN

Introduction

Physical properties data of the lunar surface are essential to the proper assessment of astronaut safety during the Apollo missions. They are necessary for the full interpretation of the geophysical data obtained by instruments in the Lunar Surface Experiments Package. The data are essential for the understanding of the mode of formation of the lunar near-surface materials, lunar near-surface structures, and other lunar geologic problems; and are necessary for a full and proper interpretation of the data obtained from the lunar-orbiting satellites.

Mission success and its corollary, astronaut safety, are first considerations of any engineering physical properties investigation. Of the engineering properties, bearing strength and trafficability are thought to be most important because they are directly related: (1) to the ability of the Early Apollo Lunar Excursion Module to land safely on the lunar surface; (2) to the ability of the astronaut to safely carry out his assigned mission, and (3) to the ability of the ascent stage of the Lunar Excursion Module to leave the surface. The physical properties measurements thus can be divided: (1) those engineering properties that are

directly related to bearing strength and trafficability of the lunar surface materials, and (2) those physical properties which will assist in interpreting geological investigations conducted on the lunar surface.

Physical properties controlling the surface bearing strength and general trafficability of the lunar surface materials will receive highest priority since these properties will be of prime importance to mission success. Engineering properties such as shear strength, creep, cohesion, compressive strength, tensile strength, Mohr's envelope, porosity, bulk density, particle size, distribution and shape, and composition will help to determine if the lunar surface materials will allow an early Apollo spacecraft to land safely and remain in a safe attitude throughout the lunar mission. These engineering properties will also largely control astronaut trafficability and safety while conducting missions on the lunar surface.

Elastic rock properties can be calculated from density, compressional wave velocity, and shear wave velocity. The interrelationship between laboratory calculated values and in situ values is being studied because the direct measurement of many of the engineering properties would be extremely difficult and time-consuming to measure on the lunar surface.

Work Plan

Objectives

The overall objective of the project is to develop methods for determining physical properties of lunar surface and subsurface materials by employing seismic parameters. Emphasis is on the interrelationship of physical properties which will assist in determining bearing strength and trafficability, and in interpreting early Apollo geophysical and geological investigations.

The effort on this project has been divided into four phases:

1. Selection of appropriate lunar analog sites;
2. Surface and subsurface geologic control and the measurement of of mechanical physical properties (laboratory and in situ);
3. Gathering seismic data on near-surface materials;
4. Correlating data and formulating criteria by which certain engineering properties can be deduced from seismic parameters.

Status of work and accomplishments to date

Eighteen potential lunar analog sites have been selected for study. These sites cover a varied spectrum of physical characteristics.

Seismic field measurements have been completed at these sites except for the possibility of some rework and minor extension recommended by future data analysis. Seismic measurements were designed primarily to record head-wave motion induced in near-surface materials by dynamite charges and weight drops. Data is

recorded in both analog and digital form. Data from seismic analog recordings have been analyzed for compressional-wave and shear-wave velocities and compressional head-wave attenuations. Several empirical and theoretical relationships have been studied that relate these parameters to observed physical properties. Two important relationships are:

1. The in situ bulk density of dry granular and fractured materials can be determined from the compressional wave velocity with an rms error of about 0.24 g per cc.
2. The calculated shear modulus and Young's modulus of granular and fractured materials can be estimated from the shear-wave velocities without consideration of the other parameters as indicated by the elastic theory. These calculated moduli are being compared with the measured in situ moduli.

In situ mechanical properties measurements include bearing strength, shear strength, penetration resistance, bulk density and moisture content. Laboratory measurements include confined and unconfined compressive strength, tensile strength, bulk density, grain density, porosity, permeability, chemical analyses, compressional-wave celocity and shear-wave velocity.

Areas of concentration in FY 1967

Geologic and physical properties investigations

Geologic personnel will complete the surface and borehole petrography of the remaining unfinished sites and will be responsible for the physical properties measurements.

Laboratory physical properties investigations will continue as in past years but on a smaller scale since most of this site data is completed. The only new measurements that will be made on existing core samples will be scleroscope hardness.

A significant part of the project effort during fiscal year 1967 will be spent measuring in situ mechanical properties. This investigation will include the measurement of bearing capacity, shear strength, bulk density, moisture content, and penetration resistance. In situ bulk density is now being measured on the surface of fine-grained sites with a 4.5 millicurie gamma ray backscattering device. The present gamma ray backscatterer has a depth of penetration of 10 inches. Since many of the lunar analog sites consist of loosely packed angular blocks of rock whose median size is greater than 10 inches, this instrument is not applicable for measurements in these areas.

Bulk density of the blocky sites is being measured by excavating a known weight of sample from a large pit whose volume can be calculated. Since a nuclear density measuring device having a penetration depth of 3-10 feet does not exist "on the shelf", In Situ Project will construct, calibrate, and use a

probe that will measure in situ bulk densities between two drill holes. This probe will use a gamma absorption technique rather than a gamma backscattering method, and the calibration will be done on sites where the bulk density is known by an excavation technique. This instrument will allow the operator to make a large number of density measurements on a site in a limited amount of time.

Geophysical investigations

Field work will be limited to rework or minor extension in areas already investigated as demanded by future data analysis.

To date, analysis of seismic data has been done manually from analog field recordings. Methods are tedious, time-consuming, and do not lend themselves to the proper analysis of the frequency spectrum of a seismic signal. All seismograms have therefore been digitized for analysis by high-speed computers.

The basic objectives are:

a. Develop computer programs for rapid computation of parameters presently obtained by hand.
b. Improve attenuation calculations by including frequency analyses of head waves.
c. Incorporate physical-property data into computer programs.
d. Develop programs to correlate seismic data with measured physical properties.

e. Interpret computer results to improve criteria already formulated by which physical properties can be obtained from seismic data.

Subroutine programs compatible with a CDC 3600 computer have already been written for reading and storing data from digital recordings and performing various frequency and amplitude analyses (frequency and amplitude spectra, frequency and velocity filtering, autocorrelation, crosscorrelation, and X-Y plotting). Additional subroutine programs for individual trace amplitude corrections and statistical analyses of seismic and physical property data will be either written or incorporated from existing library programs. Mainline programs using these subroutines for computation of significant parameters will be written and altered as the data analyses progresses. Several such mainline programs have already been completed.

Approximate schedules

An approximate schedule for completion of the work plan follows:

1. All subroutine and mainline programs written and debugged by end of second quarter;

2. Geologic field work and physical properties measurements completed by end of third quarter.

3. Data analyses and final report by end of fourth quarter.

Personnel

Lawrence A. Walters and Hans D. Ackermann of the U.S. Geological Survey, Flagstaff, Arizona, are responsible for directing the project. The project personnel will consist of:

1 Full-time geophysicist

1 Full-time geologist

1 Full-time rock mechanics engineer

2 Quarter-time geophysicists

1 Half-time geophysicist

1 Quarter-time geologist

1 Electronics technician

1 Half-time computer programmer

13 Sub-professional personnel

Existing Test Sites

Eighteen lunar analog sites have been investigated as part of the In Situ Project. The location of these sites is shown in figures 87 and 88.

S P Flow.--The flow is a Recent basaltic lava flow. The surface consists of loosely packed, angular, equant, polygonal blocks of lava that range from 20 cm to 2 m across and average about 0.3 m in diameter. The porosity of the loosely packed rubble is estimated to range between 20 and 35 percent.

The blocky basalt is dark gray to grayish-black and weathers to a mottled dark reddish- and yellowish-brown. It is fine-grained and finely vesicular; the vesicles are generally tubelike and distinctly flattened. The vesicularity of the rocks at the surface ranges from less than 5 percent to as much as 50 percent and averages about 15 percent. Small phenocrysts and plagioclase, pyroxene, and rarely olivine (which average about 1 mm in length) are sparsely scattered through the rock.

The rock has a porphyritic hyalopilitic texture mainly composed of elongate laths of plagioclase and stubby prisms of pyroxene set in a base of brown glass. The plagioclase laths usually show a distinct fluidal orientation that beds and swirls around the phenocrysts, which are mainly pyroxene. The grain size ranges from .01 mm to 5.0 mm, and averages about .07 mm. The plagioclase is mostly calcic andesite, indicating that the rock is probably a basaltic andesite or an andesitic basalt.

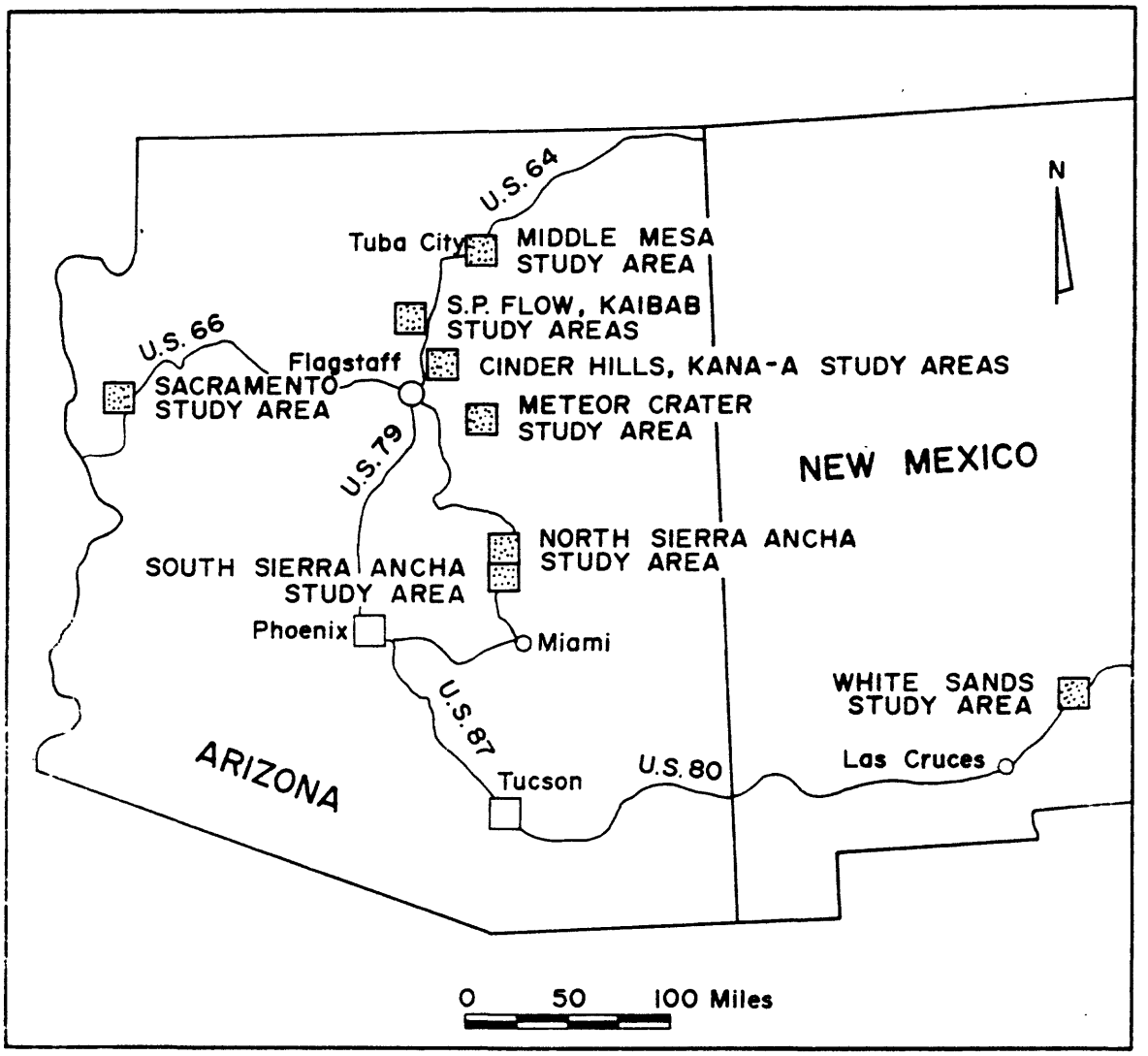

Figure 87. In Situ Arizona & New Mexico lunar analog sites.

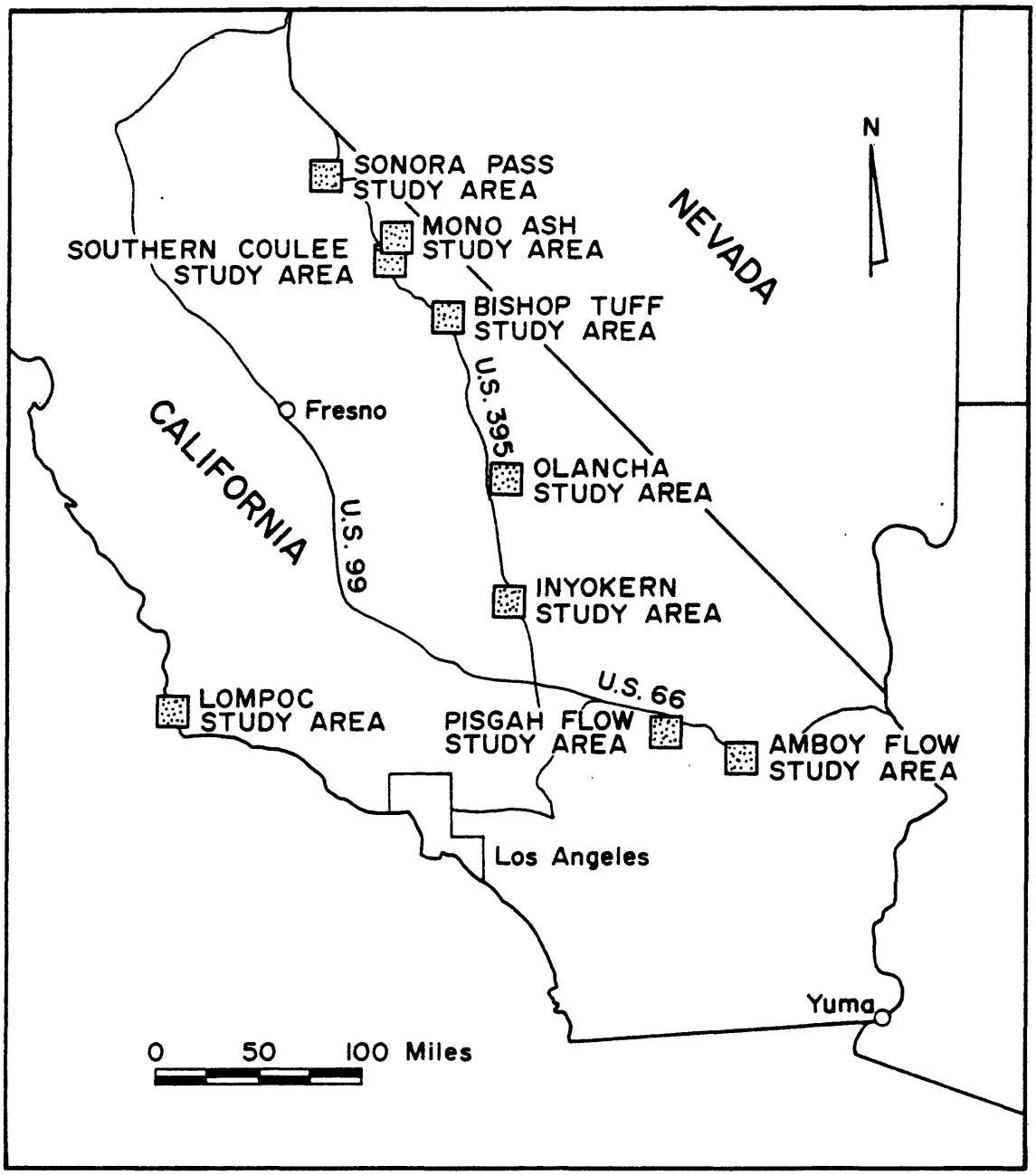

Figure 88. In Situ California lunar analog sites.

The physical properties of rocks at this site are thought to resemble those of the broken, brecciated mare surface beneath the low-density layer, or of accumulations of broken fragments thrown out along rays from craters. A preliminary map of part of the surface of this flow is available (Watkins and others, 1964).

A large pit of known volume was excavated at the S P site. The bulk density of the upper 10 feet of the flow is 1.23 g per cc.

Kana-a Flow.--This Recent olivine basalt flow is a typical aa-type lava. The flow is covered with 0-6 m of ash through which project jagged, spinose, vesicular, clinkery blocks and plates of lava which are commonly tilted up at various angles.

The lava is medium gray to medium dark gray and weathers dark gray. It is fine grained, though distinctly coarser than S P and is very sparsely and finely porphyritic. Olivine and plagioclase phenocrysts occur in about equal amounts but the larger (average diameter about 2 mm), rounded, glassy green olivine crystals are much more conspicuous. The flow is much more vesicular than S P with the vesicles ranging in diameter from less than 1 mm to more than 20 mm, and averaging about 5 mm. The vesicularity ranges from 10 to 50 percent, and averages about 25 percent.

The Kana-a flow is thought to be similar to lunar mare material overlain by a low-density layer represented in this case by the cinders and ash. A detailed geologic examination of this flow has been reported, (Loney, 1965).

Kana-a flow is covered with pine and low brush, but the adjacent Bonito flow that is thought to have been extruded from

the same vent and has nearly identical chemical and mineralogical composition is virtually free of vegetation. The Bonito flow was not used for seismic investigations because it is part of a national monument and roads cannot be built on it.

Cinder Hills.--This area, which lies north-northeast of Sunset Crater, consists of thick accumulations of ash. The ash is deposited in beds that range from 15 cm to more than a meter thick. The grain size in these beds varies markedly from bed to bed with some suggestion of grading upward from coarse to fine. The range in grain size within a meter or so varies from 1/4 to 3 mm in diameter.

The Cinder Hills area is thought to be analogous to a thick accumulation of low-density material consisting of fine fragments formed either by volcanic activity or by repeated meteorite impact.

Kaibab.--This area consists of a relatively thick sequence of Permian limestone beds and interbedded limestone-clastic beds. The thickness exceeds 80 feet in the study area.

This area was selected to test equipment and field operations techniques rather than for any possibility of lunar analogs. Nevertheless, its location near S P Flow and the availability of cores for study make it an excellent possibility for earth-orbiting satellite studies.

Meteor Crater.--Meteor Crater probably is the best example of an impact crater in the world today. Investigations designed to determine the subsurface structure of the crater have begun; specifically, the depth and configuration of the bottom of the brecciated layer in the crater, the thickness of the debris layer

on the rim, and the variation of physical properties within the debris and brecciated zones in and around the crater.

Sierra Ancha.--Two localities of Precambrian quartzite have been selected for study. Both are located between Young, Arizona, and Roosevelt Dam, Arizona. The quartzite in one area is not fractured vertically to any extent but does have prominent bedding planes at intervals of 0.3-1.0 m. The other site is massive with respect to bedding, but it is vertically fractured to some extent. The fractures are filled with soil and may be recemented at depth. One area is tree-covered and probably not applicable for remote sensing tests; however, the other area is mostly free of vegetation.

Middle Mesa.--The Navajo Sandstone is a slightly cemented sandstone having a porosity of approximately 28 percent. An outcrop of this unit at Middle Mesa, approximately 25 miles northeast of the junction of highways U.S. 89 and Arizona 64 in Coconino County, Arizona, has been selected as the study area.

Sacramento.--The Sacramento site is located south of Kingman, Arizona, in the Sacramento Valley. The site is situated on a great thickness of dry valley-fill alluvium which has grain size ranging from clay-size materials to cobbles.

White Sands.--The White Sands site is located on the Recent gypsum dunes of the White Sands National Monument near Alamogordo, New Mexico.

Sonora Pass.--This granite is coarsely porphyritic, pale pink, and characterized by numerous large euhedral phenocrysts of pink potassium feldspar, which average about 5-cm long and in places

as much as 10-cm long. Megascopically, the groundmass consists of small (average diameter about 3 mm) grains of pink potassium feldspar, white plagioclase, and glassy quartz through which are scattered fine grains of biotite and hornblende.

The granite is usually unweathered except for the upper few centimeters. It is almost homogeneous and sparsely jointed; about 2-5 cm thick. Aplite veins are present.

Forty feet of core have been taken from this granite for study. It is thought to be similar to lunar upland material.

Southern Coulee.--The top of this coulee is a chaos of spires, crags, and loosely piled, angular blocks of pumice and obsidian. Three distinct lithologic units are recognized; each has a characteristic range in density and distinctive physical characteristics. No compositional differences have been recognized--differences are related to degree and character of vesicularity. The lowest density unit ranges from 0.51 to 0.78 g per cc. The intermediate layer has a density of 1.20 g per cc and the highest density unit, where obsidian is more abundant ranges from 1.37 to 2.07 g per cc.

The rock of the coulee is predominantly layered pumice (density 0.53-2.01 g per cc) that generally lacks microscopically visible crystals. Obsidian, a minor but ubiquitous constituent of all units, occurs as lenses and laminae in the pumice. The obsidian lacks visible phenocrysts but contains sparse spherulites ranging in diameter from less than 1 mm to more than 40 mm and averaging about 2 mm. X-ray diffraction indicates that the spherulites are composed of sanidine and well-ordered cristobalite.

Glass of the pumice and obsidian is fresh and lacking in devitrification products, except the sparse spherulites in the obsidian. A few minute crystals of sanidine have been seen microscopically, but these are extremely rare and do not noticeably affect the whole rock x-ray diffraction patterns, which are characteristic of pure glass.

The Southern Coulee is the only easily accessible flow of the main chain of the Mono Craters. The extremely low densities observed in the pumice of this coulee (presumably, equally low densities can be found in the other craters), the high vesicularity of the material, and local cover of fine, low-density ash (see Mono Ash below), make this area one of the best terrestrial analog sites on the basis of what we no know about the lunar mare surface material. A preliminary geologic mapping report of this flow has been prepared (Watkins and others, 1964).

Cores from this area penetrated permafrost, thus lending additional interest to its study because of theories concerning the possible existence of ice on the lunar surface.

Mono Ash.--This area lies northeast of the northernmost of the main mass of the Mono Craters and consists of a thick layer of white pumiceous ash and lapilli that is level and free of vegetation. The ash shows a higher degree of crystallinity than the flow rocks; quartz, plagioclase, biotite, and possibly potassium feldspar have been identified by x-ray diffraction.

The lunar analogies provided by the Mono Ash are much the same as those provided by the Cinder Hills, except that the

Mono Ash consists of rhyolitic fragments, whereas the Cinder Hills area consists of basaltic fragments.

Bishop Tuff.--The rock of this large area is partially welded rhyolite tuff of Pleistocene age. The upper 20 m is hard, dense, and welded; but below this layer it is unwelded and less dense to at least 60 m. The tuff is tightly jointed into polygonal columns about 0.7 m across.

The tuff is composed of porphyritic pumice fragments that contain abundant phenocrysts of quartz, sanidine, and lesser amounts of plagioclase, and biotite sprinkled at random through a matrix of fine vitric tuff. The matrix also contains crystals similar to the pumice of Southern Coulee. Crystals compose about 10 percent of the tuff. The tuff is pink to reddish brown at the surface. White layers stratigraphically below the pink tuff crop out along the southern edge of the deposit.

The Bishop Tuff was selected because it is the best terrestrial analog found that demonstrates the proposed vacuum welding of extremely fine particles on the lunar surface.

Pisgah Flow.--The Pisgah flow is thought to have a basaltic composition similar to that of the flows in the Flagstaff area (Kana-a and Bonito). Reconnaissance of this flow indicates that the surface consists of roughly equal parts of pahoehoe and aa lava. The pahoehoe lava is smooth and trafficable. However, the aa lava is ragged, and blocky, and similar to the surfaces of the basaltic flows near Flagstaff.

The Pisgah flow also includes numerous lava tunnels, which,

if found on the lunar surface, could be used as natural shelters by the astronauts; or might possibly constitute hazards to an astronaut traversing the surface or to a lunar module landing on the surface during the early Apollo missions. These have been studied in some detail. For a partial report, see Watkins and others, 1965.

In situ measurements and studies indicate that the lateral dimensions of these cavities can accurately be determined by seismic studies on the ground. The capability exists to perform field verification tests, if desired, for remote sensing missions undertaken on behalf of early Apollo missions.

Amboy Flow.--Reconnaissance suggests that the composition of the Amboy Flow is much the same as that of the nearby Pisgah Flow. The Amboy Flow surface consists almost entirely of smooth trafficable pahoehoe lava and seismic investigations show that the lava tends to be more massive and less porous in the area of our investigations. Geologic investigations are underway to determine the causes of the variations in surface textures of the two flows having apparently similar composition.

Lompoc diatomite site.--The Lompoc diatomite site is a few miles south of Lompoc, California,

The diatomite occurs in the Miocene-Pliocene Sisquoc Formation.

The diatomite talus site is on a low-grade stockpile (no. 15)

The stockpile is approximately 11 feet thick and is underlain by a more compacted diatomite

stockpile and "in place" diatomite waste material. The diatomite talus material ranges in size from very fine aggregates to lumps of material 10 in x 10 in x 2 in.

The "in place" site is located on the crest of an anticlinal structure on hill 24 and consists of at least 100 feet of "waste diatomite." The "waste diatomite" consists of diatomite interbedded with clay and admixed clay.

Olancha bentonite site.--The Olancha bentonite site is located 10 miles east of Olancha, California, at the southern end of Owens Valley. The material is a non-swelling montmorillonite clay that has been extensively mined

for use as a filter aid and insecticide carrier.

The bentonite talus site consists of material mined from adit 29 and dumped on the slope in front of the mine adit. Minor amounts of an overlying dense volcanic rock are intermixed with the bentonite, and the bentonite talus is underlain by a talus composed predominantly of the dense volcanic rock. The bentonite talus consists of material that ranges in size from fine lumps to blocks 12 in x 12 in x 3 in.

The "in place" site is underlain by at least 12 ft of compact bentonite that is in turn underlain by a clayey siltstone.

Inyokern volcanic ash site.--The Inyokern volcanic ash site is located 14 miles south of Inyokern, California,

The material consists of volcanic ash with varying degrees of alteration (kaolinization?).

The volcanic ash stockpile is approximately 10 ft thick. It is vertically stratified into various density and moisture units.

References

Watkins, J. S., De Bremaecker, J. Cl., Loney, R. A., Whitcomb, J. H., and Godson, R. H., 1965, Investigation of in situ physical properties of surface and subsurface site materials by engineering geophysical techniques--Project ann. rept., FY 1965: Flagstaff, Arizona, U.S. Geol. Survey, Br. of Astrogeology, 163 p.

Watkins, J. S., Loney, R. A., and Godson, R. H., 1964, Investigation of in site physical properties of surface and subsurface site materials by engineering geophysical techniques--Project ann. rept., July 1, 1964: Flagstaff, Arizona, U.S. Geol. Survey, Br. of Astrogeology, 77 p.

Watkins, J. S., Loney, R. A., Whitcomb, J. H., and Godson, R. H., 1965, Quarterly report for investigation of in situ physical properties of surface and subsurface site materials by engineering geophysical techniques: Project Rept., October 1, 1964-December 31, 1964: Flagstaff, Arizona, U.S. Geol. Survey, Br. of Astrogeology, 67 p.

(page 217 follows)

APPENDIX A-D

APPENDIX A

(page 221 follows)

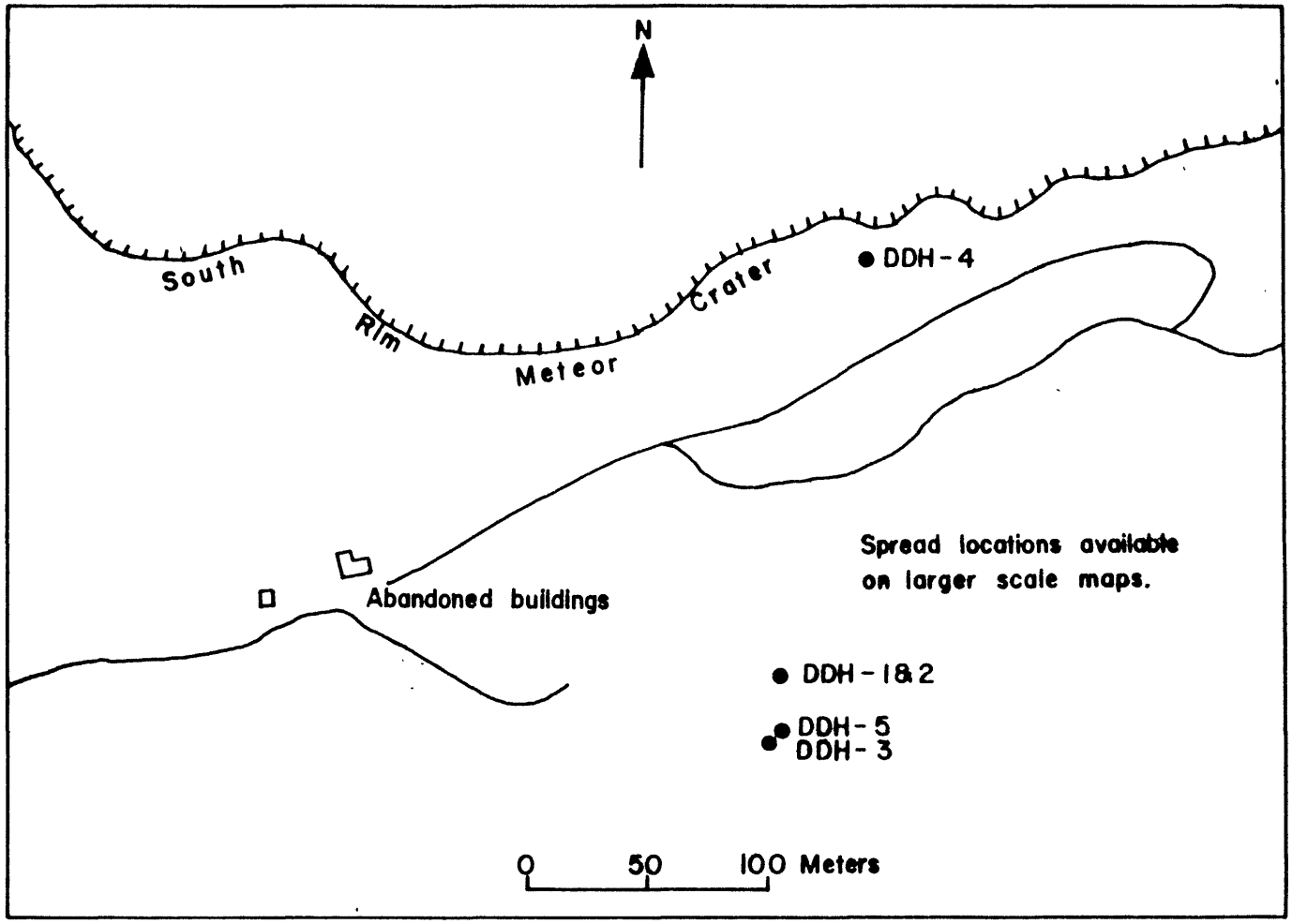

Figure 89--Meteor Crater, Arizona diamond drill hole locations.

Meteor Crater Core Hole 1
Coconino County, Arizona
Driller: Robert A. Elmer
Begun June 7, 1965 Finished June 9, 1965

Sample Depth (feet below surface)	Recovery (percent)	Description of material
3.0	0	Sandstone, white, pulverized.
4.6	93	" " "
6.0	100	" " "
11.0	0	" " "
12.4	100	" " "
22.4	30	" " "
26.0	93	" " "
32.0	17	" " "
42.0	20	Limestone, yellow, coarse, unconsolidated.
52.0	8	" " " "

Meteor Crater Core Hole 2
Coconino County, Arizona
Driller: Robert A. Elmer
Begun June 9, 1965 Finished June 17, 1965

Sample Depth (feet below surface)	Recovery (percent)	Description of material
3.0	0	Sandstone, white, pulverized.
16.0	100	" " "
26.0	20	" " "
32.0	33	" " "
35.0	66	Limestone, yellow, pulverized.
40.0	20	" " "
45.0	50	" " "

Meteor Crater Core Hole 3
Coconino County, Arizona
Driller: Robert A. Elmer
Begun June 18, 1965 Finished June 30, 1965

Sample Depth (feet below surface)	Recovery (percent)	Description of material
35.0	0	Sandstone, white, pulverized.
39.0	0	Limestone, buff, pulverized.
41.0	50	Limestone, buff, semi-consolidated.
43.0	75	" " " "
45.6	65	" " " "
55.0	100	" " " "
58.0	80	" " " "
63.0	27	" " " "
70.0	40	Shale, red, soft.
75.0	12	Shale, red, medium.
82.0	100	" " "
84.0	0	Ground up with rock bit (no core).
91.0	66	Shale, red, highly fractured cavity (91.6'-92.6').
93.0	50	Shale, red, medium.
97.0	90	Limestone, buff, medium.
100.6	55	" " "

Meteor Crater Core Hole 4
Coconino County
Driller: Robert A. Elmer
Begun January 26, 1966 Finished March 7, 1966

Sample Depth (feet below surface)	Recovery (percent)	Description of material
8.0	50	Sandstone, fractured--some rock fragments and some pulverized material most of which is washing away.
10.0	30	" " "
15.0	20	" " "
25.0	40	Sandstone and limestone, fractured.
33.0	50	Limestone, sandy, badly broken.
38.0	64	Sandstone, red, broken.
42.0	68	Sandstone, red, badly broken.

Meteor Crater Core Hole 4, Continued

Sample Depth (feet below surface)	Recovery (percent)	Description of material
47.0	20	Sandstone, red, vertical joints
60.0	77	Sandstone, red, few vertical joints, not as badly broken horizontally.
68.0	54	Sandstone, red; limestone, buff.
79.0	100	Limestone, sandy, buff to brown; some zones crystalline; all badly broken.
90.0	45	Limestone, sandy, buff; soft, air washed soft broken material away.
101.0	41	Limestone, sandy, very badly broken.
111.0	70	Limestone, sandy, buff to gray; badly broken.
121.0	90	" " "
132.0	81	" " "
142.0	60	" " "
152.0	83	" " "
162.0	79	" " "
182.0	90	Limestone, sandy, buff, badly broken.
192.0	95	" " " "
202.0	60	" " " "
212.0	65	" " " "
222.0	45	" " " "
232.0	95	" " " " (not too badly broken)
241.0	100	" " " "
251.0	30	Limestone, sandy, buff, to limestone, crystalline, tan; not too badly broken.
262.0	47	Limestone, sandy, buff; not too badly broken.
272.0	60	Limestone, sandy, buff; badly broken.
282.0	45	" " " "
292.0	50	" " " "
302.0	65	" " " "
312.5	100	" " " "
322.5	83	" " " "
332.5	95	" " " "
342.5	80	" " " "
352.5	40	" " " "
366.0	0	Sandstone, poorly cemented (?) or Sandstone, highly fractured (pulverized).

Meteor Crater Core Hole 5
Coconino County, Arizona
Driller: Robert A. Elmer
Begun March 18, 1966 Finished March 30, 1966

Sample Depth (feet below surface)	Recovery (percent)	Description of material
30.0	0	Sandstone and limestone, buff.
66.0	0	Limestone, buff, sandy--contact.
91.5	0	Sandstone, red--contact.
102.5	0	Limestone, buff, cherty.
110.0	53	Limestone, buff to yellow, badly fractured.
122.0	50	Limestone, buff, sandy, highly fractured.
126.0	75	" " " "
132.0	33	" " " "
142.0	30	" " " " (powdery yellow zones washing out completely).
152.0		Limestone, buff, sandy, not as badly broken.
162.0	90	" " " "
172.0	40	Limestone, buff, sandy, some badly broken zones.
182.0	30	" " " " "
192.0	60	" " " " "
202.0	85	" " " not too badly broken.
212.0	95	" " " " "

(page 227 follows)

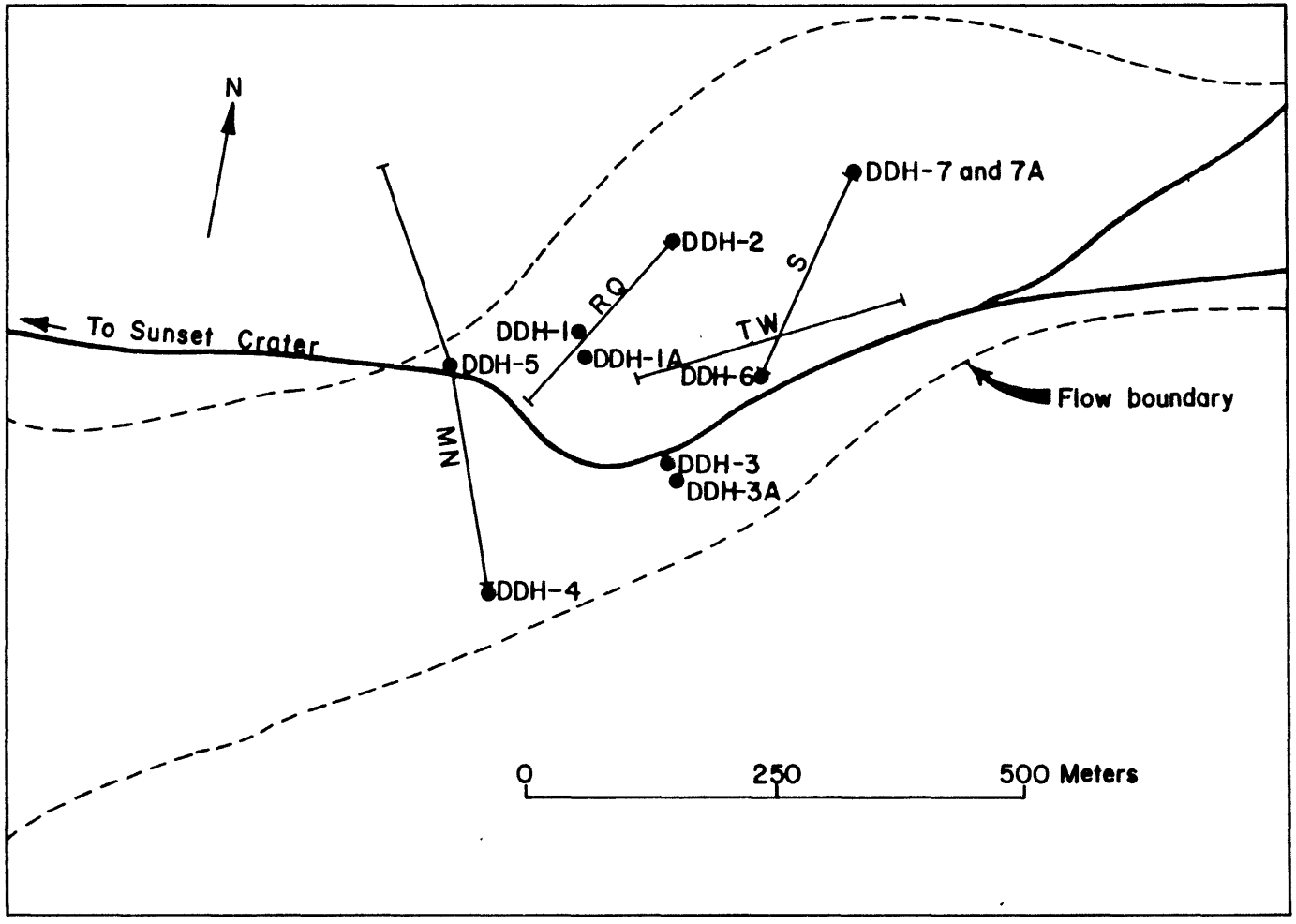

Figure 90.--Kana-a Flow, Arizona diamond drill hole and seismic spread locations.

Kana-a Flow Core Hole 1
Coconino County, Arizona
Driller: Rudy Gracey
Begun June 8, 1964 Finished June 9, 1964

Sample Depth (feet below surface)	Recovery (percent)	Description of material
17.0	0.0	Cinders, loose.
22.0	60	Basalt, vesicular.
32.0	50	" "

Kana-a Flow Core Hole 1A
Coconino County, Arizona
Driller: Rudy Gracey
Begun June 9, 1964 Finished June 10, 1964

Sample Depth (feet below surface)	Recovery (percent)	Description of material
6.5	0.0	Cinders.
11.5	96	Basalt--weathered zone 16'±.
16.0	60	" " " "
26.5	86	" " " "
30.0	65	" " " "
32.0	60	Cinders.

Kana-a Flow Core Hole 2
Coconino County, Arizona
Driller: Rudy Gracey
Begun June 11, 1964 Finished June 12, 1964

Sample Depth (feet below surface)	Recovery (percent)	Description of material
5.0	0.0	Cinders.
10.0	76	Basalt--Vesicular to 17'±; Dense to 29'±; Vesicular to 31'±.
31.0	100	" " "
40.0	0.0	Cinders.

Kana-a Flow Core Hole 3
Coconino County, Arizona
Driller: Rudy Gracey
Begun June 12, 1964 Finished June 12, 1964

Sample Depth (feet below surface)	Recovery (percent)	Description of material
8.0	0	Cinders.
9.0	70	Basalt, vesicular.
18.0	0	Cinders.

Kana-a Flow Core Hole 3A
Coconino County, Arizona
Driller: Rudy Gracey
Begun June 13, 1964 Finished June 13, 1964

Sample Depth (feet below surface)	Recovery (percent)	Description of material
5.0	0	Cinders.
10.0	100	Basalt--dense to 12'±, then vesicular.
19.5	66	" " " " "
40.0	0	Cinders.

Kana-a Flow Core Hole 4
Coconino County, Arizona
Driller: Phil Glaze
Begun July 27, 1964 Finished July 27, 1964

Sample Depth (feet below surface)	Recovery (percent)	Description of material
24.0	0	Cinders, loose.
30.0	45	Basalt, highly vesicular.
35.0	45	Cinders, loose.
37.0	20	Basalt and rubble.
40.0	20	Cinders, red, rubble.

Kana-a Flow Core Hole 5
Coconino County, Arizona
Driller: Phil Glaze
Begun July 27, 1964 Finished July 28, 1964

Sample Depth (feet below surface)	Recovery (percent)	Description of material
15.0	0	Cinders, fine size.
22.0	21	Basalt, red, highly vesicular, mostly rubble.
31.0	33	Basalt and rubble.
40.0	0	Cinders and rubble.

Kana-a Flow Core Hole 6
Coconino County, Arizona
Driller: Phil Glaze
Begun July 28, 1964 Finished July 29, 1964

Sample Depth (feet below surface)	Recovery (percent)	Description of material
10.0	78	Basalt, highly vesicular.
15.0	94	Basalt, gradually becoming less vesicular; becoming dense and layered.
25.0	86	Basalt--0.2-0.4 ft layers.
35.0	96	" " " " "
40.0	80	Basalt, layered, becoming vesicular; cinders last half foot.

Kana-a Flow Core Hole 7
Coconino County, Arizona
Driller: Phil Glaze
Begun July 24, 1964 Finished July 24, 1964

Sample Depth (feet below surface)	Recovery (percent)	Description of material
22.0	0	Cinders, loose.

Kana-a Flow Core Hole 7A
Coconino County, Arizona
Driller: Phil Glaze
Begun July 29, 1964 Finished July 29, 1964

Sample Depth (feet below surface)	Recovery (percent)	Description of material
40.0	0	Cinders, loose.

(page 233 follows)

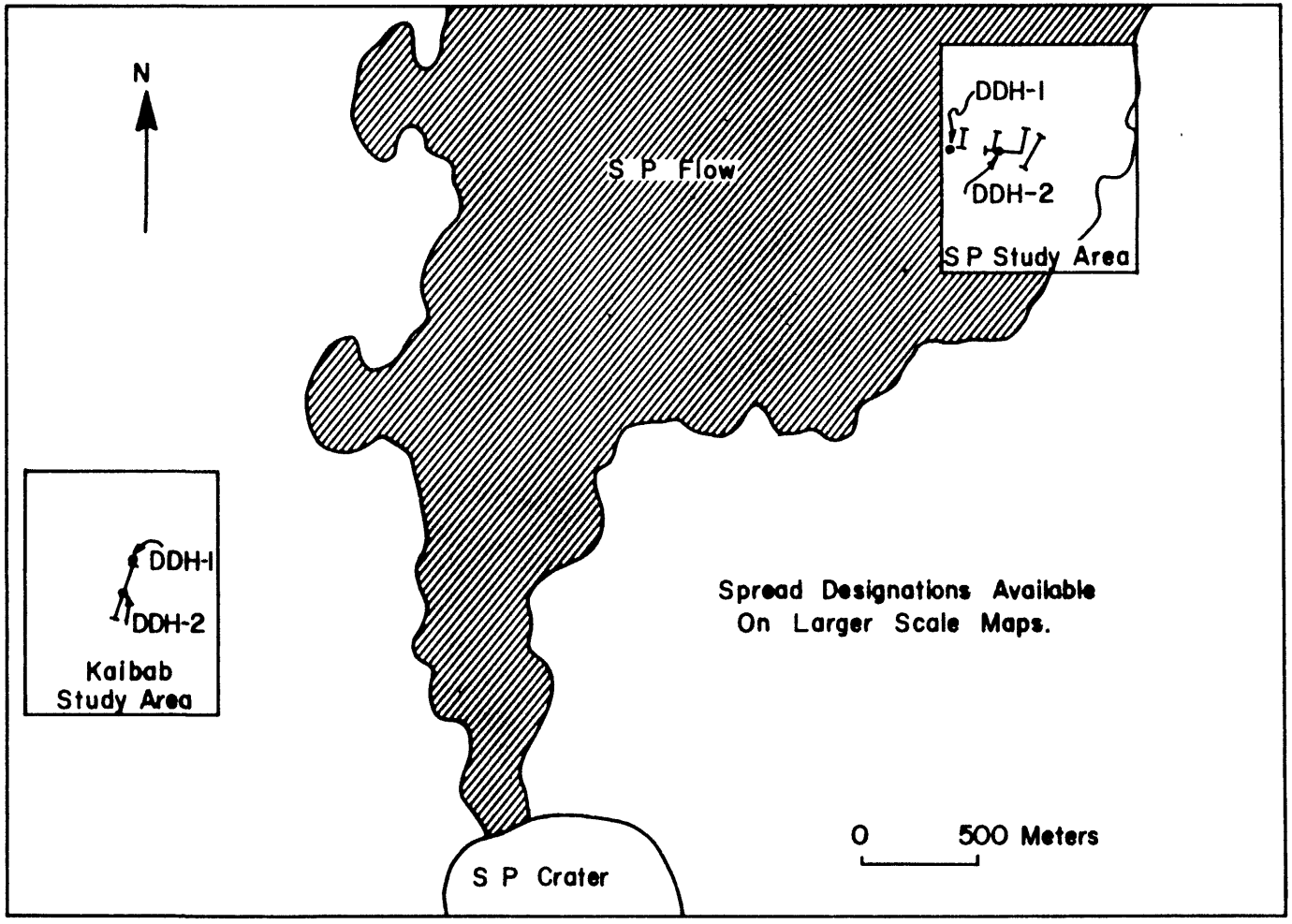

Figure 91.--S P and Kaibab flow areas, Arizona diamond drill hole and seismic spread locations.

S P Flow Core Hole 1
Coconino County, Arizona
Driller: Norman Bailey
Begun April 12, 1965 Finished April 21, 1965

Sample Depth (feet below surface)	Recovery (percent)	Description of material
11.0	0	Lava, loose blocks.
13.0	75	Basalt, gray, loose, broken.
16.2	31	" " " "
17.8	75	" " " "
18.3	100	" " " "
22.0	54	" " " "
22.5	100	Cinders and basalt, red and gray, broken.
27.0	55	Basalt, gray, hard, thin layers.
31.4		" " " " "
35.5	5	Cinders or crevices (no core).
41.0	0	" " " " "

S P Flow Core Hole 2
Coconino County, Arizona
Driller: Norman Bailey
Begun April 21, 1965 Finished April 29, 1965

Sample Depth (feet below surface)	Recovery (percent)	Description of material
2.1	21	Basalt, loose blocks.
3.5	13	" " "
4.0	0	" " "
7.0	38	" " "
11.0	49	" " "
14.5	40	" " "
15.9	77	" " "

Kaibab Core Hole 1
Coconino County, Arizona
Driller: Norman Bailey
Begun January 27, 1965 Finished January 28, 1965

Sample Depth (feet below surface)	Recovery (percent)	Description of material
52.5	100	Limestone, tan, medium hard.
82.0	100	Sandstone.

Kaibab Core Hole 2
Coconino County, Arizona
Driller: Robert A. Elmer
Begun October 19, 1965 Finished November 4, 1965

Sample Depth (feet below surface)	Recovery (percent)	Description of material
2.0	0	Overburden.
6.0	0	Limestone, buff (cuttings).
12.0	91	Limestone, buff, broken, medium hard.
17.0	100	" " well jointed, medium hard.
29.0	100	Limestone with sandstone and shaly lenses, buff, white, pale green, a lot of horizontal joints.
31.5	100	Limestone, buff, fossiliferous; well jointed.
42.0	100	Limestone, buff to gray; well jointed; lot of horizontal seams, some sandstone lenses.
42.5	40	Limestone, buff, broken.
44.0	26	" " "
47.5	50	" " " , soft layers.
53.0	27	" " badly broken, " "
63.0	0	Carbide insert broke loose and ground up core.
64.0	100	Limestone, buff, broken.
73.0	100	Limestone, buff, vertical joints; some chert and quartz lenses; limestone becoming sandy.
82.5	100	Limestone, buff to white, sandy; chert layers 1' to 2' thick; some badly broken zones.

Kaibab Core Hole 2, continued

Sample Depth (feet below surface)	Recovery (percent)	Description of material
90.0	100	Limestone, buff to white, sandy; solid, few joints and fractures.
98.5	100	Limestone, buff to gray, interbedded, and sandy limestone layers; some chert and quartz.
105.5	100	Limestone and sandy limestone interbedding buff to gray, some horizontal and vertical joints.
113.5	100	" " " " " some quartz and chert; considerable fracturing.
123.5	100	Limestone, buff, sandy; small chert and quartz nodules solid; few horizontal joints.
133.0	100	Limestone, buff, sandy, well jointed; some badly broken zones.
163.0	100	Limestone, buff to gray, sandy, fewer joints.

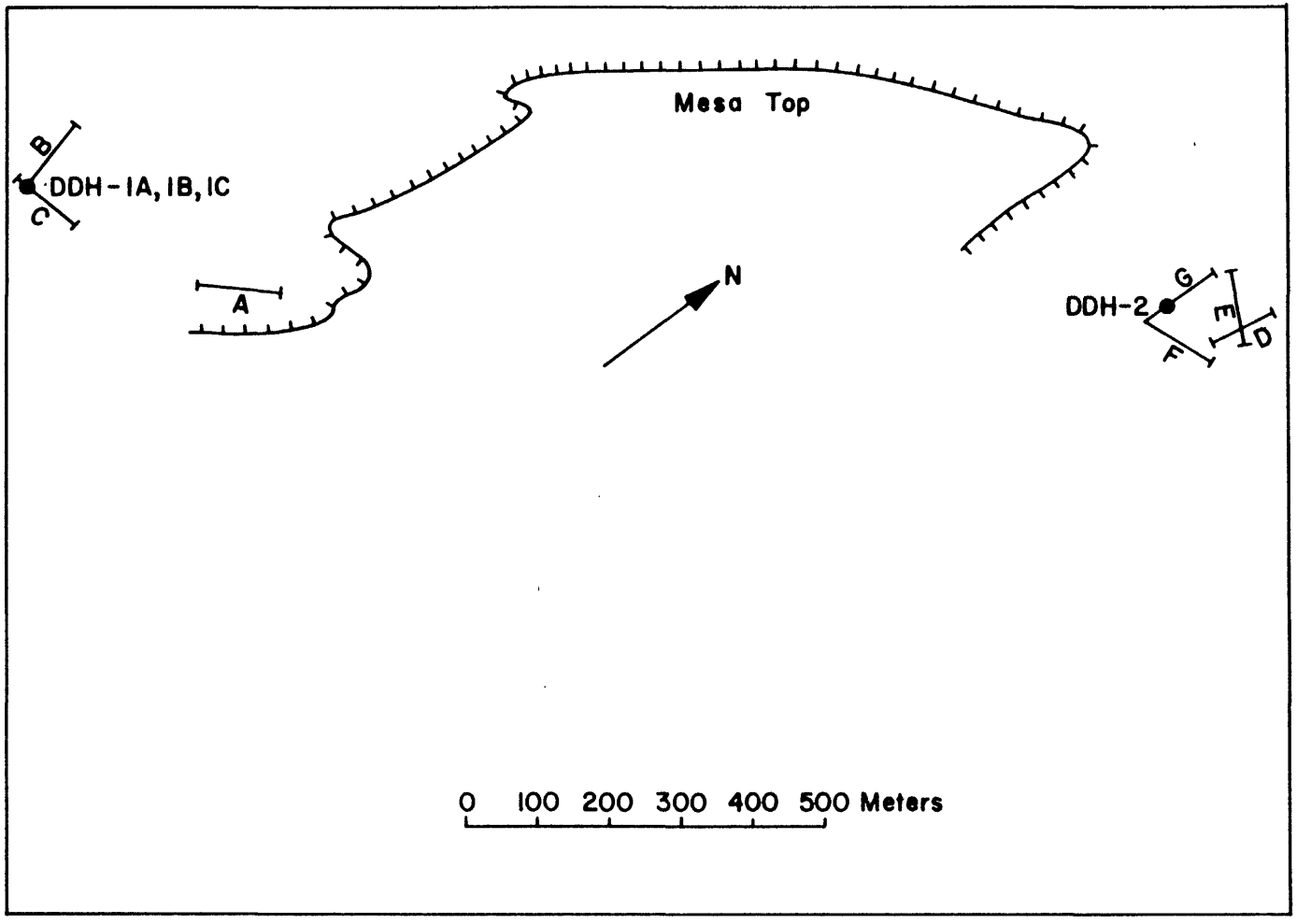

Figure 92.--Middle Mesa, Arizona diamond drill hole and seismic spread locations.

Middle Mesa Core Hole 1A
Coconino County, Arizona
Driller: Robert A. Elmer
Begun April 7, 1966 Finished April 8, 1966

Sample Depth (feet below surface)	Recovery (percent)	Description of material
1.0	0	Sandstone, cuttings.
2.0	82	Sandstone, buff, damp, broken.
3.0	0	" " " "
4.0	84	" " " "
5.0	82	" " " "
6.0	80.	" " " "
11.0	80	" " " "
21.0	83	" " " "
31.0	45	Sandstone, buff to white, damp, pulverized.
37.0	0	Core spring broke; no core recovered.

Middle Mesa Core Hole 1B
Coconino County, Arizona
Driller: Robert A. Elmer
Begun April 8, 1966 Finished April 11, 1966

Sample Depth (feet below surface)	Recovery (percent)	Description of material
1.0	0	No core.
2.0	100	Sandstone, buff, poorly cemented, broken.
4.0	65	" " " "
5.0	100	" " " "
16.0	30	" " " "
21.0	66	" " " "
30.0	37	" " " "
31.0	75	" " " "
41.0	80	" " " "
51.0	33	" " " "
61.0	45	" " " "
71.0	20	" " " "
81.0	50	" " " "

Middle Mesa Core Hole 1C
Coconino County, Arizona
Driller: Robert A. Elmer
Begun April 12, 1966 Finished April 13, 1966

Sample Depth (feet below surface)	Recovery (percent)	Description of material
1.0	0	No core.
5.5	100	Sandstone, buff, poorly cemented.
9.5	75	" " " " badly broken.
15.0	91	" " " "
20.5	96	" " " " few broken zones.
30.5	70	" " " " several broken zones.
35.0	44	" " " " badly broken.
41.0	66	" " " "
51.0	30	" " " "
55.0	75	" " " "
60.0	100	" " " "
65.0	40	" " " "
75.0	30	Sandstone, buff, poorly cemented, badly broken.
80.0	0	No core.

Middle Mesa Core Hole 2
Coconino County, Arizona
Driller: Robert A. Elmer
Begun April 15, 1966 Finished April 16, 1966

Sample Depth (feet below surface)	Recovery (percent)	Description of material
1.5	0	No core.
10.0	100	Sandstone, buff to white, poorly cemented, broken.
15.0	90	" " " "
19.5	80	" " " "
30.0	100	" " " " not too badly broken.
34.0	90	" " " " broken.
39.0	70	" " " " "
42.5	43	" " " " badly broken.
47.0	80	" " " "
51.0	50	" " " "

(page 241 follows)

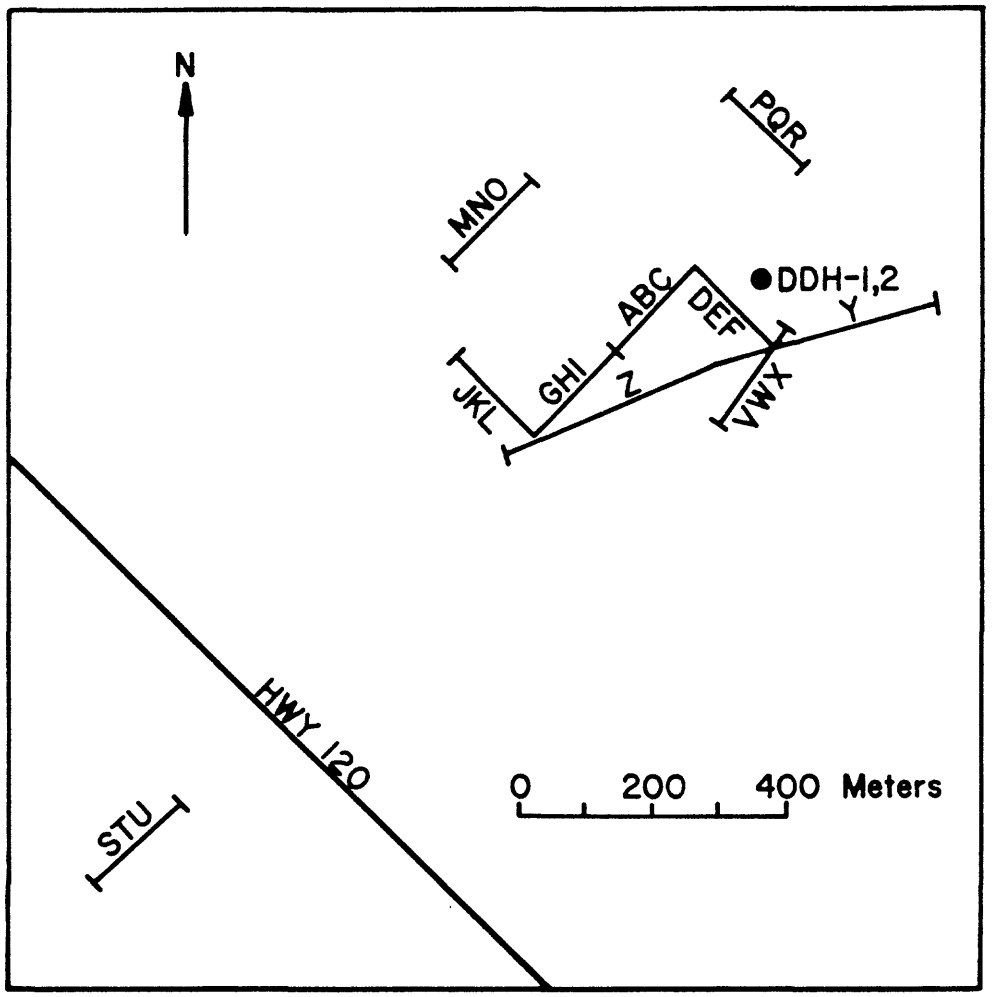

Figure93.--Mono Ash area, California diamond drill hole and seismic spread locations.

Mono Ash Core Hole 1
Mono County, California
Driller: Robert A. Elmer
Begun August 14, 1965 Finished August 25, 1965

Sample Depth (feet below surface)	Recovery (percent)	Description of material
3.0	0	No core.
4.6	33	Ash, composed of pumice and obsidian.
6.0	66	" " " " " "
9.0	43	" " " " " "
14.0	20	" " " " " "
19.0	20	Ash, fine.
21.0	0	Ash, gravel sized cuttings.
31.0	20	Ash, with pumice fragments.
33.6	90	" " " "
40.0	15	" " " "
60.0	0	" " " "
70.0	8	" " " "
80.0	25	" " " "
91.0	18	" " " "
101.0	80	Ash and lapilli.
111.0	8	Ash, fine.
121.0	100	" "
130.0	100	" coarse.
140.5	95	" fine to coarse.
149.0	100	" coarse.
152.6	70	" "
153.6	100	" contact with tuff.
164.0	95	Tuff, pink, some seams.
172.0	100	" " " "

Mono Ash Core Hole 2
Mono County, California
Driller: Robert A. Elmer
Begun September 30, 1965 Finished October 1, 1965

Sample Depth (feet below surface)	Recovery (percent)	Description of material
5.0	0	No core.
8.0	33	Ash, composed of pumice and obsidian.
13.0	20	" " " " " "
18.0	30	" " " " " "
23.0	40	Ash and pumice lapilli.
25.0	50	" " " "
32.0	20	" " " "
42.0	4	" " " "
52.0	1	" " " "

(page 245 follows)

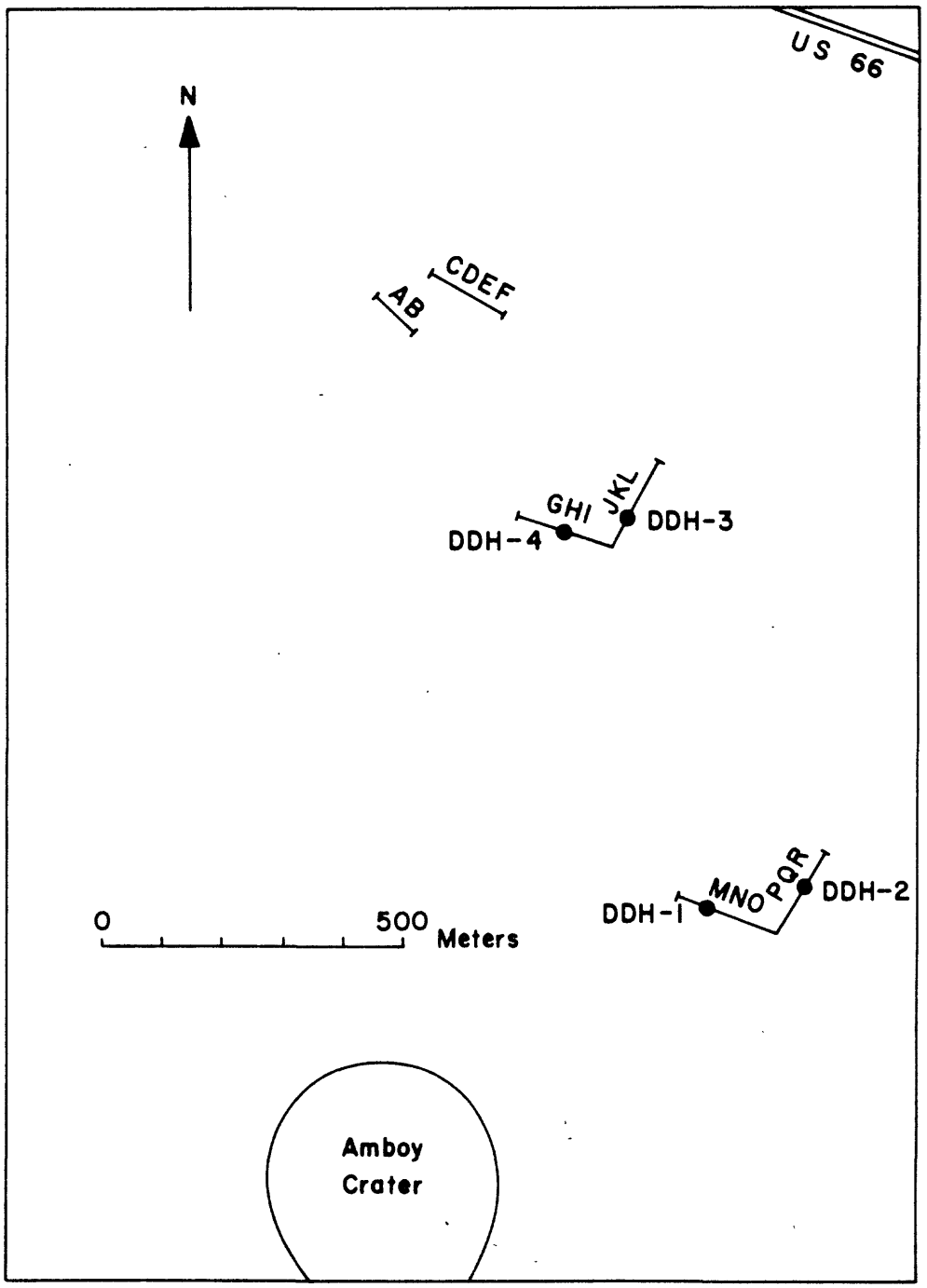

Figure 94--Amboy flow, California diamond drill hole and seismic spread locations.

Amboy Flow Core Hole 1
San Bernardino County, California
Driller: Norman Bailey
Begun March 12, 1965 Finished March 13, 1965

Sample Depth (feet below surface)	Recovery (percent)	Description of material
5.1	0	Cinders, dark gray; sand, brown; soft, loose.
11.2	0	Cinders and sand, gray; cinders fine to cobble size.
13.2	75	Lava, loose, broken.
17.0	84	Lava, hard, vesicular.
20.1	81	" " "
30.5	31	" " less vesicular.
32.0	100	" " " "
34.0	100	" " dense.
39.0	98	" " "

Amboy Flow Core Hole 2
San Bernardino County, California
Driller: Norman Bailey
Begun March 13, 1965 Finished March 17, 1965

Sample Depth (feet below surface)	Recovery (percent)	Description of material
4.7	0	Sand, brown, loose and cinders, gray-black, fine to cobble stone size.
6.0	80	Lava, gray, vesicular, broken.
7.5	80	" " " "
9.2	76	" " " "
11.0	56	" " " "
16.3	19	" " " "
17.5	67	" " " "
20.6	100	" " " "
22.8	91	" " friable, badly broken.
30.4	100	" " softer, broken.
32.5	60	" " " "

Amboy Flow Core Hole 3
San Bernardino County, California
Driller: Norman Bailey
Begun March 21, 1965 Finished March 22, 1965

Sample Depth (feet below surface)	Recovery (percent)	Description of material
6.0	0	Lava, gray, solid, dense to vesicular.
21.0	100	Lava, gray, solid, vesicular. broken 12.9-13.0; broken 15.1-15.2 solid, gray, dense.
26.0	64	Lava, gray, highly vesicular, badly broken.
31.0	80	Lava, gray, hard, solid to vesicular, broken.
38.0	50	Lava, gray, hard, broken.
40.0	95	" " "

Amboy Flow Core Hole 4
San Bernardino, California
Driller: Norman Bailey
Begun March 23, 1965 Finished March 24, 1965

Sample Depth (feet below surface)	Recovery (percent)	Description of material
0.6	0	Sand and loose cinders.
5.0	0	Lava, gray, vesicular.
10.0	100	Lava, gray, dense, vesicular.
20.0	100	" " " " vertical jointing.
30.0	36	Lava, gray, badly broken and creviced.
31.0	100	" " dense.
35.0	97	" " " non-vesicular to 34.0'
40.0	62	Cinders at 39± ?
45.0	92	Lava, gray, dense, large vesicle.
50.0	100	" " " solid.

(page 249 follows)

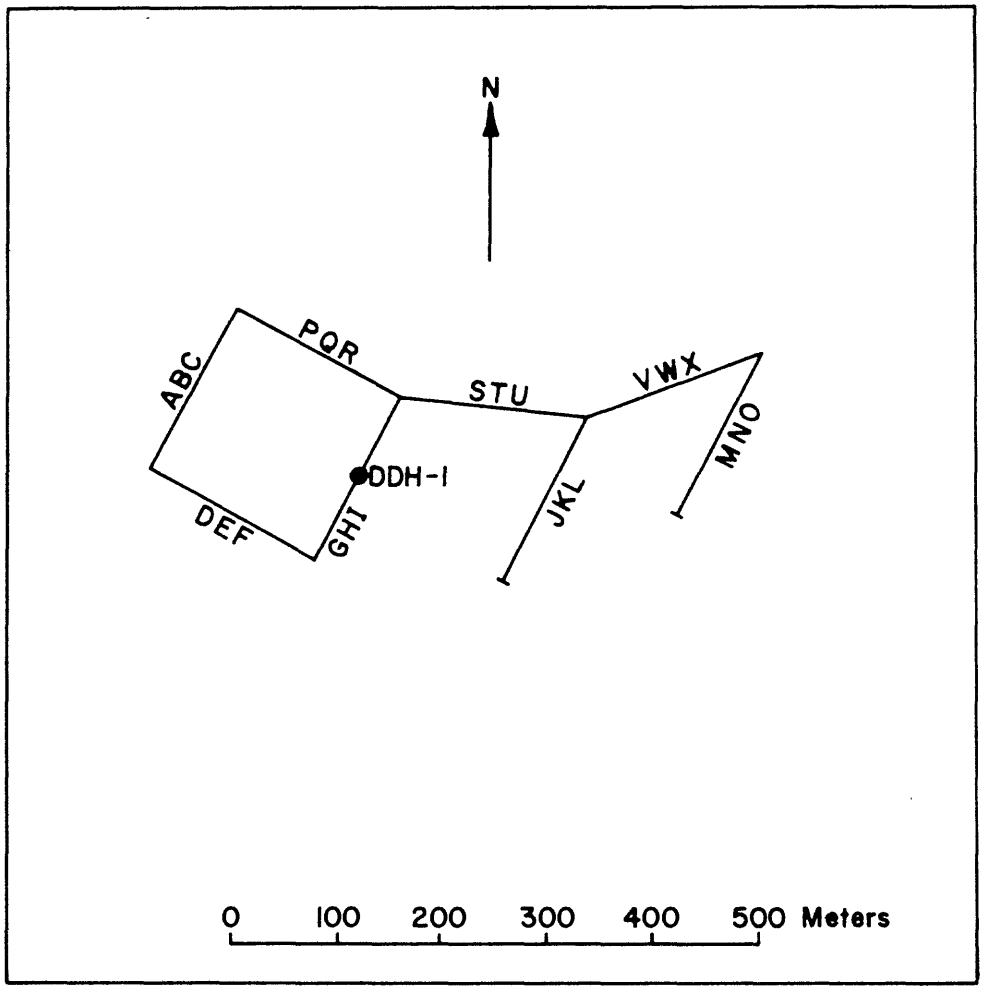

Figure95.--Bishop Tuff area, California diamond drill hole and seismic spread locations.

Bishop Tuff Core Hole 1
Inyo County, California
Driller: Robert A. Elmer
Begun September 9, 1965 Finished September 17, 1965

Sample Depth (feet below surface)	Recovery (percent)	Description of material
6.0	0	No core.
11.5	0	Core ground up by carbide bit; cuttings composed of tuff.
22.0	95	Tuff, pink, soft, horizontal joints 2' to 3' apart.
32.0	100	" " " " " 2" to 1' apart.
42.0	90	" " " " " 2" to 3" apart.
52.0	90	Tuff, buff, soft, badly broken.
62.0	90	" buff to pink, soft, badly broken.
77.5	0	Ash, pink, fine.
88.0	95	Ash, salmon, medium to coarse.
99.0	100	" " " " "
109.0	35	" " " " "
119.5	100	" " " " "
132.0	40	" " " " "
142.0	60	Ash, salmon, with colored lapilli.
152.0	5	" " " " "
162.0	0	" " " " "
172.0	10	Ash and lapilli, salmon colored.
176.5	100	" " " " "
187.0	52	" " " " "
192.0	40	" " " " "

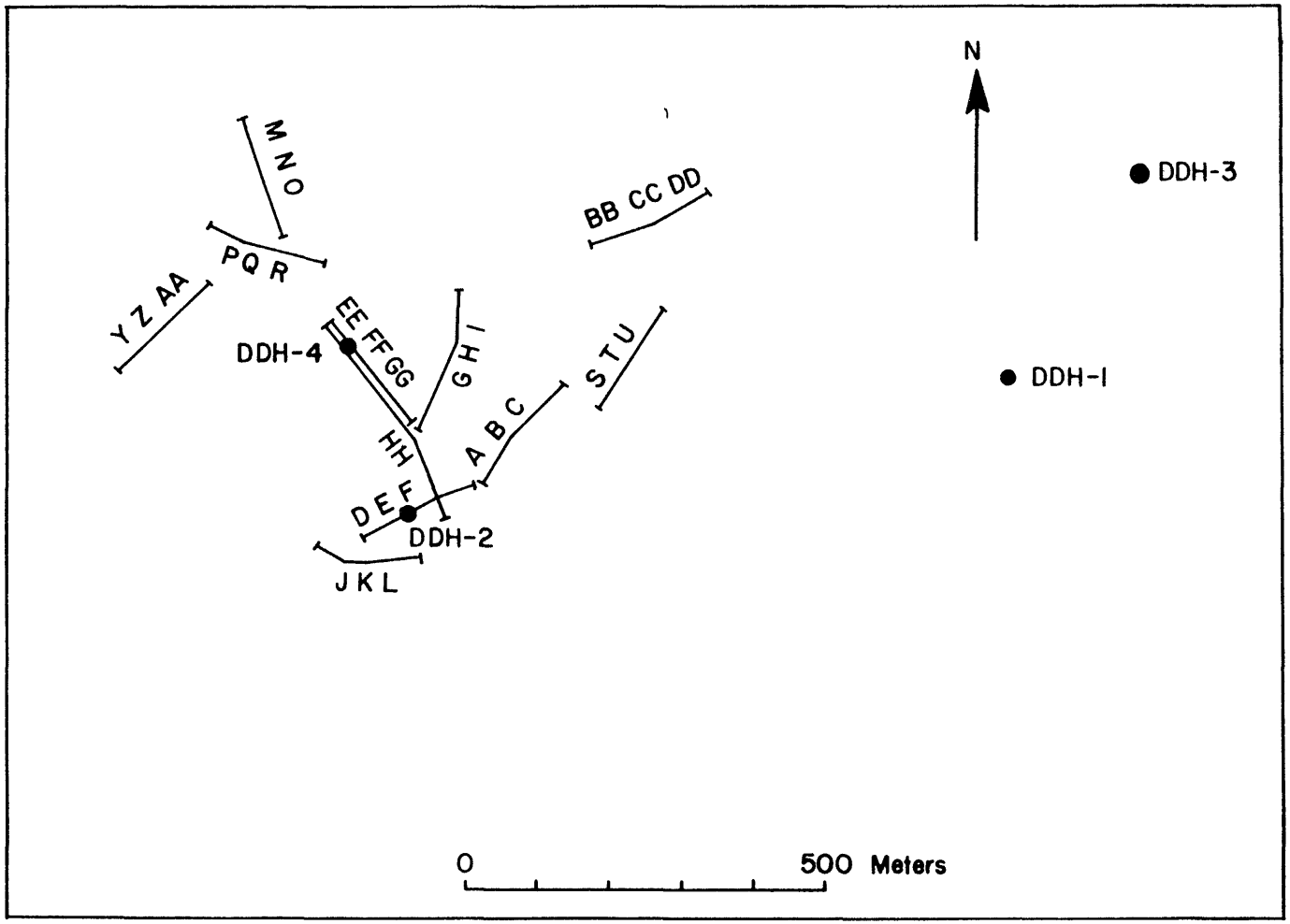

Figure 96.--Southern Coulee area, California diamond drill holes and seismic spread locations

Southern Coulee Core Hole 1
Mono County, California
Driller: Robert A. Elmer
Begun August 27, 1965 Finished August 27, 1965

Sample Depth (feet below surface)	Recovery (percent)	Description of material
7.6	0	No core (cuttings composed of light gray pumice).
17.6	90	Pumice with permafrost.
23.0	80	" " "
28.0	70	" little permafrost.
33.0	40	" broken, little ice.
40.0	29	" " " "
50.0	25	" " " "
59.0	33	" " " "
62.0	66	" " " "

Southern Coulee Core Hole 2
Mono County, California
Driller: Robert A. Elmer
Begun August 30, 1965 Finished September 7, 1965

Sample Depth (feet below surface)	Recovery (percent)	Description of material
7.0	0	No core.
13.0	33	Pumice, gray, low density.
23.0	20	" " " "
32.6	22	" " becoming dense.
42.0	37	" " " "
52.0	25	" gray to brown.
62.0	33	" tan.
72.0	20	" buff, dense, badly broken.
82.0	15	" " " " "
85.0	33	" " " " "

Southern Coulee Core Hole 3
Mono County, California
Driller: Robert A. Elmer
Begun September 8, 1965 Finished September 8, 1965

Sample Depth (feet below surface)	Recovery (percent)	Description of material
6.0	0	Pumice, gray, with permafrost.
13.0	30	" " light density, some ice.
14.5	80	" " " " " "
20.0	95	" " " " " "
31.0	91	" " " " little "
41.0	0	" " " " " "
51.0	50	" " " " " "

Southern Coulee Core Hole 4
Mono County, California
Driller Robert A. Elmer
Begun September, 20, 1965 Finished September 28, 1965

Sample Depth (feet below surface)	Recovery (percent)	Description of material
6.5	0	Pumice, gray, light, dry.
12.0	45	Pumice, gray, light density, badly broken, dry.
17.0	100	Pumice, gray, light, not too badly broken; ice at 15.0'.
22.0	80	Pumice, gray, light, ice seams that leave a pumice gravel after melting.
32.0	55	Pumice, gray, medium to dense, badly broken, ice decreasing.
42.0	60	Pumice, gray to brown, fairly dense, badly broken, ice increasing.
52.0	40	" " " " "
59.0	64	" " " " "
68.0	66	Pumice, gray brown to dark gray, banded, dense, badly broken, permafrost.
79.0	36	Pumice, gray to buff to brown, dense, some obsidian, permafrost throughout, all badly broken.

Southern Coulee Core Hole 4, continued

Sample Depth (feet below surface)	Recovery (percent)	Description of material
91.0	0	Did not pick up any core; badly broken formation; probably obsidian, cavities--83.0'-85.0', 88.0'-90.0'
97.0	50	Obsidian and dense pumice, gray, badly broken, little ice, almost dry.
101.0	0	Obsidian and dense pumice, badly broken.
106.5	9	" " " " "
112.5	50	Obsidian, dense pumice, rhyolite. gray, badly broken, ice throughout.
118.0	45	" " " "
127.0	28	" " " some ice.
137.0	50	" " " " "
143.5	31	" " " " "
147.0	0	" " " " "

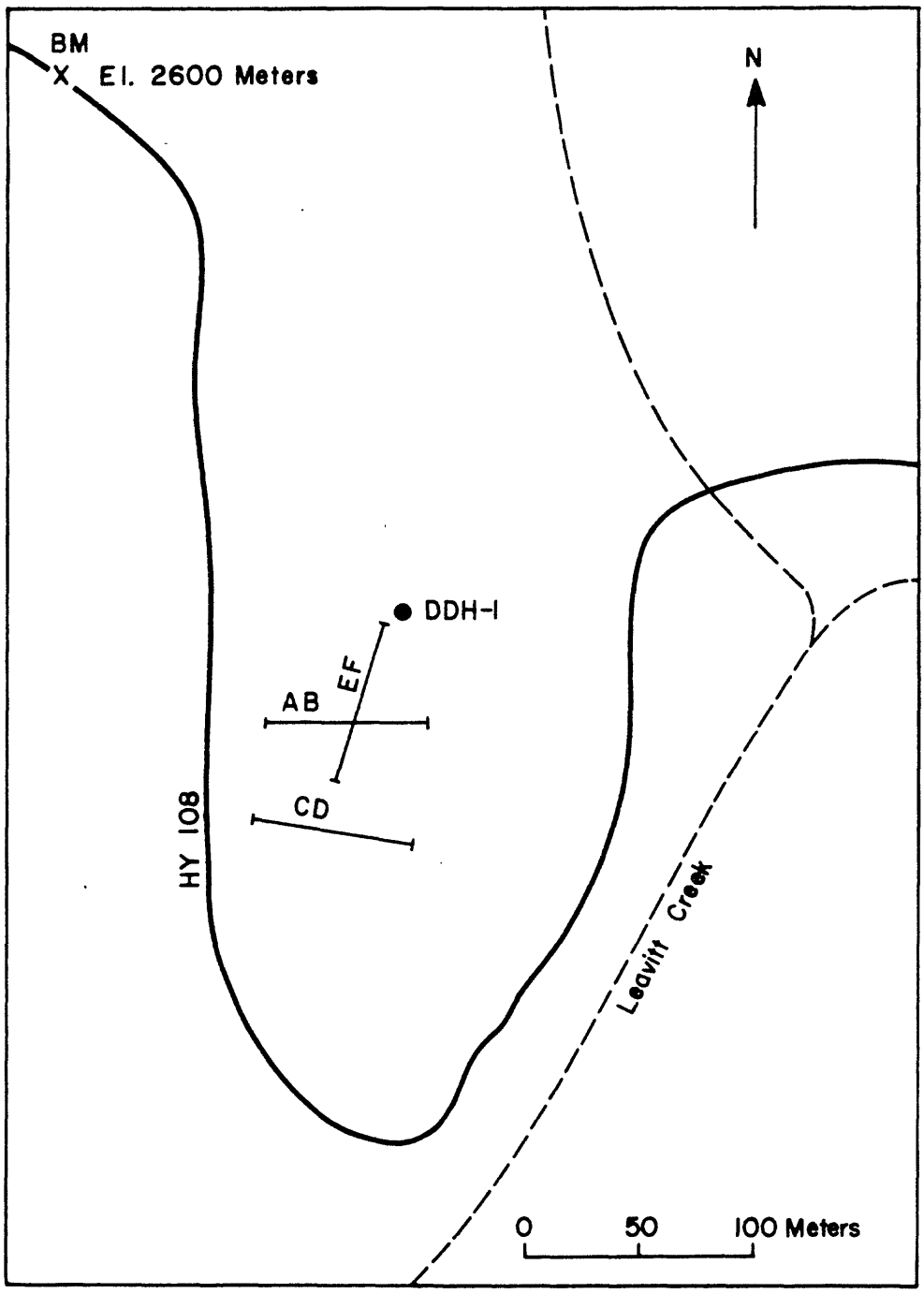

Figure 97.--Sonora Pass area, California diamond drill hole and seismic spread locations.

Sonora Pass 1
Mono County, California
Driller: Robert A. Elmer
Begun August 6, 1965 Finished August 13, 1965

Sample Depth (feet below surface)	Recovery (percent)	Description of material
1.0	0	No core.
2.2	92	Granite, few joints.
3.3	100	" " "
4.5	92	" " "
4.7	0	" " "
6.3	100	" " "
9.0	87	" " "
15.0	100	" many horizontal seams.
15.3	17	" seam 15.1'-15.3'.
31.7	100	" solid, few joints.
40.0	98	" " " "

APPENDIX B

(page 259 follows)

LABORATORY PHYSICAL PROPERTY MEASUREMENTS ON CORE AND SURFACE SAMPLES FROM SIX LUNAR ANALOG TEST SITES

by

Joel S. Watkins and Lawrence A. Walters
Flagstaff, Arizona

This appendix includes available physical properties data measured in laboratories from samples of the Kana-a Lava Flow, Arizona (an a-a basalt), S P Flow, (a blocky andesitic basalt), Amboy Flow, California (a pahoehoe basalt), Meteor Crater, Arizona (primarily fractured and shocked sandstone and limestone), Kaibab Limestone Site, Arizona (primarily limestone with lesser amounts of dolomite and sandstone), and the Sonora Pass Site (massive, relatively unweathered granite). All measurements were made on NX core or on segments taken from NX core except those on rocks from the S P Flow, where coring to date has been unsuccessful. S P measurements were based on surface samples.

The pulse and density measurements, except as noted below, were made by the Branch of Special Projects Laboratory of the U.S. Geological Survey under the direction of James Scott. The static measurements were made by the Branch of Engineering Geology Laboratory under the direction of Thomas Nichols. The density and nitrogen permeability measurements for MCC-4 were made in the

Branch of Astrogeology Laboratory under the direction of C. H. Roach.

For other laboratory physical properties data previously published by the In Situ Project, see Watkins and others, 1964, p. 39-42 and Roach and Johnson, 1966, p. 22-40. Drilling logs of core holes from which core samples were taken are given in Appendix A, this volume.

A limited amount of in situ physical properties data have been published by Walters (1966 and in this volume).

For a geologic description of the test site on S P Flow, see Watkins and others (1964); for the test site on Kana-a Flow, see Loney (1965); for Meteor Crater, see Shoemaker (1963); and also see Godson and others (1966). The Sonora Pass has been described by Haines in this volume. Brief descriptions of the Amboy and Kaibab sites are available in the Work Plan and Operating Budget for the In Situ Physical Properties Project, FY-66.

Tables 12-17

Core-sample analyses

Table 12. Core from Kana-a Flow, Arizona (a-a basalt).

Laboratory Number	Depth	Dry Bulk Density	Grain Density	Porosity	Pulse Measurements						Static Measurements					
					V_p	V_s	Poisson's Ratio	Young's Modulus	Shear Modulus	Bulk Modulus	Unconfined Compressive Strength	Tensile Strength	Poisson's Ratio	Young's Modulus	Shear Modulus	Bulk Modulus
	meters	g per cc		percent	mps	mps		10^{11} dynes per cm^2			10^8 dynes/cm^2	10^7 dynes/cm^2		10^{11} dynes per cm^2		
Drill Hole 1-A																
D701325	2.3	2.71	3.05	11.3	3700	2230	0.218	3.25	1.34	1.92	12.33		0.16	2.16	0.93	1.05
D701326	3.0	2.28	3.02	24.6	3150	1980	0.172	2.09	0.89	1.07	16.19		0.13	2.70	1.19	1.21
D701327	3.9	2.67	3.01	11.5	3010	1830	0.207	2.16	0.89	1.23	9.71		0.11	2.11	0.95	1.03
D701328	5.1	2.08	3.02	31.2	3440	2040	0.230	2.12	0.86	1.31		3.86				
D701329	5.7	2.48	3.00	17.5	3990	2520	0.175	3.67	1.56	1.88		1.52				
D701330	6.8	2.34	3.02	22.6	3260	1860	0.260	2.04	0.81	1.41	2.62		0.16	4.98	2.15	2.44
D701331	7.7	1.65	3.02	45.4	3280	2040	0.181	1.63	0.69	0.85		1.93				
D701332	8.6	2.27	3.01	24.8	3320	1900	0.256	2.05	0.82	1.41	3.93		0.23	2.09	0.85	1.29
D701333	9.2	2.60	3.02	13.9	3930	2450	0.181	3.70	1.52	1.93	11.85		0.13	3.24	1.43	1.46
Averages		2.34	3.02	22.5	3460	2090	0.209	2.52	1.04	1.45	9.44	2.44	0.15	2.88	1.25	1.41
Drill Hole 2																
D701334	1.9	2.09	3.00	30.5	3260	1810	0.274	1.76	0.69	1.30	3.24		0.20	1.79	0.74	0.99
D701335	3.4	2.54	3.01	15.8	3340	1880	0.270	2.25	0.89	1.63		3.44				
D701336	4.2	2.64	3.01	12.4	3260	2010	0.193	2.54	1.07	1.38	4.34		0.06	1.61	0.76	0.61
D701337	5.1	2.64	3.01	12.4	3580	2120	0.233	2.90	1.18	1.67		5.10				
D701338	5.4	2.80	3.01	7.2	3660	2170	0.229	3.22	1.31	1.98	15.16		0.12	2.44	1.09	1.07
D701339	6.4	2.77	3.02	8.3	3600	2260	0.179	3.31	1.41	1.72		7.58				
D701340	7.4	2.78	3.02	7.7	3690	2130	0.249	3.15	1.26	2.09		5.10				
D701341	8.3	2.79	3.01	7.3	3570	2260	0.165	3.31	1.42	1.65	15.57		0.12	3.00	1.33	1.32
D701342	9.4	2.62	3.05	14.0	3520	2150	0.203	2.90	1.21	1.62	8.75		0.09	2.98	1.37	1.21
Averages		2.63	3.02	12.8	3500	2090	0.222	2.82	1.16	1.67	9.41	5.31	0.12	2.36	1.06	1.04

Drill Hole 3-A																
D701343	1.6	2.71	3.01	10.0	3960	2550	0.152	4.03	1.75	1.93	10.13		0.19	3.27	1.38	1.76
D701344	2.2	2.79	3.02	7.5	3780	2420	0.150	3.78	1.65	1.80	19.08		0.18	3.71	1.57	1.93
D701345	3.0	2.82	3.01	6.6	3430	2290	0.102	3.22	1.46	1.35		6.20				
D701346	5.1	2.02	3.02	33.2	3350	1910	0.261	2.77	1.10	1.94		1.10				
D701347	5.9	2.62	3.02	13.1	3490	2170	0.190	3.36	1.41	1.81		6.54				
Averages		2.59	3.02	14.1	3600	2270	0.171	3.43	1.47	1.77	14.60	4.62	0.18	3.49	1.47	1.84
Drill Hole 4																
D701348	8.8	2.59	3.01	14.0	4220	2530	0.216	4.71	1.94	2.76	7.37		0.22	3.75	1.54	2.23
Drill Hole 5																
D701349	4.8	1.81	3.01	40.0	3480	1940	0.274	2.89	1.13	2.13	2.14		0.11	2.34	1.05	1.00
D701350	7.2	2.15	3.03	29.0	3670	2120	0.247	3.41	1.36	2.25		4.75				
Averages		1.98	3.02	34.5	3580	2030	0.260	3.15	1.25	2.19						
Drill Hole 6																
D701351	1.9	2.34	3.02	22.4	3170	2030	0.150	2.87	1.25	1.36	4.48		0.17	2.55	1.09	1.29
D701352	3.1	2.34	3.03	22.7	3310	1840	0.272	2.63	1.03	1.92		4.34				
D701353	4.0	2.54	3.01	15.7	3290	1780	0.292	2.48	0.96	1.98		3.00				
D701354	5.0	2.74	3.02	9.5	3110	2010	0.136	2.79	1.23	1.28	8.75		0.09	1.93	0.88	0.79
D701355	5.9	2.68	3.02	11.5	2680	1630	0.204	1.94	0.81	1.10		1.17				
D701356	6.8	2.74	3.01	9.0	2160	1200	0.277	1.10	0.43	0.83	2.89		0.30	3.70	1.43	3.09
D701357	7.7	2.76	3.02	8.4	3320	1830	0.285	2.58	1.00	2.00		5.24				
D701358	8.6	2.78	3.01	7.5	2790	1830	0.121	2.25	1.01	0.99	14.20		0.16	2.65	1.14	1.20
D701359	9.5	2.76	3.04	9.2	2790	1600	0.257	1.94	0.77	1.34	14.20		0.26	3.85	1.51	2.67
D701360	10.4	2.78	3.04	8.7	2640	1600	0.208	1.86	0.77	1.07		0.76				
D701361	11.4	2.85	3.06	6.8	2840	1770	0.184	2.26	0.95	1.19	16.12		0.17	2.85	1.06	1.44
D701362	12.1	2.72	3.04	10.4	3280	1980	0.212	2.89	1.19	1.67		3.93				
Averages		2.67	3.03	11.8	2950	1760	0.217	2.30	0.95	1.39	10.10	3.07	0.19	2.93	1.19	1.75

Table 13. Core from Amboy Flow, California (pahoehoe basalt).

Laboratory Number	Depth	Dry Bulk Density	Grain Density	Porosity	Pulse Measurements V_p	V_s	Poisson's Ratio	Young's Modulus	Shear Modulus	Bulk Modulus	Static Measurements Unconfined Compressive Strength	Tensile Strength	Poisson's Ratio	Young's Modulus	Shear Modulus	Bulk Modulus
	meters	g per cc		percent	mps	mps		10^{11} dynes per cm^2			10^8 dynes/cm^2	10^7 dynes/cm^2		10^{11} dynes per cm^2		
Drill Hole 1																
D701733	5.6	1.82	2.92	37.7	4450	2670	0.22	3.17	1.31	1.86		4.42	0.067	3.11	1.45	0.80
D701734	10.9	2.68	3.00	10.7	5720	3290	0.25	7.23	2.89	4.89		13.19	0.254	6.57	2.62	4.46
D701735	11.8	2.69	3.01	10.6	5690	3380	0.23	7.51	3.10	4.62	11.64		0.254	7.44	2.96	5.04
Averages		2.40	2.98	19.7	5280	3110	0.23	5.97	2.43	3.79	11.64	8.81	0.192	5.71	2.34	3.43
Drill Hole 2																
D701736	2.4	2.60	2.95	11.9	4990	2960	0.23	5.58	2.27	3.44	6.96		0.180	3.88	1.65	2.03
D701737	7.1	2.55	2.89	11.8	2500	1540	0.19	1.03	0.41	0.55		6.96	0.122	3.16	1.41	1.39
D701738	8.2	2.80	2.92	4.1	5050	3050	0.21	6.27	2.62	3.65	14.54		0.172	3.72	1.40	1.66
Averages		2.65	2.92	9.3	4180	2520	0.21	4.29	1.77	2.55	10.75		0.158	3.59	1.49	1.69
Drill Hole 3																
D701739	2.1	2.26	2.95	23.4	4150	2230	0.30	2.89	1.10	2.41	5.63		0.175	2.14	0.91	1.09
D701740	2.8	2.26	2.96	23.7	3640	2100	0.25	2.48	1.03	1.65		2.31	0.208	3.61	1.50	2.06
D701741	3.6	2.71	2.95	8.1	4770	2970	0.18	5.65	2.41	2.96		8.89	0.165	4.57	2.05	2.27
D701742	4.5	2.64	2.95	10.5	3840	2320	0.21	3.44	1.45	2.00	10.68		0.229	3.29	1.34	2.03
D701743	5.9	2.65	2.96	10.5	4830	2880	0.22	5.37	2.20	3.24	11.44		0.233	5.18	2.08	3.23
D701744	7.1	2.21	2.96	25.3	5060	2840	0.27	4.48	1.79	3.31		4.04	0.052	3.04	1.45	1.07
D701745	10.1	2.62	2.97	11.8	4950	3080	0.19	5.86	2.48	3.10		10.06	0.237	5.19	2.08	3.29
D701746	11.6	2.74	2.90	5.5	5240	3200	0.20	6.75	2.82	3.79	26.32		0.208	7.99	3.30	4.60
Averages		2.51	2.95	14.8	4560	2700	0.23	4.62	1.91	2.81	13.52	6.32	0.188	4.38	1.84	2.46

Table 14. Surface samples from S P Flow, Arizona (andesitic basalt).

Laboratory Number	Depth	Dry Bulk Density	Grain Density	Porosity	Pulse Measurements V_p	V_s	Poisson's Ratio	Young's Modulus	Shear Modulus	Bulk Modulus	Static Measurements Unconfined Compressive Strength	Tensile Strength	Poisson's Ratio	Young's Modulus	Shear Modulus	Bulk Modulus	
	meters	g per cc		percent	mps	mps		10^M dynes per cm^2			10^8 dynes/cm^2	10^7 dynes/cm^2		10^M dynes per cm^2			
D701130	Surface	2.40	2.81	14.6	5370	2970	0.279	5.42	2.12	4.09							
D701131		2.35	2.79	15.8	5240	3030	0.248	5.39	2.17	3.56	10.13		0.24	8.20			[1]
D701132		2.39	2.82	15.0	4940	2930	0.229	5.04	2.06	3.09	12.06		0.28	5.80			
D701133		2.49	2.80	11.3	5900	3260	0.280	6.75	2.64	5.12							
D701134		2.25	2.82	20.3	4980	2670	0.298	4.15	1.60	3.42	13.64		0.23	5.19			
D701135		2.52	2.82	10.6	5260	3080	0.238	5.91	2.39	3.76							
D701136		2.30	2.78	17.2	5120	2860	0.274	4.77	1.87	3.52	12.47		0.29	4.35			
D701137		2.24	2.81	20.2	5400	3090	0.257	5.37	2.14	3.67	13.99		0.25	4.57			
D701138		2.25	2.81	20.0	4920	2850	0.246	4.55	1.82	2.98	9.37		0.20	3.75			
D701139		2.30	2.82	18.4	4950	2900	0.239	4.80	1.94	3.06	10.13		0.20	3.50			
D701140		2.46	2.81	12.4	5500	3210	0.242	6.30	2.54	4.07							
D701141		2.03	2.81	27.7	4720	2630	0.275	3.58	1.40	2.64							
D701142		2.29	2.84	19.1	5530	3130	0.264	5.67	2.24	4.01	13.64		0.27	5.37			
D701143		2.32	2.80	17.3	5450	2990	0.284	5.31	2.07	4.11							
D701144		2.35	2.80	15.9	5610	3060	0.289	5.67	2.20	4.47	15.98		0.21	5.08			
D701145		2.48	2.83	12.2	5800	3190	0.283	6.46	2.52	4.97	12.06		0.26	6.44			
D701146		2.62	2.81	6.8	5520	3230	0.238	6.80	2.75	4.32	27.63		0.23	6.96			
D701147		2.17	2.85	24.0	5340	2890	0.294	4.66	1.80	3.76							
D701148		2.20	2.80	21.6	5240	2840	0.291	4.57	1.77	3.51	9.71		0.19	3.66			
D701149		2.34	2.81	16.9	5310	3040	0.256	5.43	2.16	3.71							
D701150		2.29	2.83	19.3	5250	2910	0.279	4.93	1.93	3.72	12.06		0.25	4.21			
D701151		2.40	2.79	13.9	5420	2930	0.293	5.33	2.06	4.29							
D701152		1.91	2.77	31.0	5040	2850	0.266	3.92	1.55	2.79							
D701153		2.02	2.78	27.4	5210	2820	0.292	4.15	1.61	3.33							
D701154		2.14	2.82	24.0	4720	2780	0.234	4.07	1.65	2.56							
D701155		2.17	2.81	22.9	5070	2810	0.279	4.37	1.71	3.27	9.71		0.16	3.82			
Averages		2.29	2.81	18.3	5260	2960	0.267	5.13	2.03	3.68	13.04		0.23	5.06			
D701147											12.06		0.24	4.65			[2]
D701153(a)											13.99		0.22	4.71			
D701153(b)											10.47		0.23	3.67			
D701153(c)											17.91		0.43	29.28			
Averages											13.61		0.28	10.58			

[1] Perpendicular to rock fabric.
[2] Parallel to rock fabric.

Table 15. Core from Meteor Crater, Arizona (primarily Coconino Sandstone and Kaibab Limestone).

Laboratory Number	Depth	Dry Bulk Density	Grain Density	Porosity	Pulse Measurements						Nitrogen Gas Permeability	Static Measurements					
					V_p	V_s	Poisson's Ratio	Young's Modulus	Shear Modulus	Bulk Modulus		Unconfined Compressive Strength	Tensile Strength	Poisson's Ratio	Young's Modulus	Shear Modulus	Bulk Modulus
	meters	g per cc		percent	mps	mps		10^{11} dynes per cm^2			millidarcies	10^8 dynes/cm^2	10^7 dynes/cm^2		10^{11} dynes per cm^2		
Drill Hole MCC-3																	
D701887	21.1	1.98	2.70	26.8	1470	860	0.239	0.37	0.14	0.23		Sample too soft for testing					
D701888	23.4	2.30	2.69	14.5	2260	1330	0.235	1.01	0.41	0.64		6.37		0.118	0.98	0.43	0.44
D701889	24.1	2.28	2.71	15.8	2180	1340	0.194	1.98	0.83	1.07		5.55		0.195	0.48	0.26	0.20
D701890	28.1	2.22	2.65	16.3	2410	1660	0.052	1.28	0.61	0.47			0.47	0.165	0.60	0.30	0.33
D701891	29.0	2.49	2.81	12.1	3850	-	-	-	-	-		Sample too small for testing					
D701892	29.8	2.30	2.81	18.1	4210	2630	0.179	3.75	1.59	2.98		8.68		0.172	3.83	1.95	1.63
D701893	30.0	2.14	2.90	26.3	4940	2620	0.304	3.06	1.17	2.59			2.16	0.220	1.88	1.12	0.77
D701894	30.3	2.41	2.82	14.6	1840	1100	0.222	0.71	0.29	0.43		6.44		0.197	4.55	2.50	1.90
D701895	30.4	2.44	2.80	12.9	4750	3060	0.143	5.23	2.28	2.45			2.94	0.135	6.23	2.84	2.74
Averages		2.28	2.77	17.5	3100	1830	0.196	2.17	0.92	1.36		6.76	1.86	0.172	2.65	1.34	1.14
[1]								[1]						[1]			
Drill Hole MCC-4																	
	8.2	2.18	2.85	23.5							17.3						
	9.3	2.17	2.93	25.9							2.5						
	10.7	2.19	3.63	18.2							1.3						
	16.0	2.44	2.89	15.6							< 0.4						
	20.0	2.48	2.68	7.5							< 0.4						
	21.0	2.68	2.73	1.8							< 0.4						
	21.4	2.63	2.74	4.0							< 0.4						
	22.0	2.61	2.68	2.6							< 0.4						
	29.5	2.44	3.04	20.0							< 0.4						
	34.0	2.18	2.81	23.2							26.8						
	37.5	2.22	3.03	26.7							4.7						
	47.6	2.39	2.99	20.1							3.8						
	54.4	2.15	3.05	29.5							25.1						
	61.0	2.33	2.74	15.0							1.5						
	68.0	2.17	2.89	24.9							16.8						
	75.8	2.14	2.72	21.3							16.7						
	81.7	2.12	2.82	24.8							30.6						
	87.5	2.15	3.02	28.8							37.6						
	91.5	2.24	2.68	16.7							4.2						
	94.8	2.35	2.91	19.2							1.7						
	98.3	2.13	2.87	25.8							33.3						
	101.9	2.12	2.65	22.0							80.7						
	105.9	2.18	2.65	18.3							15.5						
Averages		2.29	2.87	18.9							13.9						

[1] Pulse and static measurements currently underway.

Table 16. Core from the Kaibab Limestone site (primarily limestone with lesser amounts of dolomite and sandstone).

Laboratory Number	Depth	Dry Bulk Density	Grain Density	Porosity	Pulse Measurements						Static Measurements				
					V_p	V_s	Poisson's Ratio	Young's Modulus	Shear Modulus	Bulk Modulus	Unconfined Compressive Strength	Tensile Strength	Poisson's Ratio	Young's Modulus	Shear Modulus	Bulk Modulus
	meters	g per cc		percent	mps	mps		10^{11} dynes per cm^2			10^8 dynes/cm^2	10^7 dynes/cm^2		10^{11} dynes per cm^2		
D701764	2.5	2.49	2.88	13.5	5800	3400	0.254	7.03	2.80	4.77		6.21	0.316	7.16	2.83	6.28
D701765	5.0	2.18	2.87	24.0	4800	2900	0.198	4.42	1.85	2.44	8.54		0.264	4.45	1.76	3.14
D701766	7.2	2.29	2.66	13.9	2700	1700	0.131	1.61	0.71	0.72		1.57	0.192	1.65	0.70	1.00
D701767	8.3	2.08	2.85	27.0	4500	2800	0.205	3.82	1.58	2.16	6.60		0.249	4.12	1.65	2.74
D701768	11.2	2.49	2.85	12.6	5600	3300	0.237	6.63	2.68	4.20	9.89		0.326	6.33	2.39	6.07
D701769	15.2	2.18	2.72	19.9	3700	2400	0.147	2.85	1.24	1.34		3.03	0.125	2.42	1.08	1.08
D701770	17.9	2.23	2.85	21.8	3900	2300	0.245	2.91	1.16	1.90	4.08		0.157	3.32	1.44	1.62
D701771	18.7	2.16	2.69	19.7	2600	1800	0.060	1.45	0.69	0.55		1.20	0.088	1.28	0.59	0.87
D701772	22.3	2.09	2.78	24.8	3900	2300	0.209	2.78	1.15	1.60	8.54		0.155	2.60	1.12	1.25
Averages		2.24	2.79	19.7	4200	2500	0.187	3.72	1.54	2.19	7.53	3.00	0.208	3.70	1.51	2.67

(page 269 follows)

Table 17. Core from the Sonora Pass site (massive granite).

Laboratory Number	Depth	Dry Bulk Density	Grain Density	Porosity	Pulse Measurements						Static Measurements					
					V_p	V_s	Poisson's Ratio	Young's Modulus	Shear Modulus	Bulk Modulus	Unconfined Compressive Strength	Tensile Strength	Poisson's Ratio	Young's Modulus	Shear Modulus	Bulk Modulus
	meters	g per cc		percent	mps	mps		10^{11} dynes per cm^2			10^8 dynes/cm^2	10^7 dynes/cm^2		10^{11} dynes per cm^2		
D701920	0.5	2.65	2.70	1.9	3100	2100	0.07	2.51	1.17	0.97	7.96		Small	1.52	0.05	0.76
D701921	2.0	2.65	2.70	1.9	3290	2130	0.14	2.74	1.21	1.26	11.99		0.062	1.43	0.57	0.68
D701922	3.2	2.63	2.69	2.2	No data; sample fractured.						10.02		Small	0.61	0.14	0.31
D701923	4.7	2.64	2.71	2.6	3980	2740	0.05	4.15	1.98	1.53	> 7.79	>2.87	Small	2.36	0.78	1.21
D701924	6.4	2.63	2.68	1.9	4070	2530	0.18	3.98	1.68	2.11	9.78		Small	2.19	0.73	1.10
D701925	7.8	2.64	2.70	2.2	3840	2650	0.04	3.87	1.85	1.42	> 3.93	>2.41	Small	2.41	0.81	1.21
D701926	9.3	2.63	2.66	1.1	3990	2290	0.26	3.45	1.37	2.36	15.85		Small	1.85	0.58	0.96
D701927	10.9	2.65	2.70	1.9	4190	2740	0.13	4.49	1.99	1.99	> 6.20	>2.48	0.044	2.41	0.89	1.16
Averages		2.64	2.69	2.0	3780	2460	0.12	3.60	1.61	1.66	> 9.19	>2.59		1.85	0.57	0.92

APPENDIX C

(page 271 follows)

AUTOMATIC DATA PROCESSING

by Jean Claude De Bremaecker and James H. Whitcomb

Intoduction

Our philosophy in programming, as described in a previous report (De Bremaecker and Whitcomb, 1966), has been to subroutinize operations so that the programmer has maximum flexibility in writing and using programs for seismic data analysis. Ideally, main-line programs control input/output of data with the exception of subroutines specifically designed for data handling.

Our current library of subroutines, written in FORTRAN IV for a CDC 3600 computer, is listed in this report. Each subroutine is preceded by a brief description of its basic function.

Subroutines

UNPACK

The family of subroutines titled UNPACK reads and stores a group of analog traces in digital form. Individual traces are then unscrambled from their original data form and stored in a matrix in the computer, making them ready for further computations. The UNPACK family of subroutines is a prerequisite for any analysis of the seismic data and is the first subroutine incorporated in any main-line program. However, limitations in computer storage often may force the incorporation of UNPACK functions into the main-line program to conserve space.

```
1601161000-


      SUBROUTINE UNPACK (IA,IB,IR,V)
C     UNPACK TRACES 1 THRU 8 OF A 12 TRACE DIGITAL RECORD
C     STORE IN V(1,I) TO V(8,I) IN FLOATING POINT
C     IA IS TIME IN MSEC WHERE UNPACK BEGINS, IB WHERE IT ENDS
C     IR IS THE RECORD NUMBER ON THE DIGITAL TAPE STARTING AT 1
C     IA AND IB ARE GIVEN BY THE CONTROL PROGRAM AS INTEGERS
      COMMON/100/T,RECORD
      DIMENSION RECORD (9000)
      INTEGER T,RECORD
      DIMENSION T(4000),V(8,800)
      DO 12 I=1,IR
      BUFFER IN(1,1) (RECORD(1),RECORD(2))
100   IF(UNIT,1)100,12
12    CONTINUE
      IBEG=4+(3*IA)
      IEND=3+(3*IB)
      BUFFER IN (1,1) (RECORD(1),RECORD(IEND))
1     IF(UNIT,1)1,2,3,4
3     PRINT 7
7     FORMAT (* END OF FILE*)
      STOP
4     PRINT 8
8     FORMAT (* PARITY ERROR*)
      STOP
    2 PRINT 6,RECORD(1),RECORD(3)
6     FORMAT (1X,I10,I10)
      DO 9 J=IBEG,IEND,3
      M=(((J-IBEG)/3)*8)+1
      L=M+7
9     DECODE (16,10,RECORD(J)) (T(K),K=M,L)
10    FORMAT (8R2)
      LA=IB-IA
      DO 11 J=1,LA
      DO 11 I=1,8
      K=(J-1)*8+I
11    V(I,J)=T(K)
      RETURN
      END
```

```
1601161000-
```

```
      SUBROUTINE UNPAK2 (IA,IB,IR,V)
C     UNPACK TRACES 9 THRU 12 AND 13 THRU 16 PRESUMED ON CONSECUTIVE RECORDS
C     STORE IN V1(I) TO V8(I) IN FLOATING POINT
C     IA TIME IN MSEC WHERE UNPACK BEGINS, IB WHERE IT ENDS
C     IR IS THE RECORD NUMBER ON THE DIG. TAPE STARTING AT 1
C     IA AND IB GIVEN BY CONTROL PROGRAM AS INTEGERS
      COMMON/100/T,RECORD
      DIMENSION RECORD (9000)
      INTEGER T, RECORD
      DIMENSION T(4000),V(8,800)
      DO 12 I=1,IR
      BUFFER IN (1,1) (RECORD(1),RECORD(2))
100   IF(UNIT,1)100,12
12    CONTINUE
      I=0
      IBEG=6+(3*IA)
      IEND=5+(3*IB)
13    BUFFER IN (1,1) (RECORD(1),RECORD(IEND))
1     IF(UNIT,1)1,2,3,4
3     PRINT 7
7     FORMAT (* END OF FILE*)
      STOP
4     PRINT 8
8     FORMAT (* PARITY ERROR*)
      STOP
2     PRINT 6,RECORD(1),RECORD(3)
6     FORMAT (1X,I10,I10)
      IF(I)19,14,20
19    PRINT 22
22    FORMAT (* ERROR IN UNPACK2*)
      STOP
14    DO 9 J=IBEG,IEND,3
      M=((J-IBEG)/3)*8+1
      L=M+3
9     DECODE (8,10,RECORD(J)) (T(K),K=M,L)
10    FORMAT (4R2)
      I=2
      IBEG=4+(3*IA)
      IEND=3+(3*IB)
      GO TO 13
20    DO 21 J=IBEG,IEND,3
      M=((J-IBEG)/3)*8+5
      L=M+3
21    DECODE (8,10,RECORD(J)) (T(K),K=M,L)
      LA=IB-IA
      DO 11 J=1,LA
      DO 11 I=1,8
      K=(J-1)*8+I
11    V(I,J)=T(K)
      RETURN
      END
```

1601161000-

```
      SUBROUTINE UNPAK3 (IA,IB,IR,V)
C     UNPACK TRACES 5 THRU 12 OF A 12 TRACE DIGITAL RECORD
C     STORE IN V(1,I) TO V(8,I) IN FLOATING POINT
C     IA IS TIME IN MSEC WHERE UNPACK BEGINS, IB WHERE IT ENDS
C     IR IS THE RECORD NUMBER ON THE DIGITAL TAPE STARTING AT 1
C     IA AND IB ARE GIVEN BY THE CONTROL PROGRAM AS INTEGERS
      COMMON/100/T,RECORD
      DIMENSION RECORD (9000)
      INTEGER T,RECORD
      DIMENSION T(4000),V(8,800)
      DO 12 I=1,IR
      BUFFER IN (1,1) (RECORD(1),RECORD(2))
100   IF(UNIT,1)100,12
12    CONTINUE
      IBEG= 5+(3*IA)
      IEND= 4+(3*IB)
      BUFFER IN (1,1) (RECORD(1),RECORD(IEND))
1     IF(UNIT,1)1,2,3,4
3     PRINT 7
7     FORMAT(* END OF FILE*)
      STOP
4     PRINT 8
8     FORMAT(* PARITY ERROR*)
      STOP
    2 PRINT 6,RECORD(1),RECORD(3)
6     FORMAT (1X,I10,I10)
      DO 9 J=IBEG,IEND,3
      M=(((J-IBEG)/3)*8)+1
      L=M+7
9     DECODE (16,10,RECORD(J)) (T(K),K=M,L)
10    FORMAT (8R2)
      LA=IB-IA
      DO 11 J=1,LA
      DO 11 I=1,8
      K=(J-1)*8+I
11    V(I,J)=T(K)
      RETURN
      END
```

DTREND

In order to eliminate errors caused by a biasing of the data in computations, a least squares straight line is calculated for the seismic data window. The least squares line is subtracted from the data prior to analysis by another subroutine or the main-line program.

```
1601161000-
```

```
      SUBROUTINE DTREND (N,Y)
C     LEAST SQUARES DETREND
C     SUBTRACTS LEAST SQUARES STRAIGHT LINE FROM FUNCTION Y OF LENGTH N.
C     MAX N = 500.
      DIMENSION Y(800)
      P=N
      SX=P*(P+1.)/2.
      SX2=P*(P+1.)*(2.*P+1.)/6.
      SY=0
      SXY=0
      DO 10 I=1,N
      X=I
      SY=SY+Y(I)
10    SXY=SXY+X*Y(I)
      D=P*SX2-SX*SX
      AZ=(SY*SX2-SX*SXY)/D
      A1=(P*SXY-SY*SX)/D
      DO 20 I=1,N
      X=I
      YP=AZ+A1*X
20    Y(I)=Y(I)-YP
      RETURN
      END
```

CHNCOR

The object of the CHNCOR subroutine is to correct the obvious digitization errors in the digitized seismic record. The method computes the standard deviation of all the digitized values and then compares each value for validity with the magnitude of five times the standard deviation. If one or two errors in a row are detected, they are smoothed over using adjacent values; if three or more errors are detected, an error message is printed.

1601161000-

```
      SUBROUTINE CHNCOR (N,C,FN)
C     CHECK AND CORRECT FN(I) PROGRAM
C     C IS MAXIMUM PERMISSIBLE FIRST DIFFERENCE
C     N IS NUMBER OF VALUES OF FN(I) TO BE READ IN
C     N IS ODD INTEGER NO GREATER THAN 799
C     LAST 3 VALUES OF FN(I) SHOULD BE WITHIN ERROR LIMITS
      DIMENSION FN(800)
      J=0
      X=0
      N2=N-1
      DO 10 I=1,N2
      D=FN(I)-FN(I+1)
      IF(D)1,2,3
1     D=-D
3     IF(C-D)10,2,2
2     J=J+1
      X=X+D*D
10    CONTINUE
      Y=J
      X=5.*SQRTF(X/Y)
      I=0
5     I=I+1
12    IF(N-I-1)20,19,19
19    D1=FN(I)-FN(I+1)
      IF(D1)4,5,6
4     D1=-D1
6     IF(X-D1)7,5,5
7     D2=FN(I)-FN(I+2)
      XP=1.5*X
      IF(D2)8,11,9
8     D2=-D2
9     IF(XP-D2)13,11,11
11    FN(I+1)=(FN(I)+FN(I+2))/2.
      I=I+2
      GO TO 12
13    D3=FN(I)-FN(I+3)
      X2=2.*X
      IF(D3)14,15,16
14    D3=-D3
16    IF(X2-D3)17,15,15
15    FN(I+1)=(2.*FN(I)+FN(I+3))/3.
      FN(I+2)=(2.*FN(I+3)+FN(I))/3.
      I=I+3
      GO TO 12
17    PRINT 18,I
18    FORMAT (10H AFTER FN(I4,40H) ARE 3 ERRORS IN A ROW...DISCARD RECOR
     1D)
20    RETURN
      END
```

TRNSFM

This subroutine computes the amplitude spectrum of a function which is, in this case, the digitized seismic trace. The method uses an approximation to the integral known as "Filon's method." The method is given in many textbooks on numerical analysis that deal with quadratures (Hamming, 1962).

1601161000-

```
      SUBROUTINE TRNSFM (N,B,FMIN,FMAX,DF,FN,C)
      DIMENSION FN(800),C(100)
C     FOURIER TRANSFORMS BY FILONS METHOD
C     B IS TIME DURATION IN SECONDS, N IS NUMBER OF VALUES FROM 0 TO B
C     FREQUENCIES ARE IN CYCLES PER SECOND
C     N MUST BE AN ODD NUMBER NO LARGER THAN 799
C     (FMAX-FMIN)/DF MUST BE 50 OR LESS
C     FMIN IS LOWEST FREQUENCY, FMAX IS HIGHEST, DF IS INCREMENT
C     FN(I) IS THE VALUE OF THE FUNCTION TO BE TRANSFORMED AT THE ITH
C     POINT IN TIME (WHEN I=1, TIME IS ZERO, WHEN I=N, TIME IS B)
C     F IS THE FREQUENCY USED TO FIND THE CORRESPONDING TRANSFORM C(F)
C     READ IN VALUES OF N, B, FMIN, FMAX, DF, AND N VALUES FOR FN(I)
C     FROM MAINLINE PROGRAM
      J=0
      D=N-1
      K=N-1
      L=N-2
      DT=0.001
      DF=6.28318*DF
      F=FMIN*6.28318
      GO TO 7
8     F=F*6.28318
      F=F+DF
7     TH=DT*F
      J=J+1
70    ALF=(TH**2+TH*SINF(TH)*COSF(TH)-2.*SINF(TH)**2)/TH**3
      BET=(2.*(TH*(1.+COSF(TH)**2)-2.*SINF(TH)*COSF(TH)))/TH**3
      GAM=(4.*(SINF(TH)-TH*COSF(TH)))/TH**3
60    CEV=.5*(FN(1)+FN(N)*COSF(F*B))
      DO 10 I=3,L,2
      U=I
10    CEV=CEV+FN(I)*COSF(F*U*DT)
      COD=0
      DO 20 I=2,K,2
      U=I
20    COD=COD+FN(I)*COSF(F*U*DT)
      SEV=.5*FN(N)*SINF(F*B)
      DO 30 I=3,L,2
      U=I
30    SEV=SEV+FN(I)*SINF(F*U*DT)
      SOD=0
      DO 40 I=2,K,2
      U=I
40    SOD=SOD+FN(I)*SINF(F*U*DT)
      CD=FN(N)*SINF(F*B)
      CT=DT*(ALF*CD+BET*CEV+GAM*COD)
      SD=FN(N)*COSF(F*B)-FN(1)
      ST=DT*(-ALF*SD+BET*SEV+GAM*SOD)
      C(J)=SQRTF(ST**2+CT**2)
      F=F/6.28318
      IF(FMAX-F)9,9,8
9     CONTINUE
      DF=DF/6.28318
      RETURN
      END
```

COTRAN

COTRAN computes the cosine transform of a window in the seismic trace. Output gives the transformed values corresponding to equally spaced frequencies in an interval designated by a minimum and maximum frequency.

```
      SUBROUTINE COTRAN(C,FN,FL,DSEC,FMAX,FMIN,DF,NF)
C     COSINE TRANSFORM. C IS NAME OF TRANSFORM. FN,NAME OF FUNCTION TO
C     BE TRANSFORMED. FL IS LENGTH OF FN IN SECONDS = TIME AT LAST FN
C     VALUE.                                        DSEC IS TIME
C     SPACING OF FN IN SECONDS. FMIN AND FMAX ARE LOWEST AND HIGHEST
C     FREQUENCY DESIRED IN CYCLES PER SECOND. DF IS FREQUENCY SPACING.
C     FIRST FN VALUE, FN(1), IS VALUE OF FUNCTION AT TIME = 0.
C     COMPUTED QUANTITIES - NF IS NUMBER OF FREQUENCY VALUES= NUMBER OF
C     TRANSFORM VALUES(C(K)) TO BE CALCULATED. NT IS THE LENGTH OF THE
C     FN VECTOR
      DIMENSION C(200),FN(800)
      NF = ((FMAX-FMIN)/DF) + 1.
       NT =      (FL)/DSEC + 1.
       NT1 =  NT - 1
      DO 601 K = 1,  NF
      R = K-1
  601 C(K) =(R*DF + FMIN)*3.14159*2.
      DO 3030 K = 1, NF
      EVEN   = .5*FN(1)
      DO 602 I = 3,NT1, 2
      RI = I - 1
  602 EVEN   = EVEN   + FN(I)*COS (RI*DSEC*C(K))
      EVEN = EVEN + .5*FN(NT)*COS(FL*C(K))
      ODDSUM = FN(2)* COS (C(K)*DSEC)
      DO 603 I = 4, NT1, 2
      RI   =  I - 1
  603 ODDSUM = ODDSUM +FN(I)*COS (C(K)*RI *DSEC)
      T = C(K)*DSEC
      A = (T**2 + T*SIN (T)*COS (T) - 2.*(SIN (T))**2)/T**3
      B =  2.*(T*(1.+ (COS (T))**2)-2.*SIN (T)*COS (T))/T**3
      G = 4.*(SIN (T)- T*COS (T))/T**3
 3030 C(K) = DSEC*(A*FN(NT)*SIN (C(K)*     (FL)) + B*EVEN + G*ODDSUM)
      RETURN
      END
```

AUTCOR

AUTCOR computes the autocorrelation function for a given window and given maximum phase shift of the seismic trace. Digitally, the process simply multiplies a time window by itself at various phase shifts. The function has no real physical significance in itself, but may prove useful for interpretation of seismic data.

```
1601161000-


      SUBROUTINE AUTCOR (L,IBEG,IEND,FN,PHI)
C     AUTOCORRELATION FUNCTION PHI
C     WINDOW OF FN CORRELATED IS IBEG TO IEND INCLUSIVE.  L IS LENGTH
C     OF PHI, MAX L = 126.  CORRELATION IS FOR A TIME LAG OF ZERO TO
C     L-1 MILLISECONDS.  IEND-IBEG SHOULD BE MUCH GREATER THAN L.
      DIMENSION FN(4500),PHI(126)
      N = IEND - IBEG
      DO 10 I=1,L
      PHI(I)=0
      M=IEND - (I-1)
      DO 20 J = IBEG, M
      JI = J + I - 1
   20 PHI(I)=PHI(I) + FN(J)*FN(JI)
      A=N-(I-1)
      PHI(I)=PHI(I)/A
   10 CONTINUE
      RETURN
      END
```

CROSCR

Crosscorrelation of adjacent traces is computed by CROSCR given a specified time window and maximum phase shift. The function thus provides a measure of continuity of signal from trace to trace. However, as in AUTCOR, it has no physical significance except as an aid to interpretation.

```
1601161000-


      SUBROUTINE CROSCR (K,IBEG,IEND,FN,GN,PHI)
C     CROSS CORRELATION FUNCTION PHI
C     CROSS CORRELATES FN AND GN FROM IBEG TO IEND
C     TIME LAG IS -K/2 TO K/2 MILLISECONDS.  MAX K = 250.
      DIMENSION FN(4500),GN(4500), PHI(251)
      KD2 = K/2
      KP1 = K + 1
      KDP =  K/2 + 2
      LA = (K/2) + 1
      DO 20 J=1,KD2
      KJ1 = KD2 - J + 1
      L=IEND - J
      A=N-J
      PHI(KJ1)=0
      DO 30 I=IBEG,L
      M=I + J
   30 PHI(KJ1)=PHI(KJ1) + GN(I)*FN(M)
   20 PHI(KJ1)=PHI(KJ1)/A
      PHI(LA)=0
      A=N
      DO 10 I=IBEG,IEND
   10 PHI(LA)=PHI(LA) + FN(I)*GN(I)
      PHI (LA)=PHI(LA)/A
      DO 40 J=KDP,KP1
      L=IEND - (J-KD2-1)
      A=N-(J-KD2-1)
      PHI(J)=0
      DO 50 I=IBEG,L
      M=I + (J-KD2-1)
   50 PHI(J)=PHI(J) + FN(I)*GN(M)
   40 PHI(J)=PHI(J)/A
      RETURN
      END
```

BANDFL

This subroutine computes the positive half plus the center point of an even bandpass filter. The filter is named C of length TMAX at a time spacing DT. It passes the frequencies from FMIN to FMAX. TMAX should be at least 2/FMIN to obtain good results. The greater TMAX the better the filter, but also the slower the filtering. All parameters are presumed to be given by the main-line program.

```
1601161000-


      SUBROUTINE BANDFL (C,FMIN,FMAX,TMAX,DT,NT)
      DIMENSION C(200)
C     BAND  PASS FILTER. C IS NAME OF RESULTING FILTER. FMIN, FMAX ARE
C     LIMITS FOR INTEGRATION OF COS(2*PI*T*F) WITH RESPECT TO F. C(K)
C     IS INTEGRAL FOR T = (K-1)*DT. TMAX IS MAX VALUE OF T FOR WHICH C
C     IS COMPUTED. C IS MULTIPLIED BY A SCALED SIN(X)/X FUNCTION TO GIVE
C     FINAL FILTER C.  MAX NT (=TMAX/DT+1.) IS 200.
C     C IS POSITIVE HALF PLUS CENTER POINT OF AN EVEN FILTER
      NT = TMAX/DT +1.
      S = 3.14159/(FLOAT(NT) - 1.)
      C(1) = FMAX - FMIN
      IF(FMIN) 36,10,36
   36 DO 25 K = 2, NT
      F = K - 1
   25 C(K) = SIN(F*S)/(F**2*S*6.28318*DT)*(SIN(6.28318*FMAX*F*DT) -
     1SIN(6.28318*FMIN*F*DT))
      GO TO 40
   10 DO 26 K = 2, NT
      F = K - 1
   26 C(K) = SIN(F*S)/(F**2*S*6.28318*DT)*SIN(6.28318*FMAX*F*DT)
   40 RETURN
      END
```

DFILTR

This subroutine computes the positive half of an even filter corresponding to any frequency spectrum. It is not particularly well suited for computing a bandpass filter as in BANDFL.

1601161000-

```
      SUBROUTINE DFILTR (C,FN,FL,DSEC,FMAX,DF,NF)
C     COMPUTE EVEN FILTER.  C IS NAME OF FILTER. FN,NAME OF SPECTRUM.
C     FL, LENGTH OF FN IN CYCLES/SECOND = FREQUENCY AT LAST FN VALUE.
C     DSEC, FREQUENCY SPACING OF SPECTRUM FN.
C     FMAX , LENGTH OF FILTER C IN SECONDS.
C     DF, FREQUENCY SPACING IN FILTER, CYCLES/SECOND.
C     FIRST FN VALUE, FN(1), IS VALUE OF SPECTRUM AT FREQUENCY = 0.
C     COMPUTED QUANTITIES - NF IS NUMBER OF FREQUENCY VALUES= NUMBER OF
C      FILTER   VALUES(C(K)) TO BE CALCULATED. NT IS THE LENGTH OF THE
C     FN VECTOR.  MAX NF (=FMAX/DF+1.) = 200.  MAX NT (=FL/DSEC+1.)=500.
C     COMPUTES POSITIVE HALF PLUS CENTER POINT OF AN EVEN FILTER
      DIMENSION C(200), FN(500)
      NF = FMAX/DF + 1.
       NT =      (FL)/DSEC + 1.
       NT1 =  NT - 1
      DO 601 K = 1,  NF
      R = K-1
  601 C(K) = R*DF*3.14159*2.
      DO 3030 K = 1, NF
      EVEN    = .5*FN(1)
      DO 602 I = 3,NT1, 2
      RI = I - 1
  602 EVEN    = EVEN    + FN(I)*COS (RI*DSEC*C(K))
      EVEN = EVEN + .5*FN(NT)*COS(FL*C(K))
      ODDSUM = FN(2)* COS (C(K)*DSEC)
      DO 603 I = 4, NT1, 2
      RI  =  I - 1
  603 ODDSUM = ODDSUM +FN(I)*COS (C(K)*RI *DSEC)
      T = C(K)*DSEC
      A = (T**2 + T*SIN (T)*COS (T) - 2.*(SIN (T))**2)/T**3
      B =  2.*(T*(1.+ (COS (T))**2)-2.*SIN (T)*COS (T))/T**3
      G = 4.*(SIN (T)- T*COS (T))/T**3
 3030 C(K) = DSEC*(A*FN(NT)*SIN (C(K)*     (FL)) + B*EVEN + G*ODDSUM)
      RETURN
      END
```

TAPER

This subroutine is normally used to taper an autocorrelation function prior to transforming, or an even filter prior to using it. It multiplies the function being tapered by a smoothly decreasing curve thus preventing discontinuities at the end. Note that the function being tapered is assumed to be even and only its positive half is assumed to be given by FN.

```
1e01161000-
```

```
      SUBROUTINE TAPER(FN,L)
C     L IS LENGTH OF FN. FN IS MULTIPLIED BY THE FIRST SEGMENT (1-PI)
C     OF A SCALED SIN(X)/X FUNCTION.  MAX L = 200.
C     FN IS POSITIVE HALF + CENTER POINT OF EVEN FUNCTION.
C     USED TO SMOOTHE END OF FN TO PREVENT DISCONTINUITIES
      DIMENSION FN(200)
      FN(1) = FN(1)
      R = L - 1
      DO 614 I = 2,L
      S = I - 1
  614 FN(I) = (FN(I)*SIN(3.14159*S/R))/(S*3.14159/R)
      RETURN
      END
```

CONVO

This subroutine permits filtering data by even filters. The process in digital analysis is called convolution or rectangular integration and its analog equivalent can be thought of as a frequency filter of variable bandpass width and shape. The shape of the filter can be varied by the programmer and a relatively narrow bandpass response can be obtained.

```
      SUBROUTINE CONVO (FN,UP,LD,LF,GN)
      DIMENSION FN(800),UP(200),GN(800)
C     FILTER GIVEN BY CENTER POINT PLUS HALF LENGTH
C     DATA IN FN(I),RESULT IN GN(I), FILTER IN UP(I)
C     DATA LENGTH LD, FILTER LENGTH LF( MAXLD = 800., MAX LF = 200.
      LR=LD-2*LF+2
      I=0
    6 X=0
      I=I+1
      K=I+LF-1
      X=X+FN(K)*UP(1)
      DO 7 J=2,LF
      L=I+LF-J
      M=I+LF+J-2
    7 X=X+(FN(L)+FN(M))*UP(J)
      GN(I)=X
      IF(I-LR)6,8,8
    8 LRI=LR+1
      DO 10 I=LRI,LD
   10 GN(I)=0.0
      RETURN
      END
```

DECONO

This subroutine performs the autoregression of F by H. If a geophone is given a tap, i.e., an impulse of force, then H is the impulse velocity response. Thus if F is autoregressed with H (by this program) the result is the true ground velocity. Instability problems may occur if H is not quite correct. The problems can be detected by first checking H for stability by means of STABLY.

```
1601161000-
```

```
      SUBROUTINE DECOND (F,M,H,N)
C     DECONVOLUTION . M IS LENGTH OF F, N IS LENGTH OF H.  F  IS
C     OPERATED ON BY H AND THE RESULTS STORED IN F.  H IS NOT CHANGED.
C     MAX M = 500, MAX N = 20.
      DIMENSION F(500), H(20)
      F(1) = F(1)/H(1)
      DO 1200 I = 2,N
      DO 3030 J = 2,I
      IJ = I - J
 3030 F(I) = F(I) - H(J) * F(IJ + 1)
 1200 F(I) = F(I)/H(1)
      K = N + 1
      DO 8888 I = K, M
      DO 10 J = 2,N
      IJ = I - J
   10 F(I) = F(I) - H(J) * F(IJ + 1)
 8888 F(I) = F(I) / H(1)
      RETURN
      END
```

STABLY

This subroutine checks the stability of a deconvolution operator. The operator checked is H of length N. If the operator is stable it prints STABLE and vice versa for UNSTABLE. It uses Jury's division method (Jury, E. I., 1964).

```
1601161000-


      SUBROUTINE STABLY (H,N)
C     STABILITY CHECK FOR DECONV. H IS OPERATOR. N IS LENGTH OF H. FIRST
C     ELEMENT OF H  IS MADE POSITIVE BY REVERSING SIGNS OF H IF NECES-
C     SARY.  TEST 1, SUM OF ELEMENTS OF H MUST BE POSITIVE (GREATER THAN
C     0). TEST 2, (SUM OF EVEN ELEMENTS) - (SUM OF ODD ELEMENTS) MUST BE
C     POSITIVE. (FOR THIS TEST, FIRST ELEMENT IS COUNTED AS H(0), THE
C     FIRST EVEN ELEMENT).  TEST 3, H IS INVERTED (H(I) BECOMES H(N-I))
C     AND H OPERATES DECONV ON H-INVERTED (G) AND RESULTS ARE PUT INTO
C     G. THE FIRST N-2 ELEMENTS OF G MUST NOW BE SMALLER THAN 1 IN
C     ABSOLUTE VALUE.                                        IF ANY TEST
C     FAILS, PROGRAM IMMEDIATELY PRINTS OUT *UNSTABLE* AND ENDS. IF NO
C     TEST FAILS, *STABLE* IS PRINTED. IN EITHER CASE, CHECK IS MADE TO
C     BE SURE H(1) HAS ORIGINAL VALUE, REVERSING SIGNS AGAIN IF NECESS.
      DIMENSION H(20), G(20)
      COMMON HSUM, ESUM, USUM, G
      POINT = 1
      IF (H(1)) 32,32,1500
   32 DO 1691 I = 1,N
 1691 H(I) = -H(I)
      POINT = -1
 1500 HSUM = H(1)
      DO 64 I = 2,N
   64 HSUM = HSUM + H(I)
      IF (HSUM) 30,30,1600
 1600 ESUM = H(1)
      DO 99 I = 3, N, 2
   99 ESUM = ESUM + H(I)
      USUM = H(2)
      DO 89 I = 4, N, 2
   89 USUM = USUM + H(I)
      IF (ESUM - USUM) 30,30, 1700
 1700 DO 3 I = 1, N
      NI = N - I
    3 G(I) = H(NI+1)
      CALL DECONV (G,N,H,N)
      N2 = N - 2
      FLAG = 1.
      DO 28 I = 1, N2
      IF(ABS(G(I)) - 1.) 28,36,36
   36 FLAG = -1.
   28 CONTINUE
      IF (FLAG) 30,30,40
   40 PRINT 44
   44 FORMAT (7H STABLE  )
      GO TO 60
   30 PRINT 45
   45 FORMAT (9H UNSTABLE  )
   60 IF (POINT) 23, 23, 61
   23 DO 1961 I = 1, N
 1961 H(I) = -H(I)
   61 RETURN
      END
```

PYSLYS

The subroutine, PYSLYS, velocity filters adjacent seismic traces of a record as described in Embree and others (1963). The general operation of PYSLYS is to filter, using the CONVO subroutine, traces of the seismic record by a given, even filter. Then, amplitudes of adjacent traces are added with various time shifts to provide the velocity filtering effect. This subroutine operates on trace groups 1-9, 9-16, and 17-24.

```
1601161000-


      SUBROUTINE PYSLYS (V,R,IL,KBEG,KEND)
C     THIS PROGRAM USES A 1 MSEC/TRACE PIE SLICE BEAM. IT THEN TILTS THE
C     BEAM FROM KBEG TO KEND.  IT OPERATES ON 8 TRACES V OF LENGTH IL
C     KEND MAY BE POSITIVE OR NEGATIVE.  OUTPUT IS R(KB,J), KB = 1 TO 10
C     AS TILT = KBEG TO KEND.  MAX (KEND-KBEG) = 9.
C     TIME SPACING ON EACH TRACE IS 1 MSEC. USES CONVO
C     FOR USE ON IBM 7090, REPLACE DATA STATEMENT WITH
C     DATA OP/    .00827,.01621, . . . . ,-.00101/
C     AND RUN UNDER  -BOOTSTRAP, VERSION 9- INSTRUCTION TO OPERATOR
      DIMENSION OP(4,11),V(8,500),F(500),R(10,500),O(11),OR(8,11)
      DATA(((OP(I,J),I=1,4),J=1,11)=.00827,.01621,.04503,.40529,.00901,.
     101930,.08106,-.13510,.01228,.04503,-.05790,-.02702,.03118,-.03684,
     2-.01501,-.01156,-.02702,-.01039,-.00737,-.00643,-.00795,-.00540,-.
     300445,-.00409,-.00427,-.00340,-.00300,-.00283,-.00276,-.00237,-.00
     4217,-.00208,-.00196,-.00175,-.00164,-.00159,-.00147,-.00136,-.0012
     59,-.00125,-.00115,-.00108,-.00104,-.00101)
      DO 40 J=1,8
      AJ=J
      K=1. + ABSF(AJ-4.5)
      DO 40 I=1,11
40    OR(J,I)=OP(K,I)
         LTILT = ABSF(KEND) - ABSF(KBEG) + 1.
      DO 1 J=1,8
      DO 8 I=1,11
8     O(I)=OR(J,I)
      DO 9 I=1,IL
      DO 7 K=1,LTILT
7     R(K,I)=0.
9     F(I)=V(J,I)
      CALL CONVO(F,O,IL,11)
      DO 1 I=1,IL
1     V(J,I)=F(I)
      IF(KEND)2,3,3
3     CONTINUE
      DO 30 K=KBEG,KEND
      JEND=IL-7*K
      KB=K-KBEG+1
      DO 30 J= 1,JEND
      DO 30 I=1,8
      JI=J+(I-1)*K
30    R(KB,J)=R(KB,J)+V(I,JI)
      RETURN
2     KEND=-KEND
      KBEG=-KBEG
      DO 21 K=KBEG,KEND
      JBEG=7*K+1
      KB=K-KBEG+1
      DO 21 J=JBEG,IL
      DO 21 I=1,8
      JI=J-(I-1)*K
21    R(KB,J)=R(KB,J)+V(I,JI)
      RETURN
      END
```

References

De Bremaecker, J. Cl., and Whitcomb, J. H., 1966, Automatic data processing, in Investigation of in situ physical properties of surface and subsurface site materials by engineering geophysical techniques--Project quart. rept., Oct. 1, 1965-Dec. 31, 1965: Flagstaff, Arizona, U.S. Geol. Survey, Br. of Astrogeology, p. 93-96.

Embree, Peter, Burg, J. P., and Backus, M. M., 1963, Wideband velocity filtering--the Pie-slice process: Geophysics, v. 28, no. 6, p. 948-974.

Hamming, R. W., 1962, Numerical methods for scientists and engineers: New York, McGraw-Hill, 309 p.

Jury, E. I., 1964, Theory and application of the 3-transform method: New York, J. Wiley & Sons

APPENDIX D

(page 305 follows)

P-WAVE VELOCITY AND ATTENUATION SUMMARY, FY-66

by

Hans D. Ackermann and Richard H. Godson

U.S. Geological Survey
Flagstaff, Arizona

Data presented in this appendix are in the same form as those of the FY-65 Annual Report (see Godson and others, 1965) and details of analysis will be repeated here. Locations and brief site descriptions can be found in the Proposed Work Plan for 1967 in this volume.

Amboy Flow

Profile	a	ν	α	$Q_\alpha\alpha$	Q_α
A	0.062	166	4250	8350	1.97
B	0.072	166	4390	7300	1.66
D	0.092	77	2080	2620	1.26
E	0.237	143	2300	1890	0.82
G	0.032	67	3040	6800	2.24
H	0.050	125	2960	7850	2.65
I	0.137	167	2500	3820	1.52
J	0.032	62	3770	6170	1.64
K	0.073	91	2520	3960	1.57
L	0.139	167	2000	3770	1.89
M	0.031	53	3310	5260	1.59
N	0.429	83	2220	6060	2.73
P	0.031	67	3200	6750	2.11
Q	0.089	167	2750	5870	2.14
R	0.091	143	1740	4930	2.83

Bishop Tuff

A	0.064	91	1700	4450	2.62
B	0.097	167	1950	5400	2.77
C	0.128	250	1950	6130	3.14
D	0.042	77	1490	5750	3.85
E	0.149	200	1600	4220	2.64
F	0.153	250	1600	5130	3.20
G	0.045	83	1730	5810	3.35

Bishop Tuff (cont.)

Profile	a	ν	α	$Q_\alpha \alpha$	Q_α
H	0.132	200	1940	4800	2.47
I	0.164	333	1900	6380	3.36
J	0.063	77	1500	3830	2.55
K	0.066	125	1430	5950	4.06
L	0.153	250	1430	5120	3.56
M	0.074	125	1850	5310	2.88
N	0.084	167	2000	6230	3.12
O	0.118	200	1840	5320	2.89
P	0.082	100	1750	3830	2.18
Q	0.111	167	1820	4720	2.60
R	0.167	250	1760	4700	2.66
S	0.060	100	1610	5230	3.25
T	0.088	111	1430	3960	2.71
U	0.148	250	1430	5300	3.71
V	0.053	71	1520	4230	2.79
W	0.096	167	1820	5450	2.99
X	0.108	200	1670	5820	3.49

Cinder Hills

J	0.170	143	283	2640	9.35
K-1	0.076	59	319	2430	7.43
K-2	0.121	91	286	2380	8.50
L	0.076	62	309	2580	8.36
M	0.153	118	325	2570	7.92

Cinder Hills (cont.)

Profile	$\underline{a}$	ν	α	$Q_\alpha \alpha$	Q_α
N	0.105	77	366	2300	6.29
O	0.161	125	319	2440	7.66
P 1	0.248	200	395	2540	6.43
R 1	0.180	167	309	2910	9.41
Cinder Hills (second layer, probably not cinders)					
F	0.284	23	1030	2570	2.48
G	0.016	15	1030	3120	3.02
I	0.128	111	585	2730	4.66
Kaibab					
E	0.024	50	2380	6680	2.80
F	0.112	200	2500	5600	2.24
G	0.020	50	2550	7850	3.06
H	0.098	200	1380	6400	4.64
Kana-a Flow					
N	0.015	22	872	4680	5.37
Q	0.013	17	1205	4100	3.41
T	0.018	25	769	4460	5.81
U	0.017	27	752	4900	6.52
W	0.019	28	882	4660	5.28
X	0.010	27	1032	6070	5.87

1 Cinders at Kana-a flow site

Olancha bentonite site

Profile	$\underline{a}$	ν	α	$Q_\alpha{}^\alpha$	Q_α
A	1.327	57	120	147	1.22
B	0.595	54	187	483	2.58
B(w.d.)	0.480	91	159	383	2.41
C	0.785	112	261	449	1.72
C(w.d.)	0.755	95	268	399	1.49
D(w.d.)	0.339	110	317	1070	3.37
E(w.d.)	--	--	279	--	--

Lompoc diatomite site

B(w.d.)	0.888	52	115	197	1.71
C	1.317	126	205	298	1.45
D	1.260	157	182	394	2.16
D(w.d.)	0.813	78	170	310	1.82
E	0.808	95	130	380	2.92
E(w.d.)	0.781	62	126	262	2.08

Inyokern volcanic ash site

A	0.432	97	255	713	2.79
B	0.511	104	257	671	2.61
B(w.d.)	0.510	69	232	514	2.21

(w. d. means weight drop)

Meteor Crater bottom (first layer)

Profile	a	ν	α	$Q_\alpha \alpha$	Q_α
B-C	0.175	170	855	3050	3.58
C-D	0.126	124	1110	3100	2.79
D-E	0.114	109	840	3010	3.57
E-F	0.239	129	875	1900	2.16
F-G	0.130	104	690	2520	3.64
G-H	0.109	100	760	2930	3.85
H-I	0.103	93	670	2920	4.35
I-J	0.098	104	1010	3510	3.45
J-K	0.091	90	655	3180	4.84
K-L	0.133	88	592	2070	3.50
L-M	0.118	77	1010	2060	2.03
M-N	0.106	85	1050	2560	2.43
N-O	0.153	82	1020	1690	1.65
P	0.035	41	820	3820	4.65
Q	0.029	46	675	4940	7.31
R	0.086	46	790	1920	2.37

Meteor Crater bottom (second layer)

Q	0.040	45	990	3570	3.60
R	0.054	42	1130	2430	2.15
S	0.044	43	1030	3080	2.97

Meteor Crater bottom (third layer)

Profile	$\underline{a}$	ν	α	$Q_\alpha\alpha$	Q_α
P-Q	0.0037	50	2010	42780	21.3
R-S	0.0066	40	2000	18490	9.24

Meteor Crater south rim (first layer)

B-C	0.304	162	515	1770	3.42
C-D	0.332	135	495	1750	3.54
D-E	0.152	101	500	2220	4.44
G-H	0.616	257	521	1540	2.95
H-I	0.655	206	498	1240	2.55
K-L	0.654	211	735	1010	1.37
L-M	0.833	240	593	900	1.52
O-P	0.464	225	586	1530	2.61
P-Q	0.675	276	773	1290	1.67
Q-R	0.480	229	675	1490	2.21
R-S	0.176	234	965	2420	2.50
S-T	0.318	204	1120	2020	1.80
U-V	0.330	268	902	3290	3.64
W	0.029	28	870	2810	3.21

Meteor Crater south rim (second layer)

X	0.012	26	1770	8320	4.69
Y	0.013	30	1900	7270	3.83
Z	0.012	33	2080	6340	3.05

Middle Mesa

Profile	a	ν	α	$Q_\alpha \alpha$	Q_α
A	0.064	133	1290	6550	5.08
A	0.044	107	1670	7910	4.78
A(w.d.)	0.066	143	1200	6820	5.68
A(w.d.)	0.044	118	1780	8210	4.62
B	0.092	139	1890	4730	2.50
B(w.d.)	0.087	149	1890	5370	2.84
B(w.d.)	0.051	109	2090	7330	3.50
C	0.099	149	1100	4720	4.06
C(w.d.)	0.107	170	1160	5070	4.35
E	0.067	163	2270	6530	2.87
E(w.d.)	0.084	175	2270	6920	3.04
F	0.110	161	1400	6870	3.69
G	0.077	195	2000	8070	4.03

Mono Ash (first layer)

A	0.051	35	536	2120	3.95
B	0.079	63	487	2470	5.07
C	0.129	100	455	2440	5.36
D	0.047	37	510	2470	4.85
E	0.071	50	458	2220	4.85
F	0.119	100	421	2640	6.26
G	0.061	44	590	2230	3.78
H	0.092	71	512	2440	4.76
I	0.184	111	421	1900	4.50

(w.d. means weight drop)

Mono Ash (first layer) (cont.)

Profile	a	ν	α	$Q_\alpha{}^\alpha$	Q_α
J	0.062	36	513	1800	3.51
K	0.079	59	460	2320	5.04
L	0.150	125	459	2620	5.70
M	0.060	43	510	2280	4.47
N	0.107	71	452	2090	4.62
O	0.242	125	473	1630	3.45
P	0.069	48	564	2160	3.83
Q	0.073	59	491	2530	5.15
R	0.119	100	455	2640	5.80
S	0.052	45	500	2720	5.44
T	0.102	83	434	2560	5.90
V	0.052	40	568	2430	4.27
W	0.082	66	494	2560	5.19
X	0.130	91	508	2200	4.33
Z	0.050	40	556	2520	4.53

Mono Ash (second layer)[1/]

A	0.013	33	1760	7950	4.50
D	0.026	42	1680	5050	3.01
G	0.022	38	2080	5500	2.64
M	0.027	45	1780	5350	3.00
S	0.017	33	2050	6150	3.00
V	0.016	36	1640	7180	4.38

1/Probably Bishop Tuff, see Haines (this volume).

Mono Ash (second layer) (cont.)[1/]

Profile	a	ν	α	$Q_\alpha\alpha$	Q_α
Y	0.014	34	2160	7950	3.68
Z	0.013	27	2030	6570	3.24
		Pisgah Flow (first layer)			
E	0.154	59	611	1200	1.97
F	0.110	48	940	1360	1.45
H	0.048	32	1160	2110	1.82
I	0.117	62	1260	1680	1.33
J	0.230	91	1480	1240	0.84
N	0.037	27	1020	2290	2.24
O	0.070	62	1140	2800	2.46
P	0.121	91	1090	2360	2.16
Q	0.025	30	1280	3220	2.52
R	0.092	53	1040	1790	1.71
S	0.125	50	895	1260	1.41
T	0.057	45	1070	2500	2.34
U	0.212	71	952	1060	1.11
		Pisgah Flow (second layer)			
G	0.023	27	3420	3690	1.07
H	0.018	32	2170	5580	2.58
K	0.042	42	2970	3110	1.05
L	0.111	62	2570	1770	0.69
M	0.138	83	2870	1900	0.66

1/ Probably Bishop Tuff, see Haines (this volume).

Profile	$\underline{a}$	ν	α	$Q_\alpha \alpha$	Q_α
Sacramento Valley (first layer)					
B	0.061	96	1070	5000	4.67
B(w.d.)	0.062	98	1070	4960	4.51
E	0.043	87	1120	6290	5.59
Sacramento Valley (second layer)					
A	0.034	79	1450	7270	5.03
B	0.042	93	1350	7130	5.28
C	0.040	72	1240	5610	4.50
C(w.d.)	0.052	85	1240	5140	4.12
D	0.047	81	1230	5320	4.32
Sierra Ancha					
A	0.042	170	4400	12700	2.89
A(w.d.)	0.063	192	4400	9940	2.26
B	0.048	176	4000	11500	2.88
C	0.053	179	4060	10600	2.62
C(w.d.)	0.059	165	3890	8810	2.26
D(w.d.)	0.046	154	3900	10600	2.72
E	0.071	193	3800	8480	2.23
E(w.d.)	0.059	159	3800	5590	2.26
F	0.051	136	4600	8320	1.81
G	0.079	191	3600	8280	2.30
H	0.084	78	2200	2880	1.31
I	0.107	143	2650	4880	1.84

(w.d. means weight drop)

Sierra Ancha (cont.)

Profile	$\underline{a}$	ν	α	$Q_\alpha\alpha$	Q_α
J	0.082	97	2550	3950	1.60
J	0.060	105	2900	6170	2.13
K	0.174	70	1200	1270	1.06
K	0.081	100	3520	9750	2.78

Sonora Pass

A	0.089	333	5000	11800	2.36
B	0.084	333	5000	12500	2.50
C	0.075	333	5000	13900	2.78
D	0.084	333	5000	12500	2.50
E	0.094	200	5000	7040	1.41

Southern Coulee (first layer)

A	0.169	83	500	1550	3.10
D	0.045	24	500	1710	3.42
E	0.095	48	500	1580	3.16
F	0.139	67	500	1510	3.02
L	0.139	53	540	1190	2.20
U	0.192	83	420	1360	3.24
Z	0.096	59	350	1930	5.50
AA	0.086	71	350	2610	7.45
DD	0.096	67	440	2180	4.95
GG	0.123	62	400	1600	4.00

Southern Coulee (second layer)

Profile	$\underline{a}$	ν	α	$Q_\alpha\alpha$	Q_α
B	0.065	30	1000	1470	1.47
M	0.044	29	1250	2100	1.68
N	0.082	45	1250	1740	1.39
P	0.025	14	725	1820	2.52
S	0.049	29	1350	1880	1.39
T	0.058	39	1350	2070	1.53
Y	0.049	20	880	1250	1.42
FF	0.061	50	2100	2580	1.23
GG	0.054	43	2100	2510	1.20

S P Flow

A	0.090	55	790	1950	2.47
B	0.123	100	1000	2550	2.55
C	0.082	53	1080	2020	1.87
D	0.120	83	775	2180	2.81
E	0.090	105	1060	2330	2.20
F	0.182	32	1120	2460	2.20

References

Godson, R. H., Watkins, J. S., and Loney, R. A., 1965, Velocities and attenuation of head-wave amplitudes observed in lunar analog rocks, in Investigation of in situ physical properties of surface and subsurface site materials by engineering geophysical techniques--Project ann. rept., FY 1965: Flagstaff, Arizona, U. S. Geol. Survey, Br. of Astrogeology, p. F1-F25.